ISSN: 2153-1196 Volume 9, Number 12, October 2018

Scientific Research Publishing

Journal of Modern Physics

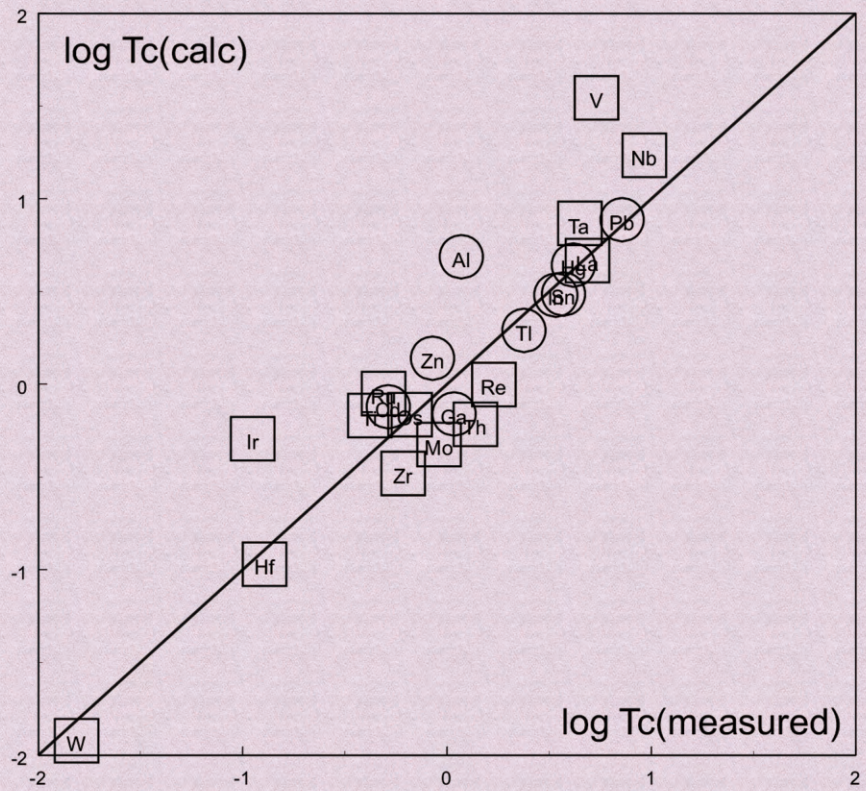

ISSN: 2153-1196

www.scirp.org/journal/jmp

Journal Editorial Board

ISSN: 2153-1196 (Print) ISSN: 2153-120X (Online)
http://www.scirp.org/journal/jmp

Editor-in-Chief

Prof. Yang-Hui He City University, UK

Editorial Board

Prof. Nikolai A. Sobolev Universidade de Aveiro, Portugal
Dr. Mohamed Abu-Shady Menoufia University, Egypt
Dr. Hamid Alemohammad Advanced Test and Automation Inc., Canada
Prof. Emad K. Al-Shakarchi Al-Nahrain University, Iraq
Prof. Tsao Chang Fudan University, China
Prof. Changle Chen University of Science and Technology of China, China
Prof. Stephen Robert Cotanch NC State University, USA
Prof. Peter Chin Wan Fung University of Hong Kong, China
Prof. Ju Gao The University of Hong Kong, China
Prof. Sachin Goyal University of California, USA
Dr. Wei Guo Florida State University, USA
Prof. Cosmin Ilie Los Alamos National Laboratory, USA
Prof. Haikel Jelassi National Center for Nuclear Science and Technology, Tunisia
Prof. Santosh Kumar Karn Dr. APJ Abdul Kalam Technical University, India
Prof. Christophe J. Muller University of Provence, France
Prof. Ambarish Nag National Renewable Energy Laboratory, USA
Dr. Rada Novakovic National Research Council, Italy
Prof. Tongfei Qi University of Kentucky, USA
Prof. Mohammad Mehdi Rashidi University of Birmingham, UK
Prof. Alejandro Crespo Sosa Universidad Nacional Autónoma de México, Mexico
Dr. A. L. Roy Vellaisamy City University of Hong Kong, China
Prof. Yuan Wang University of California, Berkeley, USA
Prof. Fan Yang Fermi National Accelerator Laboratory, USA
Prof. Peter H. Yoon University of Maryland, USA
Prof. Meishan Zhao University of Chicago, USA
Prof. Pavel Zhuravlev University of Maryland at College Park, USA

Scientific Research Publishing

Journal of Modern Physics, 2018, 9, 2101-2256
http://www.scirp.org/journal/jmp
ISSN Online: 2153-120X
ISSN Print: 2153-1196

Table of Contents

Volume 9 Number 12 October 2018

The figure on the front cover is from the article published in Journal of Modern Physics, 2018, Vol. 9, No. 12, pp. 2101-2124 by Boris V. Vasiliev.

Journal of Modern Physics (JMP)
Journal Information

SUBSCRIPTIONS

The *Journal of Modern Physics* (Online at Scientific Research Publishing, www.SciRP.org) is published monthly by Scientific Research Publishing, Inc., USA.

Subscription rates:
Print: $89 per issue.
To subscribe, please contact Journals Subscriptions Department, E-mail: sub@scirp.org

SERVICES

Advertisements
Advertisement Sales Department, E-mail: service@scirp.org

Reprints (minimum quantity 100 copies)
Reprints Co-ordinator, Scientific Research Publishing, Inc., USA.
E-mail: sub@scirp.org

COPYRIGHT

Copyright and reuse rights for the front matter of the journal:
Copyright © 2018 by Scientific Research Publishing Inc.
This work is licensed under the Creative Commons Attribution International License (CC BY).
http://creativecommons.org/licenses/by/4.0/

Copyright for individual papers of the journal:
Copyright © 2018 by author(s) and Scientific Research Publishing Inc.

Reuse rights for individual papers:
Note: At SCIRP authors can choose between CC BY and CC BY-NC. Please consult each paper for its reuse rights.

Disclaimer of liability
Statements and opinions expressed in the articles and communications are those of the individual contributors and not the statements and opinion of Scientific Research Publishing, Inc. We assume no responsibility or liability for any damage or injury to persons or property arising out of the use of any materials, instructions, methods or ideas contained herein. We expressly disclaim any implied warranties of merchantability or fitness for a particular purpose. If expert assistance is required, the services of a competent professional person should be sought.

PRODUCTION INFORMATION

For manuscripts that have been accepted for publication, please contact:
E-mail: jmp@scirp.org

Journal of Modern Physics, 2018, 9, 2101-2124
http://www.scirp.org/journal/jmp
ISSN Online: 2153-120X
ISSN Print: 2153-1196

Gilbert's Postulate and Some Problematic Physical Theories of the Twentieth Century

Boris V. Vasiliev

Dubna, Russia
Email: bv.vasiliev@yandex.com

How to cite this paper: Vasiliev, B.V. (2018) Gilbert's Postulate and Some Problematic Physical Theories of the Twentieth Century. *Journal of Modern Physics*, **9**, 2101-2124.
https://doi.org/10.4236/jmp.2018.912132

Received: August 30, 2018
Accepted: September 27, 2018
Published: September 30, 2018

Copyright © 2018 by author and Scientific Research Publishing Inc.
This work is licensed under the Creative Commons Attribution International License (CC BY 4.0).
http://creativecommons.org/licenses/by/4.0/
Open Access

Abstract

William Gilbert more than 400 years ago formulated a postulate that can be considered as main principle of natural sciences. According to this postulate, the criterion for the correctness of a theory can only be its confirmation by measurement data. In our time, all theories are confirmed by at least some experimental data. But sometimes the theory cannot explain parameters which can be considered as main for objects under study. Usually such "inexplicable" objects and dependencies are called empirical and it is assumed that they do not require theoretical explanation at all. In most cases, this means the fallacy of the used theory. So nowadays postulate Gilbert needs to be reformulated: the correct theory should describe ALL basic properties of objects of research. A number of theories developed in the twentieth century do not satisfy this formulation. In almost all cases, the reason for this is a misinterpretation of nature of objects of study. In particular, in order to satisfy Gilbert's refined postulate, it turns out necessary to revise the theoretical descriptions: 1) nature of superfluidity and superconductivity; 2) nature of neutrinos; 3) nature of neutron; 4) nature of nuclear forces; 5) model of quarks with fractional charge; 6) internal structure of stars; 7) nature of the Earth's magnetic field; 8) mechanism of thermomagnetic effect in metals.

Keywords

Superfluidity, Superconductivity, Quarks, Neutron, Nuclear Force, Neutrino, Star Physics, Terrestrial Magnetism

1. The Main Postulate of Natural Sciences

The twentieth century is in the past.

It's time to critically rethink a number of theories created by physicists during

this time.

The need for such a rethinking arises from the fact that theoretical physicists in the last century often considered the most fascinating and important thing to build theoretical models for those phenomena and objects for which experimental data have not yet been collected.

To create such theories in addition to knowledge needed fantasy, intuition and imagination. Therefore, the validity of such models, even if they are common accepted, may be questionable.

In the field of elementary particles, theoreticians often to replace the missing experimental data used symmetry considerations to systematize particles, for example, tables of particles based on Gell-Mann's quarks or a table, such as the Weinberg-Salam's standard model of elementary particles. These symmetrized tables look really nice, but the weakness of this approach is that the dropping out of even one basic particle, such as neutron (see below), violates the very principle of such systematization.

The reason that forces to reconsider a number of other theories of the XX century (for example, physics of stars) is connected with the progress of measurement techniques and obtaining new experimental data. Sometimes new measurement data do not fit into old theories. Apologists of these outdated theories often struggle hard for their survival. Several of these theories still dominate their fields of expertise and require partial or complete revision in our time.

In general, the past twentieth century brought remarkable scientific discoveries in the field of physics.

In the early twentieth century, nuclear physics was born and then rapidly developed. It was probably its greatest discovery. It radically changed the whole material and moral image of the world civilization.

At the same time, superconductivity was discovered, and a little later, and superfluidity. These super-phenomena promise mankind a giant leap of technology and economy.

At the beginning of the twentieth century, radio was born, which gradually led to television, and then radio technics spawned computers. Their importance is difficult to overestimate.

There was a science of quantum, which led to the appearance of quantum devices, among which lasers shine.

It can be a long list of branch of physical knowledge that gave us the twentieth century.

However, not all theoretical explanations for these discoveries seem perfectly correct.

William Gilbert (1544-1603) developed the criterion of correctness of the theory more than 400 years ago. He formulated a postulate that can be considered as the main principle of the natural sciences [1]:

All theoretical constructions that claim to be scientific must be verified and confirmed experimentally.

Before Gilbert, false ideas did not fear of experimental verification. At that time the world of thought was incomparably more subtle than the ordinary and gross material world. A precise coincidence of a philosophical theory with direct experience almost degraded it dignity in the eyes of dedicated. The discrepancy between pre-gilbert theory and observations did not bother anyone. There were absolutely fantastic statements, from our point of view. So, W. Gilbert writes that he experimentally denied the popular belief that the force of a magnet can be increased by rubbing it with garlic.

However, the formulation of this postulate proposed by Gilbert seems somewhat simplified nowadays. It is applicable to relatively simple theoretical models.

Nowadays, it seems impossible to find researchers who would disagree with Gilbert in principle. Indeed, all well-developed theories of the twentieth century are consistent to some measurement data. But these theories may contradict other data, the existence of which they simply do not pay attention.

Therefore, in the application to the complex theoretical constructions that made up the essence of physics of the twentieth century, Gilbert's postulate needs to be clarified:

Physical theory which claims to be an adequate description of the object of research has to explain **ALL** *the experimental data obtained by studying it.*

Without such clarification, in theoretical physics there is a paradoxical situation: there are theories of various phenomena that describe some their properties but cannot explain the main features of these phenomena.

2. Some Theories Created in the Twentieth Century, Which Can Not Explain the Main Features of Studied Phenomena

Here is a short list of such theories:

2.1. Superfluidity

Superfluidity was discovered in the late 1930s (see **Figure 1**). The main features of the phenomenon of superfluidity in liquid helium became clear soon after its discovering [2].

Now there is a generally accepted well-developed theory that describes many features characteristic of the superfluid state. For example, it explains the temperature dependence of the concentration of the superfluid component, the temperature dependence of its heat capacity, the existence of different types of "sound" and calculates their velocities, as well as other features of the superfluid state.

However, the existing theory does not explain the main thing—why the transition of helium-4 to the superfluid state occurs at temperature

$$T_\lambda \approx 2.1768\,\mathrm{K}, \tag{2.1}$$

and the density of superfluid helium is $\gamma_4 \approx 0.145\,\mathrm{g/cm^3}$.

It will be shown below that these values are well described by formulas containing only world constants

Figure 1. P.L. Kapitsa (right) and L.D. Landau. P. Kapitsa discovered the phenomenon of superfluidity, and L. Landau gave the first theoretical explanation for this phenomenon.

$$T_\lambda = \frac{M_4 c^2 \alpha^6}{3k} \approx 2.1778\,\mathrm{K}. \tag{2.2}$$

(where M_4 is mass of He-4 atom, $\alpha = \frac{e^2}{\hbar c} \approx \frac{1}{137}$ is the fine structure constant)

$$\gamma_4 = \frac{\alpha^2}{a_B^3}\sqrt{\frac{M_4^3}{2m_e}} \approx 0.1443\,\mathrm{g/cm^3}. \tag{2.3}$$

(where $a_B = \frac{\hbar^2}{m_e e^2}$ is the Bohr radius, m_e is electron mass.)

Such formulas are absolutely not typical for the description of a condensed state of a system of many particles. They speak about the fundamental nature of this phenomenon. This is not clear from the point of view of the current generally accepted theory, which should therefore be revised.

2.2. Superconductivity

Superconductivity was discovered in the early 20th century (see Figure 2), but for a long time it was thought to be the most enigmatic phenomenon in condensed substances.

Its theory appeared a few decades later.

Now the generally accepted theory of superconductivity successfully explains, for example, the temperature dependences of heat capacity and energy gap in superconductors. But it cannot calculate main property of superconductors—the critical temperature of transition into a superconducting state. Therefore, this theory should be replaced by one that is able to explain all the main properties of specific superconductors.

2.3. Neutrino

The existence of the neutrino was predicted by W. Pauli in the early 30s of the last century (see Figure 3).

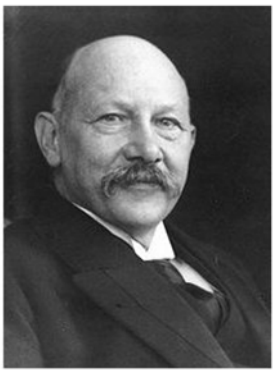

Figure 2. Heike Kamerlingh Onnes discovered the phenomenon of superconductivity in 1911.

Figure 3. Nobel laureate Wolfgang Pauli predicted the existence of neutrinos for theoretical reasons in 1932.

The effect of reactor neutrinos on the substance was found after about two decades (see **Figure 4**).

In neutrino physics, the triad—e-neutrino, μ-neutrino and τ-neutrino—and details of their mutual transformations are considered. But the main property of neutrino—its unusually high penetrating power—remains unexplained. This unusual property distinguishes neutrino from all other particles.

In addition, a special fundamental weak interaction of nature is introduced to explain neutrino-related reactions. The necessity of this introducing is justified by the special properties of the mysterious neutrino.

2.4. The Quark Theory

The quark model introduces new subparticles from which all other elementary particles must consist. At this a particular importance has the explanation of the mechanism of transformation of neutron into proton. An attractive invention is the scheme proposed by Gell-Mann (see **Figures 5-7**), in which this transformation is carried out by replacing only one quark with a fractional charge to another. However, no particle with fractional charge was experimentally discovered. That demanded to admit the existence of the specific confinement of quarks.

Figure 4. Fred Raines and Clyde Cohen, who discovered neutrinos, in the control center of their measurement equipment (1953).

Figure 5. Murray Gell-Mann.

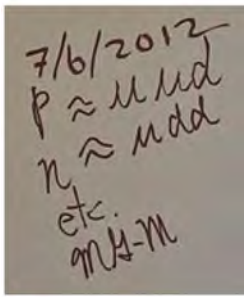

Figure 6. The main achievement of the quark theory—the structure of neutron and proton—recorded by Gell-Mann.

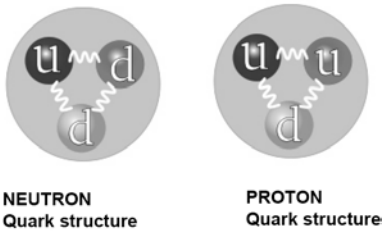

Figure 7. The quark structure of nucleons according to Gell-Mann.

This directly contradicts Gilbert's postulate: the quark model assumes that quarks with a fractional charge are real particles at their full undetectable.

It is also important that the quark model don't make possibility to calculate the basic parameters of neutron at comparing them with the properties of proton.

2.5. Nature of Nuclear Forces

The problem of nuclear forces related to the quark model required for its explanation the introduction of a new type of fundamental interactions—a strong interaction—and a new type of non-observable particles—gluons. It is assumed that they must bond the nucleons in nuclei. This approach makes it possible to obtain a fully developed picture of nuclear forces, but does not allow to solve the main problem—to calculate the binding energy of nuclei.

2.6. Astrophysics

Astrophysics in its modern state was formed by the middle of the twentieth century and is a completely unique branch of physics, because it does not rely on measurement data and ignores Gilbert's postulate.

However, the technological progress of astronomical measurements to the present time gave the ability to know about a dozen interdependence of the main parameters of the stars. These dependencies are radius-temperature-mass-luminosity of close binary stars, magnetic fields of stars, etc.

Naturally, it turned out that the existing theory of stars, built without reliance on any measurement data, cannot explain these dependencies and should be revised.

2.7. The Magnetic Field of Earth

Attempts to explain the mechanism of the Earth's magnetic field have been undertaken for several centuries. Apparently, the first model of the Earth's magnetic field was created by W. Gilbert more than 400 years ago [1].

Einstein included this problem as one of the three main tasks of the science of his time.

Currently a hydrodynamical model is accepted. Despite some difficulties, its parameters can be chosen so that the magnitude of the magnetic field near the poles of the Earth will be approximately equal to 1 Oe, which is consistent with the measurements.

However, in the second half of XX centuries space flights began and the technique of astronomical measurements obtains further developing. As a result, the magnetic fields of most objects of the Solar system and a number of stars, including pulsars, were measured. It turned out that the gyromagnetic relations of all these space objects are approximately equal to the ratio of the world constants $\frac{\sqrt{G}}{c}$ (**Figure 14**).

Because the problem of terrestrial magnetism has become a special case of a common problem for all celestial bodies. This required rejecting the hydrodynamical model to create a new general theory of cosmic bodies magnetism.

3. What Should Be Theories That They Explain All Main Features of Phenomena under Study

3.1. Superfluidity as a Consequence of the Ordering of Zero-Point Oscillations of Helium Atoms

3.1.1. Superfluidity as a Quantum Effect

L. D. Landau saw in superfluidity a quantum effect in a macroscopic manifestation. That created the basis for understanding the characteristic features of this phenomenon and further progress in its study [3].

The modern theory of superfluidity explains the general characteristics of this phenomenon: the energy spectrum of excitations, thermodynamics of superfluid helium, its heat capacity, etc.

3.1.2. λ-Transition

However, the energetically profitable transition of helium to a superfluid state should occur due to the appearance of some additional forces of attraction in the ensemble of its atoms lowering the ensemble energy.

Therefore, the most important task of the theory is to explain the mechanism of attraction that causes the transition to the superfluid state and the reason that this transition in helium-4 occurs at a temperature of about 2K.

According to Gilbert's refined principle, the theory should provide a quantitative explanation of all the characteristic parameters that are observed in this phenomenon.

Therefore, the refined theory of superfluidity should first explain the physics of the λ-transition and way this temperature is almost exactly half the boiling point of helium:

$$\frac{T_{\text{boiling}}}{T_{\lambda}} = \frac{4.215\ \text{K}}{2.177\ \text{K}} \approx 1.93. \tag{3.1}$$

3.1.3. London's Dispersion Forces

The feature of helium-4 is that the atom has no total charge or dipole moments.

Nevertheless, a certain electromagnetic mechanism should be responsible for phase transformations in its condensed state. This is evidenced by the scale of energy change in this transition, which corresponds to other electromagnetic transitions in condensed matter.

In the 30-ies of the last century F. London showed [4] (see **Figure 8**), that between the atoms He-4 in the ground state, there is an interaction of type of the van der Waals force, having a quantum nature.

At very low temperatures, all movements in liquid helium freeze. Only quantum zero-point oscillations remain. F. London considered these oscillations

Figure 8. Fritz London (1900-1954).

as three-dimensional vibrating dipoles connected with each other by electromagnetic interaction. He called this interrelation of atoms in the ground state as a dispersion interaction.

3.1.4. The Interaction of Zero-Point Oscillations of Helium Atoms

F. London showed that the electromagnetic interaction of zero-point oscillations of helium atoms leads to their attraction. Since there is no repulsion between particles of boson gas, the occurrence of attraction should lead to liquefaction of boson gas. However, F. London did not pay attention to the fact that there are two types of vibrations of the shells of symmetric atoms—the vibrations of neighboring atoms can be longitudinal or transverse with respect to the line connecting neighboring atoms. The interaction energy in these two modes turns out to be different [5]. The ordering of longitudinal oscillations leads to the liquefaction of helium. The ordering of transverse oscillations occurs at twice less temperature. It is remarkable that this temperature is described by the formula consisting of world constants only (Equation (2.2)). Below this temperature, the system of zero-point oscillations of atoms is completely ordered, *i.e.* atoms form a single quantum ensemble of the superfluid state.

Results of experimental measurements confirm the correctness of this theoretical evaluation with high accuracy Equation (2.1)).

The consideration of superfluidity as the ordering of zero-point oscillations allows to calculate all basic parameters of this phenomenon. (see **Table 1** [5])

3.2. Superconductivity as a Result of the Ordering of Zero-Point Oscillations of Electron Gas

The main difficulty of modern theory of superconductivity (BSC) is that it cannot explain why this phenomenon occurs in different metals at different temperature.

Superconductivity can be considered as superfluidity of electron gas. These phenomena are similar. Considering the superconductivity as a result of ordering of zero-point oscillations in electron gas, it is possible to show that the

Table 1. Comparison of the calculated values of liquid helium-4 [5] with the measurement data ([8] [9]).

parameter	defining formula	calculated value	measured value
the velocity of zero-point oscillations of helium atom	$\widehat{v}_0 = c\alpha^3$	116.5 m/s	
The density of atoms in liquid helium	$n = \sqrt{\frac{M_4}{2m_e}}\frac{\alpha^2}{a_B^3}$	2.172×10^{22} atom/cm^3	
The density of liquid helium-4 g/l	$\gamma = M_4 n$	144.3	$145_{T=T_\lambda}$
The dielectric constant of liquid helium-4	$\frac{\varepsilon-1}{\varepsilon+2} = \frac{4\pi}{3}\alpha^2\sqrt{\frac{M_4}{2m_e}}$	1.040	$1.048_{T=4.2}$ $1.057_{T=T_\lambda}$
The temperature λ-point, K	$T_\lambda \simeq \frac{M_4 c^2 \alpha^6}{3k}$	2.1778	2.1768
The boiling temperature of helium-4, K	$T_{boil} \simeq 2T_\lambda$	4.35	4.21
The first sound velocity, m/s	$c_{s1} = 2\widehat{v}_0$	233	$238.3_{T\to 0}$

ordering temperature of these oscillations is determined by the Fermi temperature of the metal [5]

$$T_c \approx 4\pi\alpha^3 \cdot T_F, \tag{3.2}$$

where α is the fine structure constant.

This is consistent with the measurement data (**Figure 9**, [5]).

As for the external magnetic field of the critical value, which destroys the coherence of zero-point oscillations of electronic pairs, the theoretical evaluation of this field is also in good agreement with the measurement data [5].

The consideration of superconductivity as sequens of the electron gas zero-point oscillations ordering gives possibility to explain all main properties of all separate superconductors.

3.3. Neutrino Is Magnetic Excitation of Aether

3.3.1. Magnetic Dipole Radiation in Maxwell's Theory

It is usually accepted to consider neutrino as a specific particle moving at the speed of light and having no charge and mass (the latter with some reservations). This speaks that there is much in common between neutrinos and photons, although their penetrating abilities in matter differ by many orders of magnitude. This fact forces to consider the problem of electromagnetic waves radiation in more detail.

Let, for simplicity, the problem is formulated in such a way that there are no electric charges, electric dipoles and quadrupoles. And the electromagnetic radiation in aether can arise only due to the time-varying magnetic moment $\boldsymbol{m}(t)$.

The changing moment $\boldsymbol{m}(t)$ will create in space at a distance R from it an electromagnetic disturbance described by vector potential [6]

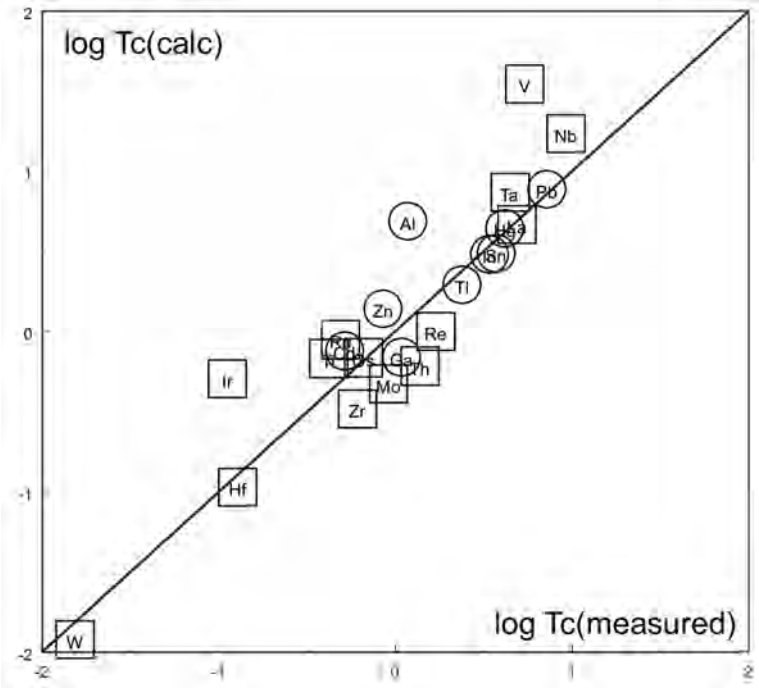

Figure 9. The comparison of the calculated values of critical temperatures of superconductors (calculated according to Equation (3.2)) with measurement data [5]. Circles relate to type-I superconductors, squares show type-II superconductors. On the abscissa, the measured values of critical temperatures are plotted, on ordinate, the calculated estimations are plotted.

$$\boldsymbol{A}(R,t)=\frac{\dot{\boldsymbol{m}}(t^*)\times\boldsymbol{n}}{cR}. \tag{3.3}$$

where t^* is retarded time.

By definition, in the absence of free charges (*i.e.* at $\varphi=0$) in this electromagnetic disturbance, the electric field strength will have the value [7]:

$$\boldsymbol{E}(R,t)=-\frac{1}{c}\frac{\mathrm{d}\boldsymbol{A}(R,t)}{\mathrm{d}t^*}=-\frac{1}{c^2R}\left[\ddot{\boldsymbol{m}}(t^*)\times\boldsymbol{n}\right], \tag{3.4}$$

and intensity of magnetic field [7]:

$$\boldsymbol{H}(R,t)=\boldsymbol{rotA}(R,t)=-\frac{1}{c^2R}\left[\boldsymbol{n}\times\left[\ddot{\boldsymbol{m}}(t^*)\times\boldsymbol{n}\right]\right]+\frac{1}{cR^2}\left[\boldsymbol{n}\times\left[\dot{\boldsymbol{m}}(t^*)\times\boldsymbol{n}\right]\right] \tag{3.5}$$

Thus, the amplitude of oscillations of the electric field generated by changes in the magnetic moment depends only on the second time derivative of the function describing its changes. At the same time, the first time derivative additionally contributes to the amplitude of the magnetic field oscillations.

In this case, two options are possible, since two types of magnetic emitters are possible.

3.3.2. Photons

This option is studied in all courses of electrodynamics. It is realized in the case when the magnetic dipole performs the motion described by the differentiable

function from time. That is, the motion of the magnetic dipole is described by such a function, in which there are at least two first derivatives in time. A typical example of such a motion is the harmonic oscillation of dipole $\boldsymbol{m}(t) = \boldsymbol{m} \cdot \sin \omega t$, in which both E and H exist, since $\dot{\boldsymbol{m}}(t) \neq 0$ and $\ddot{\boldsymbol{m}}(t) \neq 0$.

The same solution has problems where the oscillations of the magnetic moment are described by more complex formulas, if the spectrum of these oscillations can be decomposed into harmonic components.

For harmonic oscillations at a considerable distance from the oscillating dipole, the second term in the formula (3.5), which depends on $\dot{\boldsymbol{m}}$, is λ/R times smaller than the first term (here λ is the length of the generated wave).

Therefore, term $\dot{\boldsymbol{m}}$ can be neglected.

The result is that in this case fields E and H are equal to each other and only are turned relative to each other by 90 degrees.

3.3.3. Magnetic Excitation of Aether

Another solution of Equations (3.4) and (3.5) is obtained if $\boldsymbol{m}(t)$ is a discontinuous (spasmodic) function. For this function $\dot{\boldsymbol{m}} \neq 0$, but $\ddot{\boldsymbol{m}} = 0$, and therefore, the magnetic moment forms a purely magnetic wave, in which $H \neq 0$, but $E = 0$.

More precisely, this excitation of vacuum should be classified as a kind of particle, because it is characterized by a very short time interval.

An example of the radiation of such a particle is β-decay, in which a free electron carrying a large magnetic moment arises relativistically quickly.

Another example is the transformation of π-meson into μ-meson. π-meson has no magnetic moment, but μ-meson does.

The uncertainty relation makes it possible to estimate the transformation time of π-meson to μ-meson:

$$\tau_{\pi\to\mu} \approx \frac{\hbar}{\left(M_\pi - M_\mu\right)c^2} \approx 10^{-23}\,\text{sec} \tag{3.6}$$

Thus the time dependence of the magnetic moment in this reaction has the form of a very sharp Heaviside's rung, which equal to zero for negative arguments and one for positive ones. (At zero, this function requires additional definition. It is usually convenient to set it to zero equal to 1/2):

$$He(t) = \begin{cases} 0 & \text{if } t < 0 \\ 1/2 & \text{if } t = 0 \\ 1 & \text{if } t > 0 \end{cases} \tag{3.7}$$

An unusual property that pure magnetic photon $\dot{\boldsymbol{m}}$ must possess arises due to the absence of magnetic monopoles in nature. The fact that normal photons, with the electric component, scattered and absorbed in matter with electrons. In the absence of magnetic monopoles, a small energy magnetic photon must interact extremely weakly with the substance and its free path in the medium must be about two dozen orders of magnitude greater than that of a normal photon [7].

Thus, Maxwell's equations say that the radiation of free electron at β-decay should generate in vacuum a pure magnetic excitation, similar to photon, but weakly interacting with the substance.

3.3.4. Neutrino and Antineutrino

According to the electromagnetic model of the neutron, the generalized angular momentum of a relativistic electron, which forms a neutron together with a proton, is zero [10]. Therefore, the self magnetic moment of the electron is not observed.

With neutron β-decay, the electron acquires freedom, and with it spin and magnetic moment. Given that the emitted electron has a speed close to the speed of light, this process should occur abruptly.

At that a δ-shaped magnetic field burst generates, which is commonly called as antineutrino.

Since in the initial bound state (as part of the neutron) the electronic generalized angular momentum was equal to zero [10], and in the final free state its spin is $\hbar/2$, taking into account the law of conservation of angular momentum, the magnetic γ-quantum must carry with it the angular momentum equal to $-\hbar/2$.

Another implementation of the magnetic γ-quantum must occur in the reverse process—in K-capture. In this process, the electron, which originally formed the shell of the atom and had its own magnetic moment and spin, at some point is captured by proton of nucleus and forms neutron with it. This process can be described by the inverse of the Heaviside function. In this process, a magnetic γ-quantum of the inverse direction of field with respect to the vector of its propagation $\boldsymbol{R}$ should arise (**Figure 10**).

$$p^{+} + e^{-} \to n + \nu. \tag{3.8}$$

3.3.5. Results Shortly

The concept of neutrino as magnetic excitations of aether [11] explains all the basic of their properties:

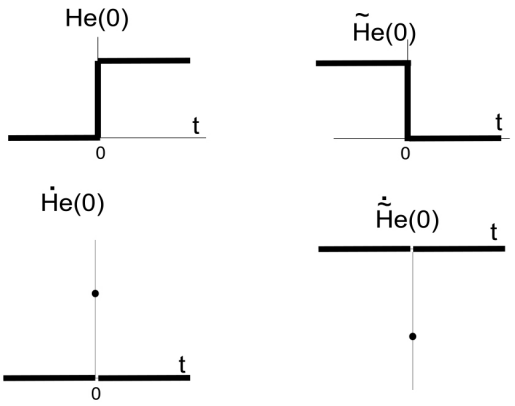

Figure 10. Two functions of Heaviside responsible for the birth of neutrinos and antineutrinos.

- extremely weak interaction with the substance is the result of the absence of magnetic monopoles in nature,
- spin neutrino is equal to $\hbar/2$ due to the fact that they have only the magnetic component,
- the birth of neutrino in beta-decay is due to the abrupt appearance of the magnetic moments of particles,
- the existence of neutrino and antineutrino is explained by the presence of two types of Heaviside steps.

In addition, this concept opens a new page in the study of mesons, with quantitatively predicting their masses.

What does tau-neutrino have to do with this concept remains unclear.

Due to the fact that neutrino radiation is a purely electromagnetic process, there is no need to introduce a fundamental weak (or electro-weak) interactions of Nature, which should be attributed to the category of speculation.

3.4. The Quark Model, Neutron Properties and Nature of Nuclear Forces

3.4.1. Proton and Neutron

In the second half of the twentieth century, scientists in the elementary particles theory began to develop the model of quarks. The formation of this theory in the chain of sciences about the structure of matter seems to be quite successive: all substances consist of molecules and atoms. The central elements of atoms are nuclei. The nuclei consist of protons and neutrons, which in turn consist of quarks.

The cornerstone of this model was the assumption that both—proton and neutron—are elementary particles and are composed of different sets of quarks (**Figure 7**).

This assumption allowed Gell-Mann quite simply to explain the transformation of neutron into proton. To do this, it only needs to replace one quark with a fractional charge to another.

It seems possible as neutron is an elementary particle.

However, the Gilbert's postulate speaks in favor of a different design of the neutron. The Gell-Mann model provides an explanation for the transformation of neutron into proton, but it cannot explain other properties of the neutron. On the contrary, the model in which neutron is a kind of hydrogen atom with relativistic electron, makes it possible to calculate all basic properties of neutron: its magnetic moment, mass, decay energy. Its transformation into proton is considered as process of simple ionisation.

3.4.2. Neutron Properties

It is commonly thought that the Bohr's atom is the only possible construction that can be constructed from proton and electron. This is true, if to use a non-relativistic electron. In this case, the equilibrium state between proton and electron is established by mutual attraction of their charges. At that the distance

between them is equal to the Bohr radius $a_B = \frac{\hbar^2}{m_e e^2} \approx 10^{-8}$ cm. The magnetic moment of proton is approximately equal to the Bohr magneton $\mu_p \approx \frac{e\hbar}{2M_p c} \approx 10^{-23}$ Gs·cm^3. Its influence on electron is very small and it can be neglected.

However, the situation changes radically at distances of the order of 10^{-13} cm. If an electron orbit has this value, magnetic field of order $\frac{\mu_p}{R^3} \approx \frac{10^{-23}}{\left(10^{-13}\right)^3} \approx 10^{16}$ Gs will act on electron. With a suitable orientation, such a huge field can keep electron in orbit even if it rotates at a speed close to the speed of light and electron mass will be hundreds of times greater than its rest mass.

Detailed calculations [10] show that the equilibrium radius of such orbit is approximately equal to 10^{-13} cm, and the mass of an electron taking into account the relativistic effect is equal approximately to $370m_e$.

However, almost all of this weighting of electron is compensated by the mass defect, which occurs due to the binding energy of electron to proton, so that the total mass of neutron only slightly exceeds the mass of proton. The result is the correct prediction for the neutron decay energy.

It is remarkable that the neutron magnetic moment can be calculated in this way, and the calculated value coincides with the measured one up to 10^{-4}.

Thus, all the measured properties of neutron (except its lifetime) in this theory find a quantitative explanation. The calculation of the neutron lifetime should be carried out taking into account additional factors.

The most important consequence of this consideration is the fact that neutron is not elementary particle but it is a kind of structure, like a hydrogen atom only with relativistic electron. It discredits the Gell-Mann's quark model completely.

3.5. Quantum-Mechanical Nature of Nuclear Forces

The rapid development of nuclear technology in twentieth century made the understanding of nature of nuclear forces a most important task of theoretical physics.

By 30s of last century, the experimenters found that the nuclei consist of protons and neutrons, and neutrons decay with the emission of electrons. For the first time attention to the possibility of explaining nuclear forces on the basis of the electron exchange effect drew apparently *I.E.* Tamm [12]. However, later the predominant model in nuclear physics was the exchange of π-mesons, and then the exchange of gluons.

The reason for this is clear. To explain the magnitude and radius of action of nuclear forces need a particle with a small natural wavelength. A nonrelativistic electron is not suitable for this.

Because of this, the assumption about the existence of a special strong interac-

tion—the fundamental interaction of Nature, which is carried out by quarks and gluons—has come into use.

However, on the other hand, models of π-meson or gluon exchange were not productive either. These models could not give a sufficiently accurate quantitative explanation of the binding energy of even light nuclei.

It turns out that this explanation can be obtained by solving the corresponding quantum mechanical problem. At the same time, to explain the nature of nuclear forces, the hypothesis of the existence of a strong interaction can be abandoned.

In 1927, a quantum mechanical description of the simplest molecule—the molecular ion of hydrogen—was published. The authors of this article V. Heitler and F. London [13] has calculated the attraction that occurs between two protons at electron exchange. This exchange is a quantum mechanical effect and does not exist in classical physics. (Some details of this calculation are given in [10] [14]).

The main conclusion of this calculation is that the binding energy between two protons, which occurs due to the electron exchange, is in order of magnitude close to the binding energy of proton and electron (the electron energy in the first Bohr orbit). This conclusion agrees satisfactorily with the measured data, which give results different from the estimated less than two times.

The calculation method developed by Heitler and London can be applied to the calculation of the binding energy of two protons that exchange with relativistic electron which is part of neutron. The energy obtained as a result of this calculation is quite satisfactory in agreement with the experimentally measured value of the deuteron coupling energy [10].

The extension of the results of this calculation to the light nuclei allows us to obtain the values of their binding energy consistent with the measurement data.

Thus, the results of this calculation show that in order to explain the nature of nuclear forces there is no need to invent some fundamental strong interaction of Nature. At least in the case of light nuclei, nuclear forces are explained by quantum-mechanic way.

3.6. Astrophysics

Star physics stands apart from other physical Sciences. Until the last decades of the twentieth century, almost nothing was with certainty known about the internal structure of stars. However, in the last decades of the twentieth century, astronomers have measured a number of dependencies of parameters of stars. To date, already there are about a dozen of such dependencies. That are interdependencies of the temperature-radius-luminosity-mass of close binary stars, spectra of seismic oscillations of the Sun, distribution of stars by mass, the magnetic fields of stars etc. All these dependencies are determined by phenomena occurring inside stars. Therefore, the construction of the theory of the internal structure of stars should be based on these quantitative data as on boundary conditions.

However, modern astrophysics prefers a more speculative approach: qualitative theories of stars are developed in detail, which are not brought to such quantitative estimates that could be compared with astronomic data.

Of course, the existence of dependencies of stellar parameters measured by astronomers is known to the astrophysical community. However, in modern astrophysics it is accepted, without finding an explanation, to refer them to the category of empirical and believe that they do not need an explanation at all.

To reach agreement of the theory with the available data of astronomical measurements, it is necessary to refuse some astrophysical constructions which are generally accepted today. First of all, we need to change the approach to describing the equilibrium of matter inside stars. It should be noted that the interior of the stars is plasma—electrically polarized medium. Therefore, the equilibrium equation of the interstellar substance should take into account the role of gravitationally induced electric polarization (GIEP). Taking into account the GIEP of intrastellar plasma allows us to construct a model of a star in which all the main parameters—the mass of a star, its temperature, radius and luminosity—are expressed by certain combinations of world constants, and the individuality of the stars is determined only by two parameters—mass and charge numbers of atomic nuclei from which plasma of these stars is constructed. Thus it is possible to explain quantitatively and with satisfactory accuracy all dependences measured by astronomers (**Figure 11**, **Figure 12**) [15].

Taking into account the gravitationally-induced polarization of the Sun's core, it is possible to calculate the spectrum of its seismic oscillations [15]. This spectrum is in good agreement with the measurement data obtained in recent decades (**Figure 13**).

Taking into account the gravitationally-induced polarization, it is possible to construct the theory of magnetic fields of stars, consistent with the observational data (**Figure 14**).

In general, taking into account the GIEP effect allows to get an explanation of all data of astronomical measurements.

An important characteristic feature of the model of a star, built taking into account the GIEP, is the absence of collapse at the final stage of development of stars, as well as the absence of "black holes" in nature, resulting from such collapse.

3.7. Thermomagnetic Effect in Metals

The theoretical explanation of the thermomagnetic effect (TME) in metals stands out among the theories discussed above, since there was no such theory in the twentieth century. Previously, there was an opinion that this effect does not exist.

By the middle of the XX century a number of thermomagnetic effects in semiconductors had been discovered, studied and theoretically explained.

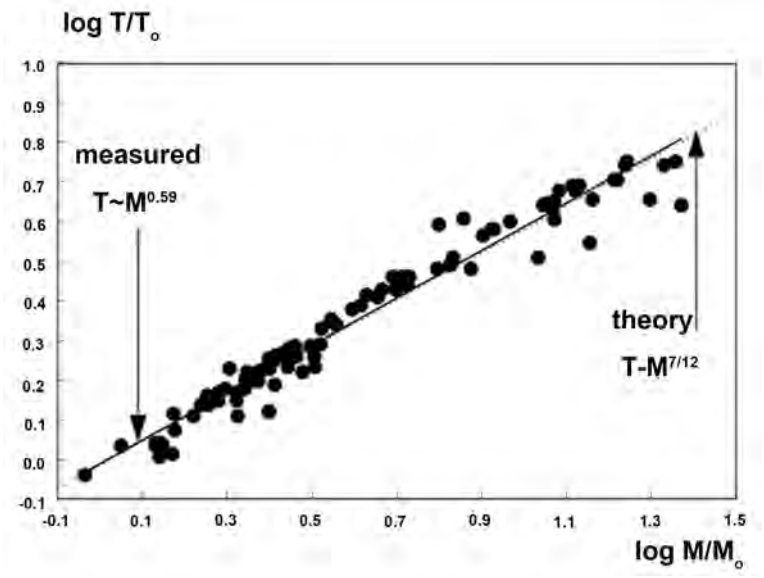

Figure 11. Comparison with measurements of the theoretical dependence of the surface temperature on the mass of the star. The theory takes into account the presence of electric polarization induced by gravity in the star plasma. Temperatures are normalized at the surface temperature of the Sun (5875 K), the mass—by the mass of the Sun.

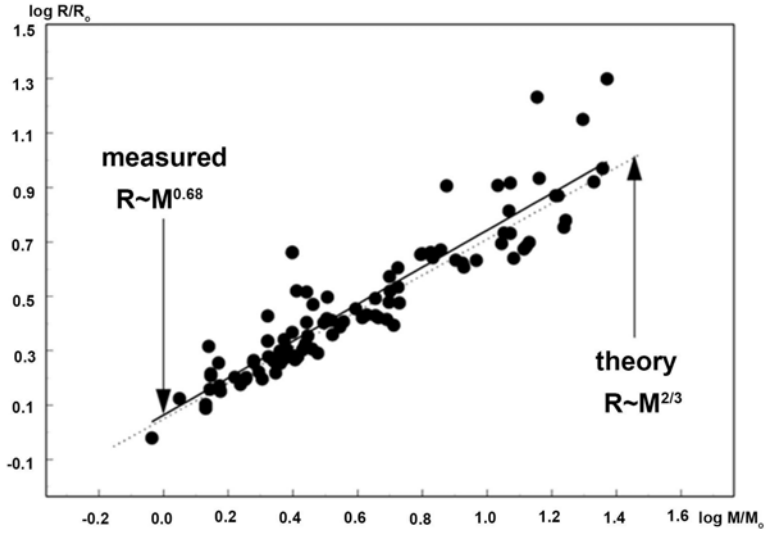

Figure 12. Comparison with measurements of the theoretical dependence of the radius of a star on its mass. The theoretical dependence is obtained taking into account the existence of electric polarization induced by gravity in the dense plasma of a star. The radius is expressed in units of the solar radius, mass—in units of the mass of the Sun.

It was believed that thermomagnetic effects do not occur in metals due to their high electrical conductivity. It was assumed that there is only a thermoelectric effect, at which electrons of conductivity from the hot region of a metal sample transfer energy (heat) to the cold region and heating it. Electrons of from cold region are forced into the hot part, reducing its temperature.

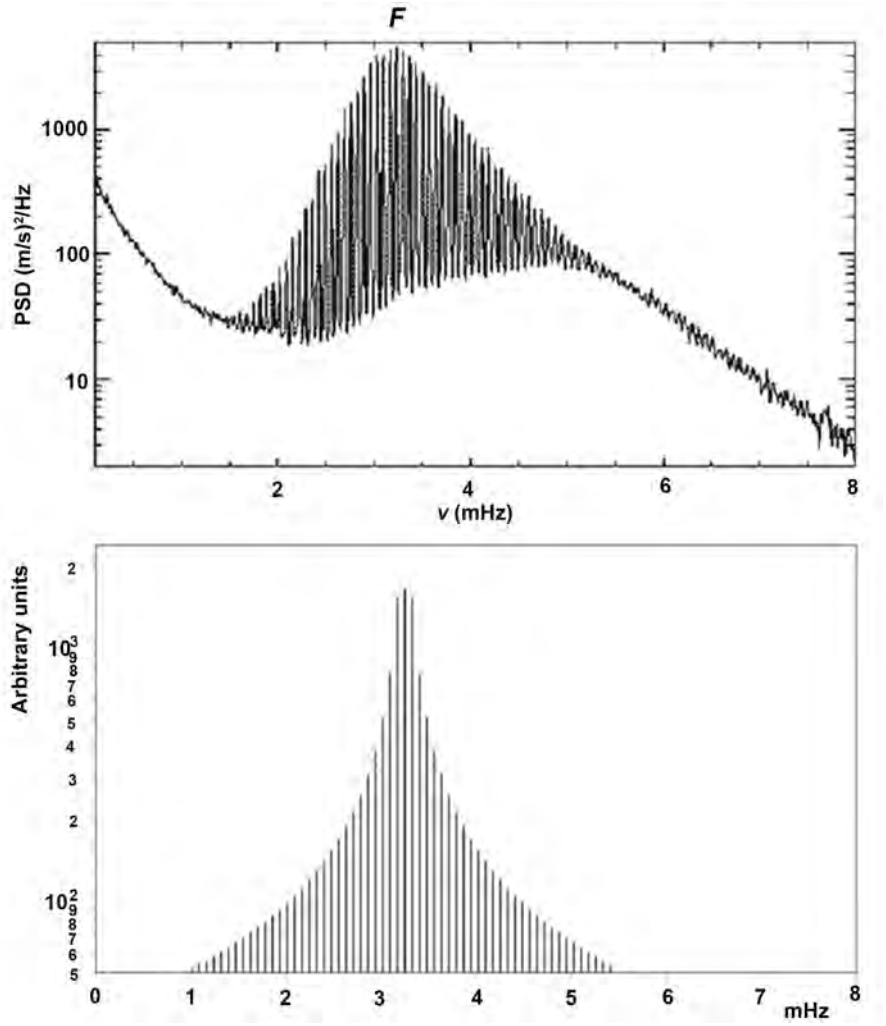

Figure 13. (a) Spectrum of solar oscillations. The data obtained in the framework of the program "SOHO/GOLF". (b) Theoretical spectrum calculated taking into account the existence of electric polarization induced by gravity in the solar plasma [15].

At the same time, the researchers who studied this phenomenon missed from attention the fact that counter electric currents due to the magnetic interaction must repel each other and flow along different trajectories in a metallic sample.

As a result of this separation of currents near the metallic sample there is a significant, quite easily measurable magnetic field (with the help of sensitive modern magnetometers), which depends on a number of parameters, such as the conductivity of the metal, its average temperature, the configuration of the temperature gradient in the metallic sample, etc.

The theoretical description of this effect makes it possible to explain all its characteristic features [17].

3.8. Nature of Magnetic Field of Earth

In the twentieth century, as before, it was believed that the most important experimental fact, which must satisfy the model of the Earth's magnetic field, is

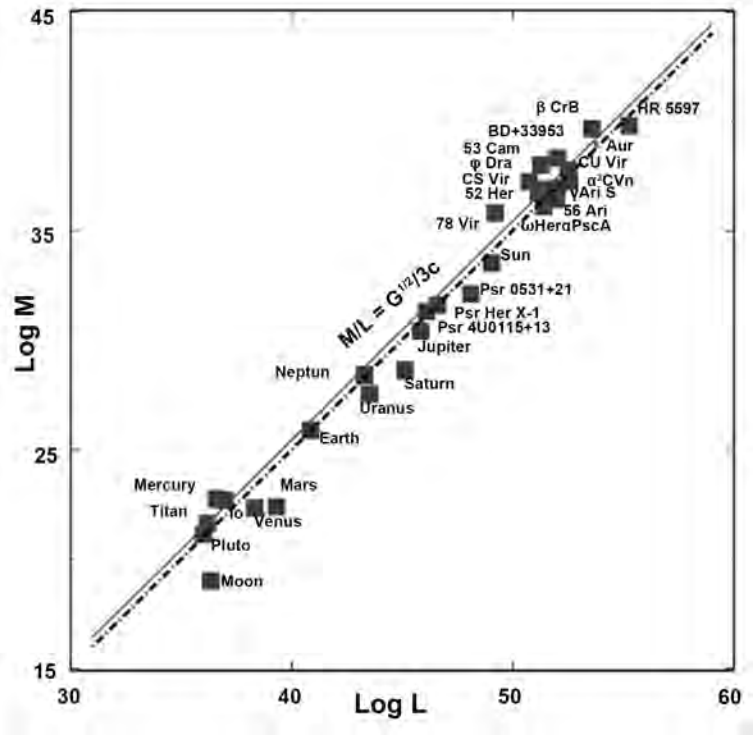

Figure 14. The measured values of the magnetic moments of celestial bodies depending on their torques [16]. By ordinate-logarithm of the magnetic moment (in Gs·cm^3), by abscissa is the logarithm of the moment of rotation (in egr·s). Line illustrates the dependence of Blackett.

the dipole character of the main field with the magnitude of the field intensity near poles of approximately equal to 1 Oe.

The first such model was proposed by W. Gilbert more than 400 years ago.

The Gilbert's model and others

W. Gilbert developed the first model of terrestrial magnetism [1] (see **Figure 15**). He assumed that inside the Earth there is an area filled with magnetized ferromagnetic (if to use the modern term). More recent studies have shown that the temperature in the central region of the Earth has high temperature—above the Curie temperature of ferromagnets. Therefore, the Earth's core can't be magnetized.

Later, many different models of the Earth's magnetic field were proposed. In particular, several models based on the thermoelectricity effect. In the 40s of the last century, the hydrodynamic model was developed [18], which won the recognition of experts.

It should be noted that the operation of such a mechanism requires the presence of a certain initial field, which can be strengthened. In the presence of only the space field (~10^{-7} Oe), the performance of this model is highly questionable.

Doubts about the performance of the hydrodynamic model in the following decades have arisen in many scientists, and for this reason, until recently, there are new models of this phenomenon.

Figure 15. Sir William Gilbert (1544-1603)—English physicist, who proposed the first model of terrestrial magnetism, introduced the concepts of electric and magnetic fields.

The Blackett's hypothesis

On another way to the problem of magnetic fields of cosmic bodies approached baron P. M. S. Blackett, Nobel laureate and President of the Royal society of London [19] (see Figure 16).

He suggested that the magnetic field is generated not only by a moving electric charge, but also by any moving neutral mass. Later began to assume that this may be a consequence of the fact that the electric charges of the electron and proton are not equal to each other. It was estimated that their difference can be very small—only 10^{-18}e. However, such a negligible difference was enough to at all cosmic bodies due to their rotation around its own axis there was a magnetic field of about the magnitude that was obtained from measurements.

Naturally, in this approach, there must be a connection between the magnetic moment of the cosmic body μ and its rotational moment L. Blackett showed that the ratio of these values (the gyromagnetic ratio) depends only on the world constants:

$$\vartheta = \frac{\mu}{L} = \frac{\sqrt{G}}{c}, \tag{3.9}$$

where G is the gravity constant, is the light velocity.

However, Blackett's hypothesis was rejected, despite its beauty and attractiveness. Blackett himself refused it. High-precision experiments conducted by Blackett, as well as other experimenters, showed that electrically neutral massive bodies do not create magnetic fields of the desired intensity in the laboratory condition.

The Measurement Data of Magnetic Fields of Cosmic Bodies

In the first half of the twentieth century many geophysicists (see Figure 17) was involved in the problem of terrestrial magnetism. Their task of the first plan saw

Figure 16. Nobel laureate baron Patrick Maynard Stuart Blackett (1897-1974).

Figure 17. My Father—Basil I. Volkov, scientist-geophysicist. He was looking for a solution to the problem of terrestrial magnetism, was killed by Stalin's torturers at 39.

the construction of such a theory, which would explain the reason why the main magnetic field of the Earth near its poles is approximately equal to 1 Oe.

In the second half of the twentieth century, this formulation of the problem becomes unacceptable, because by this time this geophysical problem has developed into a special case of a more general problem of magnetism of cosmic bodies.

Spacecraft flights in the second half of the twentieth century and the overall progress of astronomical technology have discovered a remarkable, previously unknown fact: magnetic moments of all cosmic bodies of the Solar system, as well as a number of stars and pulsars, are proportional to the moments of rotation of these cosmic bodies (Figure 14) as it should be according to Blackett's conjecture.

It is remarkable that this dependence preserves the linearity in the range of

about 20 orders of magnitude!

To explain this phenomenon is quite simple, given the phenomenon of the GIEP in the plasma of all large cosmic bodies [20].

However there is peculiarity at formation of terrestrial magnetism. Pressure and temperature inside the Earth are not as high as in stars. If stars are consist of electron-nuclear plasma, then in the central region of the Earth only electron-ion plasma can exist. That requires attentional consideration for a successful theoretical description of the Earth's magnetism [20].

4. Conclusions

The development of physics in the twentieth century led to the appearance of many new its branches. At first, many of these discoveries gave the impression of a certain mystery. So, many scientists have called superconductivity still several decades after its discovery as the most mysterious phenomenon in the physics of condensed matter. The penetrating power of neutrinos is still often called mysterious. To explain mysterious phenomena in the twentieth century, new concepts were often introduced. So, for example, strong and weak fundamental interactions, gluons, quarks with a fractional charge, etc. appeared. This method of constructing theories is valid only under one condition—it is necessary that the construction of the theory was carried out in full accordance with Gilbert's postulate.

It is obvious that without full confirmation of the measurement data, the theories constructed in this way turn out to be speculations.

In some cases, when this type of theory was presented with the help of a complex mathematical apparatus, it seemed that the conclusions following from these theories have found their mathematical confirmation and this is enough to recognize their correctness.

However, such mathematical confirmation and confirmation of the theory by means of some systematization and construction of tables should not replace experimental verification. At the same time, due to the large intricacy of some theories, it becomes important how successfully these theories explain ALL the properties of the object under study, or at least ALL MAIN its properties.

Conflicts of Interest

The author declares no conflicts of interest regarding the publication of this paper.

References

[1] Gilbert, W. (1600) De magneto magneticisque corporibus et de magno magnete tellure. Peter Short, London.

[2] Landau, L.D. (1941) *JETP*, **11**, 592.

[3] Khalatnikov, I.M. (1965) Introduction into Theory of Superfluidity. Nauka, Moscow.

[4] London, F. (1937) *Transactions of the Faraday Society*, **33**, 8.

https://doi.org/10.1039/tf937330008b

[5] Vasiliev, B.V. (2015) Superconductivity and Superfluidity Science PG (NY). http://www.sciencepublishinggroup.com/book/B-978-1-940366-36-4.aspx

[6] Landau, L.D. and Lifshitz, E.M. (1971) The Classical Theory of Fields (Volume 2 of A Course of Theoretical Physics). Pergamon Press, New York.

[7] Vasiliev, B.V. (2015) *International Journal of Modern Physics and Application*, **3**, 25-38. http://www.aascit.org/journal/archive2?journalId=909&paperId=3935

[8] Kikoine, I.K. (1978) Physical Tables. Atomizdat, Moscow. (In Russian)

[9] Donnelly, R.J. and Barenghy, C.F. (1977) *Journal of Physical and Chemical Data*, **6**, 51-104. https://doi.org/10.1063/1.555549

[10] Vasiliev, B.V. (2015) *Journal of Modern Physics*, **6**, 648-659. http://www.scirp.org/Journal/PaperInformation.aspx?PaperID=55921 https://doi.org/10.4236/jmp.2015.65071

[11] Vasiliev, B.V. (2017) *Journal of Modern Physics*, **8**, 338-348. http://www.scirp.org/Journal/PaperInformation.aspx?PaperID=74443 https://doi.org/10.4236/jmp.2017.83023

[12] Tamm, I.E. (1934) *Nature*, **134**, 1011.

[13] Heitler, W. and London, F. (1927) *Zeitschrift fur Physik*, **44**, 455-472. https://doi.org/10.1007/BF01397394

[14] Vasiliev, B.V. (2015) *International Journal of Modern Physics*, **3**, 25-38. http://www.aascit.org/journal/archive2?journalId=909&paperId=3935

[15] Vasiliev, B.V. (2018) *Journal of Modern Physics*, **9**, 257-262. http://www.scirp.org/Journal/PaperInformation.aspx?PaperID=87076

[16] Sirag, S.-P. (1979) *Nature*, **275**, 535. https://doi.org/10.1038/278535a0

[17] Vasiliev, B.V. (2014) *Journal of Physics and Application*, **8**, 221-225.

[18] Campbell, W.H. (2001) Earth Magnetism. Academic Press, New York.

[19] Blackett, P.M.S. (1947) *Nature*, **159**, 658. https://doi.org/10.1038/159658a0

[20] Vasiliev, B.V. (2015) *International Journal of Geosciences*, **6**, 1233-1247. http://www.scirp.org/journal/PaperInformation.aspx?PaperID=61451

Journal of Modern Physics, 2018, 9, 2125-2134
http://www.scirp.org/journal/jmp
ISSN Online: 2153-120X
ISSN Print: 2153-1196

Neutrinos from CERN, Reaching Too Early to Gran Sasso, Do Not Exceed the Velocity of Light. They in Fact Reveal the True Physical Mechanism of Gravity

Jacob Schaf

Universidade Federal do Rio Grande do Sul (UFRGS), Instituto de Fsica, Porto Alegre, Brazil
Email: schaf@if.ufrgs.br

How to cite this paper: Schaf, J. (2018) Neutrinos from CERN, Reaching Too Early to Gran Sasso, Do Not Exceed the Velocity of Light. They in Fact Reveal the True Physical Mechanism of Gravity. *Journal of Modern Physics*, **9**, 2125-2134.
https://doi.org/10.4236/jmp.2018.912133

Received: September 12, 2018
Accepted: October 8, 2018
Published: October 11, 2018

Copyright © 2018 by author and Scientific Research Publishing Inc.
This work is licensed under the Creative Commons Attribution International License (CC BY 4.0).
http://creativecommons.org/licenses/by/4.0/

Open Access

Abstract

In 2011 neutrinos from CERN in Geneva-CH were announced to reach to the OPERA Lab in Gran Sasso-IT 60 ns earlier than light. In reality, the velocity of the neutrinos was compared, not with the measured one-way velocity of light, however with the *presumed* velocity of light *c*. As this conclusion breaks the light postulate, the data were withdrawn. In fact, to compare the neutrino velocity with the presumed velocity of light violates a fundamental precept of scientific methodologies. Such a comparison could make a sense only if the velocity of both neutrinos and light had been measured along the same path in vacuum. Actually the absence of the solar gravitational slowing of the GPS clocks, absence of light anisotropy with respect to earth etc. demonstrates that the Higgs Quantum Fluid Space (HQFS), giving mass to the elementary particles and thus ruling their inertial motion, is moving round the sun according to a Keplerian velocity field, consistently with the planetary motions. It is also moving round earth consistently with the orbital motion of the Moon. The Keplerian velocity fields are the quintessence of the gravitational fields. In the earth's field, the velocity of the HQFS achieves 7.91 km/sec on surface and drags both the neutrinos and light toward the East. In the South-East direction, from CERN to OPERA Lab, making ~58 degrees with the Meridians, this drag adds 6.7 km/sec to the conventional light velocity *c*, making neutrinos from CERN (and light) to reach the OPERA Lab ~60 ns earlier than *presumed* by the current theories.

Keywords

Fundamental Physics, Theory of Relativity, Relativistic Effects, Relativistic Experiments, Gravitational Physics, Higgs Theory, Neutrino Physics

1. Introduction

From the view of the Special Theory of Relativity (STR) [1] [2], empty space contains nothing that can be a reference for rest and for motions, nor contains a medium of propagation for light. Also time intervals and distances depend on the relative velocity in the observer's reference. Within this scenario, the velocity of light, *measured in free space* (*vacuum*) *by light go-return round-trips between two mirrors and a clock*, is an invariant and a universal constant c. Moreover, according to the STR, the rate of the time evolution t of all physical processes (clocks) depends of the relative velocity v according to:

$$t = t_0\left(1 - v^2/c^2\right)^{-1/2}. \tag{1}$$

where t_0 is the time interval in a proper reference. Although the basic postulates of the STR are well confirmed by experimental observations, many paradoxes remain unsolved or badly resolved.

According to general relativity (GR) [1] [2], the rate of evolution of the coordinate time, within a gravitational field, is seen as an effective velocity c' along the time axis. It is given by $c'(r) = c\left(1 - 2U/c^2\right)^{1/2}$, where $2U = 2GM/r$ is the square of the local escape velocity from the gravitational field. The oscillation period $T(r)$ of the time standard, by which a clock counts time intervals, is given by $T(r) = T_0\left(1 - 2U/c^2\right)^{-1/2}$, where T_0 is the period of the time standard in the absence of gravity. Clocks count time in terms of the frequency of the time standard. Therefore, measuring the velocity of light by the method of light go-return round-trips between two mirrors and a clock, within a gravitational field, gives the same value as in free-space, independently from $U(r)$. It simply is the ratio of the frequencies of the light roundtrips and of the clock's time standard. In particular, from the view of an external observer, the velocity of a light pulse, along the radial coordinate, decreases toward the gravitational center.

In GR, the gravitational acceleration is due to spacetime curvature. This curvature is characterized by the invariant length of the line element ds that for weak fields, has the approximate form:

$$\mathrm{d}s^2 \approx \left[1 - \frac{2U}{c^2}\right]^{-1} \mathrm{d}r_0^2 + r^2\mathrm{d}w^2 - c^2\left[1 - \frac{2U}{c^2}\right]\mathrm{d}t_0^2 \tag{2}$$

in which the negative sign before the last term accounts for the orthogonality of the time axis with respect to ordinary space coordinate axes. The coefficients $\left(1 - \frac{2U}{c^2}\right)^{-1}$ and $-c^2\left(1 - 2U/c^2\right)$ are respectively the diagonal g_{11} and g_{44} components of the Schwarzschild metric tensor.

The first indication of shortcomings of GR became evident from the absence of the gravitational slowing of the solar field on the GPS clocks, moving with earth round the sun. GR associates the gravitational time dilation with the escape velocity that is fixed at each point of space. Hence, the gravitational time dilation by the solar field should not be affected by the orbital velocity of the

GPS clocks with earth round the sun. Current theories explain this absence in terms of the principle of equivalence [3]. Accordingly, the orbiting earth is free-falling in the solar field. It is asserted that the orbital velocity of earth cancels locally the effects of the solar gravitational field. It cancels locally the gravitational slowing, the local spacetime curvature, the gravitational pull, and all the other effects of the solar gravitational field on matter, on light and on clocks. Strangely however, motion of the GPS clocks within the GPS satellites round earth in exactly the same conditions does not cancel the gravitational slowing by the earth's field.

Another much more serious trouble, which however also is much more difficult to realize, is that the model of the free-falling inertial references of GR cannot give rise to the observed gravitational pull. It cannot because the free-fall velocity of the inertial references at each fixed point r_0 does not change with time ($\mathrm{d}v/\mathrm{d}t\big|r_0 = 0$). In order to turn this model able to create the observed gravitational pull, it would be necessary that locally $\mathrm{d}v/\mathrm{d}t\big|r_0 = g(r_0)$. This however would rapidly increase the free-fall velocity beyond the velocity of light.

In order to create a central field of centrifugal effects (gravitational pull) toward the gravitational center, it is necessary that the local inertial references (IRs) be not free-falling, however be rotating, in the ordinary space, *round an over-head axis*. Rotating references are well-known to be non-inertial references. However, if it is *the physical space, ruling the inertial motion of matter-energy* that is itself so rotating, things are quite different. Such *rotating inertial references* can be created if this physical space circulates like a fluid round earth according to a circular velocity field, in which *the velocity increases toward the gravitational center*. In such a velocity field, a body, stationary in the ordinary space, will locally be *implicitly* moving along an opposite circular path round the same over-head axis as the local rotating IRs. This motion is implicit because it cannot be described in ordinary space. This body will be stationary within a *non-IR*, implicitly rotating within the local true IR. The Higgs theory introduces exactly such a physical space.

The Higgs theory [4] [5] introduces profound changes in the current view about the nature of empty space. According to this theory, a quantum fluid medium, stabilized by a huge energy gap exists, which, according to the Glashow-Weinberg-Salam electroweak model achieves 200 GeV. This quantum fluid medium fills up the whole of space and is described by a complex order parameter. It gives inertial mass to the elementary particles by the Higgs mechanism, providing them with mechanical properties. This Higgs Quantum Fluid Space (HQFS) is much more than simply a reference for rest and for motions. It literally governs the inertial motion of matter-energy and is the local *ultimate reference* for rest and for motion.

The Higgs mechanism is closely analogous to the Meissner effect [6] in superconductivity that gives inertial mass to the electromagnetic field quanta (photons) within superconductors [7]. The HQFS materializes the local Lorentz

frames (LFs) turning them into local proper LFs, *intrinsically stationary with respect to the local HQFS* [8] [9]. LFs moving with respect to the local HQFS are not proper LFs. Velocity with respect to the local HQFS and *not relative velocity*, is the origin of all the effects of motion. Within this context, the one-way velocity of light c is fixed with respect to the local HQFS and not with respect to all possible inertial references. The velocity of light c in free (empty) space is the maximum velocity at which the HQFS can propagate the phase perturbations in its order parameter.

The superconducting condensate (SCC) can be put in motion by an electromotive forces (or of a varying vector potential). In the presence of a magnetic field, it develops a velocity field of the SCC, screening, confining and quantizing it, or expelling it out from the superconductor by the Meissner effect, thereby reducing its own energy. Analogously, the Higgs condensate or HQFS in the presence of weak and strong nuclear fields develops a screening velocity field, confining and quantizing them by the Higgs mechanism. This screening velocity field of the HQFS, thrusts the matter fields toward large matter agglomerates, where the Higgs order parameter is weakened, thereby too reducing its energy. The HQFS governs the inertial motion of matter-energy and is the ultimate reference for rest and for motion. Therefore, a uniform velocity field of the HQFS drags the matter waves of particles and of light. However, a non-uniform velocity field drags and *refracts the matter waves*, thereby creating inertial dynamics, which, according to Einstein's principle of equivalence, is gravitational dynamics.

Within the context of the HQFS dynamics, the effects of the gravitational fields must be explained in terms of a non-uniform velocity field of the HQFS, instead of spacetime curvature. This means that Einstein's spacetime curvature, created by astronomical bodies and the model of the free-falling IRs must be replaced by a velocity field of the HQFS, in which the local IRs are rotating round a fixed overhead axes. Actually a large number of experimental observations systematically and definitely show that the HQFS is moving round the astronomical bodies according to a Keplerian velocity field, consistent with the local orbital motions. In terms of spherical coordinates (r,θ,ϕ) this Keplerian velocity field of the HQFS has the very simple form:

$$\boldsymbol{V}(r)=(GM/r)^{1/2}\boldsymbol{e}_{\phi} \tag{3}$$

where G is the gravitational constant, and M is the mass of the gravitational source. In this Keplerian velocity field the magnitude of the velocity of the local HQFS is spherically symmetric.

The Keplerian velocity field round the sun is consistent with the planetary orbital motions and round earth it is consistent with the orbital motion of the Moon. *The Keplerian velocity field of the HQFS is the quintessence of the gravitational fields*. It naturally and accurately gives rise to the gravitational pull, the gravitational acceleration and the orbital motions within the gravitational fields. Keplerian velocity fields of the HQFS perfectly and accurately create all the observed effects of the gravitational fields on matter, on light and on clocks. Refer-

ences [8] [9] give the full details. Most importantly, the Keplerian velocity field of the HQFS Equation (3) is the only possible physical mechanism, able to implement the ingenious *outside-inside and inside-outside centrifuge mechanism*, and create the central field of *centrifugal accelerations toward the gravitational center*. No other imaginable physical mechanism is able to create this intriguing inertial dynamics. It also naturally and appropriately creates all the observed effects of the gravitational fields on light and on clocks.

In the solar Keplerian velocity field, earth and the GPS clocks, moving with it, are stationary with respect to the local moving HQFS and with respect to the local proper LFs, which predicts the absence of the gravitational slowing of the GPS clocks by the solar field, exactly as observed [8] [9]. It also straightforwardly predicts the absence of light anisotropy with respect to the orbiting planet earth, exactly as shown by a large number of light anisotropy experiments. The velocity of light is isotropic with respect to earth, not because of the intrinsic isotropy of light, however because earth is stationary with respect to the local HQFS that is the medium propagating light. The Keplerian velocity field of the HQFS round the sun predicts correctly the excess time delay of radar signals in go-return round-trips from earth to Venus and back to earth within the solar system (Shapiro effect) [10]. It predicts very precisely the observed light lensing effect by the solar field. It predicts the non-synchronous arrival of the Pulsar signals to equidistant earth-based antennas along the orbital motion of earth, however the synchronous arrival to antennas along transverse directions to the earth's orbital motion etc. Ref. [8] gives the full details.

In its turn, the earth's Keplerian velocity field of the HQFS precisely predicts the observed first order anisotropy effect of 8 km/sec of the electromagnetic signals between the twin satellites of the GRACE project in the same polar orbit round earth. This anisotropy is due essentially to the orbital velocity of these satellites. Clocks moving round earth along direct, circular equatorial orbits, analogously as in the motion round the sun, are predicted to be not slowed by the earth's gravitational field, an experiment that to now has not been realized. The earth's field also predicts the very small light anisotropy, with respect to the earth-based laboratories, that is due only to the local earth's Keplerian velocity field, a very small (10^{-10}) second order effect, observed by only a few of the most sensitive *Michelson light anisotropy experiments*. It also predicts correctly the gravitational time dilation, observed by the atomic clocks stationary in the earth's gravitational field, which also is predicted by general relativity. It predicts precisely the gravitational slowing of the GPS clocks, moving round earth along non-equatorial orbits, by the earth's field. It predicts the spectral red-shifts, measured by Mössbauer experiments in earth-based laboratories. Detailed description of all these observed effects can be seen in Ref. [8]. Here, it is shown that this HQFS dynamics gravitational mechanism too predicts very precisely the *too early arrival* of the neutrinos from CERN-CH to Gran Sasso-IT by closely 55 ns, which is a first order effect, due to the earth's Keplerian velocity field. This observation does not show that neutrinos exceed the velocity of light, but

simply shows that the one-way velocity of neutrinos and of light is anisotropic, due to the drag by the earth's field. The HQFS is the medium propagating light and neutrinos. Therefore, its motion according to Equation (3) drags and causes anisotropy on the velocity of light and of neutrinos.

2. Precise Time of Flight of Neutrinos from CERN-CH to OPERA Lab IT

Recently the one-way time of flight of neutrinos, from CERN in Geneva-CH to the OPERA laboratory at the Gran Sasso Mountains-IT, distant 732 km South-East and direction making ~58˚ with the Meridians, have precisely been measured. These very precise measurements are possible thanks to help by the tightly synchronized atomic clocks of the GPS clocks. The CERN and Gran Sasso laboratories can precisely be localized and their local atomic clocks can be tightly synchronized. In 2011 the neutrinos were announced to speed faster light, reaching the OPERA Lab 60 ns earlier than expected for light [11]. Later the data were put in doubt because these data run into conflict with the light postulate [12]. It was informed that, because of this conflict the distance between CERN and the OPERA Lab was monitored by a common view technique with the help of a GPS satellite. From the present viewpoint this method can be very precise along North-South directions. However, along West-East directions, it incorporates the effect of the Keplerian velocity field of the earth's field that can introduce deviations of tens of meters in the localizations on the earth's surface. The effect of this velocity field is decreasing the apparent distance from CERN to OPERA by about 19 m. Due to the rotation of earth, during the neutrino flight of 2.44 milliseconds, the Gran Sasso Lab displaces it by nearly one mater toward East. Hence, the true displacement of the common view method is 18 m. Calculating the time of flight for light, by using this decreased distance, leads to the conclusion that light and neutrinos complete the flight in the same 2.44 milliseconds.

Within the scenario of the HQFS gravitational mechanism, the Keplerian velocity field drags both neutrinos and light, reducing their time of flight with respect to the presumed time of flight of light c by 55 ns (please see calculations in the coming Section hereafter). From this viewpoint the too early arrival of the neutrinos does not exceed the velocity of light and does not break the light postulate. In reality this observation simply shows that the one-way velocity of the neutrinos and of light is anisotropic along the path from CERN to the OPERA lab. If neutrinos and light could be sent the opposite sense, from Gran Sasso do Geneva, both would reach to CERN *too late* by nearly the same 55 ns. Adding up the effects for complete cycles of go-return round-trips, would give for both neutrinos and light very closely an average value of c. In this case, the second order effect, of only a fraction of a picosecond, would fall within the experimental error. This second order effect however is sufficient to cause a gravitational slowing of the atomic clocks on ground by (6.16×10^{-10} sec/sec).

3. The Physical Mechanism Responsible for the Apparently Faster than Light Motion of Neutrinos

In the solar Keplerian velocity field the orbiting earth is stationary with respect to the local moving HQFS (proper LFs) and the solar system is stationary in the velocity field of the Milky-Way galaxy etc. This is why the GPS clocks, moving with earth round the sun, do not show the gravitational slowing by the solar field and also is why the velocity of light is isotropic with respect to earth. This orbital velocity effectively cancels locally all the effects of the solar field. The HQFS too moves round earth according to a Keplerian velocity field, consistently with the orbital motion of the Moon. On the earth surface, the velocity of the HQFS reaches 7.91 km/sec from West to East. As earth rotates only very slowly, the earth-based laboratories are not stationary with respect to the local HQFS. The HQFS is flowing through the earth-based laboratories from West to East at nearly this velocity.

The fixed velocity of the neutrinos as well as of light *with respect to the local moving HQFS* is closely 3×10^5 km/sec. The South-East path of the neutrinos from Geneva to Gran Sasso makes ~58 degrees with the Meridians. The path is along a straight line from CERN to Gran Sasso, passing deeply, up to 12 km, under-ground. There is no problem, because the neutrinos practically do not interact with ordinary matter. Along this path the average velocity of the HQFS through the neutrino path is estimated to be about 7.92 km/sec. The velocity component of the HQFS along the neutrino path is:

$$7.92 \times \sin 58^\circ = 6.716541 \text{ km/sec}. \tag{4}$$

This is the velocity that the neutrinos get because of drag by the moving HQFS in the Keplerian velocity field, creating the earth's gravitational field, an effect analogous to the drag of flowing water on the water waves. Note that this velocity is exactly the excess velocity of the neutrinos as estimated by the CERN neutrino team. This velocity adds up to the fixed speed ($c = 3 \times 10^5$ km/sec) of the neutrinos with respect to the local HQFS, giving:

$$300000 + 6.716541 = 300006.716541 \text{ km/sec} \tag{5}$$

The time spent by the neutrinos in the travel from CERN to the OPERA Lab at Gran Sasso is:

$$732/300006.716541 = 0.00243994537 \text{ sec} \tag{6}$$

According to the current theories, light would spend more time:

$$732/\left(3 \times 10^5\right) = 0.002440 \text{ sec} \tag{7}$$

The difference between Equation (7) and (6) is:

$$0.00244 - 0.00243994537 = 54.63 \text{ ns}. \tag{8}$$

The Gran Sasso Lab moves about 1.112 m toward East during the 2.44 ms of the neutrino flight, due to the rotation of earth of 330 m/sec at the latitude of the experiment, which makes ~280 m/sec along the neutrino path. In 2.44 ms this

corresponds to the total of ~0.6 m. The additional travel time of the neutrinos takes ~2 ns. Therefore, the neutrinos are predicted to reach about ~53 ns too early to the actual position of the OPERA laboratory at Gran Sasso.

No doubt that, if the too early arrival of the neutrinos from CERN to the OPERA Lab is confirmed, *it will be one of the most significant discoveries about the nature of the gravitational fields and of their effects on light and on clocks*. It will provide direct and unquestionable evidence that the Keplerian velocity field of the HQFS, creating the gravitational fields, effectively exists. In reality the too early arrival of the neutrinos to the Gran Sasso laboratory is not due to a faster than light velocity. It is an obvious effect, due to drag by the moving HQFS, creating the earth's gravitational field. This observation is not at all an isolated predicted observation. Practically all of the observed effects, listed at the end of the Introduction, are directly created by the Keplerian velocity field of the sun or of earth.

The wrong step by the leaders of the neutrino experiment was imputing the too early arrival of the neutrinos to faster than light velocity *c*, without giving any reasonable justification. The velocity of light *c* is the maximum velocity at which any measurable effect can be transmitted by the HQFS. It is one of the most extensively verified and well established observational facts. The hypothesis of the faster than light neutrinos has set off very strong criticisms by the scientific community. In the context of the HQFS dynamics gravitational mechanism, the fixed velocity of light *c* too is the maximum velocity at which the HQFS can propagate perturbations of its order parameter. However, this velocity is fixed with respect to the local HQFS and not with respect to every possible observer as stipulated by the theory of relativity. If the HQFS moves through the laboratory, at a velocity $\boldsymbol{V}$, this velocity adds up to the velocity $\boldsymbol{c}$ at which it propagates light.

In the scenario of the HQFS dynamics, the apparent faster than light neutrinos with respect to the earth-based laboratories, like CERN and OPERA, which are nearly stationary in the ordinary space within the earth's gravitational field, is a fundamental prediction. It unquestionably and perfectly corroborates the HQFS dynamics gravitational mechanism and, if confirmed, will constitute one of the most significant experimental achievements from all times.

Within the Keplerian velocity field of the HQFS, creating the gravitational fields, the effect of this HQFS velocity field on the effective velocity of light $\left(\boldsymbol{c}'=\boldsymbol{c}+\boldsymbol{V}\right)$ and of neutrinos, depending on the direction of the path with respect to the direction of the local Keplerian velocity field of the HQFS, the *effective* one-way velocity, can be smaller or larger than *c*. On earth the one-way velocity of light or of neutrinos (c') along North-South or South-North directions is predicted to be smaller than *c*: $c'_{N,S}=\left(c^2-V^2\right)^{1/2}$ where V is given by Equation (3). However, for Eastward or Westward neutrinos or light, the one-way velocity is $c'=\left(c\pm V\right)$ respectively.

In the mega neutrino experiment, being developed in the USA, neutrinos will

be sent underground from Fermilab (Chicago) to Stanford (South Dakota), distant ~1300 km *toward the West*. In this case, the neutrinos are predicted by HQFS dynamics gravitation to reach Stanford more than 115 ns *too late*. Again the neutrinos do not move slower than light *c*. Light along the same path in vacuum too would reach 115 ns too late to Stanford. The reason of this simply is the anisotropy, due to the opposite drag by the earth's Keplerian velocity field of the HQFS. Neutrino anisotropy measurements could turn into an excellent and powerful technique to map up the HQFS velocity field, inside and outside earth. However, at the Polar Regions this map up would be especially interesting and important.

4. Conclusion

The apparent faster than light neutrinos from CERN to OPERA Lab does not break the light postulate. It in fact reveals anisotropic velocity of neutrinos and of light, caused by the Keplerian velocity field of the HQFS, creating the earth's gravitational field. The apparent faster than light neutrinos, precisely and unquestionably, corroborates a fundamental prediction of the HQFS dynamics gravitational mechanism. It directly and fully ratifies the implications of the large number of observations, listed at the end of the Introduction, which all thoroughly back the HQFS dynamics gravitational mechanism. This affair is about to turn into an immense scientific discovery, the discovery of the Higgs quantum space dynamics that creates and governs our universe.

Conflicts of Interest

The authors declare no conflicts of interest regarding the publication of this paper.

References

[1] Laue, M.V. (1955) *Annalen der Physik*, **38**, 777.

[2] Lorentz, H.A., Einstein, A., Minkowski, H. and Weyl, H. (1923) The Principle of Relativity. Dover Publications, New York.

[3] Ashby, N. (1996) *Mercury*, **25**, 23-27.

[4] Higgs, P.W. (1964) *Physical Review Letters*, **13**, 508. https://doi.org/10.1103/PhysRevLett.13.508

[5] Englert, F. and Brout, R. (1964) *Physical Review Letters*, **13**, 321. https://doi.org/10.1103/PhysRevLett.13.321

[6] Meissner, W. and Ochsenfeld, R. (1933) *Naturwissenschaften*, **21**, 787-788. https://doi.org/10.1007/BF01504252

[7] Anderson, P.W. (1963) P*hysical Review*, **130**, 439. https://doi.org/10.1103/PhysRev.130.439

[8] Schaf, J. (2018) *Journal of Modern Physics*, **9**, 1111-1143. https://doi.org/10.4236/jmp.2018.95068

[9] Schaf, J. (2018) *Journal of Modern Physics*, **9**, 395-418. https://doi.org/10.4236/jmp.2018.93028

[10] Shapiro, I.I., *et al.* (1971) *Physical Review Letters*, **26**, 1132. https://doi.org/10.1103/PhysRevLett.26.1132

[11] Autiero, D., *et al.* (2011) Measurement of the Neutrino Velocity with the OPERA Detector in the CNGS Beam. arXiv:1109.4897v2 [hep-ex]

[12] Adam, T., *et al.* (2012) Measurement of the Neutrino Velocity with the OPERA Detector in the CNGS Beam. arXiv:1109.4897v4 [hep-ex]

Journal of Modern Physics, 2018, 9, 2135-2140
http://www.scirp.org/journal/jmp
ISSN Online: 2153-120X
ISSN Print: 2153-1196

Homeostasis Processes Expressed as Flashes in a Poincaré Sections

Yehuda Roth

Oranim Academic College, Oranim Campus, K. Tivon Town, Israel
Email: yudroth@gmail.com

How to cite this paper: Roth, Y. (2018) Homeostasis Processes Expressed as Flashes in a Poincaré Sections. *Journal of Modern Physics*, **9**, 2135-2140.
https://doi.org/10.4236/jmp.2018.912134

Received: September 12, 2018
Accepted: October 8, 2018
Published: October 11, 2018

Copyright © 2018 by author and Scientific Research Publishing Inc.
This work is licensed under the Creative Commons Attribution International License (CC BY 4.0).
http://creativecommons.org/licenses/by/4.0/
Open Access

Abstract

We describe a homeostasis system with a discrete map that is revealed by stroboscopic "flashes" (Poincaré sections) that are synchronized with the measurement events.

Keywords

Homeostasis, Poincaré Sections, Regulation, Discrete Map

1. Introduction

Homeostasis is a process that corresponds with biological measurements that are conducted over the internal and external body environments. Its purpose is to keep the body in a steady phase under a varying environment [1]. A regulation is obtained by a negative feedback process, as described in **Figure 1**. A negative feedback system has a sensor that monitors a physiological value. The collected data is transferred to the control center in the brain that compares the received data to the normal range. If the value is far from the set point, then the control center activates an effector which, through the negative feedback loop, balances the value to the normal range. For example, in a thermo-regulation process, sensors in the blood vessels are constantly sending the brain updates on internal temperatures. This information is sent to the hypothalamus area, where four different types of neurons analyze the data. Then, if necessary, an effector is triggered to balance the temperature to the range of the fixed point [2] (see also ref. [3] [4] for the Hammel's model and ref. [5] for an extensive review).

Oscillatory behavior in a range of 10 - 100 [ms] is commonly observed in many neurons [6]. Because Homeostasis processes are activated by the brain, we propose that the time between these measurement events will be at that scale. Negative feedback systems are mostly described by recursive maps [7] [8]. By

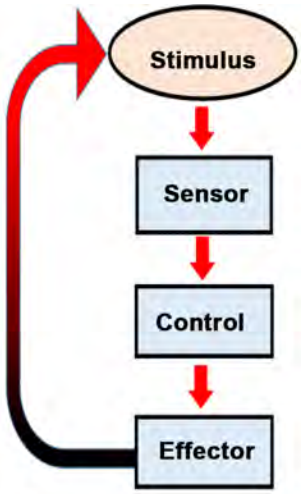

Figure 1. Feedback loop description: Data is collected by the sensors and transferred to the control center. If the value is far from the set point, then the effector, through the negative feedback loop, balances the value to the normal range.

synchronizing the maps' evolution with the measurement events, we describe a regulation process by the Poincaré stroboscopic "flashes". Note that although negative feedback corresponds with nonlinear maps' in practice, we can also analyze maps that in the transition from the n to the $n+1$ stages are linear.

2. Maps

Suppose that σ are a set of numbers over $\mathbb{R}$. The measurement's dynamics are determined by a discrete map $\mathbf{S}$: in a Poincaré stroboscopic style where the "flashes" are synchronized with the neuron detections events. Once an initial value σ_0 is detected, the homeostasis iteration starts, such that

$$\mathbf{S}:\sigma_n=\sigma_{n+1}. \tag{1}$$

Considering a regular map that converges to a single value σ_∞ such that

$$\lim_{n\to\infty}\mathbf{S}:\sigma_n=\sigma_\infty. \tag{2}$$

where σ_∞ is the regulation point such as 37˚C in the temperature regulation.

3. Homeostasis Process Expressed by Linear Maps

In this part we introduce the general description of Homeostasis maps. This will be demonstrated for temperature regulation process in the following subsection.

4. General Description of Homeostasis Linear Maps

The numerical values of σ depend on the system-unit such as the Celsius or Fahrenheit scales for temperature detections. Consider two observers who implement different system units I and II—say, the Celsius and Fahrenheit scales—to measure the same process. Mathematically speaking, the conversion is

obtained by the linear combination,

$$\sigma[\mathrm{I}] = A\sigma[\mathrm{II}] + B. \tag{3}$$

For example, converting from [Celsius] to [Fahrenheit] corresponds with,

$$T[^{\circ}\mathrm{F}] = 1.8T[^{\circ}\mathrm{C}] + 32. \tag{4}$$

At the initial stage, where $n = 0$, both observers measure the same state but with different numerical values. Actually, they describe the same data. Our aim is to find a recursive relation that conserves the converting formula between different measurement units.

For any arbitrary functions f_1 and f_2, a recursion relation that conserves the conversion equation must be of the form:

$$f_1\left(\frac{\sigma_{n+1} - \sigma_1}{\sigma_3}\right) = f_2\left(\frac{\sigma_2 - \sigma_n}{\sigma_4}\right) \tag{5}$$

where σ_1, σ_2, σ_3 and σ_4 are constants possessing the same units of measurement. A simple case is of the linear maps that appear as:

$$\sigma_{n+1} - \sigma_i = a\left(\sigma_e - \sigma_n\right) \tag{6}$$

where σ_i is an internal reference parameter determined by the body's biology, such as the liver's desired temperature, σ_e is an external parameter such as the external environment temperature and *a* stands for the rate of body-surrounding iteration. Simplifying this expression we obtain,

$$\sigma_{n+1} = \sigma_i + a\sigma_e - a\sigma_n \tag{7}$$

or

$$\mathbf{S}: \sigma_n = \sigma_i + a\sigma_e - a\sigma_n \tag{8}$$

This map fluctuates until it eventually reaches the final value $\sigma_\infty = \frac{\sigma_i + a\sigma_e}{1+a}$. The negative feedback can be observed if instead of expressing the transition $n \to n+1$ we follow iteration $n \to n+2$. Now, Equation (7) becomes

$$\sigma_{n+2} = (1-a)\sigma_i + a(1-a)\sigma_e + a^2\sigma_n \tag{9}$$

By comparing Equation (7) with Equation (9), we see that the parameters are rescaled such that $\sigma_i \to (1-a)\sigma_i$ and $\sigma_e \to (1-a)\sigma_e$ only now the negative term $-a\sigma_n$ is transformed into a positive variable $\to a^2\sigma_n$. This reflects the negative feedback process: while in the single iteration σ_n reduces σ_{n+1}, the positive sign in the proceeding iteration increase σ_{n+2}, and so on. This fluctuation decays along the iterations until the map reaches a final value, as shown in Figure 2.

4.1. Temperature Regulation Maps

Core body temperature, T_c, refers to the temperature of the internal body environment, such as the liver temperature. Relatively to the other body zones, T_c varies in a very small range [9], which makes it appropriate to serve as an

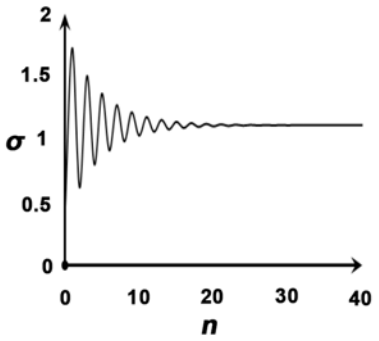

Figure 2. Graphs describing the map $\mathbf{S}:\sigma_n=\sigma_r-a\sigma_n$.

internal reference temperature ($\sigma_i=T_i$). We also consider $\sigma_e=T_s$, where T_s is the external environment temperature.

Suppose that at a stage n, the sensors detect a temperature of T_n that is lower than T_c. This means that at that time the body emits heat calculated as $H_\beta=\beta\left(T_n-T_s\right)$, where β represents a body isolation factor, such that, in the extreme scenario where $\beta=0$, no heat is transmitted to the external environment. Following this measurement result, the body responds (in the $n+1$ iteration) by generating internal heat to increase its temperature. This is represented with the heat term $H_\alpha=\alpha\left(T_c-T_{n+1}\right)$ where α is a parameter representing the heat production rate.

By comparing the two terms, $H_\beta=H_\alpha$, we obtain the recursive equation,

$$T_{n+1}=T_c+aT_s-aT_n, \tag{10}$$

where $a=\dfrac{\beta}{\alpha}$, is a dimensional variable that determines the body-surrounding heat exchange. This equation is with agreement with Equation (8).

For a sufficient number of iterations, the temperature is regulated at T_∞, which satisfies the relation

$$T_{n+1}=T_n\overset{\text{def}}{=}T_\infty, \tag{11}$$

where

$$T_\infty=\frac{T_c+aT_s}{1+a}. \tag{12}$$

For example, for $T_c=37^\circ\text{C}$, $T_s=25^\circ\text{C}$ and $a=0.034483$ we find the final temperature at $T_\infty=36.6^\circ\text{C}$.

4.2. Control of Temperature Level

There are extreme cases in which the conventional regulation process is not sufficient to balance the body parameter. For that scenarios, the brain initiate an additional process that we refer to a $\mathbf{S}_R$: map.

A few scenarios affect temperature regulation, such as:

1) The internal "heat engine" increases or decreases heat production as reflected through α in the heat term $H_\alpha=\alpha\left(T_0-T_{n+1}\right)$. In an extreme heat

production such as occurs in a physical activity like jogging, the body initiate an additional process such as sweating. This we describe by $\mathbf{S}_R$:.

2) The external environment temperature drops or increases dramatically. This is mostly reflected though T_s. For a cold surrounding environment in which heat runs away rapidly from the body environment, the control is on the isolation factor β. A behavioral control can include wearing warm clothing, which will reduce β. A physiological alternative is to initiate a $\mathbf{S}_R$ process, such as shivering that causes the muscles to produce extra heat.

Let us demonstrate the scenario of a temperature reduction process: For high T_s, the body temperature may reach temperatures higher than 37˚C. For example, using the earlier parameters $T_c = 37^{\circ}\mathrm{C}$ and $a = 0.034483$ but with $T_s = 40^{\circ}\mathrm{C}$, we obtain $T_\infty = 37.1^{\circ}\mathrm{C}$ (see Equation (11)). In this scenario, the body initiates $\mathbf{S}_R$: in the following way: after applying the standard map $\mathbf{S}_S$: the outcome temperature T_{n+1} initiates the second map. Using a linear model while implementing the unit of measurements conservation, we define $\mathbf{S}_R$: through the following recursion equation:

$$T_{n+2} = T_{n+1} - bT_s + bT_c \tag{13}$$

where b is a new coefficient of the heat exchange term. By using Equation (10), we obtain that,

$$T_{n+2} = (1-b)T_c + (a-b)T_s - aT_n \tag{14}$$

where for $T_{n+2} = T_n \overset{\text{def}}{=} T_\infty$ we obtain,

$$T_\infty = (1-b)T_\infty^{(s)} \tag{15}$$

where $T_\infty^{(s)}$ is the standard regulation temperature (only now we added the superscript (s)) as appeared in Equation (12) By reusing the data $T_c = 37^{\circ}\mathrm{C}$, $a = 0.034483$ and $T_s = 40^{\circ}\mathrm{C}$, that leads to $T_\infty^{(s)} = 37.1^{\circ}\mathrm{C}$, we can apply $b = 0.01348$ to obtain $T_\infty = 36.6$.

5. Summary

We introduced simple maps that describe homeostasis processes. Finding fundamental equations that describe the homeostasis processes allows us to simplify its description and may contribute a new perspective in analyzing these processes.

Conflicts of Interest

The author declares no conflicts of interest regarding the publication of this paper.

References

[1] Homeostasis. https://www.nature.com/subjects/homeostasis

[2] Morrison, S.F. and Nakamura, K. (2011) *Frontiers in Bioscience* (*Landmark Ed*), **16**, 74-104. https://doi.org/10.2741/3677

[3] Hammel, H.T. (1965) Neurons and Temperature Regulation. In: Yamamoto, W.S. and Brobeck, J.R., Eds., *Physiological Controls and Regulations*, Saunders, Philadelphia, 71.

[4] Boulant, J.A. (2006) *Journal of Applied Physiology*, **100**, 1347-1354. https://doi.org/10.1152/japplphysiol.01064.2005

[5] Chan, L.T., Elizabeth, K.C., David, E.L., Yen, E.C.L., Gwendolyn, E.D., Christopher, A.Z. and Zachary, A.K. (2015) *Cell*, **167**, 47-59.

[6] Buonomano, D.V. (2007) *Nature Chemical Biology*, **3**, 594-597. https://doi.org/10.1038/nchembio1007-594

[7] Prigogine, I. (1980) From Being to Becoming. W. H. Freeman and Company, New York, 123.

[8] Erik, P., Mestl, T. and Omholt, S.W. (1995) *Journal of Biological Systems*, **3**, 409-413.

[9] Tansey, E.A. and Johnson, C.D. (2015) *Advances in Physiology Education*, **39**, 139-148. https://doi.org/10.1152/advan.00126.2014

Journal of Modern Physics, 2018, 9, 2141-2155
http://www.scirp.org/journal/jmp
ISSN Online: 2153-120X
ISSN Print: 2153-1196

Irradiation Energy Effect on a Silicon Solar Cell: Maximum Power Point Determination

Mamadou Lamine Ba[1], Hawa Ly Diallo[2], Hamet Yoro Ba[1], Youssou Traore[2], Ibrahima Diatta[2], Marcel Sitor Diouf[2], Mamadou Wade[1], Gregoire Sissoko[2]

[1]Laboratory of Sciences and Techniques of Water and Environment, Polytechnic School of Thiès, Thiès, Senegal
[2]Laboratory of Semiconductors and Solar Energy, Physics Department, Faculty of Science and Technology, University Cheikh Anta Diop, Dakar, Senegal
Email: gsissoko@yahoo.com

How to cite this paper: Ba, M.L., Diallo, H.L., Ba, H.Y., Traore, Y., Diatta, I., Diouf, M.S., Wade, M. and Sissoko, G. (2018) Irradiation Energy Effect on a Silicon Solar Cell: Maximum Power Point Determination. *Journal of Modern Physics*, **9**, 2141-2155.
https://doi.org/10.4236/jmp.2018.912135

Received: August 29, 2018
Accepted: October 8, 2018
Published: October 11, 2018

Copyright © 2018 by authors and Scientific Research Publishing Inc.
This work is licensed under the Creative Commons Attribution International License (CC BY 4.0).
http://creativecommons.org/licenses/by/4.0/
Open Access

Abstract

The aim of this study is to determinate the electrical parameters of a white biased silicon solar cell submitted to an irradiation energy of particles (protons, helium, electrons and heavy ions). A theoretical study of the influence of irradiation energy on the photocurrent density, the photovoltage, the maximum power, as well as the maximum efficiency of the solar cell is presented through a resolution of the continuity equation relative to excess minority carrier. Then the expressions of the photocurrent density Jph, the photovoltage Vph, and the excess minority carrier recombination velocity at the back side *Sb* are established dependent of irradiation parameters ϕp, *Kl* respectively irradiation flux and intensity. In this work, we propose a method for determining the recombination velocity of the excess minority carrier at the junction Sf_{max} corresponding to the maximum power point delivered by the photovoltaic generator under the influence of the irradiation. It is then obtained by calculating the derivative of the power with respect to the excess minority carrier recombination velocity *Sf* at the junction emitter-base. A transcendental equation solution is deduced as eigenvalue, leading to the junction recombination velocity of excess minority carrier and also yields the solar cell maximum conversion efficiency.

Keywords

Silicon Solar Cell, Irradiation, Electrical Parameters, Maximum Power Point

1. Introduction

The study of the effect of radiation on solar cells designed for space applications has long occupied research fields, in order to understand the stakes in their per-

formance opposite the high-energy radiating particles of the space environment [1] [2] [3]. These same concerns are studied at the terrestrial level in order to investigate the relationship between the solar cell parameters and those of the irradiation [4].

The aim of this study is to show the influence of irradiation energy on the electrical parameters of a silicon solar cell: photocurrent density, photovoltage, I-V characteristic, electric power and efficiency.

This work deals with a method, to determinate the maximum power point of the solar cell under the effect of the irradiation energy. Maximum Power Point Trackers (MPPT) is a well-known technique allowing the solar cell to operate at the maximum power point under varying illumination and temperature [5] [6] [7] [8] [9].

This work gives the expressions the excess minority carrier density continuity equation in the base. Then, the expressions [10] [11] of the photocurrent density, the photovoltage, the excess minority carrier excess minority carrier recombination velocity at the back side Sb and the electrical power, all depending on the irradiation energy are deduced. These parameters are also represented graphically as a function of the excess minority carrier recombination velocity at the junction.

The characteristic curve of the photocurrent density as a function of the photovoltage I(Sf)-V(Sf) [12] [13] [14], is produced as irradiation parameters dependent. The power [15] [16] [17], as a function of both the recombination velocity of the excess minority carrier at the junction and the photovoltage, is also represented graphically.

A transcendental equation giving the velocity of recombination of the excess minority carrier at the points of maximum power Sf_{max} is determined and the numerical values of Sf_{max} are extracted graphically. We then calculated the fill factor FF of the solar cell for different values of the irradiation energy. Finally, the profiles of Sf_{max}, V_{max}, I_{max} and η_{max} versus irradiation energy are shown graphically.

2. Theory

Consider a crystalline silicon solar cell (n^+-p-p^+) [18]. Its structure is illustrated in **Figure 1**. Where:

x is the depth in the base of the solar cell measured from the emitter-base junction, called space charge region (SCR) ($x = 0$) to the back side face ($x = H$). H is the base thickness, where a back surface field (BSF) is created by help of the p^+ zone.

Kl is the damage coefficient while ϕp is the irradiation energy.

The set of different processes taking place in the base can result in the so called continuity equation:

$$\frac{\partial^2 \delta(x, kl, \phi p)}{\partial x^2} - \frac{\delta(x, kl, \phi p)}{\left[L(kl, \phi p)\right]^2} = -\frac{1}{D(kl, \phi p)} \cdot G(x) \tag{1}$$

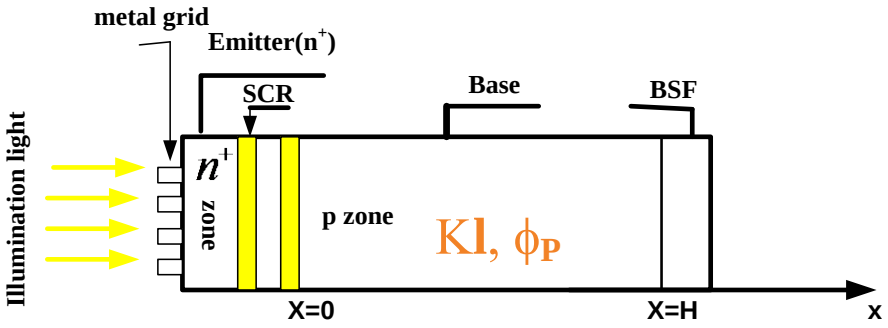

Figure 1. Structure of the silicon solar cell (n^+-p-p^+).

with:

$$D(kl,\phi p)=\frac{\left[L(kl,\phi p)\right]^2}{\tau} \tag{2}$$

$$L(kl,\phi p)=\frac{1}{\left(\frac{1}{L_0^2}+kl\cdot\phi p\right)^{1/2}} \tag{3}$$

$D(kl,\phi p)$ is the diffusion coefficient of the electrons in the base under irradiation.

$L(kl,\phi p)$ is the diffusion length of the excess minority carriers in the base as a function of the irradiation energy flux (Φp) and the damage coefficient intensity (Kl). It also represents the average distance traveled by the minority carriers before their recombination in the base under irradiation.

$\delta(x,kl,\phi p)$ represents the excess minority carrier density in the base of the solar cell at the x-position, dependent of the irradiation energy.

$G(x)$ is the excess minority carrier generation rate, given by [19] [20]:

$$G(x)=\sum_{i=1}^{3}a_i e^{-b_i\cdot x} \tag{4}$$

The coefficients a_i and b_i take into account the tabulated values of solar radiation and the dependence of the absorption coefficient of silicon with the wavelength. The resolution of the differential equation gives the expression of the excess minority carrier density in the base as:

$$\delta(x,kl,\phi p)=A\cdot\cosh\left[\frac{x}{L(kl,\phi p)}\right]+B\cdot\sinh\left[\frac{x}{L(kl,\phi p)}\right]-\sum K_i\cdot e^{-b_i\cdot x} \tag{5}$$

The expressions of, A and B are determined from the following boundary conditions:

2-4-a: At the junction: emitter-base ($x=0$)

$$D(kl,\phi p)\frac{\partial\delta(x,kl,\phi p)}{\partial x}\bigg|_{x=0}=S_f\cdot\delta(0,kl,\phi p) \tag{6}$$

2-4-b: At the back side ($x=H$)

$$D(kl,\phi p)\frac{\partial\delta(x,kl,\phi p)}{\partial x}\bigg|_{x=H} = -S_b\cdot\delta(H,kl,\phi p) \tag{7}$$

S_f is the excess minority carrier recombination velocity at the junction and also indicates the operating point of the solar cell [21] [22].

S_b is the excess minority carrier recombination velocity on the back side surface [23] [24] [25]. Its expression is obtained from the derivative of the photocurrent density for large Sf values [21] [26] [27] that can be seen on **Figure 2**.

$$\left[\frac{\partial Jph}{\partial Sf}\right] = 0 \tag{8}$$

From the relation (Equation (8)), the calculation gives the recombination velocity S_b [10] [28] of the excess minority carrier at the back side of the solar cell, depending on parameters influenced by irradiation energy, such as, $L(kl, \varphi p)$ and $D(kl, \varphi p)$:

$$Sb(kl,\phi p) = \frac{D(kl,\phi p)}{L(kl,\phi p)} \cdot\sum_{i=1}^{3}\frac{L(kl,\phi p)\cdot b_i\left(e^{b_i\cdot H}-\cosh\left(\frac{H}{L(kl,\phi p)}\right)\right)-\sinh\left(\frac{H}{L(kl,\phi p)}\right)}{L(kl,\phi p)\cdot b_i\cdot\sinh\left(\frac{H}{L(kl,\phi p)}\right)+\cosh\left(\frac{H}{L(kl,\phi p)}\right)-e^{b_i\cdot H}} \tag{9}$$

3. Photocurrent Density

The expression of the photocurrent density is deduced from the excess minority carrier density in the base. It is given by the following relation:

$$Jph(Sf,kl,\phi p) = q\cdot D(kl,\phi p)\cdot\left[\frac{\partial\delta(x,kl,\phi p)}{\partial x}\right]_{x=0} \tag{10}$$

Figure 2 shows the profile of the photocurrent density as a function of the excess minority carrier recombination velocity at the junction for different given values of the irradiation energy.

We note in this figure that the photocurrent density is almost zero for recombination velocity lower than 10 cm/s (solar cell operating in open circuit). Then for 10 cm/s < Sf < 3×10^3 cm/s, the photocurrent density increases with the recombination velocity to reach a maximum of amplitude. This shows that the excess minority carrier has acquired some energy to cross the junction.

Indeed, for recombination velocity greater than 3×10^3 cm/s, the photocurrent density is maximum and constant, corresponding to the short-circuit photocurrent.

The figure also shows that as the irradiation energy increases, the maximum amplitude of the photocurrent density decreases. This phenomenon can be explained by the interaction of the irradiating particles with the silicon material which increases and reduces the density of the excess minority carrier.

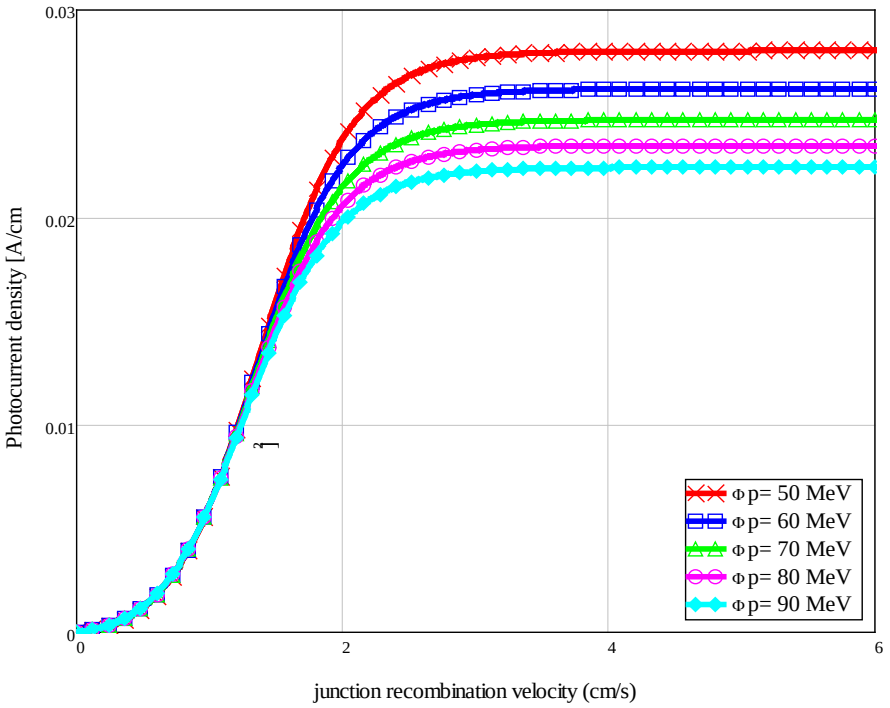

Figure 2. Photocurrent density versus junction recombination velocity for different irradiation energy values.

4. Photovoltage

The illuminated solar cell photovoltage expression, is obtained by the Boltzmann relation.

$$Vph(Sf,kl,\phi p)=V_T\cdot\ln\left(\frac{Nb}{n_i^2}\cdot\delta(0,kl,\phi p)+1\right) \tag{11}$$

V_T is the thermal voltage, defined by:

$$V_T=\frac{K_b}{q}T \tag{12}$$

- T is the absolute temperature = 300 K
- Nb is the doping rate in acceptor atoms in the base
- n_i is the intrinsic concentration
- K_b is the constant of Boltzmann
- q is the elementary charge of the electron

Figure 3 shows the profile of the photovoltage as a function of the excess minority recombination velocity at the junction for different values of the irradiation energy.

We note in this figure that the photovoltage is maximum and constant for recombination velocity lower than 2×10^2 cm/s; thus corresponding to solar in open circuit condition. Beyond this recombination velocity, the photovoltage linearly decreases very rapidly to reach almost zero value in the vicinity of the short-circuit and consequently, yields the crossing of almost all excess minority carrier at the junction.

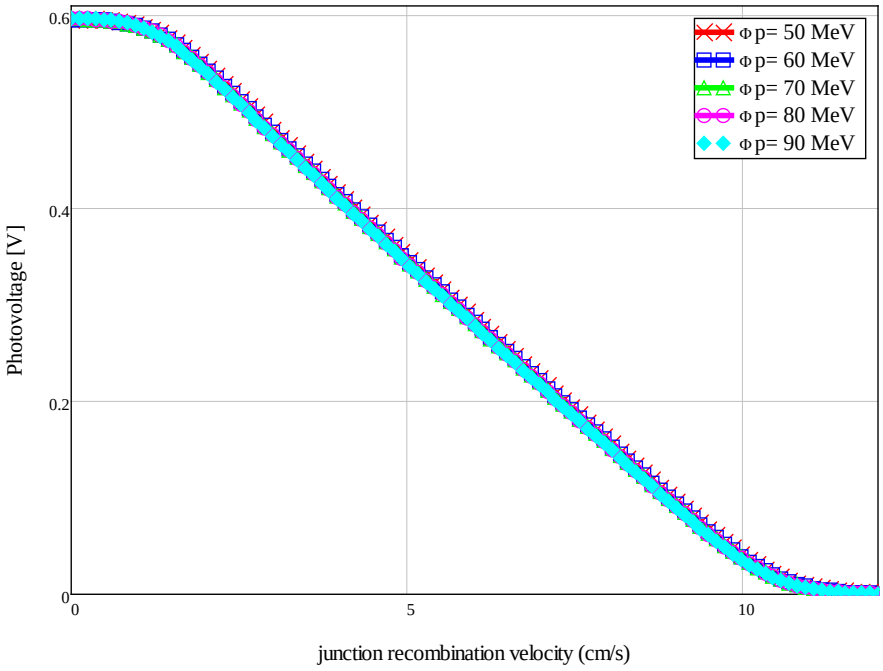

Figure 3. Photovoltage versus junction recombination velocity for different irradiation energy values.

Then, we note in this figure that the increase of the irradiation energy influences weakly the photovoltage.

5. Illuminated Solar Cell I(Sf)-V(Sf) Characteristic Study

The profile of the illuminated solar cell I(Sf)-V(Sf) characteristic for different values of the irradiation energy is shown in **Figure 4**.

We note that the photocurrent density decreases with the increase of the irradiation energy. And the photovoltage increases slightly.

6. Study of the Power and the Maximum Power Point

6.1. Electrical Power of the Solar Cell

The equivalent electric circuit of a real solar cell under illumination is shown in **Figure 5**. This circuit gives the solar cell as an ideal current generator that outputs an illumination depending photocurrent density Iph, connected in parallel with a diode and a shunt resistor Rsh and in series with a series resistor Rs [29].

The ohm law applied to the circuit in **Figure 5** yields the electric power delivered by the base of the solar cell to an external load as follows:

$$P\left(Sf,kl,\phi p\right)=V_{ph}\left(Sf,kl,\phi p\right)\cdot I\left(Sf,kl,\phi p\right) \tag{13}$$

Applying the first Kirchhoff law to the circuit of **Figure 5** the current delivered by an illuminated solar cell to an external load, is given by the following relationship:

$$I\left(Sf,kl,\phi p\right)=J_{ph}\left(Sf,kl,\phi p\right)-I_{d}\left(Sf,kl,\phi p\right) \tag{14}$$

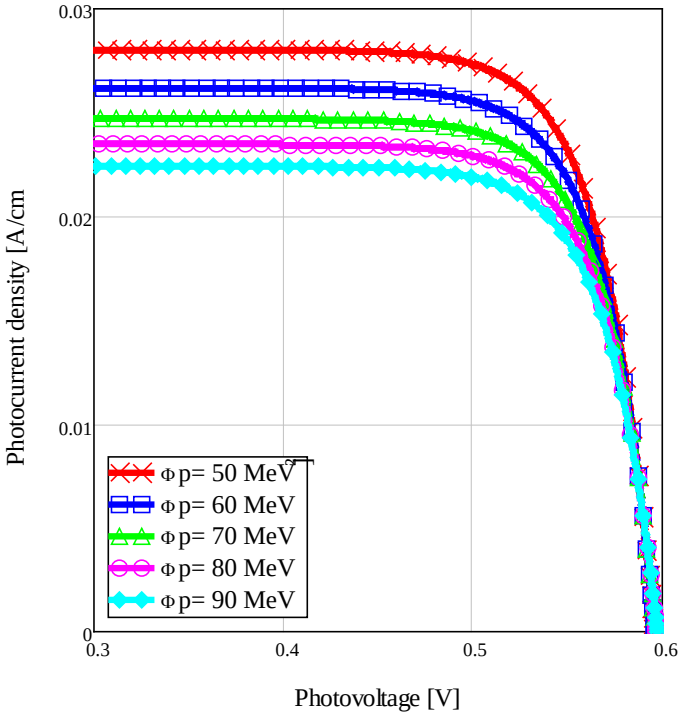

Figure 4. Photocurrent density versus photovoltage for different irradiation energy values.

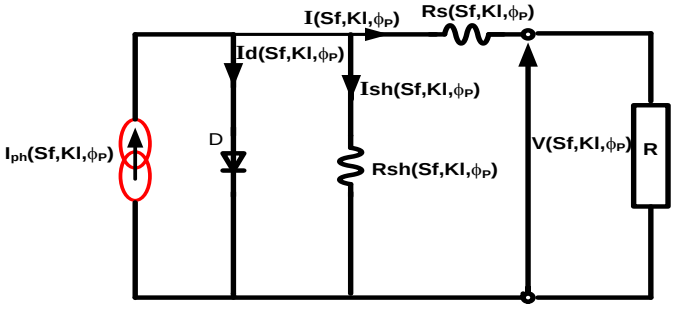

Figure 5. Equivalent electrical circuit of an illuminated solar cell.

I_d is the diode current, its expression is given by the following relation:

$$I_d\left(Sf,kl,\phi p\right)=q\cdot Sf_0\cdot\frac{n_i^2}{Nb}\cdot\exp\left(\frac{V_{ph}\left(Sf,kl,\phi p\right)}{V_T}-1\right) \tag{15}$$

Sf_0 is the excess minority carrier recombination velocity associated with shunt resistance-induced charge carrier losses [30] [31], which characterizes the good quality of the solar cell [21] [22] [24].

Figure 6 and **Figure 7** show the variations in electrical power as a function of both, the excess minority carrier recombination velocity at the junction and the photovoltage for different values of the irradiation energy.

We note that the power grows from the high recombination velocity at the junction (**Figure 6**) and reaches a maximum amplitude where it decreases to tend to zero value. The maximum of this power amplitude decreases with the

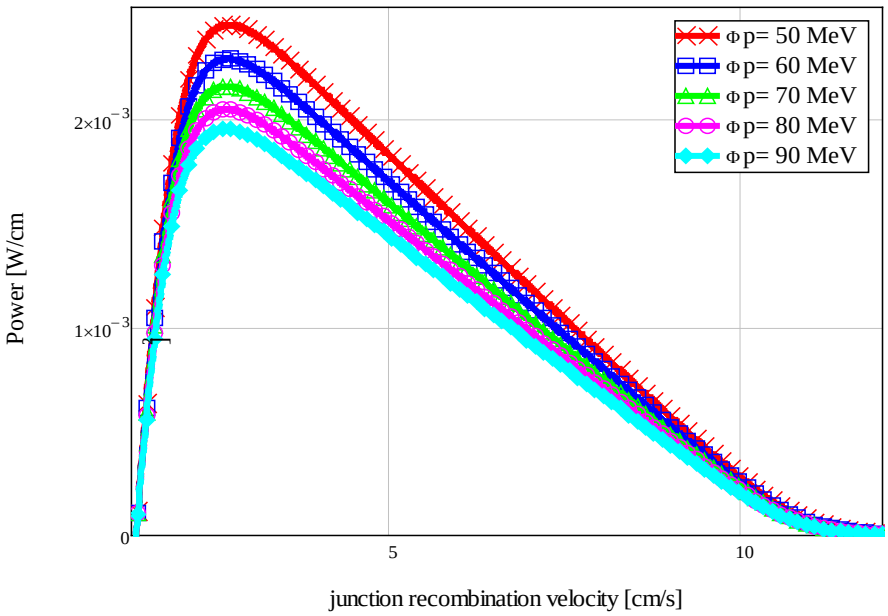

Figure 6. Solar cell power versus junction recombination velocity for different irradiation energy values.

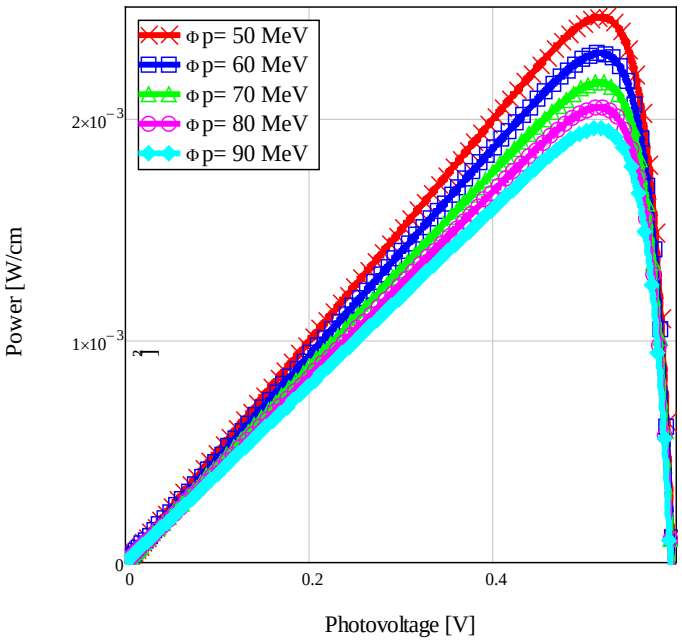

Figure 7. Solar cell power versus photovoltage for different irradiation energy values.

increase of the irradiation energy. There are three zones of variation of the power as a function of the photovoltage (Figure 7):

- A short-circuit zone with a maximum photocurrent density (where the photovoltage is zero) gives a power equally zero;
- A region in the vicinity of the open circuit with a maximum photovoltage (with a zero photocurrent density) provides such a zero power;

- And an intermediate zone with increasing and decreasing power passing through a maximum which is located at an intermediate operating point.

It is also observed a decrease in power with the increase of the irradiation energy.

6.2. Maximum Power Point and Efficiency

The maximum power point of a photovoltaic generator corresponds to the photocurrent density-photovoltage couple generating the maximum electrical power [17]. The product of the maximum photocurrent density Jph_{max} and the maximum photovoltage Vph_{max} gives a maximum power as $P_{max} = Jph_{max} \times Vph_{max}$.

The recombination velocity Sfmax of the excess minority carrier at the junction corresponding to the maximum power point is bring out by solving the following equation [17].

$$\frac{\partial P}{\partial Sf} = 0 \tag{16}$$

Let Sf_{max} denote the recombination velocity of the excess minority carrier at the junction corresponding to the maximum power point. It depends on both the phenomenological and geometrical parameters of the solar cell, respectively,

$L(kl, \varphi p)$, $D(kl, \varphi p)$, $Sf(kl, \varphi p)$, $Sb(kl, \varphi p)$, μ, τ, n_i, Nb, b_i and H in the one dimensional model.

From Equation (16), the transcendental equation depending on recombination velocity Sf and the irradiation energy is obtained. It is given by the following expressions:

$$M\left(Sf, kl, \phi p\right) = \frac{1}{Sf_{\max} L\left(kl, \phi p\right)} \cdot \left[1 - \frac{Sf_{\max} L\left(kl, \phi p\right)}{Y_1 \cdot D\left(kl, \phi p\right) + Sf_{\max} L\left(kl, \phi p\right)}\right] \tag{17}$$

And:

$$N\left(Sf, kl, \phi p\right) = \left[\frac{\Gamma_{\max}\left(0, kl, \phi p\right)}{\left(\Gamma_{\max}\left(0, kl, \phi p\right) + \frac{n_i^2}{Nb}\right) \cdot \left(Sf_{\max} \cdot L\left(kl, \phi p\right) + Y_1 \cdot D\left(kl, \phi p\right)\right)}\right] \times \left[\frac{1}{\log\left(\frac{Nb \cdot \Gamma_{\max}\left(0, kl, \phi p\right)}{n_i^2} + 1\right)}\right] \tag{8}$$

$\Gamma_{\max}\left(0, kl, \phi p\right)$ is the density of the minority excess minority carrier at the point of maximum power, its expression is given by the following relation:

$$\Gamma_{\max}\left(0, kl, \phi p\right) = \beta \cdot D\left(kl, \phi p\right) \cdot \left[\frac{Y_2 + Y_1 - b_i \cdot L\left(kl, \phi p\right)}{Sf_{\max} \cdot L\left(kl, \phi p\right) + Y_1 \cdot D\left(kl, \phi p\right)}\right] \tag{19}$$

with:

$$\beta = \frac{n \cdot a_i \cdot L(kl,\phi p)^2}{D(kl,\phi p) \cdot \left(L(kl,\phi p)^2 \cdot b_i^2 - 1\right)} \tag{20}$$

$$Y_1 = \frac{\frac{D(kl,\phi p)}{L(kl,\phi p)} \cdot \sinh\left(\frac{H}{L(kl,\phi p)}\right) + Sb(kl,\phi p) \cdot \cosh\left(\frac{H}{L(kl,\phi p)}\right)}{\frac{D(kl,\phi p)}{L(kl,\phi p)} \cdot \cosh\left(\frac{H}{L(kl,\phi p)}\right) + Sb(kl,\phi p) \cdot \sinh\left(\frac{H}{L(kl,\phi p)}\right)} \tag{21}$$

$$Y_2 = \frac{\left(D(kl,\phi p) \cdot b_i - Sb(kl,\phi p)\right) \cdot \exp(-b_i \cdot H)}{\frac{D(kl,\phi p)}{L(kl,\phi p)} \cdot \cosh\left(\frac{H}{L(kl,\phi p)}\right) + Sb(kl,\phi p) \cdot \sinh\left(\frac{H}{L(kl,\phi p)}\right)} \tag{22}$$

The graphical resolution of this transcendental equation as a function of the excess minority carrier recombination velocity Sf at the junction, for different values of the irradiation energy, gives the Sf_{max} values by the intercept point of the two curves represented by Figure 8. At each Sf_{max} operating point, the electrical power delivered by the photovoltaic generator, is maximum.

Figure 8 shows a decrease in the Sf_{max} values as the irradiation energy increases. This reflects the decrease in maximum power as the irradiation energy increases. We observe the intercept points in the figure, corresponding to the values of Sf_{max}. These values of Sf_{max} correspond to a condition of solar cell operating at its maximum power point.

The results obtained from Figure 8 corresponding to the numerical values of Sf_{max} for each maximum power point, are given in Table 1.

The influence of the irradiation energy on the Sf_{max} is represented by Figure 9.

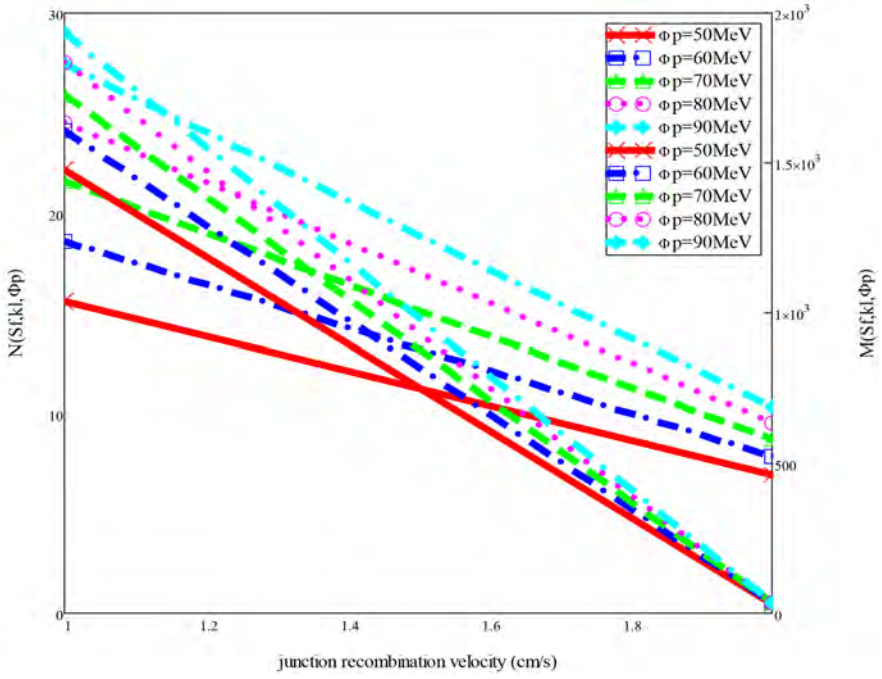

Figure 8. Representation of transcendental equation versus junction recombination velocity for different irradiation energy values.

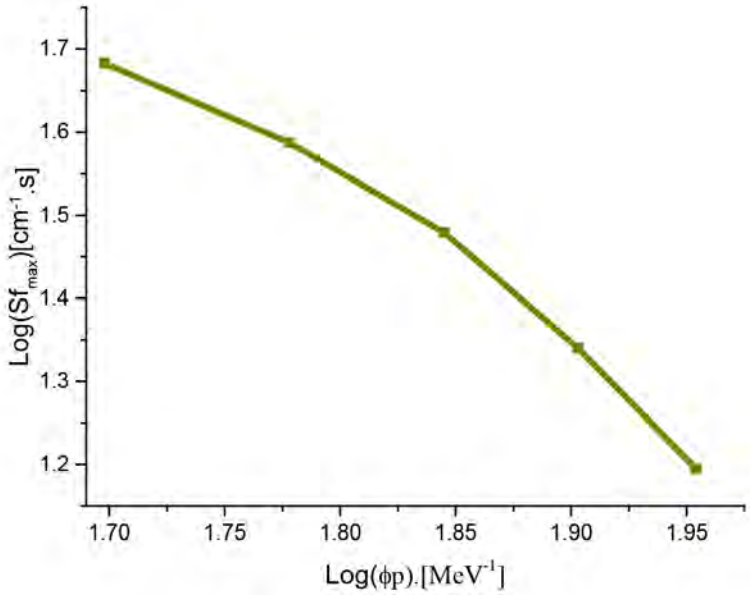

Figure 9. Sf_{max} versus irradiation energy.

Table 1. The numerical values of Sf_{max} corresponding to the maximal power point for different irradiation energy values.

Irradiation energy (MeV)	Intercept points for given irradiation energy values (p)	Sf_{max} (p·10^{p}cm/s)
50	1.506	47.624
60	1.432	35.970
70	1.349	26.924
80	1.251	24.967
90	1.139	15.728

The recombination velocity Sf_{max} of the excess minority carrier at the junction decreases with the irradiation energy.

7. The Efficiency

The conversion efficiency of a solar cell is the ratio between the maximum power supplied provided by the solar cell and the incident light power absorbed. It is written as follows:

$$\eta = \frac{I_{max} \cdot V_{max}}{P_{incident}} \tag{23}$$

$P_{incident}$ is the incident light power absorbed by the solar cell, with $P_{incident} = 100\ \mathrm{mW/cm^2}$ in the standard conditions Air Mass 1.5.

The representation of the efficiency is deduced from the I-V characteristic curve (Figure 4). The graphical values corresponding to the maximum power point, leading to both, the maximum photocurrent and the maximum photovoltage, allowed to obtain the photovoltaic efficiency conversion for different values of the irradiation energy. These results are noted in Table 2.

Table 2. Table of parameters leading to the efficiency η_{max} corresponding to the maximal power point for different irradiation energy values.

Irradiation energy (MeV)	50	60	70	80	90
I_{max} (A/cm²)	0.02802	0.02619	0.02470	0.02346	0.02241
I_d (Sf_{max}) (A)	0.19578×10^{-3}	0.19616×10^{-3}	0.19655×10^{-3}	0.19692×10^{-3}	0.19729×10^{-3}
V_{max} (V)	0.59549	0.59606	0.59652	0.59692	0.59726
P_{max} (W/cm²)	0.016569	0.015494	0.014617	0.013886	0.013267
FF	0.016682	0.015605	0.014731	0.014003	0.013381
η_{max} (%)	16,569	15.494	14.617	13.886	13.267

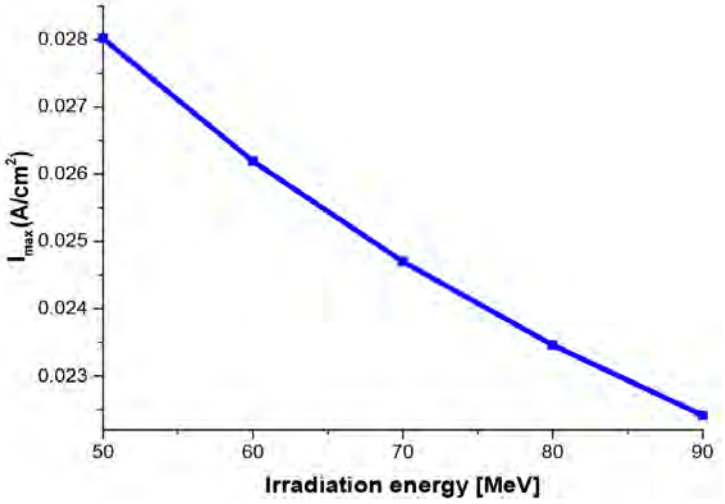

Figure 10. Maximal photocurrent versus irradiation energy.

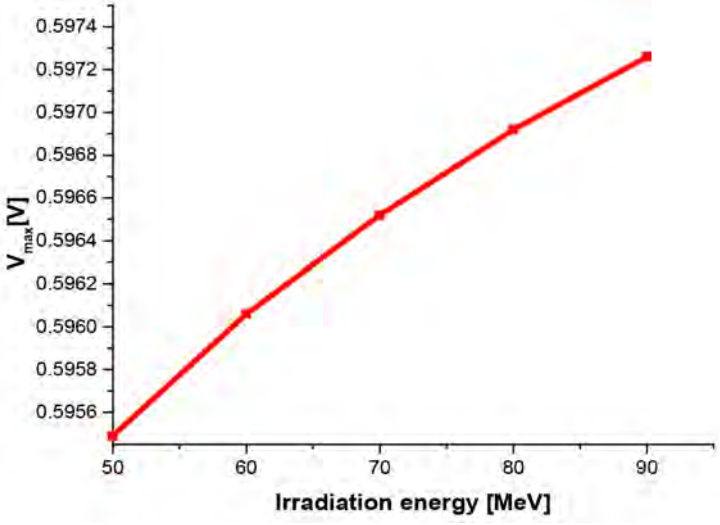

Figure 11. Maximal photovoltage versus irradiation energy.

Figures 10-12 show the maximum photocurrent I_{max}, the maximum photovoltage V_{max} and the maximum conversion efficiency η_{max} of the solar cell as a function of the irradiation energy.

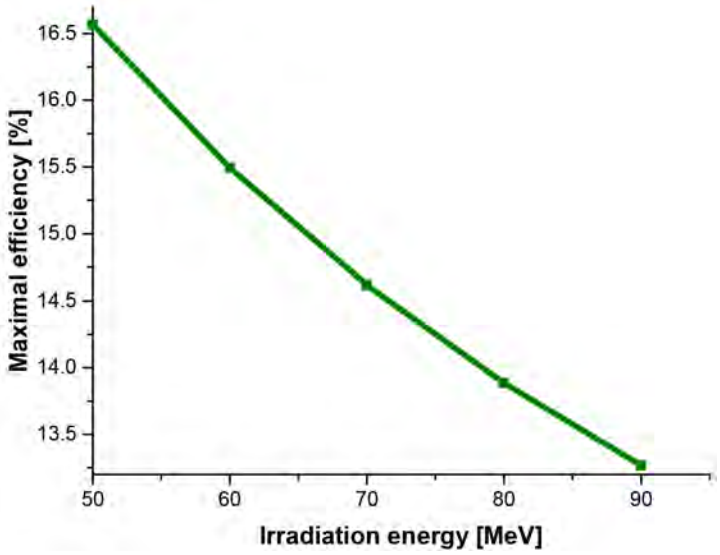

Figure 12. Maximal conversion efficiency versus irradiation energy.

These results show that, the recombination velocity of the excess minority carrier Sf_{max} at the junction yielding, the maximum photocurrent as well as the photovoltaic conversion efficiency, decrease when the irradiation energy increases, contrary to the maximum photovoltage which increases with the energy of irradiation. This results in a variation of the peak power point as the irradiation energy increases.

8. Conclusions

In this work, from the expression of the excess minority carrier density in the base, the photocurrent density and the photovoltage, lead to the illuminated I-V characteristic of the solar cell under irradiation. This study showed us a decrease in short-circuit photocurrent and an increase in open-circuit photovoltage as irradiation energy increases. The decrease of the short-circuit photocurrent is manifested by a decrease in the excess minority carrier density that crosses the junction as the irradiation energy increases.

From the dark and illuminated I-V characteristics, we have studied the electric power delivered by the base of the solar cell as a function of the excess minority carrier recombination velocity Sf at the junction. The power increases with the recombination velocity Sf as well as the photovoltage up to a maximum value which represents the maximum power point. Then it decreases to cancel at a value corresponding to the open circuit voltage (very low Sf).

A transcendental equation graphically resolved, gives eigenvalue, represented by the recombination velocity of the excess minority carrier Sf_{max} corresponding to the maximum power point of the solar cell under different values of the irradiation energy.

Finally we calculated and plotted solar cell electrical parameters I_{max}, V_{max} and η_{max} versus the applied irradiation energy.

Conflicts of Interest

The authors declare no conflicts of interest regarding the publication of this paper.

References

[1] Martin, J.E. (2006) Physics for Radiation Protection: A Handbook. 2nd Edition, Wiley-VCH, Weinheim. https://doi.org/10.1002/9783527618798

[2] Fatemi, N.S., Sharps, P.R., Stan, M.A., Aiken, D.J., Clevenger, B. and Hou, H.Q. (2001) Radiation-Hard High-Efficiency Multi-Junction Solar Cells for Commercial Space Applications. *Proceedings of the* 17*th European Photovoltaic Solar Energy Conference*, 2155-2158.

[3] Kreinin, L., Bordin, N. and Eisenberg, N. (2007) Spectral Response of Light Biased Si Solar Cells at Open Circuit Voltage. *Proceedings of the* 14*th Sede Boqer Symposium on Solar Electricity Production*, 19-21 February 2007, 71-76.

[4] Ohshima, T., Sumita, T., Imaizumi, M., Kawakita, S., Shimazaki, K., Kuwajima, S., Ohi, A. and Itoh, H. (2005) Evaluation of the Electrical Characteristics of III-V Compounds Solar Cells Irradiated with Protons at Low Temperatures. *Proceedings of the* 31*st IEEE Photovoltaic Specialists Conference*, Lake Buena Vista, FL, 3-7 January 2005, 806.

[5] Ould El Moujtaba, M.A., Ndiaye, M., Diao, A., Thiame, M., Barro, I.F. and Sissoko, G. (2012) *Research Journal of Applied Sciences, Engineering and Technology*, **4**, 5068-5073.

[6] Gaye, I., Sam, R., Seré, A.D., Barro, I.F., Ould El Moujtaba, M.A., Mané, R. and Sissoko, G. (2012) *International Journal of Emerging Trends & Technology in Computer Science* (*IJETTCS*), **1**, 210-214,

[7] Sow, O., Diarisso, D., Zénobe, N., MBodji, A., Diallo, M.S., Diao, A., Gaye, I., Barro, F.I. and Sissoko, G. (2013) *International Journal of Innovative Technology and Exploring Engineering* (*IJITEE*), **2**, 330-334.

[8] Dione, B., Sow, O., Wade, M., Ibrahima, L.Y., Mbodji, S. and Sissoko, G. (2016) *Circuits and Systems*, **7**, 3984-4000. https://doi.org/10.4236/cs.2016.711330

[9] Barro, F.I., Seidou Maiga, A., Wereme, A. and Sissoko, G. (2010) *Physical and Chemical News*, **56**, 76-84.

[10] Diallo, M.M., Tamba, S., Seibou, B., Cheikh, M.L.O., Diatta, I., El Hadji Ndiaye, Traore, Y., Sarr, C.T. and Sissoko, G. (2017) *Journal of Scientific and Engineering Research*, **4**, 29-40.

[11] Gaye, I., Ould El Moujtaba, M.A., Thiam, N., Tall, I. and Sissoko, G. (2014) *Current Trends in Technology and Science*, **3**, 98-104.

[12] Dieye, M., Mbodji, S., Zoungrana, M., Zerbo, I., Dieng, B. and Sissoko, G. (2015) *World Journal of Condensed Matter Physics*, **5**, 275-283. https://doi.org/10.4236/wjcmp.2015.54028

[13] Ly, I., Wade, M., Ly Diallo, H., El Moujtaba, M.A.O., Lemtabott, O.H., Mbodji, S., Diasse, O., Ndiaye, A., Gaye, I., Barro, F.I., Wereme, A. and Sissoko, G. (2011) Irradiation Effect on the Electrical Parameters of a Bifacial Silicon Solar Cell under Multispectral Illumination. *Proceedings of* 26*th European Photovoltaic Solar Energy Conference and Exhibition*, 785-788.

[14] Sow, O., Zerbo, I., Mbodji, S., Ngom, M.I., Diouf, M.S. and Sissoko, G. (2012) *International Journal of Sciences and Technology*, **1**, 230-246.

[15] Sissoko, G., Correa, A., Nanema, E., Diarra, M.N., Ndiaye, A.L. and Adj, M. (1998) Recombination Parameters Measurement in Silicon Double Sided Surface Field Cell. *Proceeding of the World Renewable Energy Congress*, Florence, 20-25 September 1998, 1856-1859.

[16] Madougou, S., Made, F., Boukary, M.S. and Sissoko, G. (2007) *Advanced Materials Research*, **18**-**19**, 303-312.

[17] Sylla, B.D.D., Ly, I., Sow, O., Dione, B., Traore, Y. and Sissoko, G. (2018) *Journal of Modern Physics*, **9**, 172-188. https://doi.org/10.4236/jmp.2018.92011

[18] Nam, L., Rodot, M., Nijs, J., Ghannam, M. and Coppye, J. (1992) *Journal de Physique III*, *EDP Sciences*, **2**, 1305-1316.

[19] Furlan, J. and Amon, S. (1985) *Solid State Electronics*, **28**, 1241-1243. https://doi.org/10.1016/0038-1101(85)90048-6

[20] Mohammad, S.N. (1987) *Journal of Applied Physics*, **28**, 767-772. https://doi.org/10.1063/1.338230

[21] Sissoko, G., Sivoththanam, S., Rodot, M. and Mialhe, P. (1992) Constant Illumination-Induced Open Circuit Voltage Decay (CIOCVD) Method, as Applied to High Efficiency Si Solar Cells for Bulk and Back Surface Characterization. 11*th European Photovoltaic Solar Energy Conference and Exhibition*, Montreux, 352-354.

[22] Diallo, H.L., Seïdou Maiga, A., Wereme, A. and Sissoko, G. (2008) *The European Physical Journal Applied Physics*, **42**, 203-211. https://doi.org/10.1051/epjap:2008085

[23] Rose, B.H. and Weaver, H.T. (1983) *Journal of Applied Physics*, **54**, 238-247. https://doi.org/10.1063/1.331693

[24] Joardar, K., Dondero, R.C. and Schroder, D.K. (1989) *Solid-State Electronics*, **32**, 479-483. https://doi.org/10.1016/0038-1101(89)90030-0

[25] Sissoko, G., Museruka, C., Corréa, A., Gaye, I. and Ndiaye, A.L. (1996) *Renewable Energy*, **3**, 1487-1490.

[26] Bocande, Y.L., Corréa, A., Gaye, I., Sow, M.L. and Sissoko, G. (1994) *Proceedings of the World Renewable Energy Congress*, **3**, 1698-1700.

[27] Sissoko, G., Nanéma, E., Corréa, A., Biteye, P.M., Adj, M. and Ndiaye, A.L. (1998) *Renewable Energy*, **3**, 1848-1851.

[28] Diallo, M.M., Seibou, B., Ba, H.Y., Zerbo, I. and Sissoko, G. (2014) *Current Trends in Technology and Sciences*, **3**, 416-421.

[29] Mbodji, S., Ly, I., Diallo, H.L., Dione, M.M., Diasse, O. and Sissoko, G. (2012) *Research Journal of Applied Sciences*, *Engineering and Technology*, **4**, 1-7.

[30] Thiam, N., Diao, A., Ndiaye, M., Dieng, A., Thiam, A., Sarr, M., Maiga, A.S. and Sissoko, G. (2012) *Research Journal of Applied Sciences*, *Engineering and Technology*, **4**, 4646-4655.

[31] Ly Diallo, H., Wade, M., Ly, I., Ndiaye, M., Dieng, B., Lemrabott, O.H., Maïga, A.S. and Sissoko, G. (2002) *Research Journal of Applied Sciences*, *Engineering and Technology*, **4**, 1672-1676.

Journal of Modern Physics, 2018, 9, 2156-2169
http://www.scirp.org/journal/jmp
ISSN Online: 2153-120X
ISSN Print: 2153-1196

The Negative Entropy in Organisms; Its Maintenance and Extension

Jinya Otsuka

JO Institute of Biophysics, Tokyo, Japan
Email: jin.otsuka @kyj.biglobe.ne.jp

How to cite this paper: Otsuka, J. (2018) The Negative Entropy in Organisms; Its Maintenance and Extension. *Journal of Modern Physics*, **9**, 2156-2169.
https://doi.org/10.4236/jmp.2018.912136

Received: August 3, 2018
Accepted: October 8, 2018
Published: October 11, 2018

Copyright © 2018 by author and Scientific Research Publishing Inc.
This work is licensed under the Creative Commons Attribution International License (CC BY 4.0).
http://creativecommons.org/licenses/by/4.0/
Open Access

Abstract

Life has been a mystery for most physicists since the question of Maxwell's demon. In the present paper, the self-reproduction, which is characteristic of the organism, is shown to be essential in resolving the paradox of Maxwell's demon. For this purpose, a new thermodynamic quantity of biological activity is introduced to represent the molecular events in an organism recently revealed by molecular biology. This quantity gives a measure that the entropy production arising from the difference between acquired energy and stored energy compensates for the negative entropy of systematizing the organism, and is considered to be proportional to the self-reproducing rate of the organism as the first approximation. The equation of replicator dynamics consisting of self-reproducing rate, death rate and mutation terms contains all known types of evolution of unicellular organisms. When the mutation term is restricted to the point mutation mainly due to the nucleotide base changes in genes, this equation automatically leads to Darwinian evolution that the mutant with the higher increase rate is selected to become prevailing in the population. Throughout this evolution, the nucleotide bases in genes are converged to the special arrangement exhibiting the optimal increase rate of the organism. Moreover, the mutants having experienced gene duplication first decline to the minor members in the population but some of the descendants recover as a new style of organisms by generating new gene(s) from the counterpart of duplicated genes. This evolutionary process to expand the repertoire of genes is mathematically formulated by solving the equation of replicator dynamics up to the higher order of mutation terms. The present theoretical approach can be not only extended to the multicellular diploid eukaryotes but also applied to explain the origin of genes in the self-reproducing proto-cells formed anciently.

Keywords

Evolution, Gene, Maxwell's Demon, Mutation, Self-Reproduction

1. Introduction

When the first and second laws of thermodynamics have been established, Maxwell has raised the question about the compatibility of life with the second law in terms of a sorting demon [1]. This question has been discussed by many physicists. For example, Szilard suggests that the demon actually transforms "information" into "negative entropy" [2]. In 1949, Brillouin [3] has summarized different opinions of life among physicists, chemists and biologists into the following three groups. 1) Our present knowledge of physics and chemistry is practically complete, and these physical and chemical laws will soon enable us to explain life. 2) We know a great deal about physics and chemistry, but it is presumptuous to pretend that we know all about them. We admit that life obeys all the laws of physics and chemistry at present known to us, but we definitely feel that something more is needed before we can understand life. 3) The principles of thermodynamics, especially the second law, apply only to inert objects. Life is an exception to the second law, and a new principle of life will have to explain conditions contrary to the second law.

According to the suggestion by Szilard [2], Brillouin [4] has then analysed the operation of Maxwell's demon that at least one quantum of light emitted from electric torch is scattered by a molecule and is absorbed in the eye of the demon. In this analysis, he shows that the increase in entropy of the demon by accepting the light quantum is greater than the decrease in entropy by acquiring the information about the molecule, and concludes that the demon ultimately dies by the repetition of such operation. Schrödinger has pointed out that the organism acquires negative entropy by assimilating food [5], but he has not considered how the food restores the demon. Although the thermodynamics is extended afterwards to treat the irreversible process far from equilibrium, this approach is directed to evaluate the entropy production arising from the dissipative structure [6], and does not inquire into the problem how the organism maintains and further strengthens its lower entropy state. This is also the case for the hypercycle proposed by a series of catalytic reactions [7]. Any of these approaches to life lacks the consideration of self-reproduction. The self-reproduction is discussed in terms of automata [8], but the problem of Maxwell's demon is left untouched in this mathematical model.

Recently, the studies of molecular biology have revealed the central dogma in the free-living organism; the proteins are translated from messenger RNAs (mRNAs) by the aid of ribosomal RNAs (rRNAs) and transfer RNAs (tRNAs), and the three kinds of RNAs are all transcribed from the DNA genes, which are replicated upon self-reproduction [9]. These proteins play the respective roles in acquiring the material and energy sources from the outside and in converting them into the biomolecules for the growth and self-reproduction of the organism, according to their specific amino acid sequences. To represent these molecular events in an organism, a new thermodynamic quantity of "biological activity" has been proposed previously [10] [11]. In the present paper, this quantity

will be first outlined again and then shown to be useful for explaining the maintenance and extension of negative entropy in organisms by the evolution through self-reproduction.

2. The Thermodynamic Quantity of Biological Activity

A free-living organism is generally characterized by two internal variables; the size N of its genome (a set of genes) and the systematization S_N of the genome and its products. The systematization is the degree of negative entropy, $-S_N$, which should be measured for the arrangement of deoxynucleotide bases in genes, the arrangement of amino acid residues in the proteins which is transmitted from the genes, the metabolic pathways formed by the catalytic reactions of enzyme proteins, the regulation and control of translation, transcription and replication of DNAs, the cell structure constructed by the intrinsic property of lipid molecules to form a vesicle of lipid bilayer and by the cell wall to support the lipid vesicle, and for furthering the communication between differentiated cells in the case of a multicellular organism.

The energy acquired by such an organism depends on its genome size N and systematization S_N as well as on the material and energy source M available from the environment. Thus, the acquired energy is expressed to be $E_a(M;N,S_N)$, which is an increasing function of N and S_N as well as M. On the other hand, the organism utilizes the material and energy to produce the biomolecules for its growth and self-reproduction. The energy $E_s(N, S_N)$ stored in the biomolecules such as polynucleotides, proteins, lipids and cell wall is also another increasing function of N and S_N. These biomolecules to exhibit biological functions have the higher energy than the inorganic molecules, into which they are finally decomposed, and the energy stored in these biomolecules should be measured in comparison with the energy of the decomposed state. The difference between the acquired energy and the stored energy, $E_a(M;N,S_N) - E_s(N, S_N)$, is released as heat. If the entropy production by the heat compensates for the entropy reduction—S_N due to the systematization, this is consistent with the second law of thermodynamics. In the organism, the acquired energy is transiently trapped in ATP and NADPH molecules as chemical energy, and it is gradually consumed in the syntheses of other biomolecules under the guidance of enzyme proteins without drastic change in temperature T. Thus, the following quantity will be proposed as biological activity BA.

$$BA \equiv E_a(M;N,S_N) - E_s(N,S_N) - TS_N > 0. \quad (1)$$

The positive value of this quantity has been illustrated for simple organisms and also estimated for higher organisms except for the developmental stage of the latter [11]. In the multicellular eukaryotes such as animals and seed plants, the parent endows the egg or seed with the material and energy source and the endowed energy is used for the development of cell differentiation until the cooperative action of differentiated cells begins to acquire the energy and materials from the outside. Thus, BA retains the positive value in such higher organisms

throughout their lifetime if $E_a(M;N,S_N)$ includes the endowed energy. The larger value of BA means that the biological process tends to proceed more smoothly, and this quantity is considered to be proportional to the self-reproducing rate of an organism as the first approximation. The biological activity has the thermodynamic connotation as a departure from equilibrium, but this is in a reverse relation to the well-known "free energy" which decreases upon any change in a given system by the decrease in internal energy and/or the increase in entropy. This is due to the property of the genome that is almost constant during the lifetime of an organism but changes enough to increase the biological activity by the evolution during longer time, as will be shown in the next section.

3. Evolution of Unicellular Organisms

To illustrate simply that organisms maintain and further extend their negative entropy, we consider the behaviour of unicellular organisms that self-reproduce, sometimes mutate, and die. The set of internal variables (N, S_N) of the organism will be simply denoted by a single variable x, unless the description of changes in the genome is necessary. In the population of such organisms taking a common material and energy source M from the outside, the number $n_{xi}(t)$ of i-th variants x_i changes with time t according to the following equation of replicator dynamics.

$$\frac{\mathrm{d}}{\mathrm{d}t}n_{xi}(t)=\left\{Q_{xi}(t)R(M;x_i)-D(x_i)\right\}n_{xi}(t)+\sum_{j(\neq i)}q_{xi,xj}(t)R(M;x_j)n_{xj}(t). \quad (2)$$

Here, the self-reproducing rate and death rate of the variant x_i are denoted by $R(M; x_i)$ and $D(x_i)$, respectively. The apparent decrease factor $Q_{xi}(t)$ for the self-reproducing rate of variant x_i means the mutation of variant x_i to other kinds of variants and is related with the mutation term $q_{xj,xi}(t)$ in the following way.

$$Q_{xi}(t)=1-\sum_{j(\neq i)}q_{xj,xi}(t). \quad (3)$$

The population behaviour becomes transparent by transforming Equation (2) into two types of equations; one concerning the total number $B(t)$ of all kinds of variants defined by

$$B(t)=\sum_i n_{xi}(t). \quad (4)$$

and another concerning the fraction $f_{xi}(t)$ of variants x_i defined by $n_{xi}(t)/B(t)$. By simple calculation, these equations are obtained from Equation (2) to the following forms, respectively, using the relation (3).

$$\frac{\mathrm{d}}{\mathrm{d}t}B(t)=W_{av}(M;t)B(t). \quad (5)$$

and

$$\frac{\mathrm{d}}{\mathrm{d}t}f_{xi}(t)=\left\{W(M;x_{xi})-W_{av}(M;t)\right\}f_{xi}(t)+\sum_j q_{xi,xj}(t)R(M;x_j)f_{xj}(t). \quad (6)$$

Here, $q_{xi,xi}(t)$ is defined by $Q_{xi}(t) - 1$. The increase rate $W(M; x_i)$ of the variant x_i is defined by

$$W(M;x_i) \equiv R(M;x_i) - D(x_i). \tag{7}$$

and the average increase rate of organisms in the population is defined by

$$W_{av}(M;t) \equiv \sum_i W(M;x_i) f_{xi}(t). \tag{8}$$

If the mutation term is the point mutation such as the nucleotide base change in a gene, this only changes S_N in a definite size of genome and the time change in fraction can be evaluated in the following way by the first order of mutation term. When the increase rate of an occasionally arisen mutant x_i is larger than the average increase rate of the population, that is, $W(M; x_i) - W_{av}(M; t) > 0$, the fraction $f_{xi}(t)$ of the mutant x_i increases with time according to the first term on the right side of Equation (6). This raises the average increase rate $W_{av}(M;t)$, resulting in the increase in the total number $B(t)$ of organisms according to Equation (5), although this increase in $B(t)$ is ultimately stopped by the decrease in available material and energy source M. On the other hand, the fraction $f_{xi}(t)$ decreases when $W(M;x_i) - W_{av}(M;t) < 0$. Thus, the organisms taking a common material and energy source M are elaborated by the mutation and above selection, and most of them reach the ones x_{opt} with the optimum increase rate.

This is Darwinian evolution of unicellular organisms. This evolution is first proposed qualitatively to explain the generation of new species from the observation of unique species in a geographically isolated region and of domestic animals and plants [12]. After the discovery of mutants and the rediscovery of Mendelian heredity, Darwinian evolution is mathematically formulated in the population genetics to estimate the probability that a spontaneously arisen mutant is fixed in the population according to its selective parameter value [13] [14]. Although these studies of multicellular organisms have hardly influenced the physical and chemical approaches to life, the present derivation of Darwinian evolution indicates that this evolution converges the nucleotide bases in genes to the special arrangement exhibiting the optimum increase rate and is the essentially important process to maintain the negative entropy of an organism. While RNAs and proteins are continuously transcribed and translated, respectively, to make up for their destruction, the DNA genome also suffers damages, especially in the nucleotide bases. However, such damaged bases are repaired and proofread. By this molecular mechanism, nucleotide bases are substituted with the rate of $u \sim 10^{-9}$ per site per year in both prokaryotes and eukaryotes [15] [16] [17]. The prokaryote carries the genome, whose size s is of the order of 10^6 base pairs (bp) [18], and it only suffers the base changes with the probability of $sut = 10^{-3}$ after one year. During this period, the prokaryote repeats many times of self-reproduction. Thus, most of the descendants retain the original genome and only a small fraction of descendants receive changed bases. Among the descendants receiving changed bases, some show the higher increase rate while the others are defective or selectively neutral, and the ratio of the former to the latter

decreases in the mature population. It depends on the environment what arrangement of nucleotide bases in genes is the best one, and the new species are generated in Darwinian evolution by geographical isolation and/or climate change. This is essentially the same for the multicellular diploid eukaryotes discussed in the last section, although the reproduction of these eukaryotes through hybridization makes the evolutionary process somewhat complicated.

The gene and genome sequencing started in the latter half of last century has brought new information about the evolution of organisms. The amino acid sequence similarities of paralogous proteins strongly suggest that the repertoire of protein functions has been expanded by gene duplication and by the succeeding changes in the counterpart of duplicated genes due to the nucleotide base changes, partial deletion and/or insertion, and domain shuffling [19] [20] [21] [22]. For the theoretical formulation of this evolution by gene duplication, the concept of biological activity is especially useful, and this evolution is also derived from Equation (6) as far as the unicellular organisms are concerned. The gene duplication enlarges the genome size to $N + \Delta N$. This increases the stored energy to $E_s\left(N+\Delta N, S_N\right)$, while the value of acquired energy $E_a\left(M; N+\Delta N, S_N\right)$ is almost the same as that of $E_a\left(M; N, S_N\right)$. Thus, the biological activity of the variant having experienced gene duplication is first lowered than that of the original style organism, especially when the counterpart of duplicated genes loses the original function by its change in nucleotide bases. However, such variants are not necessarily compelled to extinction but can exist as minor members in the population. Moreover, new function(s) can arise from such a changing gene. If the product(s) of such new gene(s) become suitable for the variant to acquire a new material and energy source L and/or the ability of moving to a new area, the acquired energy $E_a\left(L; N+\Delta N, S_{N+\Delta N}\right)$ turns to increase, overcoming the increase in systematization from S_N to $S_{N+\Delta N}$ as well as the increased stored energy $E_s\left(N+\Delta N, S_{N+\Delta N}\right)$. Thus, a new style organism appears with the recovered biological activity
$E_a\left(L; N+\Delta N, S_{N+\Delta N}\right) - E_s\left(N+\Delta N, S_{N+\Delta N}\right) - TS_{N+\Delta N}$.

For formulating mathematically the above evolutionary route, the fraction of variants with the lower increase rate has to be considered more accurately than in Darwinian evolution, after the organisms x_{opt} become dominant in the population, because the gene duplication occurs less frequently than the nucleotide base change. For this purpose, Equation (6) will be formally integrated with respect to time *t*, *i.e.*,

$$f_{xi}(t) = \exp\left[\int_0^t \left\{W\left(M; x_i\right) - W_{av}\left(M; \tau\right)\right\} \mathrm{d}\tau\right] \left[\int_0^t \sum_j q_{xi,xj}(\tau) R\left(M; x_j\right) f_{xj}(\tau) \exp\left[-\int_0^\tau \left\{W\left(M; x_i\right) - W_{av}\left(M; \tau'\right) \mathrm{d}\tau'\right\}\right] \mathrm{d}\tau + f_{xi}(0)\right] \tag{9}$$

Among the fractions $f_{xi}(t)$'s in this expression, we focus on the fraction $f_{xi1}(t)$ of the variants x_{i1}, which have arisen from the dominant organism x_{opt} by the duplication of one kind of gene. Then, the average increase rate, $W_{av}(M; \tau)$ and

$W_{av}(M; \tau)$, is approximated to be $W(M, x_{opt})$ and the fractions of other variants expect for x_{opt} are neglected on the right side of Equation (9). The mutation term $q_{xi1,xopt}(\tau)$ is averaged over a sufficiently long time to be regarded as the rate of gene duplication;

$$q_{xi1,xopt} = \frac{1}{t}\int_0^t q_{xi1,xopt}(\tau)\,\mathrm{d}\tau. \tag{10}$$

This quantity $q_{xi1,xopt}$ is used as the occurrence rate of gene duplication. Even in this large time scale, the fraction $f(x_{i1})$ of variants x_{i1} is present with the following relation to the fraction $f(x_{opt})$ of dominant organisms x_{opt} as a semi-stationary state.

$$f(x_{i1}) = \frac{q_{xi1,xopt}R(M;x_{opt})}{W(M;x_{opt}) - W(M;x_{i1})} f(x_{opt}) \tag{11-1}$$

The fraction $f(x_{i2})$ of the variants x_{i2}, which have further experienced the second kind of gene duplication, is also obtained from Equation (9). By focusing on the mutation term $q_{xi2,xi1}(\tau)$ of $f_{xi1}(\tau)$ on the right side of this equation, the fraction $f(x_{i2})$ of variants x_{i2} is shown to be related with the fraction $f(x_{i1})$ in the following way.

$$f(x_{i2}) = \frac{q_{xi2,xi1}R(M;x_{i1})}{W(M;x_{opt}) - W(x_{i2})} f(x_{i1}) \tag{11-2}$$

By repeating the similar procedure, the fraction $f(x_{in})$ of variants x_{in}, which have experienced n kinds of gene duplication, is obtained as

$$f(x_{in}) = \frac{q_{xin,xin-1}R(M;x_{in-1})}{W(M;x_{opt}) - W(x_{in})} f(x_{in-1}). \tag{11-n}$$

A new style of organisms y can appear from such a minor member x_{in} by changing the counterparts of n kinds of duplicated genes into new genes. When this change probability is denoted by $q_{y,xin}$, the probability $P_n(y \leftarrow x_o)$ that a new style organism y appears from the original style organism x_o is expressed as

$$P_n(y \leftarrow x_o) = q_{y,xin}\prod_{m=1}^{n}\frac{q_{xim,xim-1}R(M;x_{im-1})}{W(M;x_o) - W(M;x_{im})}. \tag{12}$$

Here, x_{opt} in Equations (11-1) - (11-n) is replaced by x_o *or* x_{io}, with the meaning of original.

If the new style organisms y are elaborated to utilize the material and energy source M more efficiently by Darwinian evolution, they compel the original style organisms x to be extinct. If the new style organisms y utilize a new material and energy source L other than M, on the contrary, they form a new population, where the fraction $f_{yk}(t)$ of variant y_k obeys the following equation, apart from the population of original style organisms x_i in Equation (6).

$$\frac{\mathrm{d}}{\mathrm{d}t} f_{yk}(t) = \left\{W(L;y_k) - \overline{W}(t)\right\} f_{yk}(t) + \sum_l q_{yk,yl}(t)R(L;y_l) f_{yl}(t). \tag{13}$$

Here, the average increase rate of new and original styles of organisms is de-

fined by

$$\overline{W}(t) \equiv \sum_i W(M; x_i) f_{xi}(t) + \sum_k W(L; y_k) f_{yk}(t). \tag{14}$$

and the total number $B(t)$ of new and original style organisms obeys

$$\frac{\mathrm{d}}{\mathrm{d}t} B(t) = \overline{W}(t) B(t). \tag{15}$$

This divergence of new and original styles of organisms can occur without geographical isolation and/or climate change. Generally, the material and energy sources L and M are not completely independent to each other but are connected through the circular flow of materials in the global scale. This gives the fundamentals for forming an ecological system, which is also considered to be the systematization of organisms and environment [23].

The evolution by gene duplication is investigated systematically at the molecular level about the O_2-releasing photosynthesis and O_2-respiration in eubacteria, which produce the circular flow of oxygen molecules. In addition to the amino acid sequence similarities of the proteins constituting these systems to the ubiquitous proteins [24], the intermediate stages of eubacteria on the way to the photosynthesis and O_2-respiration are also detected [25]. This suggests that the evolution by gene duplication in prokaryotes has taken place in a relatively stepwise manner, *i.e.*, the suffix n of the probability (12) is a small number and the process from Equation (6) to Equation (13) has been repeated to accomplish the O_2-releasing photosynthesis and O_2-respiration [26]. The above mathematical formulation also holds for the evolution of chemical syntheses in other prokaryotes and for the evolution of unicellular eukaryotes. The evolution of organisms before and after the unicellular organisms in the DNA-RNA-protein world will be discussed in the next section.

4. Conclusions and Discussion

In an organism, the entropy production due to the heat released from the difference between acquired energy and stored energy compensates for the negative entropy, which is so designed as to self-reproduce itself by the special arrangement of nucleotide bases in DNA genes. This is realized by the difference in stability and function between DNAs, RNAs and proteins. These molecular events in such an organism are represented by a thermodynamic quantity of biological activity. This quantity more directly reflects the genome change in an organism than the "characters" such as shape, colour, size etc. used customarily in evolutionary biology and the change in this quantity is the better measure to formulate any type of evolutionary process of organisms. The negative entropy in an organism is maintained through the selection of self-reproduced organisms. Moreover, the organisms have the potential to extend the range of negative entropy, even if their increase rate is transiently lowered. This is illustrated for unicellular organisms in the present paper, using the concept of biological activity and the equation of replicator dynamics containing the mutation terms. This

concept and the equation are specific to the organism, and they correspond to the answer to the opinion (B) among the three opinions summarized by Brillouin [3].

The present mathematical formulation of self-reproducing unicellular organisms also has a possibility to explain the origin of genes. Although the RNA replicase has been proposed as the start of life [27], various organic compounds including nucleotides and amino acids would have been synthesized non-biologically when the RNA replicase appeared. Some satellite variants of RNA replicases would have catalyzed the polymerization of amino acids as primitive rRNA and tRNA [9] [28]. Even if several amino acids are only polymerized at this stage, the random sequences of amino acid residues amount to enormously many kinds of polypeptides. When five of 20 kinds of amino acids are randomly polymerized, for example, 20^5 kinds of polypeptide chains are yielded and they sufficiently cover the active centres of enzyme proteins in a free living organism at the present time. By the catalytic reactions of these polypeptides, therefore, it is plausible that primitive cells are formed and self-reproduce in the following way, as inferred from the relation between lipid synthesis and the cell wall construction in the prokaryote [29] [30] [31] [32]. 1) First, lipid synthesis occurs to form intrinsically lipid vesicles each containing the polynucleotides and polypeptides to synthesize lipids and cell wall elements. 2) The cell wall elements synthesized within the vesicle are then transported to the outside across the lipid bilayer and form the cell wall network by the catalytic activity of the polypeptides on the outer surface of the vesicle. 3) When the lipid synthesis progresses faster than the enlargement of cell wall, the density of lipid bilayer becomes gradually higher to prevent the newly synthesized cell wall elements from passing through the lipid bilayer of the vesicle, resulting in the increase in the concentration of lipids and cell wall elements within the vesicle. 4) Thus, the division of the vesicle occurs spontaneously to lower the free energy by increasing the ratio of surface to volume. The density of lipid bilayer is lowered in each of divided vesicles, and this again makes it possible for the cell wall elements to be transported to the outside. 5) The network of cell wall is newly constructed especially in the interspace between the divided vesicles to be connected with the old area of the network distant from the interspace but the old area of cell wall outside the newly constructed cell wall is finally broken to separate the divided vesicles each covered with cell wall, because this area is far from the polypeptides catalysing the connection of cell wall elements on the respective surfaces of divided vesicles.

Such self-reproducing proto-cells also obey the equation of replicator dynamics with the following mutation terms. If the first formed proto-cells are specified by x_i's on their RNA contents, these RNA contents would have changed upon their replication by the primitive RNA polymerase as well as RNA replicase activity. Thus, most of proto-cells are elaborated to x_{opt} by Darwinian evolution, especially with respect to the primitive rRNA and tRNAs to catalyze the polym-

erization of amino acids. However, this evolution increases the concentration of primitive RNA polymerases and thus increases the concentration of non-functional RNAs in the cell. This yields the variant proto-cells x_{i1}, in which the increased non-functional RNAs interfere with the primitive tRNAs and rRNAs by the hydrogen bonds transiently formed between their nucleotide bases. Such variant cells are declined to the minor members in the population but produce the translation apparatus after the following steps of variation. A part (anticodon) of tRNA originally embracing the side chain of amino acid residue alternatively attaches to the complementary bases in non-functional RNAs which become later the codon of RNA genes of proteins. Such ancestral RNA gene then comes into the contact with the other type of RNAs which become later the initiation complex. The primitive rRNA is enlarged to form the sites for the successive acceptance of amino acid residues carried by tRNAs aligned on ancestral genes of proteins. After the above series of variant cells, x_{i2}, x_{i3}, $\cdots$, x_{in}, a new style of self-reproducing cells, in which *L*-type of amino acids are polymerized according to the sequence of codons in ancestral RNA genes, appear with the probability such as Equation (12). In this new style of cells, the polymerization rate of amino acids is raised in comparison with the random collision of charged tRNA and primitive rRNA, and the substituted bases in the ancestral RNA genes are selected so as to encode the proteins for raising the increase rate of the cell by Darwinian evolution, compelling the original proto-cells x_o to be extinct.

The deoxidization of RNAs would have then occurred in some of such new style cells that began the glycolysis releasing protons. The DNAs thus generated would have been first rubbish and decreases the increase rate of such variant cells. If the optimum RNA content of the self-reproducing cell with the translation apparatus is rewritten into x_{opt}, the internal variable of the variant cell suffering deoxidization corresponds to x_{i1}. For utilizing the DNAs as genes, the variant cells x_{i1} must have further experienced the succeeding steps of variation x_{i2}, x_{i3}, $\cdots$, x_{in} to induce the genes of proteins for the transcription and replication of DNAs as well as of auxiliary proteins for the unwinding of double-stranded DNAs. Such induction of DNA-associated genes from the RNA-associated genes is suggested from the fact that DNA-dependent DNA polymerases and RNA polymerases form a protein superfamily together with the RNA-dependent RNA polymerases in RNA viruses [33] and that the DNA helicases show the similarities to RNA helicases in a superfamily [34] [35]. After the parallel usage of RNA genes and DNA genes, the decisive turning point for the variant cells x_{in} to enter the DNA-RNA-protein world would have been the direct or indirect attachment of DNAs under replication to the cytoplasmic membrane in cooperation with the cell division. This mechanism not only makes the cell division mechanical but also makes it possible for the replicated DNAs to be equi-partitioned into daughter cells. In the case of direct attachment to the membrane, the DNA genes are gradually fused to a single circular molecule,

leading to the appearance of ancestral prokaryote. On the other hand, DNA genes in the ancestral eukaryote get together to the plural number of chromosomes and each of chromosomes under replication is attached to the membrane through contractive microtubules. In this innovation, the probability $P_n\left(y \leftarrow x_o\right)$ in Equation (12) is divided into $P_n\left(y_p \leftarrow x_o\right)$ and $P_n\left(y_e \leftarrow x_o\right)$ where y_p and y_e denote the prokaryotic and eukaryotic styles of DNA genomes, respectively. Accordingly, Equation (13) of fraction $f_{yk}(t)$ is also divided into the equation of fraction $f_{ypk}(t)$ and that of fraction $f_{yek}(t)$.

In fact, the analyses of neutral base changes in rRNAs reveal that all free-living organisms are traced back to the ancient divergence of prokaryote and eukaryote, probably occurred 4×10^9 years ago [36] [37]. Among them, the prokaryote has first diverged to evolve chemical syntheses, photosynthesis and O_2-respiration [37]. During this period, the ancestral eukaryote probably lived as the predator of prokaryotes, evolving nuclear membrane, endocytosis and exocytosis. Such living style and cell structure have made it possible for the eukaryote to acquire the mitochondria as the endosymbionts of O_2-respiratory eubacteria around 1.8×10^9 years ago [37] and to acquire further photosynthetic plastids as the endosymbionts of cyanobacteria [38]. Some of such eukaryote-shaving acquired endosymbionts have then evolved multicellularity and cell differentiation, especially in green plants and animals whose divergence is estimated to have occurred around 1.2×10^9 years ago [16] [39]. These multicellular organisms have further evolved to take the diploid state through the intermediate stages of alternating the monoploid generation with the diploid one. This is due to the following situation. Although the cooperative action of differentiated cells is a powerful strategy to raise the acquired energy and to spread the living area of the organisms, the genome of each cell in the multicellular organism is expanded to 10^8 bp or more, e. g., ~10^8 bp in *Arabidopsis* and *Drosophila*, 3×10^9 bp in *Homo sapience* and ~10^{10} bp in *Taxodials*, while 1.2×10^7 bp in the unicellular *Saccharomyces* [18]. Nevertheless, the duration time of differentiated cells has to be elongated against nucleotide base changes to exhibit the cooperative action effectively. In the diploid cell, it suffers serious influence only when base substitutions occur concurrently at homologous sites. Thus, the diploid eukaryote consisting of N cells retains the following number of cells not suffering base substitutions at any pair of homologous s sites in their genome during time t; $N\left\{1-(ut)^2\right\}^s \sim N\left\{1-s(ut)^2\right\}$. For example, this number is calculated to be $N(1-10^{-5})$ even during one hundred years for the genome size $s = 10^9$ bp using $u = 10^{-9}$ per site per year. The life-times of these multicellular diploid eukaryotes seem to be secondarily regulated within the duration time estimated from the genome size, because they are considerably different even between closely related species. If the base substitution rate became slower, the cell differentiation would have more evolved in the monoploid state. However, much more energy than that for taking the diploid state is required for the increase in the times of proofreading to lower the substitution rate [40]. The multicellular diploid eu-

karyotes produce the children by the combination of egg and sperm (fertilization). This way of reproduction not only decreases the fraction of children receiving defective nucleotide bases homologously but also yields the descendants receiving various combinational sets of new genes generated from gene duplication in different lineages of parents, causing the explosive divergence on the way to establish the respective new genes [41] [42] [43]. This explains the punctuated mode of explosive divergence of body plans in animals, which is first pointed out by paleontology [44] [45] [46] and then ascertained to have occurred during the period of $12\sim4 \times 10^8$ years ago by the study of molecular evolution [47].

While the organisms in the DNA-RNA-protein world have evolved overcoming the decrease in organic compounds synthesized non-biologically, the organisms in the RNA-protein world would have turned to utilize the translation apparatus as well as nucleotides and amino acids in the prokaryotes and eukaryotes, and survive as RNA phages and viruses under the common codon usage. In this connection, it should be noted that the biological activity is degenerate, that is, almost the same strength of biological activity can be attained by either a small genome, low systematization and a small amount of acquired energy or a large genome, high systematization and a large amount of acquired energy.

Conflicts of Interest

The author declares no conflicts of interest regarding the publication of this paper.

References

[1] Maxwell, J.C. (1871) Theory of Heat. Longmans, Green, and Company, London, New York and Bombay, 328.

[2] Szilard, L. (1929) *Zeitschrift für Physik*, **53**, 840-856. https://doi.org/10.1007/BF01341281

[3] Brillouin, L. (1949) *American Scientist*, **37**, 554-568.

[4] Brillouin, L. (1951) *Journal of Applied Physics*, **22**, 334-337. https://doi.org/10.1063/1.1699951

[5] Schrödinger, E. (1945) What Is Life? Cambridge University Press, London and The Macmillan Company, New York.

[6] Prigogine, I. (1967) Introduction to Thermodynamics of Irreversible Process. 3rd Edition, Interscience Publishers, A Division of John Wiley & Sons, New York, London, Sydney.

[7] Eigen, M. and Schuster, P. (1977) *Naturwissenschaften*, **64**, 541-565. https://doi.org/10.1007/BF00450633

[8] Von Neumann, J. (1966) Theory of Self-Reproducing Automata. The University of Illinois Press, Chicago, IL.

[9] Watson J.D., Hopkins, N.H., Roberts, J.W., Steitz, J.A. and Weiner, A.M. (1987) Molecular Biology of the Gene. Volumes I and II. 4th Edition, The Benjamine/Cumming Publisher Company, California.

[10] Otsuka, J. (2008) *Journal of Theoretical Biology*, **255**, 129-136. https://doi.org/10.1016/j.jtbi.2008.07.006

[11] Otsuka, J. (2017) *Journal of Physical Chemistry & Biophysics*, **7**, 1-6.

[12] Darwin, C. (1859) The Origin of Species. John Murry, London.

[13] Fisher, R.A. (1930) General Theory of Natural Selection. Oxford University Press, London, New York.

[14] Wright, S. (1949) Adaptation and Selection. In: Jepson, G.L., Simpson, G.G. and Mayer, E., Eds., *Genetics*, *Paleontology and Evolution*, Princeton University Press, Princeton, New Jersey, 365-389.

[15] Kimura, M. (1980) *Journal of Molecular Evolution*, **16**, 111-120. https://doi.org/10.1007/BF01731581

[16] Otsuka, J., Nakano, T. and Terai, G. (1997) *Journal of Theoretical Biology*, **184**, 191-186. https://doi.org/10.1006/jtbi.1996.0277

[17] Sugaya, N. and Otsuka, J. (2002) *Journal of Molecular Evolution*, **55**, 584-594. https://doi.org/10.1007/s00239-002-2354-9

[18] Wheeler, D.L., Church, D.M., Edgar, R., Federhen, S., Helmberg, W., *et al.* (2004) *Nucleic Acids Research*, **32**, D35-D40.

[19] Ingram, V.M. (1963) The Haemoglobin in Genetics and Evolution. Columbia Press, New York.

[20] Ohno, S. (1970) Evolution by Gene Duplication. Spring-Verlag, Berlin. https://doi.org/10.1007/978-3-642-86659-3

[21] Gilbert, W. (1978) *Nature*, **271**, 501. https://doi.org/10.1038/271501a0

[22] Ferris, S.D. and Witt, G.S. (1979) *Journal of Molecular Evolution*, **12**, 267-317. https://doi.org/10.1007/BF01732026

[23] Otsuka, J. (2004) *Ecological Complexity*, **1**, 237-252. https://doi.org/10.1016/j.ecocom.2004.04.002

[24] Otsuka, J. (2002) *Recent Research Developments in Proteins*, **1**, 229-256.

[25] Otsuka, J. and Kawai, Y. (2006) *Trends in Photochemistry & Photobiology*, **11**, 1-21.

[26] Otsuka, J. (2017) *Physical Science & Biophysics Journal*, **1**, 105-114.

[27] Cech, T.R. (1986) *Proceedings of National Academy of Sciences USA*, **83**, 4360-4363. https://doi.org/10.1073/pnas.83.12.4360

[28] Weiner, A.M. and Maizels, N. (1987) *Proceedings of National Academy of Sciences USA*, **84**, 7383-7387. https://doi.org/10.1073/pnas.84.21.7383

[29] Botta, G.A. and Park, J.T. (1981) *Journal of Bacteriology*, **145**, 333-340.

[30] Begg, K.J. and Donachie, W.D. (1985) *Journal of Bacteriology*, **163**, 615-622.

[31] Cooper, S. (1988) *Journal of Bacteriology*, **170**, 422-430. https://doi.org/10.1128/jb.170.1.422-430.1988

[32] Otsuka, J. (2001) *Research Communications in Biochemistry, Cell and Molecular Biology*, **5**, 49-73.

[33] Otsuka, J., Kikuchi, N. and Kojima, S. (1999) *Biochimica et Biophsica Acta*, **1434**, 221-247. https://doi.org/10.1016/S0167-4838(99)00187-9

[34] Bork, P. and Koonin, E.V. (1993) *Nucleic Acid Research*, **21**, 751-752. https://doi.org/10.1093/nar/21.3.751

[35] Pyle, A.M. (2008) *Annual Review of Biophysics*, **37**, 317-336. https://doi.org/10.1146/annurev.biophys.37.032807.125908

[36] Woese, C.R. (1987) *Microbiological Reviews*, **51**, 221-271.

[37] Otsuka, J., Terai, G. and Nakano, T. (1999) *Journal of Molecular Evolution*, **48**, 218-235. https://doi.org/10.1007/PL00006461

[38] Van den Eynde, H., De Baere, R., De Roeck, E., van de Peer, Y., Vandenberk, A., *et al.* (1988) *Journal of Molecular Evolution*, **27**, 126-132. https://doi.org/10.1007/BF02138372

[39] Dickerson, R.E. (1971) *Journal of Molecular Evolution*, **1**, 26-45. https://doi.org/10.1007/BF01659392

[40] Hopfield, J.J. (1974) *Proceedings of National Academy of Sciences USA*, **71**, 4135-4139. https://doi.org/10.1073/pnas.71.10.4135

[41] Otsuka, J. (2011) *Journal of Theoretical Biology*, **278**, 120-126. https://doi.org/10.1016/j.jtbi.2011.03.006

[42] Otsuka, J. (2011) A Theoretical Scheme of the Large-Scale Evolution by Generating New Genes From Gene Duplication. In: Friedberg, F., Ed., *Gene Duplication*, In-Tech, Croatia, 3-26. https://doi.org/10.5772/22618

[43] Otsuka, J. (2014) *Advances in Genetics Research*, **11**, 85-116.

[44] Gould, S.J. (1989) Wonderful Life. The Burgess Shale and the Nature of History. W. W. Norton & Company Inc., New York.

[45] Rozanov, A.Y. and Zhuravlev, A.Y. (1992) The Lower Cambrian Fossil Record of the Soviet Union. In: Lipps, J.H. and Signor, P.W., Eds., *Origin and Early Evolution of Metazoa*, Plenum Press, New York, London, 205-282. https://doi.org/10.1007/978-1-4899-2427-8_7

[46] Rassmussen, B., Bengtson, S., Fletcher, I.R. and McNaughton, N.J. (2002) *Science*, **296**, 1112-1115. https://doi.org/10.1126/science.1070166

[47] Otsuka, J. and Sugaya, N. (2003) *Journal of Theoretical Biology*, **222**, 447-460. https://doi.org/10.1016/S0022-5193(03)00057-2

Journal of Modern Physics, 2018, 9, 2170-2192
http://www.scirp.org/journal/jmp
ISSN Online: 2153-120X
ISSN Print: 2153-1196

Discovery & Proofs of a Nucleus of Mass and Charge in the Photons/Quantum Particles

Narendra Swarup Agarwal

Gurgaon, India
Email: nsagarwal@gmail.com

How to cite this paper: Agarwal, N.S. (2018) Discovery & Proofs of a Nucleus of Mass and Charge in the Photons/Quantum Particles. *Journal of Modern Physics*, **9**, 2170-2192.
https://doi.org/10.4236/jmp.2018.912137

Received: August 30, 2018
Accepted: October 12, 2018
Published: October 15, 2018

Copyright © 2018 by author and Scientific Research Publishing Inc.
This work is licensed under the Creative Commons Attribution International License (CC BY 4.0).
http://creativecommons.org/licenses/by/4.0/

Open Access

Abstract

This work discovers and proves that all the photons/quantum particles have a "**Nucleus of mass and charge.**" The nucleus is located off-center in the particles. ***The constructive, destructive and intermediate Interference phenomena decisively discover and prove the presence of only one nucleus of the mass located off-center in a photon, like an atomic nucleus.*** The mass in the nucleus of a photon develops varying forces to move the photon as a wave. The Wave-Particle Duality is the most significant proof of such a nucleus of mass. The formation of an electromagnetic wave by a photon proves the presence of a charge in the nucleus of the photon. The Quantum Theory, developed about 100 years back, simplified the understanding of matter and energy at the atomic/subatomic levels. However, the Quantum Theory remains incomplete and cannot explain even a single quantum phenomenon. The New Quantum Theory, developed in the year 2012, is based on the similarity of an atomic nucleus as well as the solar system with the Sun as its nucleus of the mass and the charge. The New Quantum Theory explains all the Quantum Phenomena and matches with the Classical Mechanics as well as the Theory of Electromagnetism. The experiments described in this work, using high precision instruments, determine the mass, the charge and the diameter of a photon/quantum particle.

Keywords

Nucleus, Off-Center Location, Mass, Acceleration, Force and Charge

1. Introduction

Everything around us consists of very tiny atoms. Every atom has a nucleus of the mass > 99.9% occupying only negligibly small volume. The nucleus of an atom is not in the center of the atom but located off-center. Similarly, the solar system has the Sun as its nucleus having >99.86% mass and occupying only neg-

ligibly small volume. The solar system also has the Sun in the off-center position. The Sun is the most significant source of electromagnetic radiations.

Based on the above facts of nature, **the New Quantum Theory [1] states:**

"A photon/quantum particle has a nucleus of the mass and the charge located off-center."

A nucleus of the mass and the charge, located off-center in the spinning photon/quantum particle, bestows unique characteristics and displays strange behaviours. ***This constitutional essence of a photon/quantum particle explains not only the Wave-Particle Duality but all the Quantum Phenomena and completes the Quantum Theory.***

The New Quantum Theory can also explain the phenomenon such as "Raman Effect" with the additional information about the external forces (varying forces in the molecular bond of a compound). The "**Multiple Slits in Series**" experiments describe the procedure to determine the mass, the charge and the diameter of a photon. The physical energies of a photon calculate the mass of the photon by the formula $m = af$ where "a" is a constant.

Unlike the Quantum Theory which does not match with the Classical Mechanics, the New Quantum Theory is consistent with the Classical Mechanics as well as the Theory of Electromagnetism. Moreover, the New Quantum Theory can also predict the interactions of the photons/quantum particles with other objects at the quantum level for the new developments in the scientific and commercial segments including the improvements in the PV cells.

2. Hidden Mysteries of the Photons

All the photons/quantum particles display mysterious phenomena known for the last several centuries. For these fundamental particles, only nature provides the hints to solve their mysteries.

A mysterious particle of the photon has its mysteries hidden inside. The following characteristics of the photons and their analysis discover the mysteries hidden within a photon:

- A photon never travels in a straight line; it moves like a helix/a smooth space curve in all the three planes or as a wave in a single two-dimensional plane.
- A photon travels with an average speed of light in the direction of its travel, irrespective of its frequency and the amplitude of the wave it forms.
- A photon always spins in one plane only. This plane does not change unless and until an external force or object interacts with the photon. A polarised photon keeps on spinning in the same plane and can travel hundreds of light years.
- A photon continuously changes its velocity and the direction to move as a wave without any external force. Whereas, according to Newton's laws of motion, a force is necessary to change the velocity and the direction of a particle.
- Therefore, a photon must develop the "**Internal Forces**" from within in all the 3 X, Y & Z-directions to form a helix or the forces only in 2-directions to form a wave in a single two-dimensional plane.

- The magnitudes of these internal forces in the different directions change continuously with the spin of the photon to move the photon as a wave.
- A mass generates the force on acceleration. For a photon to generate variable internal forces, it must have a "mass" along with accelerations in the different directions.
- Since the mass of the photon is constant, the acceleration/deceleration in the different directions must vary continuously to generate variable internal forces in the different directions to move the photon as a wave.
- A spinning photon with uniformly distributed mass or the mass in the center cannot develop internal forces to move the photon as a wave.
- However, if a photon has its mass in an off-center position, the mass rotates at a constant linear speed with the spin of the photon around the center of the photon. The continuous rotation of the mass develops acceleration/deceleration in the different directions continuously.
- Therefore, the mass in the spinning photon experiences variable accelerations/decelerations and develops variable internal forces in the different directions.
- ***Only the presence of a mass, located off-center in a photon, develops the variable forces in the different directions by accelerating/decelerating with the spin of the photon. These internal forces, created by the mass of a photon, move the photon as a wave.***
- Similarly, a charge located off-center in the spinning photon accelerates/decelerates and generates the electric and the magnetic fields of the varying intensities and directions to form an electromagnetic wave.
- Both the mass and charge coexist in a so-called nucleus located off-center in the photon. There is nothing unique about the existence of such a nucleus in the photons; all the atoms have a similar nucleus of the mass and the charge.
- Similarly, all the quantum particles must also have a nucleus of the mass and the charge located off-center. An electron has a definite mass, always moves as a wave and forms an electromagnetic wave due to its charge. ***An electron has to have both the mass and the charge located off-center in a nucleus to travel as a wave and generate a3 dimensional electromagnetic wave.***
- A photon/quantum particle spins in the plane consisting the circular path of the nucleus and the center of the photon. The nucleus of the mass and the charge rotates in this plane only.
- It appears that all the tiny particles in the universe have a nucleus of the mass and the charge located off-center. Exceptions, if any, are rare.

The above peculiarities of a photon indicate the presence of a nucleus of the mass and the charge located off-center in the photon, as stated in the New Quantum Theory.

Figure 1 shows a spinning photon as a yellow sphere with a small nucleus of mass and charge located off-center as a red sphere along with an enlarged view of the central photon. As the photon spins, the nucleus rotates in a circular path around the center of the photon. At the origin (0, 0), the nucleus is at 0˚ from

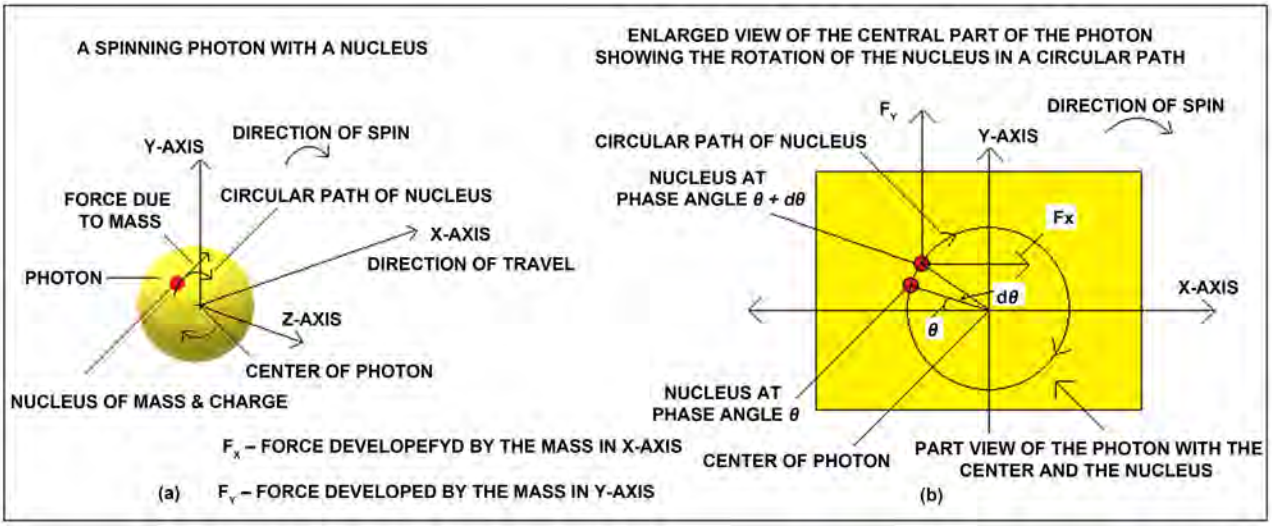

Figure 1. Shows a spinning photon as a yellow sphere with a small nucleus of mass and charge located off-center as a red sphere. As the photon spins, the nucleus rotates in a circular path around the center of the photon. **Figure 1(a)** shows a complete photon, and **Figure 1(b)** shows an enlarged view of only the central part of the photon with a red nucleus rotating around the center of the photon from the phase angle (θ) to ($\theta + d\theta$) in time (dt). The phase angle (θ) of the nucleus (or the photon) is the angular position of the nucleus in the photon from X-axis with center of the photon as reference.

the direction of travel of the photon (X-axis) with center of the photon as the reference point. The phase angle or the angular position of the nucleus from the X-axis increases from 0˚ to 360˚ with the spin of the photon in a single wave cycle. From 360˚, the next cycle of the wave of the photon starts again from 0˚. **Figure 1(a)** shows a complete photon, and **Figure 1(b)** shows an enlarged view of only the central part of the photon with a red nucleus rotating around the center of the photon from the phase angle (θ) to ($\theta + d\theta$) in time (dt) and developing the accelerations and the forces.

A spinning photon develops the following forces:

a) Mechanical Forces:

If the angle of the nucleus is θ_1 from X-axis and the photon spins from the phase angle θ_1 to $\theta_1 + d\theta_1$ in time dt, the force in X-axis develops as under:

- The circumference of the rotating Nucleus: $2\pi r$
- The linear speed of the rotating Nucleus: $2\pi rf$
- The velocity of the nucleus in the X-axis at phase angle θ_1: $2\pi rf \sin\theta_1$
- The velocity of the nucleus in X-axis at phase angle $\theta_1 + d\theta_1$: $2\pi rf \sin(\theta_1 + d\theta_1)$
- The change in velocity in X-axis in time dt: $2\pi rf\{\sin(\theta_1 + d\theta_1) - \sin\theta_1\}$
- Acceleration in X-axis: $2\pi rf\{\sin(\theta_1 + d\theta_1) - \sin\theta_1\}/dt$
- **The force developed by the mass in the X-axis:**

$$2\pi rfm\{\sin(\theta_1 + d\theta_1) - \sin\theta_1\}/dt \quad (1)$$

If the phase angles of the nucleus in the photon are θ_2 & θ_3 in Y-axis & Z-axis respectively, the mass in the nucleus of the photon develops the following forces:

- **The force developed by the Nucleus:**

$$2\pi rfm\left\{\sin\left(\theta_2+d\theta_2\right)-\sin\theta_2\right\}/dt \quad (2)$$

In the Y-axis

- **The force developed by the Nucleus:**

$$2\pi rfm\left\{\sin\left(\theta_3+d\theta_3\right)-\sin\theta_3\right\}/dt \quad (3)$$

In the Z-axis

where:

- The frequency of the photon: f
- Mass of the photon: m
- The distance of the nucleus from the center: r
- The phase angle of the photon: θ
- Incremental change in phase angle: $d\theta$ degree in time dt

Therefore, the mass in the nucleus of a spinning photon develops the forces of the variable magnitudes in all the three directions. Depending on the phase angle θ, the directions of these forces reverse in each cycle of the wave.

In case of a linearly polarised photon, the forces develop in only two axes. If θ is the phase angle from X-axis, the forces develop as under:

- The force developed by the Nucleus:

$$2\pi rfm\left\{\sin\left(\theta+d\theta\right)-\sin\theta\right\}/dt \quad (4)$$

in the horizontal X-axis

- The force developed by the nucleus:

$$2\pi rfm\left\{\cos\left(\theta+d\theta\right)-\cos\theta\right\}/dt \quad (5)$$

in vertical Y-axis

The velocities, accelerations and the internal forces of the photon in the different directions vary with the values of $\sin\theta$ & $\cos\theta$ in the range between +1 to (−)1 with the spin of the photon from 0˚ to 360˚ to complete one cycle of the wave.

b) Electromagnetic Force:

As a photon spins and moves, the nucleus of the mass and the charge located off-center accelerates/decelerates. Any moving charge generates both the electric as well as the magnetic fields. The charge in the photon generates the electromagnetic force along with the electromagnetic wave with the varying intensities and the changing directions.

A nucleus of the mass & the charge located off-center in a photon/quantum particle generates the mechanical forces as well as the electromagnetic forces.

3. Mass & Energy of the Photons—The Facts & the Myth

THE FACTS:

- The mass and energy always exist together.
- The energy is only the "quantitative property" of a matter. No form of energy can exist without an object of mass. Any form of energy needs an object of mass to hold the energy.
- Similarly, every object of mass has some form of the energy.

- A photon has its mass which is always constant. A photon possesses energy in various physical forms in addition to its mass.
- Planck's equation $E = hf$ relates to the physical forms of energies of a photon.
- The mass of a photon is proportional to its frequency. Equation $m = af$ calculates the "Mass (m)" of the photon of frequency f, where "a" is constant ($a = 1.474499440284 \times 10^{-50}$ kg·sec) [2].
- Einstein's equation $e = mc^2$ relates to the conversion of energy to mass and vice versa involving the nuclear conversion. This energy "e" is in addition to the physical forms of the energy's "E" possessed by the photon. Both the forms of the energies "e" and "E" relate to the different types of the energies.
- The mass of a photon can be calculated theoretically as well as determined by the experiments using high precision instruments.
- A nucleus of the mass and the charge exists in an off-center position and rotates around the center of the spinning photon. The nucleus of the mass and the charge continuously accelerates and decelerates to create the variable mechanical forces and the electromagnetic forces to exhibit all the quantum phenomena.

THE MYTH:

- The Photons have no mass & no charge.

The above myth must go.

4. Theoretical Proofs

All the Quantum Phenomena are the proofs and can only take place if a photon has a "nucleus of mass and charge, located off-center." Some of the important Quantum Phenomena as the proof of the presence of a nucleus of mass and the charge in a nucleus located off-center in the photons are presented below:

4.1. Polarisation Phenomenon

In the polarisation phenomenon, a photon/quantum particle forms a wave in a single two-dimensional plane. The continuously accelerating mass develops forces in a single two-dimensional plane to form a wave by a polarized photon. The following characteristics describe the Polarisation Phenomenon:

- A critical feature of a photon is: "A photon spins only in one plane and continues to spin in the same plane unless it interacts with an external force/object."
- If a photon/quantum particle is a uniform particle with zero mass, there is nothing to restrict the plane of the spin of the photon and the formation of the wave in one single plane only. The photon is always at the liberty to keep on changing the plane of spin and to form the waves in the different planes, in such a case, the polarisation phenomenon for a photon with zero mass cannot take place.
- Only the forces, developed in a single two-dimensional plane by the mass in the nucleus located off-center in a photon/quantum particle, limit the photon particle to form a wave in a single two-dimensional plane and display the pola-

risation phenomenon. The direction of travel of a linearly polarized photon confines in the plane of the circular path of the nucleus/spin of the photon.

- The axis of rotation of the nucleus or the spin of the photon is the same and always perpendicular to the direction of travel of the polarised photon.
- As a polarised photon spins and travels in X-direction, the mass in the nucleus located off-center accelerates/decelerates to develop variable forces only in X & Y-directions. These forces, from within the photon, form a wave in a single two-dimensional plane.
- Figure 2 shows a polarised photon developing the variable forces F_X and F_Y with the spin of the photon to form a wave in a two-dimensional X, Y plane. The one full wave cycle of the photon shows the position of the nucleus as a small red sphere at different phase angles with the spin of the photon starting from 0˚ to 360˚ with an interval of 45˚ along with the magnitudes of the forces F_X and F_Y being indicated by the size of the arrows approximately.
- The electric field wave of a polarised photon forms in a single two-dimensional plane; but the magnetic field wave always forms in the three-dimensional planes.

There are two types of polarisation phenomena:

- **Linear Polarisation Phenomenon:**

Already explained above.

- **Circular Polarisation Phenomenon:**

If the direction of travel of a photon is outside the plane of its spin, the photon is circularly polarised. For a circularly polarised photon, the axis of rotation of the photon is not perpendicular to the direction of travel of the photon.

A circularly polarised photon moves as a smooth curve in three-dimensional space/a helix. The curve may be either clockwise or anticlockwise.

Whereas, the photon spins in the plane consisting the nucleus of the mass and the center of the photon, the circularly polarised photon travels in a direction outside this plane. Therefore, the whole photon along with the nucleus of the mass moves in all the 3 X, Y & Z-directions and creates variable internal forces F_X, F_Y & F_Z in all the X, Y & Z-directions respectively.

These variable internal forces in X, Y & Z-directions move the photon to form a wave in the three-dimensional plane.

The Polarisation Phenomenon discovers and proves the presence of a mass located off-center in a photon.

4.2. Interference

"Interference" is the most critical phenomenon of the Quantum Physics. The Interference phenomenon discovered the Dual Wave-Particle nature of the photon's way back in the year 1801 by the Double Slit experiment.

- The two photons of the same frequency superpose in the different phases to display different types of Interferences with different amplitudes of the resultant waves.

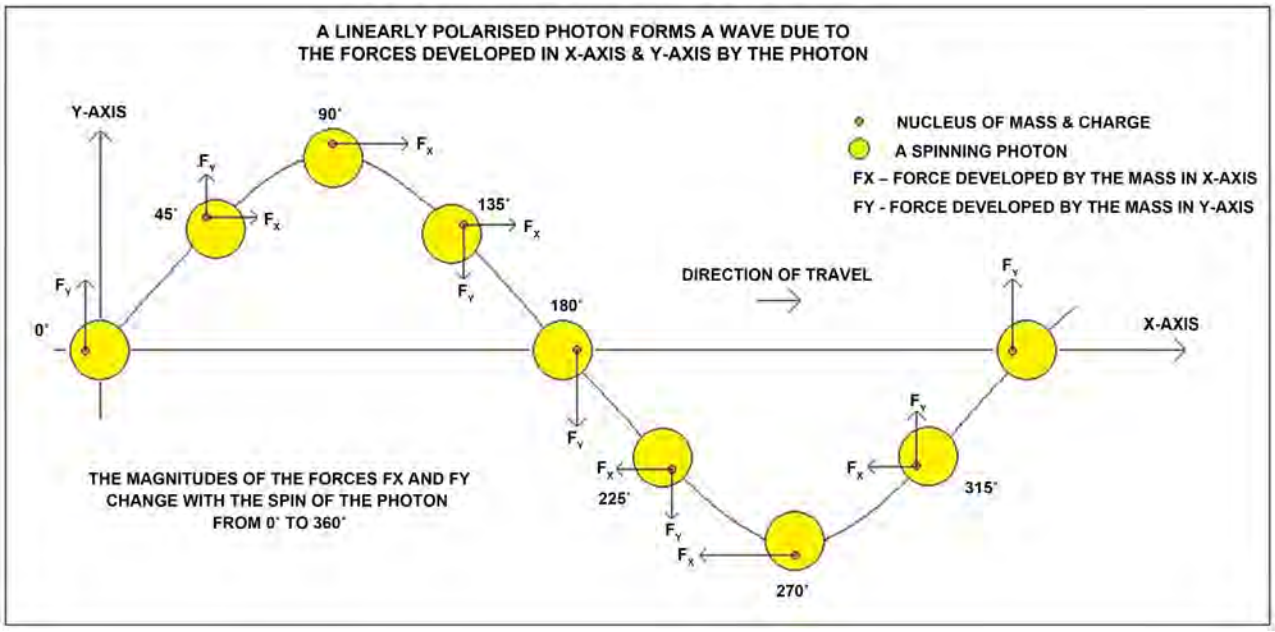

Figure 2. The mass in the nucleus of a spinning photon rotates around the center of the photon and generates forces of varying magnitudes in X-axis as well as Y-axis to form a wave in a single two-dimensional X-Y plane. The wave shows the direction of the forces F_X and F_Y at different phase angles of the photon.

- The phase angle of a photon refers to the angle of its nucleus from the direction of travel (generally, the X-axis) with the center of the photon as the reference. At the start of a new wave cycle or the origin, the phase angle/angular position of the nucleus or the photon is 0˚. As the photon spins, the nucleus of the mass and the charge rotates around the center of the photon, and the phase angle increases from 0˚ up to 360˚ and from the 360˚ a new wave cycle of the photon starts.
- If the photons are uniform particles with no substructure, whatever are their orientations or the phase angles or the degree of spins, all the photons remain identical with no difference. Therefore, all the photons of the same frequency must display the same character/properties in all the 360˚ spins or the phase angles, and the phase angles or the degree of the spin of the photons has no meaning.
- In the above situation of the photons as the uniform particles, the different types of the Interference Phenomena are not possible.
- *The phase angle or the degree of spin of a photon from* 0˚ *to* 360˚ *refers to the angular position of a substructure in the photon.* ***This proves the presence of a substructure in a photon.***
- The 0˚ phase angle of a photon indicates the position of the nucleus (substructure of the photon) at 0˚ angular position from the X-axis with the center of the photon as the reference. At the 0˚, the photon is at the origin (0, 0) or the start point of a new cycle of the wave.
- As the photon spins and forms a wave the nucleus of the mass and the charge located off-center rotates around the center of the photon and the phase an-

gle or the angular position of the nucleus increases from 0˚ to 360˚ in the photon in one wave cycle of the wave.

- The two photons of the same frequency can superpose in the different phases to display different types of the Interference effects.

If the two photons of the same frequency and in the same direction superpose, the two photons can join only in side by side position. Both the superposed photons keep on spinning in their direction of spin and move together. The mass in each photon being close enough, the strong force is applied to keep the superposed photons together. Figure 3 shows the two spinning photons joined side by side.

4.2.1. Constructive Interference

In the Constructive Interference of the two photons, the amplitude of the resultant wave doubles. When the two photons of the same frequency and in the same phase superpose, the angular positions of the nuclei of both the photons are also the same as shown in the part (a) of Figure 4. The mass, in the nucleus of both the photons, accelerates/decelerates and develops the forces of the same magnitude all the time. The force F_Y in the vertical direction, developed by the mass of each photon, adds to double as under:

- The force developed by the nucleus of: $2\pi rfm\{\cos(\theta+d\theta)-\cos\theta\}/dt$
  Photon No. 1 in Vertical Y-axis
- The force developed by the nucleus of: $2\pi rfm\{\cos(\theta+d\theta)-\cos\theta\}/dt$
  Photon No. 2 in Vertical Y-axis
- Total Force developed by the nuclei of: $4\pi rfm\{\cos(\theta+d\theta)-\cos\theta\}/dt$
  Photons 1 & 2 in Vertical Y-axis

If a photon has zero mass, it cannot develop any force to double the amplitude.

Only the presence of a mass in each photon generates the vertical forces in both the photons to double the amplitude. The phenomenon of Constructive Interference' with the double amplitude of the resultant wave discovers and proves: "*A Photon has Mass.*"

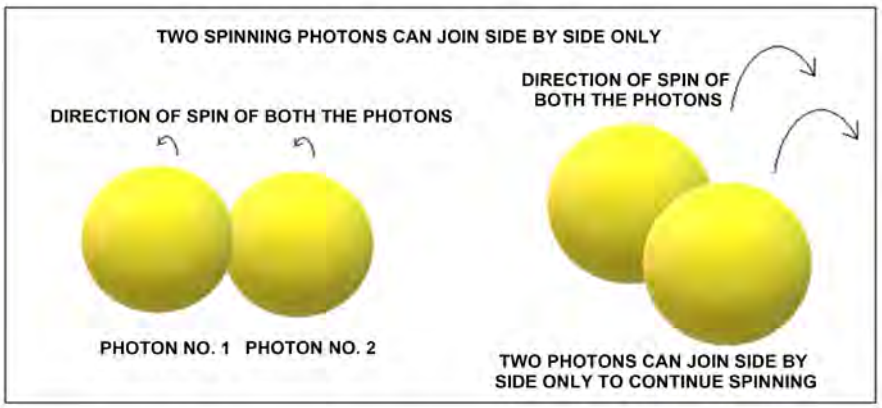

Figure 3. Two same frequency spinning photons moving in the same direction can join in side by side position only so that both the photons continue spinning in the same direction.

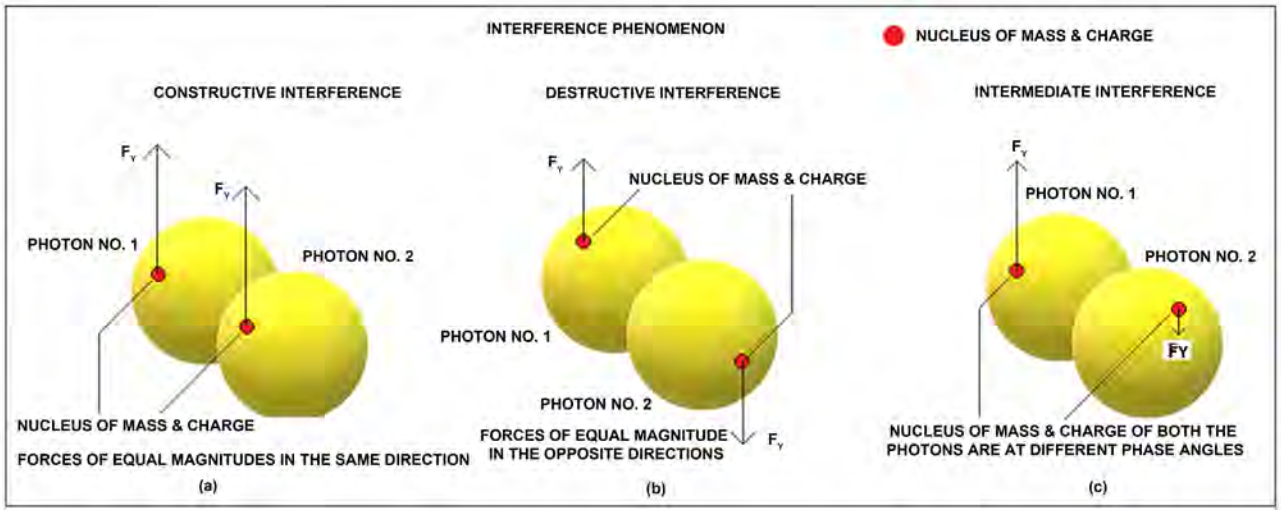

Figure 4. Part (a) shows the two photons in the same phase developing forces of equal magnitudes in the same direction. Part (b) shows the two photons in the opposite phase developing forces of equal magnitudes in the opposite directions. Part (c) shows the two photons developing forces of the different magnitudes and directions.

Even though the Constructive Interference proves the presence of the mass in the photons, it does not indicate the location of the mass in the photon.

4.2.2. Destructive Interference

In the Destructive Interference, the two photons superpose with a phase difference of π and form the resultant wave with the zero amplitude. The part (b) of Figure 4 shows the two photons of the same frequency with a phase difference of π in the superposed position developing the forces of equal magnitudes in the opposite directions.

The nuclei of the mass of both the spinning photons have a phase angle difference of π. The directions of the forces developed by the mass in the nucleus of each photon are always opposite to each other with a phase difference of π. If the phase angle of the Photon No. 1 is (θ) and the phase angle of the Photon No. 2 is ($\theta+\pi$). The two photons develop forces in the vertical direction as under:

- The force developed by the nucleus of: $2\pi rfm\{\cos(\theta+d\theta)-\cos\theta\}/dt$
  Photon No. 1 in Vertical Y-axis
- The force developed by the nucleus of:
  $2\pi rfm\{\cos(\theta+\pi+d\theta)-\cos(\theta+\pi)\}/dt$
  Photon No. 2 in Vertical Y-axis
  Or: $-2\pi rfm\{\cos(\theta+d\theta)-\cos\theta\}/dt$
- The resultant force developed by the nuclei: Zero
  Of both the Photons in Vertical Y-axis

Since the net vertical force of both the photons is always zero, the amplitude of the resultant wave is also always the zero. The Destructive Interference phenomenon is not possible if the mass is uniformly distributed or in the center of the photon. In such a situation, whatever is the phase difference between the two photons, only the Constructive Interference can take place.

The Destructive Interference is possible only in a condition: "The location of the nucleus of the mass is in the off-center position in the photons." However, the Destructive Interference phenomenon can also take place even if a photon has more than one nucleus of the mass, located off-center in the photon.

The phenomenon of Destructive Interference with the zero amplitude of the resultant wave discovers and proves: "***A photon has the mass located in an off-center position.***"

4.2.3. Intermediate Interference

When the two photons, with a phase difference other than 0˚ or π, superpose the resultant wave with the amplitude > 0 but < double the amplitude forms due to the phenomenon of the Intermediate Interference. **Figure 3(c)** shows such two interfering photons.

If the two photons of the same frequency with phase angles θ_1 & θ_2 interfere, the mass in the nucleus of each photon develops the force in the vertical direction as under:

- The force developed by the nucleus of: $2\pi rfm\left\{\cos\left(\theta_1+d\theta_1\right)-\cos\theta_1\right\}/dt$
  Photon No. 1 in Vertical Y-axis
- The force developed by the nucleus of: $2\pi rfm\left\{\cos\left(\theta_2+d\theta_2\right)-\cos\theta_2\right\}/dt$
  Photon No. 2 in Vertical Y-axis
- Total force developed by the nuclei of both the Photons in Vertical Y-axis:

$$2\pi rfm\left\{\cos\left(\theta_1+d\theta_1\right)-\cos\theta_1\right\}/dt+2\pi rfm\left\{\cos\left(\theta_2+d\theta_2\right)-\cos\theta_2\right\}/dt$$

The amplitude of the resultant wave depends on the difference in the phase angles θ_1 & θ_2 of the two photons. If a photon has more than one nucleus of the mass, the two photons on intermediate interference must form a resultant wave with two or more peaks. However, the resultant wave has only a single peak (there is no reference of the resultant wave with the Intermediate Interference of more than one peak). The single peak of the resultant wave confirms the presence of only one nucleus of the mass located off-center in a photon.

The phenomenon of Intermediate Interference produces the resultant wave with the sum of the amplitudes of both the photons discovers and proves:

"***A photon has only one nucleus of the mass located in the off-center position.***"

Note: The horizontal forces developed by the mass in the nucleus of the photons are not required here to prove the presence of only one nucleus of the mass located off-center in the photons.

4.3. Wave-Particle Duality

The Dual Wave-Particle nature of a photon awaits explanation since the year 1801. A particle of a photon/quantum always moves like a wave and displays the properties of the particle as well as the wave. Only the New Quantum Theory explains the Wave-Particle Duality. The followings describe the characteristics of a linearly polarised photon traveling in the horizontal X-axis and forming a wave

in X-Y plane:

- A photon particle continuously changes its velocity and direction to move as a wave.
- The photon spins and completes one cycle of the wave in 360˚ spins with half the wave above the line of the travel and the other half below. Both the halves have a single peak.
- For a wave starting from the origin (0, 0), the photon moves up with the maximum vertical velocity in the Y-axis which reduces to zero at 90˚ phase angle. The photon descends from 90˚ phase angle achieving the maximum downward velocity at 180˚ phase angle but this velocity again turns to zero at 270˚ phase angle, and from there the photon ascends.
- In addition to the speed of light in the horizontal X-axis, the mass in the nucleus of the photon also develops the acceleration/velocity in the horizontal direction. Therefore, the horizontal velocity of a photon varies continuously in a wave cycle with the speed of light being always the average in a single wave cycle.
- The horizontal velocity of the photon (due to the mass in the nucleus) is zero at the origin, the maximum at 90˚ phase angle, again zero at 180˚ phase angle and the maximum in the reverse direction at 270˚ phase angle.
- The up and down cyclical movement of a photon to form a wave is only possible by the presence of a mass located off-center in the photon. The mass, in the nucleus of a photon located off-center, continuously accelerates/decelerates to produce variable forces in both the horizontal X-axis and the vertical Y-axis.

The following is the science of the "**Formation of a wave by a particle of a linearly polarised photon**":

- The horizontal velocity of a photon at phase angle θ: $2\pi rf\sin\theta + c$
- The force developed by the Nucleus: $2\pi rfm\{\sin(\theta + d\theta) - \sin\theta\}/dt$

in the horizontal X-direction

- The vertical velocity of a photon at phase angle θ: $2\pi rf\cos\theta$
- The force developed by the nucleus: $2\pi rfm\{\cos(\theta + d\theta) - \cos\theta\}/dt$

in the vertical Y-direction

where, "c" is the average speed of light in X-axis.

The horizontal velocity and the force in the horizontal direction are the functions of $\sin\theta$. The vertical velocity and force in the vertical direction are the functions of $\cos\theta$. With the spin of the photon from 0˚ to 360˚ phase angle, the values of $\sin\theta$ and $\cos\theta$ change between +1 and (−)1. For the same frequency photons, the values of r, f & m are constant. The internal forces, developed from within the photon, move the photon as a wave as under:

A) Formation of 1st Quarter of Wave: Phase Angle from 0˚ to 90˚:

- At 0˚ phase angle or the origin of a new wave cycle, the value of Sin θ is zero. Therefore, the horizontal velocity (due to the mass in the photon) is also zero. In this quarter as the photon spins and moves from 0˚ to 90˚ phase angle,

the value of $\sin\theta$ increases from 0 to +1.

- The horizontal velocity and the horizontal force change from 0˚ to 90˚ as under:

The horizontal velocity: Zero at 0˚ phase angle and the maximum at 90˚

The horizontal force: The maximum force at 0˚ phase angle and reduces to zero at 90˚

- At 90˚ phase angle, the value of $\sin\theta$ is 1. Therefore, the horizontal velocity at 90˚ phase angle grows to the maximum.
- At 0˚ phase angle or the origin of a new wave cycle, the value of $\cos\theta$ is +1. Therefore, its vertical velocity (due to the mass in the photon) is the maximum. In this quarter as the photon spins and moves from 0˚ to 90˚ phase angle, the value of $\cos\theta$ decreases from +1 to 0.
- The vertical velocity and the vertical force change from 0˚ to 90˚ as under:

The vertical velocity: The maximum at 0˚ phase angle and reduces to zero at 90˚

The vertical force: Zero at 0˚ phase angle and increases to the maximum at 90˚ in (−)Y-axis

- At 90˚ phase angle, the value of $\cos\theta$ is zero. Therefore, the vertical velocity at 90˚ phase angle turns to zero, and the photon cannot move further up anymore in the Y-axis from the phase angle 90˚. The photon reaches the highest point of the wave at 90˚ phase angle.

B) Formation of 2nd Quarter of Wave: Phase Angle from 90˚ to 180˚:

- At 90˚ phase angle, the value of $\sin\theta$ is +1 with the maximum horizontal velocity. In this quarter as the photon spins and moves from 90˚ to 180˚ phase angle, the value of $\sin\theta$ decreases from +1 to 0.
- The horizontal velocity and the horizontal force change from 90˚ to 180˚ as under:

The horizontal velocity: The maximum at 90˚ phase angle and reduces to zero at 180˚

The horizontal force: Zero at 90˚ phase angle and increases to the maximum at 180˚ in (−)X-axis

- At 180˚ phase angle, the value of $\sin\theta$ is zero. Therefore, the horizontal velocity at 180˚ phase angle (due to the mass in the photon) turns to zero.
- At 90˚ phase angle, the value of $\cos\theta$ is zero with the zero vertical velocity. In this quarter as the photon spins and moves from 90˚ to 180˚ phase angle, the value of $\cos\theta$ decreases from 0 to (−)1.
- The vertical velocity and the vertical force change from 90˚ to 180˚ as under:

The vertical velocity: Zero at 90˚ phase angle and increases to the maximum at 180˚ in (−)Y-axis

The vertical force: The maximum at 90˚ phase angle and reduces to zero at 180˚ in (−)Y-axis

- At 180˚ phase angle, the value of $\cos\theta$ is (−)1 with the maximum vertical velocity in (−)Y-axis and the photon completes the upper half cycle of the wave formation. From 180˚ phase angle, the photon moves below the line of travel

(X-axis) of the photon.

C) Formation of 3rd Quarter of Wave: Phase Angle from 180˚ to 270˚

- At 180˚ phase angle, the value of $\sin\theta$ is zero with the zero-horizontal velocity (due to the mass of the photon). In this quarter as the photon spins and moves from 180˚ to 270˚ phase angle, the value of $\sin\theta$ decreases from 0 to (−)1.
- The horizontal velocity and the horizontal force change from 180˚ to 270˚ as under:

The horizontal velocity: Zero at 180˚ phase angle and increases to the maximum at 270˚ in (−)X-axis

The horizontal force: The maximum at 180˚ phase angle and reduces to zero at 270˚ in (−)X-axis

- At 270˚ phase angle, the value of $\sin\theta$ is (−)1 with the maximum horizontal velocity in (−)X-axis.
- At 180˚ phase angle, the value of $\cos\theta$ is (−)1 with the maximum vertical downward velocity. In this quarter as the photon spins and moves from 180˚ to 270˚ phase angle, the value of $\cos\theta$ increases from (−)1 to 0.
- The vertical velocity and the vertical force change from 180˚ to 270˚ as under:

The vertical velocity: The maximum at 180˚ phase angle in (−)Y-axis and reduces to zero at 270˚

The vertical force: Zero at 180˚ phase angle and increases to the maximum at 270˚ in +Y-axis

- At 270˚ phase angle, the value of $\cos\theta$ is zero with the zero-vertical velocity; therefore, the photon cannot go down further. The photon reaches the lowest point of the wave at 270˚ phase angle.

D) Formation of 4th Quarter of Wave: Phase Angle from 270˚ to 360˚

- At 270^0 phase angle the value of $Sin\ \theta$ is (−)1 with the maximum horizontal velocity (due to the mass of the photon) in the (−)X-direction. In this quarter as the photon spins and moves from 270˚ to 360˚ phase angle, the value of $\sin\theta$ increases from (−)1 to 0.
- The horizontal velocity and the horizontal force change from 270˚ to 360˚ as under:

The horizontal velocity: The maximum at 270˚ phase angle in (−) X-axis and reduces to zero at 360˚

The horizontal force: Zero at 270˚ phase angle and increases to the maximum at 360˚ in +X-axis

- At 360˚ phase angle, the value of $\sin\theta$ is zero; therefore, the horizontal velocity at 360˚ turns to zero.
- At 270˚ phase angle the value of $\cos\theta$ is zero with the zero-vertical velocity. In this quarter as the photon spins and moves from 270˚ to 360˚ phase angle, the value of $\cos\theta$ increases from 0 to +1.
- The vertical velocity and the vertical force change from 270˚ to 360˚ as under:

The vertical velocity: Zero at 270˚ phase angle and increases to the maximum

at 360˚ in +Y-axis

The vertical force: The maximum at 270˚ phase angle and reduces to zero at 360˚ in +Y-axis

- At 360˚ phase angle, the value of $\cos\theta$ is +1 with the maximum vertical velocity in +Y-axis and the photon completes the lower half of the wave.

Figure 2 shows a wave formed by a linearly polarised photon spinning from 0˚ to 360˚ phase angle to form one full cycle of the wave. This figure also shows the forces with their directions developed by the mass in the nucleus located off-center in the photon at different phase angles or the angular position of the nucleus in the photon.

The Wave-Particle Duality is only possible if, and only if, a spinning photon has a mass located off-center in the photon and proves the presence of a mass located off-center in a photon.

If a photon has either the zero mass or uniformly distributed mass, the Wave-Particle Duality and other quantum phenomena are not possible.

4.4. To Find the Location of a Photon in Wave at Any Phase Angle

The following equations calculate the exact location of a photon in a wave cycle:

A photon of frequency *"f"* spins from the phase angle θ to $\theta + d\theta$, the time and the average velocity are as under:

- The time required by a photon to spin $d\theta$ degree: $d\theta/(360f)$
- The average horizontal velocity in $d\theta$ spin: $\left[c + \pi rf\left\{\sin\theta + \sin\left(\theta + d\theta\right)\right\}\right]$
- The horizontal distance covered in $d\theta$ spin:

$$\left[c + \pi rf\left\{\sin\theta + \sin\left(\theta + d\theta\right)\right\}\right] d\theta \Big/ \left(360 f\right) \tag{6}$$

- The average vertical velocity:

$$\pi rf\left\{\cos\theta + \cos\left(\theta + d\theta\right)\right\}$$

- The vertical distance covered in $d\theta$ spin:

$$\pi rf\left\{\cos\theta + \cos\left(\theta + d\theta\right)\right\} d\theta \Big/ \left(360 f\right) \tag{7}$$

The integration, of the equation nos. (6) & (7) from the phase angle θ_1 to θ_2 calculates the location of the photon in a quadrant. The integration of the equation no. (7) from 0˚ to 90˚, calculates the amplitude of the wave formed by a photon. The above equations need calculations for each quadrant separately since the same values of $\sin\theta$, and $\cos\theta$ between 0˚ to 360˚ phase angle repeat at different phase angles.

For the photon of known amplitude of the wave, the equation no. (7) calculates the value of "*r*" for the photon.

4.5. Formation of an Electromagnetic Wave

The following is the science of "**The Formation of an Electromagnetic Wave by a photon**":

- A moving point charge generates both the electric field as well as the magnetic field.

- As the velocity of the charge increases, the intensities of both the electric and the magnetic fields increase and vice versa. If the charge moves in the reverse direction, the directions of both the electric and magnetic fields generated are also in the reverse directions.
- During the 1st half cycle of the spin of the photon from 0˚ to 180˚ phase angle, the charge, in the nucleus located off-center in the photon, moves in the *forward direction* in comparison to the center of the photon. **Figure 5** shows a spinning photon with the nucleus moving in the *forward direction*.
- The velocity of the charge in the nucleus in the forward direction increases from 0˚ to 90˚ spin and decreases from 90˚ to 180˚ spin of the photon or the phase angle. Therefore, the intensities of both the electric and the magnetic fields increase from 0˚ to 90˚ and decrease from 90˚ to 180˚ spin of the photon or the phase angles.
- During the 2nd half cycle of the spin of the photon from 180˚ to 360˚ phase angle, the charge, in the nucleus located off-center in the photon, moves in the *backward direction* in comparison to the center of the photon. **Figure 5** also shows a spinning photon with the nucleus moving in the *backward direction*.
- As the charge moves in the backward direction during 180˚ to 360˚ spin, now both the electric and the magnetic fields are generated in the reverse/opposite direction.
- The velocity of the charge in the nucleus (in the reverse direction) increases from 180˚ to 270˚ spin and decreases from 270˚ to 360˚ spin of the photon or the phase angle. Therefore, the intensities of both the electric and the magnetic fields increase from 180˚ to 270˚ and decrease from 270˚ to 360˚ spin of the photon or the phase angle, but in the opposite directions.
- After completing one cycle of the electromagnetic wave formation in 360˚ spin of the photon, the new cycle of the electromagnetic wave starts again from 0˚ phase angle.

The charge in the nucleus accelerates/decelerates to produce the electric field wave in a two-dimensional plane and the magnetic field wave in three-dimensional plane. **Figure 6** shows one full cycle of the Electromagnetic Wave formed during the 0˚ to 360˚ spin of a polarised photon. The above describes the formation of an electromagnetic wave briefly only, as the "New Quantum Theory explains all the Mysterious Quantum Phenomena" [2] explains the formation of an electromagnetic wave by a photon with enough details.

The formation of an Electromagnetic Wave by a photon discovers and proves the presence of a charge in the nucleus located off-center in the photon.

4.6. Refraction

The phenomenon of refraction changes the direction and the velocity of a photon in the new medium. The secret of the refraction phenomenon are the interactions between the electromagnetic fields of both the photon as well as the new

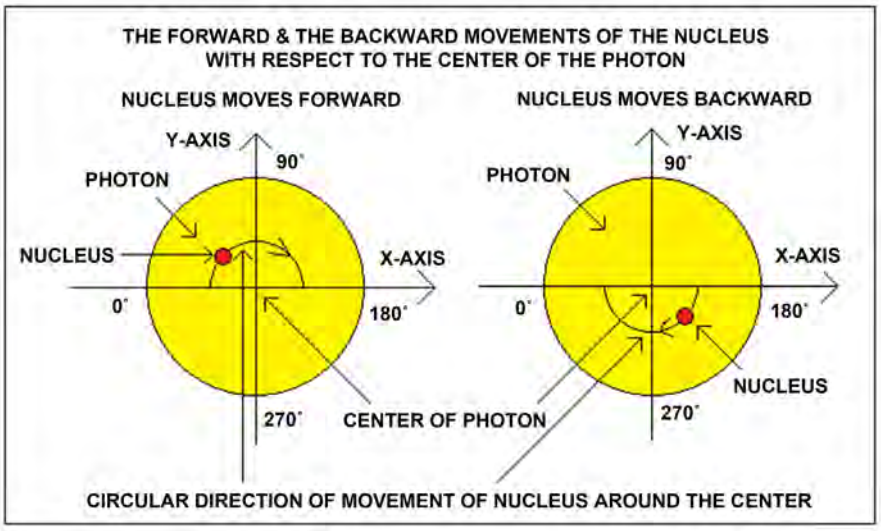

Figure 5. The nucleus of the mass circles around the center of the spinning photon. The nucleus moves in the forward direction during 0˚ to 180˚ phase angle with respect to center of the photon. The nucleus moves in the backward direction during 180˚ to 360˚ phase angle with respect to center of the photon.

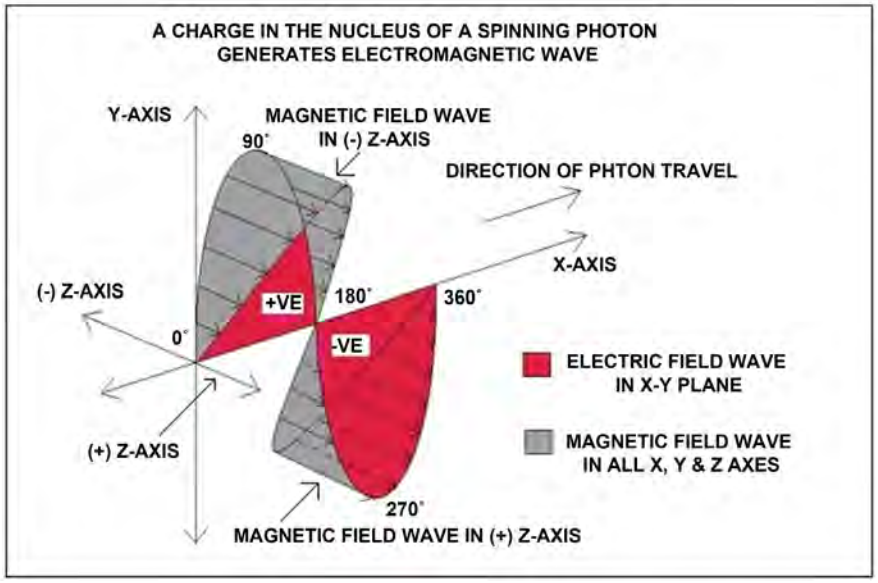

Figure 6. A charge in the off-center nucleus circles the center of photon and moves in the forward as well as the backward directions. The forward movement above the line of travel (X-axis) and backward movement below the line of travel generate the electric and the magnetic field waves in the opposite directions.

medium. A linearly polarised photon explains the phenomenon of refraction as under:

- As a rule, a photon spins in the plane of the rotation of the nucleus around the center of the photon. The mass in the nucleus of a linearly polarised photon generates the forces in the X-Y plane only and the photon travels in X-axis. The charge in the nucleus generates the electric field in the X-Y plane

on both up & down sides of the line of travel of the photon. The magnetic field generates in all the three directions on both the sides of the line of travel in the plane perpendicular to X-Y plane of the electric field. Figure 6 shows the planes of the Electromagnetic Wave formed by a linearly polarized photon.

- When a polarised photon travels in the vacuum in the absence of any external electromagnetic field, the charge in the photon generates the uniform electric field and the uniform magnetic field on both the sides of the line of travel of photon.
- A medium consists of atoms bonded together as the molecules. The molecular bonds of the medium generate their distinct electromagnetic fields.
- As the photon enters from the vacuum to the new medium, it experiences a new environment of the external electromagnetic field. Both the electromagnetic fields of the photon and the medium interact.
- A photon is an independent moving identity whereas a medium, in comparison to the photon, is a solid or liquid with a rigid structure and molecular bonds with the electromagnetic field.
- The external electromagnetic field forces the photon to tilt its plane of spin to adjusts to the new external electromagnetic field. The tilt of the photon changes the directions of its electric and the magnetic fields and finds the path of the least electromagnetic resistance to travel in the medium.
- With the tilt of the plane of spin of the photon, the nucleus of the mass and the charge rotates around the center of the photon in a new plane. The mass in the nucleus now generates the forces in the new plane and the photon now travels in a new direction matching with the plane of spin of the photon. Therefore, the direction of the travel of photon changes in the new medium.
- Figure 7 shows a photon moving from vacuum to a medium and again to the vacuum, the electromagnetic field of the medium changes the direction of the photon in the medium.
- As the photon travels out from the medium and its electromagnetic field, the photon is now out of the external magnetic field. Therefore, the photon tilts back to its regular plane of spin and direction, and all the above changes revert to the normal status.

As the photon enters a new medium and its electromagnetic field, the plane of the spin of photon tilts resulting in the following changes in the photon:

1) The photon travels in a new direction matching with the new plane of the spin of the photon as the forces developed by the mass in the nucleus are in the new directions.

2) The photon forms a wave in a new two-dimensional plane.

3) A medium always contracts the electric field of the photon in comparison to the vacuum. The reduction in the size of the electric field wave now formed by the photon reduces the wavelength of the photon in the medium. *Therefore*, *the velocity of the photon reduces in the new medium*.

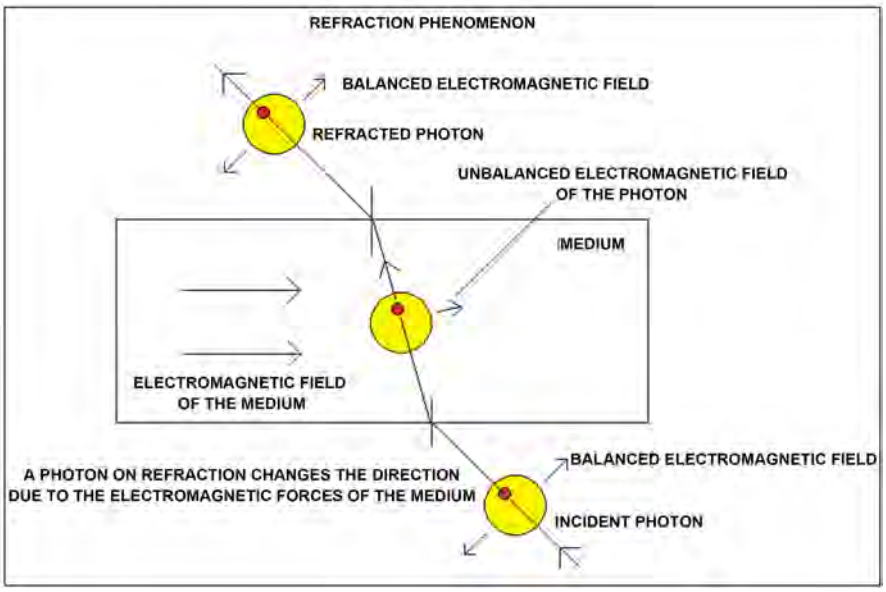

Figure 7. Shows a photon traveling from the vacuum to a medium resulting in the change of direction of travel. As the photon exits to the vacuum, the plane of spin tilts again to return to its original direction.

The phenomenon of Refraction discovers and proves the presence of a nucleus of the mass and the charge in a photon.

5. Experiments

When a photon reflects on a mirror, the rotating mass in the nucleus of the photon generates an inertial torque at the contact point of the mirror. This inertial torque deviates the photon very slightly in all the three axes. The new equation of reflection for a photon is as under:

$$i = i + d$$

where "*i*" is the angle of incidence and "*d*" is the angle of deviation of the photon in an axis.

This little deviation of the photons depends on the angle of incidence and the angle of polarisation of the photons. Generally, this deviation is tiny and below the noticeable limit. However, this little deviation on the reflection can be multiplied by the followings:

a) By the second reflection of the deviated photons from a circular surface coated mirror.

b) By reflecting a long chain of the photons.

By repeating the constructive interference again and again, a long chain of the photon forms. When only the 1st photon at the beginning of the chain contacts and reflects on a mirror, the torque of all the spinning photons transfers to the contact point of the 1st photon with the mirror. Therefore, the angle of the deviation of the whole chain of the photons multiplies in all the three axes. **Figures 8(a)-(c)** shows the horizontal, inclined and the vertical chains of the photons for the reflection at the mirror.

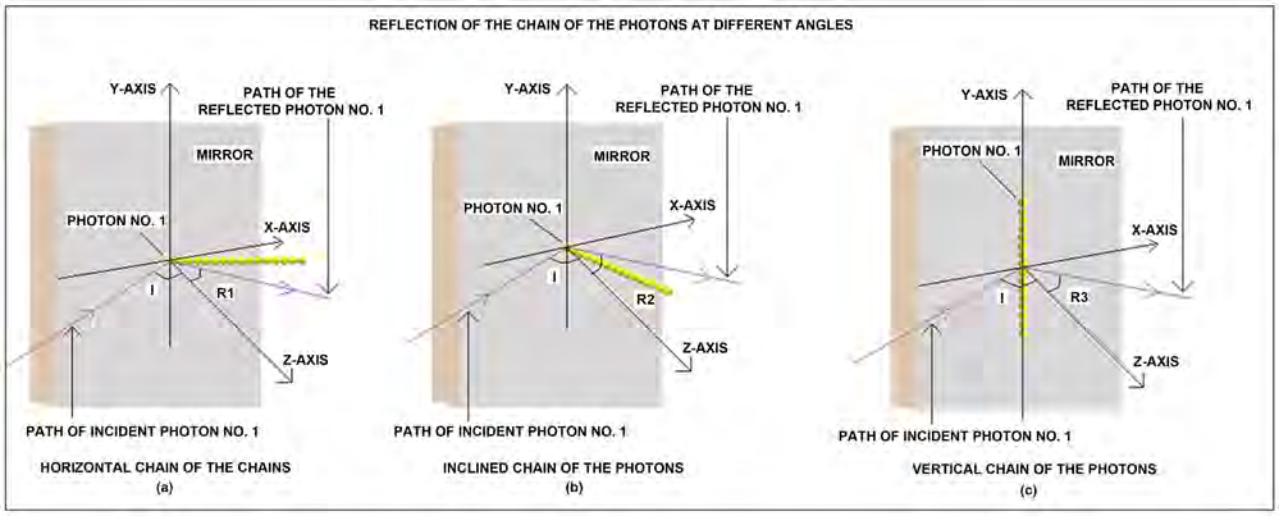

Figure 8. The reflection of the long chain of the photons on a vertical mirror. **Figure 8(a)** shows a horizontal chain of the photons reflecting on a mirror. **Figure 8(b)** shows an inclined chain of the photons reflecting on a mirror. **Figure 8(c)** shows a vertical chain of the photons reflecting on a mirror. All the figures are not to scale.

The most critical feature of any reflection experiment is the increase in the angle of deviation with the increase in the frequency of the photons under the same conditions. If the photons have zero mass, no inertial torque develops, and on reflection there is no deviation of the photons.

The deviation of the photons on reflection and the increase in the angle of deviation with the higher frequency photons prove the presence of a mass located off-center in the photons.

The following experiments prove and determine the mass, diameter & charge of the photons:

5.1. Multiple Slits in Series Experiment

- A set of a single and a double slit creates constructive interference of the two photons and join them side by side. A typical frame mounts several sets of such single & double slits in the series in perfect alignment with the facility to rotate all the slits together in 360˚ angles.
- Every set of the slits doubles the number of the photons joined together side by side from 2 to 4, 4 to 8, 8 to 16, 16 to 32 and so on by the constructive interference.
- When the same frequency photons join side by side, the strong force due to the mass in the photons is applied, and the photons join to produce a long chain of the photons spinning together.
- All the slits in the same vertical plane produce a horizontal chain of the spinning photons. The chain of the spinning photons forms in a line perpendicular to the plane of all the slits.
- As all the slits rotate, the angle of the chain of the spinning photons changes. With all the slits in the horizontal plane, the chain of photon forms in a vertical line.

- A vertical plain surface coated mirror, in an inclined position, reflects the long chain of the spinning photons. A detector, installed at a distance, detects and records the position of the reflected chain of the photons and the changes in the angles of deviation in different directions.
- The above set up determines the mass, the charge and the diameter of the photons of different frequencies.

5.2. To Determine the Mass of the Photons

- An inertial torque develops on reflection of a chain of the spinning photons by the rotating mass in each photon of the chain. **Figure 8(a)** and **Figure 8(b)** show the chain of the spinning photons and the mirror. Only the first photon of the chain contacts the mirror and reflects along with the whole chain of the photons attached to the first photon.
- All the photons transfer the torques generated to the first photon. The first photon at the contact point of the mirror turns, due to all the inertial torques from all the photons, to deviate on reflection in the different directions.
- After the reflection, the angle of the whole chain of the spinning photons also changes in the different directions.
- The angles of the deviation depend on the angle of the chain of the spinning photons at the contact point of the mirror.

The following equations can calculate the mass of the photon:

- The angle of deviation in X-direction:

$$\Phi_X : kmf\left[\left(r\sin\theta\right)^2+\left\{\left(D+r\right)\sin\theta\right\}^2+\left\{\left(2D+r\right)\sin\theta\right\}^2 +\cdots+\left\{\left(nD-D+r\right)\sin\theta\right\}^2\right] \tag{8}$$

- The angle of deviation in Y-direction:

$$\Phi_Y : kmf\left[\left(r\cos\theta\right)^2+\left\{\left(D+r\right)\cos\theta\right\}^2+\left\{\left(2D+r\right)\cos\theta\right\}^2 +\cdots+\left\{\left(nD-D+r\right)\cos\theta\right\}^2\right] \tag{9}$$

where:

- k: a constant
- θ: Polarisation angle of the photons
- D: Diameter of the photon
- n: Number of photons in the chain

A set of data generates by varying the angle of the chain of the spinning photons and the angle of incidence on the mirror to calculate the mass of the photon.

5.3. To Determine the Charge of the Photons

- The multiple slits produce a long chain of the photons joined together side by side in any required number by the constructive interference.
- All the photons are in the same phase in the chain of the spinning photons.

As all the photons are close enough, the magnetic fields of all the photons combine to form a single peak of the strong magnetic field.

- A magnetic field detector detects and records the combined magnetic field.
- The division of the combined magnetic field by the number of the photons calculates the strength of the magnetic field of a single photon which in turn calculates the charge of the photon using already known equations.

5.4. To Determine the Diameter of a Photon

- All the multiple slits in the horizontal plane form a long vertical chain of the spinning photons. Figure 7(c) shows a vertical chain of the photons with the mirror.
- A detector can detect both the ends of the chain of the photon after reflection or directly without reflection. The distance between the first and the last photon divided by the number of the photons calculates the diameter of the photon.

Note: The instruments with the required high precision are not available in the private laboratory of the author.

6. Conclusions

The essence of a photon/quantum particle is the presence of a nucleus of the mass and the charge, and the most critical feature is the off-center location of the nucleus in the particle. The intermediate interference decisively discovers and proves the presence of only one nucleus of the mass located off-center in the photons.

The nucleus of the mass and charge rotates around the center of the photon with the spin of the photon and continuously accelerates/decelerates in the different directions, and these accelerations of the mass in the nucleus generate the forces of varying magnitudes in the different directions. ***The continuously varying forces in the different directions move a photon as a wave and explain the Wave-Particle Duality pending since the year*** **1801.** *Similarly, the regular accelerations/decelerations of the charge in the nucleus explain the formation of an electromagnetic wave by a photon/quantum particle.*

During reflection of a photon, the rotating mass in the photon creates inertial torque at the contact point of the mirror in different directions. These inertial forces deviate the photon a little in different directions after the reflection. The increase in the frequency of the photons increases the angles of deviation in the different directions. Higher the frequency, the higher is the inertial torque developed by the mass of the photons. The generation of the inertial torque, at the contact point of the mirror, proves the presence of a mass located off-center in the photons.

All the quantum phenomena prove the presence of a nucleus of the mass and the charge located off-center in the photons/quantum particles as stated in the New Quantum Theory. The experiments using high precision instruments can

determine the mass, the charge and the diameter of the photons.

Conflicts of Interest

The authors declare no conflicts of interest regarding the publication of this paper.

References

[1] Agarwal, N.S. (2012) *Indian Journal of Science and Technology*, **5**, 3612-3617.

[2] Agarwal, N.S. (2016) *Journal of Modern Physics*, **7**, 2135-2154. https://doi.org/10.4236/jmp.2016.715186

Scientific Research Publishing

Journal of Modern Physics, 2018, 9, 2193-2205
http://www.scirp.org/journal/jmp
ISSN Online: 2153-120X
ISSN Print: 2153-1196

Available Face-Changing Effect

Xiaobai Ai

Shanghai Institute of Applied Physics, The Chinese Academy of Sciences, Shanghai, China
Email: hsiaobaiai@outlook.com, mraixiaobai@163.com

How to cite this paper: Ai, X.B. (2018) Available Face-Changing Effect. *Journal of Modern Physics*, **9**, 2193-2205.
https://doi.org/10.4236/jmp.2018.912138

Received: August 15, 2018
Accepted: October 12, 2018
Published: October 15, 2018

Copyright © 2018 by author and Scientific Research Publishing Inc.
This work is licensed under the Creative Commons Attribution International License (CC BY 4.0).
http://creativecommons.org/licenses/by/4.0/

Open Access

Abstract

Based on mathematical foresight and beyond the mainstream inertial thinking pattern, the author believes that if neutrinos were really tachyons, the mystery of neutrinos might be solved. Fortunately, the space-like theory of special relativity reveals that there would exist an observable effect *i.e.* a "face-changing effect", not oscillation, which was just related to the superluminal motion. As long as the motion velocity of an electron anti-neutrino was greater than c^2/v, where v was the instantaneous thermal motion velocity of its mother neutron at the time of β-decay, a corresponding electron neutrino formed from the face-changing would be observed on the journey. Therefore, a special and easy way to judge the physical nature of neutrinos may be suggested the reactor neutrino experimental groups all over the world, in addition to the current studies involving the disappearance mode of $\bar{\nu}_e$, to add a new experimental search after ν_e in the $\bar{\nu}_e$ current, to see whether a few ν_e neutrinos would exceed the background counting. "Yes" result would reveal the neutrinos being tachyons, and "no" would be not.

Keywords

Special Relativity in Space-Like Region, Tachyon, Face-Changing Effect, Mother Neutron in β-Decay, Reactor Neutrino Experiments

1. Introduction

Neutrino oscillation has received the Nobel Prize for physics in 2015, but there are still mysteries of neutrino, especially after the neutrino oscillation has been confirmed, which would be still in very contradiction with the Standard Model (SM) of particle physics. That is because according to the historical works of Pontecorvo B. *et al.* to study neutrino oscillations firstly, neutrinos had been supposed to have nonzero rest mass [1]. Hence, the experimental confirmation of neutrino oscillation seems to have no doubt that neutrinos with different fla-

vors do have different masses, although these masses may be tiny and not known so far. Moreover, the mainstream physical community believes that on May 31, 2010, OPERO researchers observed firstly the candidate events of the muon neutrino transforming to tau neutrinos, which provided further evidence for the problem of neutrinos with nonzero rest mass [2]. Nevertheless the SM assumed that neutrinos are massless. As a result, an irreconcilable contradiction with SM was produced necessarily, making the mystery of the neutrino more difficult to understand. The historical footprint of solving this contradiction to get rid of the dilemma was: along the speculation and conjectural way of massive neutrinos, some ingenious ideas such as the concepts of Dirac mechanism, Majorana mechanism, Mikheyev-Smirnov-Wolfenstein effect (MSW effect), seesaw mechanism, the possibility of sterile neutrinos, the Standard-Model Extension and Lorentz-violating oscillations and so on, have been put forward in the past few decades. However, concerning above new concepts, the present author is very sorry to be sure that they do not bring us nearer to the true solution of the fundamental difficult problems, or in other words, none of the above theories are perfect enough to explain the true meaning of the neutrino puzzles. The trend is often unstoppable. The mainstream scientists of today's physics believe firmly that the observations of neutrino oscillations are strong evidence in favor of massive neutrinos. On June 11th this year, the Karlsruhe Tritium Neutrino Experiment (German acronym-KATRIN) [3] [4] [5], which will be going to measure neutrino mass, has officially started operation. Despite this trend, beyond the mainstream inertial thinking pattern, the author still holds that the whole way previous researchers in the big direction of thinking and approaching neutrino puzzles may be a hindrance. This is an issue that should be really worried about by us.

Hegel (George Wilhelm Friedrich, 1770-1831) wrote: "Dialectics constitutes the soul that drives scientific progress. … Dialectics is the driving principle of all movements, all life and all undertakings in the real world. Similarly, dialectics is the soul of all true scientific understanding within the scope of knowledge." (§81 in Chinese translation < SYSTEM DER PHILOSOPHIE ERSTER TEIL. DIE LOGIK). Follow Hegel, in the understanding of any existing thing, it also contains a negative understanding of that. The following questions will naturally be asked: are there three-generations of neutrinos in nature, which have different flavors but massless? Actually, the answer is yes: provided neutrinos being tachyons, not only all of the results of previous studies about neutrinos and neutrino oscillations do not have to change, but also the main neutrino puzzle which is in contradiction with SM might be solved [6].

In Section 2, a review of the main judgments in [6] is given, which positively pointed out that the tachyons may exist in nature, which would be neutrinos with different flavors but massless. In Section 3, based on the inferences in [6], some suggestions are made for those studies of weighing neutrinos. In Section 4, it can readily verify that the composition theorem of velocities is applicable to

tachyons, which ensures the Lorentz invariance of the superluminal motion. In Section 5, a special "face changing effect" would be revealed. That is, when the condition ($|\vec{u}'| > c^2/|\vec{v}|$) being satisfied, where $\vec{u}'$ is the velocity of a tachyon in one used inertial frame Σ' which moving with a velocity $v = |\vec{v}| < c$ relative to another inertial frame Σ in the negative direction, as a result, a corresponding anti-tachyon might be observed by observers in Σ. This space-like relativistic observable effect would give us a new <yes-no> measuring method to study the nature of neutrinos, which cost is low and the technology used has been mature. In Section 6, the author suggests those reactor neutrino experimental groups all over the world that, in addition to the current reactor experimental research concerning the disappearance mode of $\bar{\nu}_e$, to add a measurement to search after ν_e in the $\bar{\nu}_e$ current, to see if a few ν_e neutrinos in excess of the background might be detected. "Yes" result shows that the neutrinos would be tachyons, "no" would be not. Two remarks are given in Section 7.

2. If Neutrinos Being Tachyons

It is well known that Minkowski's metric $\mathrm{d}s^2$ [7] is as follows

$$\mathrm{d}s^2 = c^2\mathrm{d}t^2 - \mathrm{d}x^2 - \mathrm{d}y^2 - \mathrm{d}z^2 = \begin{cases} >0 & \text{time-like} \\ =0 & \text{light-like} \\ <0 & \text{space-like} \end{cases} \tag{1}$$

As long as to adhere the Lorentz invariance of Minkowski's space-like metric ($\mathrm{d}s^2 < 0$), if there exist tachyons in nature, they should be neutral point-like particles with lepton appearance, which are very much like our early understanding about neutrinos before.

The relativistic energy-momentum relationships for a free bradyon, a photon and a free tachyon are as follows

$$p^2 = p_\mu p^\mu = E^2/c^2 - |\vec{p}|^2 = \begin{cases} m_0^2c^2 \\ 0 \\ -p_0^2 \end{cases} \tag{2}$$

One may see that in space-like region there is no physical quantity "rest-mass" m_0, but there is physical quantity "lowest limited momentum" p_0 [8], which may be called the space-like physical quantity. According to Equation (2), the time-like representation of the space-like physical quantity p_0^2 may be indicated by $-m_0^{*2}c^2$ (or $p_0 \sim im_0^*c$), which comes from $p_0^2c^2 = -m_0^{*2}c^4$.

Based upon the probability expression of the neutrino oscillation derived in [8] [9] and [10], due to

$$\Delta m_{\ell\ell'}^2 = m_{0\ell}^{*2} - m_{0\ell'}^{*2} = \left(p_{0\ell'}^2 - p_{0\ell}^2\right)/c^2 = -\Delta p_{0\ell\ell'}^2/c^2 < 0,$$

where

$$\Delta p_{0\ell\ell'}^2 = p_{0\ell}^2 - p_{0\ell'}^2 > 0.$$

Using SI units, the probability of the neutrino oscillation $\nu_\ell \to \nu_{\ell'}$ for extremely relativistic neutrinos $E \approx |\boldsymbol{p}|$ may also be described by means of fol-

lowing function [6]:

$$P\left(\nu_\ell \to \nu_{\ell'}, \nu_\ell \neq \nu_{\ell'}; L\right) = \sin^2 2\theta_{\ell\ell'} \sin^2\left(\frac{c}{4\hbar}\frac{\Delta p_{\ell\ell'}^2 L}{E}\right), \tag{3}$$

where ℓ, ℓ' are the flavor of neutrinos (e, μ, τ neutrinos and their antineutrinos), $L_{\ell\ell'} = \left|E/\Delta p_{0\ell\ell'}^2\right|$ being the oscillation length. That is to say: neutrino oscillation $\nu_\ell \to \nu_{\ell'}$ may be the conversion between massless neutrinos with different flavors expressed in different $p_{0\ell'}$ ($\ell: e, \mu, \tau$ neutrinos and their anti-neutrinos) during their flight journey.

During the 70s-80s last century, several research teams used different experimental methods to explore the rest mass of neutrinos, but had obtained some negative square values of masses [11] [12] [13] [14] [15]. The mainstream physics community at that time and up to date believed that some non-physics issues involved in. For example, Bornschein B. summarized the conditions for measuring the mass of neutrinos by means of tritium beta decay in six decades and he attributed the unphysical reasons, systematic errors, some statistical fluctuation and additional energy loss involved in those measuring results of the negative mass square of neutrinos [3].

In the light of [6], one should know that $-m_0^2$ makes physical sense now, which is just the time-like representation of a positive space-like physical quantity p_0^2/c^2. Actually those experimental researches in [11] [12] [13] [14] [15] had confirmed that the neutrinos being tachyons.

In fact, on the basis of the experimental measurements in [11] [12] [13] [14], one had known that

$$p_{0e} \to 1.38 \sim 6.2 \text{ eV}/c,$$

from [15] we know

$$p_{0\mu} \to 0.126 \text{ MeV}/c.$$

Of course, above experimental measurements are not the most accurate and the final results, but we must not forget their historical contributions.

3. To Scientists Who Are Going to Weigh Neutrinos

KATRIN will be going to weigh neutrino mass by means of an improved sensitivity for $m_{\bar{\nu}_e}^2$ from $2 \text{ eV}/c^2 \to 0.2 \text{ eV}/c^2$. It is designed to detect the behaviour of electrons and electronic anti-neutrinos that are emitted by ultra-pure molecular (gaseous) tritium source. The basic principle is to investigate the electron spectrum of tritium beta decay

$$^3H \to {}^3H_e^+ + e^- + \bar{\nu}_e,$$

that is to try to find the answer by observing following β decay:

$$n \to p + e + \bar{\nu}_e.$$

In this process, although the energy $E_{\bar{\nu}_e}$ taken away by the electronic anti-neutrino cannot be measured directly, but which might be deduced by the conservation of energy:

$$E_{\bar{\nu}_e} = E_n - E_p - E_e .$$

The electron and electronic anti-neutrino share only ($E_n - E_p =$) 18.6 keV between them. According to the conventional cognitive understanding, if the electron anti-neutrino is a massless particle, the high-energy "end point" of the electron energy spectrum should be $E_{e0} = 18.6$ keV . All of the scientists believe that the subtle changes near E_{e0} contain important information about the nature of neutrinos. However, there is a significant difference between KATRIN's and the authors' view. The negative neutrino mass square $m_{0\ell}^2 (< 0)$ ($\ell : e, \mu, \tau$ neutrinos or their anti-neutrinos) makes sense, the present author firmly believes that the results of those careful, precise, and unbiased measurements would certainly be one of the following results:

$$E_e \begin{cases} > \left(E_n - E_p =\right) 18.6 \text{ keV} \to m_{e\bar{\nu}}^2 < 0 \to p_{0e}^2 / c^2 \\ = \left(E_n - E_p =\right) 18.6 \text{ keV} \to m_{e\bar{\nu}} = 0 \\ < \left(E_n - E_p =\right) 18.6 \text{ keV} \to m_{e\bar{\nu}} > 0 \end{cases} \tag{4}$$

Because we only care about the "end point" of the spectrum, the high-energy "end point" $E_{e0} > 18.6$ keV or "$m_{e\bar{\nu}}^2 < 0$" ($-m_{e\bar{\nu}}^2 \to p_0^2 / c^2$) might be the final answer, which does not exist in the preconceived idea of KATRIN, because KATRIN appreciates MAC-E filter with high resolution very much, that were used in the experiments at Mainz [11] and Troitsk [12] to try to get rid of the large negative values of $m_{e\bar{\nu}}^2$ in small energy intervals (50 - 100 eV) below the endpoint 18.6 keV [3]. In the sketch Fig.6 of [3], Bornschein B. attributed a shift of the endpoint to $E_{e0} < 18.6$ keV as a result of "an additional energy loss" that would be arbitrarily regarded as some physical cause to yield "a negative neutrino mass square". In fact, according to Equation (4) one knows that if "E_{e0}" were less than 18.6 keV, without doubt, some "masses of electron anti-neutrinos" would be obtained. But unfortunately, they will artificially discard the real information about the nature of neutrinos.

The author has already pointed that "the negative squared mass" were important physical evidence for the neutrinos being as tachyons and sincerely hopes that all the scientists who are going to weigh neutrinos will not presuppose the ultimate goal, will respect all the pleasant or alternative experimental results in their future experiments, not deliberately reduce "the negative squared mass". Hope is a good thing, but let it goes. Scholars should not be subjective, not be paranoid and not be stubborn, otherwise to make up a story may lose the game. This is historical experience and lessons.

4. The Addition Theorem of Velocities for Tachyon

If a tachyon is generated from its moving mother, without loss of generality, we must firstly study whether the movement of its mother will change the superluminal characteristics of the tachyon.

Let us consider two reference frames Σ and Σ', assume that at time $t_0' = t_0 = 0$, the reference axes of two systems coincide, the clocks in two frames

are synchronized, Σ' moving at a velocity $v=|\mathbf{v}|<c$ relative to Σ in the positive or negative direction of x axis. If a tachyon is emitted in Σ' (mother's body) at a velocity $|\vec{u}'|\left(=\mathrm{d}x'/\mathrm{d}t'\right)$ along the common positive or negative $x(x')$ direction from the common origin of Σ and Σ', the Lorentz transformation is

$$\begin{cases} \mathrm{d}x=\dfrac{\mathrm{d}x'\pm v\mathrm{d}t'}{\sqrt{1-v^2/c^2}} \\ \mathrm{d}t=\dfrac{\mathrm{d}t'\pm v\mathrm{d}x'/c^2}{\sqrt{1-v^2/c^2}} \end{cases} \tag{5}$$

Then, its velocity $|\vec{u}|\left(=\mathrm{d}x/\mathrm{d}t\right)$ in Σ is given by the addition theorem for velocities

$$|\vec{u}|=\frac{u'\pm v}{1\pm u'v/c^2}. \tag{6}$$

For an addition of a velocity $|\vec{u}'|$ ($>c$) and a velocity $|\vec{v}|$ of Σ', Equation (8) would yield a velocity $|\vec{u}|$ greater than c also, which may be proved easily as follows. Let us denoting $|\vec{u}'|$ by $|\vec{u}|=c^2/w'$, where $|\vec{w}'|<c$, it turns

$$|\vec{u}|=\left|\frac{u'\pm v}{1\pm u'v/c^2}\right|=\left|\frac{\dfrac{c^2}{w'}\pm v}{1\pm\dfrac{c^2v}{w'c^2}}\right|=\frac{c^2}{\left|\dfrac{w'\pm v}{1\pm w'v/c^2}\right|}>c. \tag{7}$$

That is, the composition theorem of velocities is applicable to tachyons, which ensures the Lorentz invariance of the superluminal motion. Consequently, if tachyons were yielded in some reactions, they will keep their superluminal nature in their later motions.

5. Face-Changing Effect

According to special theory of relativity (SR) in space-like continuum, there exist an available "face-changing effect" in nature, which is related to the superluminal motion and is also related to the existence of antimatter.

The SR is an axiom system with formal logic. All the rational arguments of an axiom system may be inferred from its premises or so-called axioms with consistence, independence as well as completeness by means of the formal logic method. Einstein's SR in the current physical textbooks is just SR in the time-like region. "Time-like region" as a constraint, its equivalent representation is "objects with nonzero rest mass" or "the speed of objects is less than the speed of light in vacuum", which is actually the third hypothesis hidden in Einstein's SR. Hence, all efforts to use the SR in the time-like region to demonstrate the absence of the superluminal motion can only get a misunderstanding. Because the conclusion, *i.e.* "less than the speed of light in vacuum", is early already contained in the premises. Einstein adhered that superluminal speeds would be of "non-physicality" and his SR did not allow superluminal speeds at all [16]:

The infinite contraction of objects moving at the speed of light and a clock runs infinitely slowly as it moves with the velocity of light (in Section 4 of [16]

and in [17] [18] [19] [20]);

The infinite intensity that a light source would have for an observer approaching it at the speed of light (in Section 7 of [16]);

The infinite amount of energy that would needed to accelerate an electron to the speed of light (in Section 10 of [16] and in [21]);

Einstein developed a new argument against superluminal motion in [22] [23] [24] [25], which was that he used the addition theorem for velocities to show that a signal superluminal propagating from cause to effect in one rest frame of those two events would propagate from effect to cause in another frame moving relatively to the first.

Other scholars followed the SR in time-like region did something similar, such as Tolman in 1917 [26] and Pauli in 1921 [27] supported Einstein's reversed causality argument.

The academic significance of their argument was the existence of $1/\sqrt{1-v^2/c^2}$ factor reflected that there were no inertial systems of light speed and superluminal speed in nature. However, they should not assert that there is no superluminal motion in nature, because their discussions in time-like region can not cover the knowledge of space-like physics, which is an area that they have neglected to develop. Whatever, nobody tried to believe this point at that time. In the first decades of last century, the scientific community was not yet aware of the presence of anti-matter in nature, so that the scholars who followed the famous masters would rather believe some of the non-physical components implied in the Lorentz transformation and from which some inferences going beyond common sense might be derived certainly.

Up to 1940's Stückelberg and Feynman raised a view of positrons as negative-energy electrons traveling backwards in time [28] [29] [30] [31]. In 1962, Bilaniuk *et al.* argued that the superluminal particle would be traveling "backward in time", should carry negative energy and would act as the antiparticle of the original one [32]. However, after 1962, Physics Textbooks that contain only the time-like SR still teach that there is no superluminal motion in nature, for instance, see [33]-[38], except Weinberg, S. discussed "Temporal Order and Antiparticles" briefly in his book [39]. Nevertheless, the problem Bilaniuk *et al.* studied in [32] is meaningful. Of course, their research that only considered time order and the sign of energy was not enough.

Set two reference frames Σ and Σ' like in Section 4, Σ' now moving at a velocity $v=|\vec{v}|<c$ relative to Σ in the negative direction of x (x') axis. If a tachyon would be emitted in Σ' (mother's body) at a velocity $|\vec{u}'|(=\mathrm{d}x'/\mathrm{d}t')$ along the common positive x (x') direction from the common origin of Σ and Σ', under the same condition $u'v>c^2$, let us check up that whether the symbols of the momentum, "(lepton) charge" and helicity seeing in Σ are changed.

We already know the following answers (a) and (b), merely with a focus on answers (c), (d) and (e).

a) *The time order*

Under condition $\mathrm{d}x'/\mathrm{d}t' > c^2/v$, the time order changes:

$$\mathrm{d}t = \frac{\mathrm{d}t' - v\mathrm{d}x'/c^2}{\sqrt{1-v^2/c^2}} < 0. \tag{8}$$

b) *The sign of energy*

Under $E'/p' = c^2/u' < v$ *i.e.* $u' > c^2/v$, the sign of energy changes:

$$E = \frac{E' - vP'}{\sqrt{1-v^2/c^2}} < 0. \tag{9}$$

c) *The sign of velocity and the sign of momentum*

Under $u'v > c^2$, *i.e.* $u'\left(=\mathrm{d}E'/\mathrm{d}p'\right) > c^2/v$, the sign of velocity and the sign of momentum change:

$$\left|\vec{u}\right| = \frac{\vec{u}' - \vec{v}}{1 - \frac{\left|\vec{u}'\right|\cdot\left|\vec{v}\right|}{c^2}} < 0$$

$$\left|d\vec{p}\right| = \frac{\left|d\vec{p}\right| - vE/c^2}{\sqrt{1-v^2/c^2}} < 0. \tag{10}$$

Very obviously, $\vec{p}$ in Σ is equivalent to the opposite direction of $\vec{p}'$ in Σ', $\vec{u}$ in Σ is equivalent to the opposite direction of $\vec{u}'$ in Σ'.

d) *The sign of* "(*lepton*) *charge*"

Just similar to the composition of the electronic current-density four-vector, "(Lepton) current-density" four-vector is defined as J_μ $(\rho\vec{u}, i\rho c)$, where ρ represents the abstract lepton charge in Σ (ρ' in Σ'), $\vec{u}$ is the current velocity of "(lepton) charge" in Σ ($\vec{u}'$ in Σ'). As $\left|\vec{u}'\right| = u' > c^2/v$, "(lepton) charge" ρ changes sign.

$$\rho = \frac{\rho'\left(1 - vu'/c^2\right)}{\sqrt{1-v^2/c^2}} < 0. \tag{11}$$

e) *The sign of helicity*

If vector $\vec{\sigma}$ denoting the spin of a neutrino-like lepton, its helicity is

$$\mathrm{H} = \frac{\vec{p}\cdot\vec{\sigma}}{\left|\vec{p}\right|\left|\vec{\sigma}\right|}.$$

As $u' > c^2/v$, the momentum $\vec{p}$ changes sign, of course, the helicity H changes sign too, *i.e.*

$$\mathrm{H} = \frac{\vec{p}\cdot\vec{\sigma}}{\left|\vec{p}\right|\left|\vec{\sigma}\right|} < 0. \tag{12}$$

In [39], considering the existence of space-like metric, Weinberg S. wrote "One of the most striking features of the Lorentz transformation is that they do not leave invariant the order of events", "There is only one known way out of this paradox". Weinberg's way would just be "the existence of antiparticles". In this Section one may see that according to the Lorentz transformation of physical quantities, the time order, the sign of energy, the sign of velocity, the sign of momentum, the sign of "(lepton) charge" and the sign of helicity, all of them

become negative under the same condition $u'v > c^2$, which means that the original tachyon has really appeared in its corresponding anti-tachyon in front of the observers. It should be emphasized again that for anti-tachyon, $\bar{p}$ in Σ and $\bar{u}$ in Σ were only equivalent to moving in the opposite direction of $\vec{p}'$ in Σ' and $\vec{u}'$ in Σ'. This effect may be called "face-changing effect", which is a space-like SR effect, should be experimentally observable.

6. Suggestion

Based on the studies in [6], one should know that the experimental confirmation of neutrino oscillation has provided two solutions:

a) Which would demonstrate that neutrinos have masses, → how to explain the related frame-independent property of their helicity and chirality → no violation examples have been observed so far. In addition, the theoretical speculations referring to Lorentz-violating, the violation of lepton number conservation, a tiny magnetic moments and so on, there are still not supported in experiments as yet [40] [41] [42], [42] even hopes for the future KATRIN experiments. → Is it necessary to think about that or the measurement accuracy is not enough? Or are there no such effects at all?

b) If neutrino were tachyon with massless which would not only ensure the unshakable fact of neutrino oscillations and but dispel the contradiction between massive neutrinos and the SM also, → but which proposes an urgent and difficult task *i.e.* to determine the tachyonic nature of neutrinos by experiments as soon as possible.

The author pointed in [8] that due to oscillation, it is impossible to measure the velocity of neutrino of a pure kind precisely by means of the classical "distance of flight/time of flight" measurement. In fact, the efforts of many experimenters in this way are very arduous, for instance see [43] [44]. Because of oscillations, such as electron neutrino $\leftrightarrow$ muon neutrino oscillation, even if the measurements have results, we don't know whose it is. Another proposal was put forward by the author in [6]: to test whether the energy-velocity relation is a monotonic decreasing function with increasing energies. But, due to the energy calibration being a hard job, it is still very difficult to perform.

On the basis of Section 5 we know that as long as the velocity $u'\left(=\mathrm{d}x'/\mathrm{d}t'\right)$ of a tachyon in Σ' would be greater than c^2/v, where Σ' moving at a velocity $v\left(|\vec{v}|<c\right)$ in the negative direction relative to Σ, there would exist one "face changing effect" related to this tachyon *i.e.* an anti-tachyon might be observed in Σ. This "face changing effect" provides a very important revelation: if neutrino were really superluminal particle, as long as its speed $u'\left(=\mathrm{d}x'/\mathrm{d}t'\right)$, at which it were created in Σ' (its mother body), would be greater than c^2/v, where v being the instantaneous motion velocity of its mother body relative to Σ (the laboratory) in the negative direction, an anti-neutrino related original neutrino might be observed in Σ. Fortunately, nuclear beta decays in nuclear reactors offer us with a technically sophisticated, less difficult and less costly way to determine the physical properties of neutrinos. There are two reasons:

1) Nuclear reactors are the major source of human-generated neutrinos. In a nuclear reactor the release energy is generated in the majority from the fission of four fissile isotopes ^{235}U, ^{238}U, ^{239}Pu and ^{241}Pu, then the resultant neutron-rich daughter nucleus rapidly undergo additional beta decays: each converting neutron inside a daughter nucleus decays into a proton, an electron and releasing an electron anti-neutrino $\bar{\nu}_e$

$$n \to p + e + \bar{\nu}_e .$$

At the nuclear level the movement of decay neutron is associated with the mother nuclei (A, Z) where it resides, that is the following process:

$$(A, Z) \to (A, Z+1) + e + \bar{\nu}_e .$$

The mother nucleus (A, Z) of the decay neutron is the desired inertial system Σ'.

2) Each nuclear fission released 200 MeV of energy on average, most of energy remained in the reactor core as heat, and a small amount of energy is radiated away as electron anti-neutrinos radiation. Roughly speaking, for example, a nuclear reactor with a thermal power of 5000 MW, the total power produced from fission atoms is around 4800 MW, only 200 MW is radiated away as electron anti-neutrino radiation. Considering the thermal effect of the nuclear reactor core and velocity distribution, the magnitude and orientation of the vibration velocity of the mother nucleus in the metal lattice would have a wide range, so that it also brings us hope.

Hence, as a display of "face changing effect", a few electron neutrino ν_e might be observed in Σ (the laboratory) so long as the velocity of some electron anti-neutrino $\bar{\nu}_e$ being greater than c^2/v, where v being the instantaneous thermal vibration velocity of its mother neutron in a beta decay with the speed of (A, Z). It should be noted that a) "face changing effect" of electron anti-neutrino $\bar{\nu}_e$ is not neutrino oscillation $\bar{\nu}_e \to \nu_e$ because $\Delta p_{ee}^2 = p_{0e}^2 - p_{0e}^2 = 0$; b) "face changing effect" would not be produced during a beta decay process, so that, this observing effect of space-like SR in Σ (any earth laboratories) does not violate lepton charge conservation and is very different from the experimental approach envisaged by Goldhabers [41], their expected observed helicity would be related to the relative velocity between neutrinos and Σ, but Σ needs to be skillfully designed and selected by experimenters. This detectable diagnostic measurement is just to search after ν_e in excess of the background counting in the $\bar{\nu}_e$ current. Only according to the measuring result, measured or not, there is or is not, this survey method offered by "face changing effect" mentioned above may be also called <yes-no> measurement. "Yes" result shows that the neutrinos are tachyons, "no" is not.

The author suggests the reactor neutrino experimental groups such as Double Chooz, Daya Bay, KAM LAND, Braidwood, Diable Canyon, Krasnoyarsk, RENO and other reactor neutrino experimental groups all over the world, in ad-

dition to the current reactor experimental research to the disappearance mode of $\bar{\nu}_e$, to add a measurement study of ν_e, to see if a few ν_e neutrinos in excess of the background might be detected. Although it is well known that on average, a nuclear power plant may generate over 10^{23} electron antineutrinos per second and the threshold for measuring electron neutrinos is less than the threshold for measuring electron anti-neutrinos, but this search is still a very small probability event.

By the way, according to the same physical reasons, in the solar neutrino current, there might be electronic anti-neutrinos in excess of the background, but it is difficult to measure. On May 30, 2018, there is an important scientific pulse submit to arXiv: the MiniBooNE experiment at Fermilab for 15 years reports an excess of electron neutrino events [45] [46], its data are consistent in energy and magnitude with the excess of events reported by the Liquid Scintillator Neutrino Detector (LSND) in the 1990s, and has not yet found a reasonable non-oscillation explanation. The author believes that if there are atomic power plants within tens of thousands of square kilometers around, the face-changing effect might be responsible for the observed abnormality.

Consequently, no need to measure the speed of $\bar{\nu}_e$ any more, it only needs to take patience and time, the outcome of this survey, whether it is positive or negative, is of great significance in physics.

7. Remarks

1) Mathematics does not lose its ability to foresee, especially for elementary mathematics. Historical experience is that the secrets revealed by elementary mathematics are often correct, no matter how much they seem to be unphysical according to our normal habit or even if we do not understand them at the moment. On the contrary, because of Heisenberg's uncertainty, those conclusions that were derived from higher mathematics relating to the limit $r \to 0$, or $|\vec{p}| \to \infty$, would be not necessarily correct. And so, we should treat the predictions from elementary mathematics in an equal manner, study them, verify them carefully, and should not reject some of them lightly. Otherwise, one false step will make a great difference and we may lose the decades of time.

2) The emergence of modern physics is marked by the establishment of classical mechanics in the sixteenth century, less than 400 years ago. It is believed that we already have some excellent theories; however it was often the case that the reality about our so many assumptions, theoretical models, and "beyond" theories had often been short-lived, so that these transitional theories would just guide our understanding. Remember that in fact we are just beginning a long and exciting journey to explore the natural world including the universe, and the exploration will go from the first level to the second level, to the third level, …, and need to go deeper and deeper. So in the face of nature there are many things that need to learn; in the face of the preliminary knowledge we have today, there is much to be discarded, much to be modified. This process has no end.

Acknowledgements

This work was supported by the National Science Foundation of China Grant No. U1532260. The author is very grateful to Dr. Chunlei Wang for his donation of historical literature for this study and help to deal with many chores.

Conflicts of Interest

The author declares no conflicts of interest regarding the publication of this paper.

References

[1] Pontecorvo, B. (1968) *Soviet Physics—JETP*, **6**, 429.

[2] Agafonova, N., *et al.* (2010) *Physics Letters*, **B691**, 138-145. https://doi.org/10.1016/j.physletb.2010.06.022

[3] Bornschein, B. (2008) *Fusion Science and Technology*, **54**, 59-66. https://doi.org/10.13182/FST54-59

[4] Babutzka, M., *et al.* (2012) *New Journal of Physics*, **14**, Article ID: 103046. https://doi.org/10.1088/1367-2630/14/10/103046

[5] Bornschein, L., *et al.* (2015) *Fusion Science and Technology*, **67**, 274-277. https://doi.org/10.13182/FST14-T9

[6] Ai, X.B. (2018) *Journal of Modern Physics*, **9**, 1432-1440. https://doi.org/10.4236/jmp.2018.97087

[7] Minkowski, H. (1952) The Principle of Relativity, A Collection of Original Memoris. Dover Publications, New York, 75.

[8] Ai, X.B. (2012) *Physica Scripta*, **85**, Article ID: 045005.

[9] Pontecorvo, B. (1968) *Soviet Physics—JETP*, **26**, 984.

[10] Gribov, V. and Pontecorvo, B. (1969) *Physics Letters*, **B28**, 493-496. https://doi.org/10.1016/0370-2693(69)90525-5

[11] Weinheimer, Ch., *et al.* (1993) *Physics Letters*, **B300**, 210-216. https://doi.org/10.1016/0370-2693(93)90355-L

[12] Belesev, A.I., *et al.* (1995) *Physics Letters*, **B350**, 263-272. https://doi.org/10.1016/0370-2693(95)00335-I

[13] Weinheimer, Ch., *et al.* (1999) *Physics Letters*, **B460**, 219-226. https://doi.org/10.1016/S0370-2693(99)00780-7

[14] Lobashev, V., *et al.* (1999) *Physics Letters*, **B460**, 227-235. https://doi.org/10.1016/S0370-2693(99)00781-9

[15] Assamagan, K., *et al.* (1996) *Physical Review*, **D76**, Article ID: 027005.

[16] Einstein, A. (1989) The Collected Papers of Albert Einstein. Vol. 2, Princeton University Press, New Jersey, 140.

[17] Einstein, A. (1989) The Collected Papers of Albert Einstein. Vol. 2, Princeton University Press, New Jersey, 262.

[18] Einstein, A. (1989) The Collected Papers of Albert Einstein. Vol. 3, Princeton University Press, New Jersey, 133.

[19] Einstein, A. (1989) The Collected Papers of Albert Einstein. Vol. 4, Princeton University Press, New Jersey, 257.

[20] Einstein, A. (1989) The Collected Papers of Albert Einstein. Vol. 3, Princeton Uni-

versity Press, New Jersey, 348.

[21] Einstein, A. (1989) The Collected Papers of Albert Einstein. Vol. 4, Princeton University Press, New Jersey, 35.

[22] Einstein, A. (1989) The Collected Papers of Albert Einstein. Vol. 2, Princeton University Press, New Jersey, 247.

[23] Einstein, A. (1989) The Collected Papers of Albert Einstein. Vol. 2, Princeton University Press, New Jersey, 265.

[24] Einstein, A. (1989) The Collected Papers of Albert Einstein. Vol. 3, Princeton University Press, New Jersey, 136.

[25] Einstein, A. (1989) The Collected Papers of Albert Einstein. Vol. 4, Princeton University Press, New Jersey, 40.

[26] Tolman, R.C. (1917) The Theory of Relativity of Motion. University of California Press, Berkeley, 54.

[27] Pauli, W. (1958) Theory of Relativity. Pergamon Press Ltd., London, 16.

[28] Stückelberg, E.C.G. (1941) *Helvetica Physica Acta*, **14**, 588.

[29] Stückelberg, E.C.G. (1942) *Helvetica Physica Acta*, **15**, 23-37.

[30] Feynman, R.P. (1948) *Physical Review*, **74**, 939-946. https://doi.org/10.1103/PhysRev.74.939

[31] Feynman, R.P. (1949) *Physical Review*, **76**, 749-759. https://doi.org/10.1103/PhysRev.76.749

[32] Bilaniuk, O.M.P., *et al.* (1962) *Amercan Journal of Physics*, **30**, 718-723. https://doi.org/10.1119/1.1941773

[33] Bohm, D. (1965) Special Theory of Relativity. W. A. Benjamin Inc., New York, 155.

[34] Taylor, E.F. and Wheeler, J.A. (1966) Space-Time Physics. W. H. Freeman Co., San Francisco, 40.

[35] Kacser, C. (1967) Introduction to Special Theory of Relativity. Prentice Hall Inc., Englewood Cliffs, 77.

[36] French, A.P. (1968) Special Relativity. W. W. Norton Co., New York, 117.

[37] Resnick, R. (1968) Introduction to Special Relativity. John Wiley and Sons Inc., New York, 106, 196.

[38] Schwartz, H.M. (1968) Introduction to Special Relativity. McGraw-Hill Book Co., New York, 59.

[39] Weinberg, S. (1972) Gravitation and Cosmology: Principles and Applications of the General Theory of Relativity. John Wiley &Sons Inc., New York, 61.

[40] Kostelecký, A. and Mewes, M. (2004) *Physical Review D*, **69**, Article ID: 016005. https://doi.org/10.1103/PhysRevD.69.016005

[41] Goldhaber, A. and Goldhaber, M. (2011) *Physics Today*, No. 5, 40. https://doi.org/10.1063/1.3592004

[42] Giunti, C. and Studenikin, A. (2015) *Reviews of Modern Physics*, **87**, 531. https://doi.org/10.1103/RevModPhys.87.531

[43] Adamson, P., *et al.* (2007) *Physical Review D*, **76**, Article ID: 072005. https://doi.org/10.1103/PhysRevD.76.072005

[44] Antonello, M., *et al.* (2012) *Physics Letters B*, **713**, 17-22. https://doi.org/10.1016/j.physletb.2012.05.033

[45] https://arxiv.org/abs/1805.12028

[46] https://en.wikipedia.org/wiki/MiniBooNE

Journal of Modern Physics, 2018, 9, 2206-2222
http://www.scirp.org/journal/jmp
ISSN Online: 2153-120X
ISSN Print: 2153-1196

Superluminality and Entanglement in an Electromagnetic Quantum-Relativistic Theory

Massimo Auci[1,2]

[1]Maths and Physics Department, Statal European International School "Altiero Spinelli", Torino, Italy
[2]Space Science Department, Odisseo-Space, Milano, Italy
Email: massimo.auci@gmail.com

How to cite this paper: Auci, M. (2018) Superluminality and Entanglement in an Electromagnetic Quantum-Relativistic Theory. *Journal of Modern Physics*, **9**, 2206-2222.
https://doi.org/10.4236/jmp.2018.912139

Received: September 13, 2018
Accepted: October 15, 2018
Published: October 18, 2018

Copyright © 2018 by author and Scientific Research Publishing Inc.
This work is licensed under the Creative Commons Attribution International License (CC BY 4.0).
http://creativecommons.org/licenses/by/4.0/

Open Access

Abstract

An electromagnetic theory that links quantum and relativistic phenomena in a single context is built. Wave-particle duality is the experimental proof of their common origin. In this context, Quantum Mechanics and Special Relativity are two compatible synergistic theories. The developed theory shows the existence of superluminal effects that suggest an explanation to the entanglement between pairs of particles and photons.

Keywords

Electromagnetic Interactions, Electrodynamics, Dipoles, Quantum-Relativistic Effects, Photons Exchange, Quanta, Superluminality, Entanglements

1. Introduction

The Bridge Theory (BT) is a quantised electromagnetic approach to electrodynamics [1]. The theory is based on the proof of the conjecture [2] of the physical meaning of the transversal component of the Poynting vector in the dynamics of the interactions among pairs of charged particles. Starting from the BT, will extend in a self-consistent way the theory to Special Relativity, proving as the wave-particle duality principle is the experimental evidence that Quantum Mechanics and Special Relativity derive from a common quantum-relativistic phenomenology [3]. In this context an explanation to superluminality and to quantum entanglement is proposed.

The theory is based on the lack of spherical symmetry in the electromagnetic emission of a dipole, which is localising in its neighbourhood an amount of energy and momentum at charge of the transversal component of the Poynting

vector of the Dipolar Electromagnetic Source (DEMS). The theoretical results concerning the localised energy and moment are in agreement with those of a photon. The BT provides two incertitude principles, one for observers inside the wave front of the DEMS, and one for observers placed outside the wave front in agreement with the Heisenberg's one. Also the theoretical and numerical estimations of the fine structure constant and consequently of the Planck constant, provided self-consistently from the theory, give results in agreement with the experimental one [4] [5].

To develop the outline of the theory it is assumed that the elementary particles in the lab system are already created in pair, each with a rest energy, whose origin and value are not now relevant for our purposes.

Following the BT, the total energy and momentum of each interacting pair settle the wavelength of the corresponding DEMS, which is equivalent to an exchanged photon with an energy and a momentum defined by particles dynamics. Three fundamental statements based on the actual theory are:

1) When a charged particle is moving in a medium, it produces with all the anti-particles with which it is in causal contact a spacetime distribution of DEMS;

2) The value of action characterising the production of a DEMS is the Planck constant which is depending by the internal structure of the electromagnetic field;

3) The DEMS is an electromagnetic source localising an energy and a momentum identical to those of the photon exchanged in the interaction between the pairs of particles forming the dipole; its wavelength is the synthesis of all the information about the dynamical state of the interacting particles.

Spacetime Distribution of DEMS, Real Waves-Packet and Virtual Photons

In order to observe a charged particle, according to the statement (I) we need that it interacts with at least another anti-particle producing a DEMS with a specific wavelength, this is equivalent to perform a measure of energy and momentum on the particle. When a charged particle crosses a space filled of matter feels the electromagnetic fields originated by the other particles and it interacts with them producing a distribution of DEMS. The multi-interaction shares the energy and momentum carried by the particle in motion with the distribution of DEMS, each with a different wavelength, the overlap of the waves originates a localised electromagnetic waves-packet which motion describes the incoming particle in spacetime.

The process producing a DEMS can be broken up into two phases:

- the approach or Alpha phase (A-phase), the interaction localises the energy and momentum of a photon inside the source zone;
- the removal or Omega phase (Ω-phase), the initial source zone is destroyed and the products emerging go away from one another continuing to interact.

The wave emission occurs during both phases, only during the A-phase a part of the mechanical energy and momentum of the incoming charged particles is localised inside the source zone supplying the energy and momentum of the exchanged photon between the two interacting particles. Since in BT the Planck's action is weakly varying with external constrains, only for free interactions among pairs of charges its value is perfectly equal to the that of the Planck's constant, so the presence of phenomena strictly depending on Planck's action can be considered the evidence of the formation in spacetime of DEMS. If a DEMS is existing, a photon and an electromagnetic wave associated respectively to the transversal and radial components of the Poynting vector are coexisting in the same phenomenon. Following this idea, for a particle crossing a medium a distribution of DEMS in space realises a net of direct (photon exchange) and indirect electromagnetic connections among different observers, producing a phenomenology which agrees both with the quantum and waves behaviours.

2. Formulation of a Quantum-Relativistic Principle

When a DEMS is produced, an observer placed in the laboratory S sees a fraction of the energy and momentum carried by the interacting particles exchanged between the particle as a photon, the residual amounts of energy and momentum provide respectively the kinetic energy and the momentum of the centre of mass of the source in motion with respect to S.

In order to characterise dynamically the interacting particles with respect to an observer S, we assign the initial energies and momenta $(E_1, \boldsymbol{P}_1)$ and $(E_2, \boldsymbol{P}_2)$. Before the beginning of the A-phase, the available total energy and momentum of the particles are given by

$$\begin{cases} E = E_1 + E_2 \\ \boldsymbol{P} = \boldsymbol{P}_1 + \boldsymbol{P}_2 \end{cases} \tag{1}$$

Considering the interaction occurring with the energy and momentum (1) with respect to the observer S; let E_Γ and $\boldsymbol{P}_\Gamma$ be respectively energy and momentum of the exchanged photon, the conservation laws applied to the interacting particles and to the DEMS produced require:

$$\begin{cases} E_\Gamma = P_\Gamma c \\ \Delta_0 = E - E_\Gamma \\ \dfrac{\boldsymbol{\Delta}}{c} = \boldsymbol{P} - \boldsymbol{P}_\Gamma \end{cases} \tag{2}$$

where Δ_0 and $\boldsymbol{\Delta}/c$ are respectively energy and momentum not involved in the DEMS formation, associated to the transverse projection of the motion of the source when it is observed along the sight line of the observer placed in the lab frame S.

To solve the Equation (2) we consider the length of the residual momentum not observed along the sight line

$$\Delta = \left\| \boldsymbol{P} - \boldsymbol{P}_\Gamma \right\| c = \sqrt{P^2c^2 + P_\Gamma^2 c^2 - 2PP_\Gamma c^2 \cos\theta} \tag{3}$$

Considering the difference between the squared of the momentum (3) and the squared of the energy non-involved in the DEMS formation as defined in Equation (2), we obtain

$$\Delta^2 - \Delta_0^2 = 2E_\Gamma \left(E - Pc\cos\theta\right) - \left(E^2 - P^2c^2\right) \tag{4}$$

where θ is the angle between the total momentum $\boldsymbol{P}$ and the momentum $\boldsymbol{P}_\Gamma$ associated to the photon emitted along the direction of the sight line of the observer S.

In order to define the value of the left side term of the Equation (4), we consider initially the case of an observer S_0 in the centre of mass (c.m.) of the DEMS during a head-to-head interaction. The energy and the momentum (1) of the particles are completely involved in the DEMS formation, so the residual energy Δ_0 and the transversal momentum $\boldsymbol{\Delta}/c$ for this observer must be both equal to zero. If during the production of the DEMS a migrating inertial observer moves along its sight line transiting trough the c.m. of the source, the total energy and momentum observed cannot change, so the changing in energy and momentum of the source emission is balanced by the energy and momentum of the relative motion between c.m. of the source and observer in such a way that the value of the left side term of the Equation (4) continue to be zero for all the inertial observers even if the residual energy and transversal momentum are not zero as in c.m. Therefore, for each inertial observer embedded in the electromagnetic field of a DEMS, the squared difference at left side of the Equation (4) equal to the rest energy of the interacting particles not involved in the DEMS production is zero:

$$\Delta^2 - \Delta_0^2 = 0, \tag{5}$$

using (5), the (4) can be solved with respect E_Γ obtaining:

$$E_\Gamma = \frac{E^2 - P^2c^2}{2\left(E - Pc\cos\theta\right)} \tag{6}$$

able to measure along the direction defined by the observation angle θ the energy E_Γ emitted by a DEMS in relative motion with respect the observer S.

The Equation (6) is able to manage energy and momentum of the DEMS observed in the frame S, its validity is general and introduces a fundamental principle involving the energy-momentum invariance for whatever system observer-source, independently from their relative inertial motion. Using the Equation (5) we propose the invariant

$$\left(E - E_\Gamma\right)^2 - \left(P - P_\Gamma\right)^2 c^2 = 0 \tag{7}$$

as a Quantum-Relativistic Principle (QRP).

The QRP Applied to a Single Moving Particle

By considering an observer S placed in a frame associated to one of two interacting particles of a pair, for the effect of the relative motion the two particles can have symmetrically the roles of impinging particle and target. Let θ be the

angle between the directions of the dipole moment $\boldsymbol{P}_\Gamma$ of the DEMS formed by the direct interaction and the momentum $\boldsymbol{P}$ of the trajectory of the impinging particle, according to the θ angle definition, if we place arbitrarily the observer in the frame S_2 coinciding with the target particle, no energy and momentum can be associated to this observer because he cannot interact with himself, so assuming for example m_1 and $\boldsymbol{\beta}_1$ respectively the observed mass and the dimensionless velocity of an impinging particle #1, from the Equation (1) we get

$$\begin{cases} \boldsymbol{P}c \equiv \boldsymbol{P}_1 c = m_1 \boldsymbol{\beta}_1 c^2 \\ E \equiv E_1 \end{cases} \tag{8}$$

In the BT approach exist a correlation between the first interaction distance and the wavelength that will have the source. In fact, the instant when two particles begin to interact corresponds to the birth of the DEMS which starts to emit with null luminosity when the particles are at 3/2 of the minimal effective distance λ that will be reached at the end of the A-phase. Following BT, the minimal effective distance defines the value of the characteristic wavelength of emission of the DEMS and is correlated with the instant in which the DEMS achieves the maximum luminosity. Since the delay time between the effective and the real positions of the impinging particle along its trajectory is always within the time interval $0 \le t_{\text{delay}} < T$, the ratio between the distance $R\left(t_{\text{delay}}\right)$ of the two interacting particles at time t_{delay} and the minimal effective distance of interaction λ is equal to:

$$\rho = \frac{R\left(t_{\text{delay}}\right)}{\lambda} = 1 + \beta \cos\theta, \tag{9}$$

which value is in the interval $1 \le \rho < 2$. By using the Equation (8) and (9) we obtain the identity

$$Pc\cos\theta = \left(\rho - 1\right) m_1 c^2 \tag{10}$$

from which using Equation (8) and (10), the Equation (4) for the QRP becomes

$$2E_\Gamma \left[E_1 - \left(\rho - 1\right) m_1 c^2 \right] - \left[E_1^{\,2} - m_1^2 \beta^2 c^4 \right] = 0 \tag{11}$$

Considering a head-to-head collision at very high energy with $\theta \cong 0$ and $\beta \cong 1$, the Equation (9) converges to $\rho = 2$ and the DEMS is created with the maximum available energy $E_\Gamma \equiv E_1$ coinciding with that one of the impinging particle measured by the observer placed in the frame of the target #2. In these conditions the Equation (11) has solution

$$E_\Gamma \equiv E_1 = m_1 c^2 \tag{12}$$

i.e. when the interaction occurs at very high velocity the energy of the DEMS converges to all the available relativistic energy of the source, equivalent to the total energy of the impinging particle #1.

For interactions with energies involved lower than the maximum value of the

available energy (12), the energy (6) is depending by the energy and momentum of the interacting particles.

In order to define a characteristic invariant term characterising the available energy for the DEMS, we use the numerator of the Equation (6).

Let

$$\varepsilon_1^2 = E_1^2 - P_1^2 c^2 \tag{13}$$

be a non-null non-impulsive squared term associated to the energy of the impinging particle #1, using the momentum of the Equation (8) and the solution (12), we define

$$E = \frac{\varepsilon_1}{\sqrt{1-\beta_1^2}} = \gamma_1 \varepsilon_1 \tag{14}$$

where ε_1 is the rest energy involved in the DEMS production, measured in the c.m. of the interacting particle #1 and E_1 is the total energy of the DEMS equivalent to that of the particle #1 measured by the point of view of the observer placed on a the target particle #2. Equation (14) is in agreement with the Special Relativity. Using the Equation (8) and (14), the energy and momentum of the DEMS produced or equivalently the energy and momentum of the impinging particle became

$$\begin{cases} \boldsymbol{P} = \boldsymbol{\beta}_1 \gamma_1 \dfrac{\varepsilon_1}{c} \\ E = \gamma_1 \varepsilon_1 \end{cases} \tag{15}$$

Since the Equation (6) represent the electromagnetic energy of the DEMS produced during the interaction between the impinging particle and the observer, the energy and momentum (15) are coinciding with the electromagnetic energy and momentum of a photon exchanged (statement (III)) between the two particles, which energy is characterised by a Doppler frequency due to the relative motion between source and observer.

The Equation (12) proves that the energy E_Γ of the DEMS converges on the total electromagnetic energy E of the interacting particles showing that the production of the DEMS is a physical process able to transform the rest energy ε of a particle in the electromagnetic energy of the DEMS. The result (15) is the proof that the DEMS process produces a typical relativistic result starting from a typical quantum result. Since the total energy (14) of the impinging particle resulting from (13) can be positive or negative depending on whether we consider a particle or an antiparticle. The values of total energy inside the interval $-\varepsilon_1 < E < \varepsilon_1$ are forbidden because an excitation of the particle with an energy greater than $2\varepsilon_1$ may excite a negative energy particle up into the positive energy states [6].

3. Wave-Matter Duality: Compton and de Broglie Waves

Many authors have conjectured that the de Broglie wave describing a particle is a

real wave modulated by relativistic effects [7]. In agreement with the statement (III), using the Equations (6) and (15) to rewrite the electromagnetic energy and momentum exchanged between particle and observer

$$\begin{cases} E_{\Gamma} = \dfrac{\varepsilon}{2}\gamma\dfrac{1-\beta^2}{1-\beta\cos\theta} \\ P_{\Gamma} = \dfrac{\varepsilon}{2}\dfrac{\gamma\beta}{c}\dfrac{\dfrac{1}{\beta^2}-1}{\dfrac{1}{\beta}-\cos\theta} \end{cases} \tag{16}$$

the first of the Equation (16) can be interpreted as a relativistic Doppler effect due to the relative motion of the source emitting from its c.m. an energy $\varepsilon/2$ along the sight line of the observer [8]. The Equation (16) describes energy and momentum of the impinging particle as a real electromagnetic wave source, emitting along the specific sight line on which is placed the observer on the target. For symmetry, we can exchange the roles of impinging particle and observer. During their reciprocal interaction if the angle of interaction is inside the interval $0<\theta\le\pi$, and the particle moves with $\beta \ll 1$, frequency and wavelength of the exchange photon converge to the Compton values for an energy $\varepsilon/2$ that can be considered the non-relativistic approximation:

$$\begin{cases} \nu_c = \varepsilon/2h \\ \lambda_c = 2hc/\varepsilon \end{cases} \tag{17}$$

on the otherwise for a very high energy collision, the angle of interaction during the interaction could be considered close to zero in such a way that frequency and wavelength converge to the de Broglie values for the relativistic energy $\gamma\varepsilon$

$$\begin{cases} \nu_{db} = \gamma\varepsilon/h \\ \lambda_{db} = hc/\beta\gamma\varepsilon \end{cases} \tag{18}$$

By considering the observer interacting with an impinging particle #1, let $\varepsilon_1 = m_1c^2/\gamma_1$ be the rest energy of the particle converted in electromagnetic energy and momentum (16), the correspondence between electromagnetic and mechanical values allows to consider a massive particle as an wave associated to de Broglie frequency and wavelength

$$\begin{cases} \nu_{db} = \dfrac{\gamma_1\varepsilon_1}{h} = \dfrac{m_1c^2}{h} \\ \lambda_{db} = \dfrac{hc}{\beta_1\gamma_1\varepsilon_1} = \dfrac{h}{\beta_1 m_1 c} \end{cases} \tag{19}$$

in general, the Compton wave of a particle is a de Broglie wave in non-relativistic conditions.

3.1. Observation of an Interacting Pair in the Lab

From the symmetry of the observers placed in the frames S_1 and S_2, each of them measures reciprocally the energy of the respective impinging particle without

being able to measure their own rest energy. In fact, in order to make a measure of energy in these two frames, they need to create a local DEMS, but in each one of the frames S_1 and S_2 just a single charge is placed, so the observers cannot perform local measurements of their energy and momentum.

By defining a lab-frame in which a polarisable neutral medium as ordinary matter or vacuum can interact, when an interaction between a pair of charges coinciding with the frames #1 and #2 occurs, the neutral medium reacts with the particles producing two independent DEMS: SS_1, SS_2.

From the experimental point of view, in order to observe the collision of the two particles we cannot use directly the frames S_1 and S_2, because the DEMS S_1S_2 and the symmetrical one, do not allow simultaneous measurements of energy and momentum of the two colliding particles. Instead, using the lab S we can measure energy and momentum of the c.m. of all the subjects involved in the collision. In fact, the lab is sensible to the total energy involved, so applying the Equation (16) to the interaction between the lab at rest and each of the two particles #1 and #2, we get for each particle involved in the interaction:

$$SS_j \begin{cases} E_j = \gamma_j \varepsilon_j \\ \boldsymbol{P}_j = \gamma_j \boldsymbol{\beta}_j \dfrac{\varepsilon_j}{c} \end{cases} \tag{20}$$

where ε_j is the rest energy of each particle involved. The Lorentz factor and the relative velocity of the particles in Equation (20) are both referred to the same lab.

3.2. Observation of a DEMS in the Lab

To calculate in the lab S the total energy and momentum of the c.m. S_0 of the DEMS produced by the two interacting particles, we must obtain the explicit expressions of the total rest energy and of the factors $\boldsymbol{\beta}$ and γ. By using the invariant (13) and the Equation (1) and (20) for the two involved particles with rest energy and dimensionless velocity $(\varepsilon_i, \boldsymbol{\beta}_i)$, is obtained the total rest energy:

$$\varepsilon = \sqrt{\left(E_1 + E_2\right)^2 - \left\|\boldsymbol{P}_1 + \boldsymbol{P}_2\right\|^2 c^2} = \sqrt{\varepsilon_1^2 + \varepsilon_2^2 + 2\varepsilon_1\varepsilon_2\gamma_1\gamma_2\left(1 - \beta_1\beta_2\cos\delta\right)} \tag{21}$$

where δ is the angle between the momenta $\boldsymbol{P}_1$ and $\boldsymbol{P}_2$ of the two colliding particles with respect to the lab-frame S.

Since the c.m. S_0 moves with respect S with a velocity $\boldsymbol{\beta}$

$$\boldsymbol{\beta} = \frac{\left(\boldsymbol{P}_1 + \boldsymbol{P}_2\right) c}{E_1 + E_2} = \frac{\varepsilon_1\gamma_1\boldsymbol{\beta}_1 + \varepsilon_2\gamma_2\boldsymbol{\beta}_2}{\varepsilon_1\gamma_1 + \varepsilon_2\gamma_2}. \tag{22}$$

To obtain γ, by using the total rest energy (21) we get:

$$\gamma = \frac{E_1 + E_2}{\varepsilon} = \frac{\varepsilon_1\gamma_1 + \varepsilon_2\gamma_2}{\varepsilon}. \tag{23}$$

Using now the Equation (21) and (22) with the (23), energy and momentum of the c.m. of the DEMS produced during the interaction of the two particles with respect to the lab-frame, in agreement with the Equation (1) and (15) is

given by

$$SS_0 \quad \begin{cases} E = \gamma\varepsilon \equiv \varepsilon_1\gamma_1 + \varepsilon_2\gamma_2 \\ \boldsymbol{P} = \gamma\boldsymbol{\beta}\dfrac{\varepsilon}{c} \equiv \dfrac{\varepsilon_1}{c}\gamma_1\boldsymbol{\beta}_1 + \dfrac{\varepsilon_2}{c}\gamma_2\boldsymbol{\beta}_2 \end{cases}. \tag{24}$$

In this case SS_0 is a connection between lab-frame and c.m. of the DEMS S_1S_2, Equation (24) is equivalent to a pair of DEMS SS_1 and SS_2.

3.3. Doppler Effect in the Lab-Frame

The dynamical state of one interacting particle respect an observer is defined by the energy and momentum of the DEMS produced. Since the frame S_0 associated to the c.m. of a DEMS is in motion with respect each observer in the universe, using the energy of the Equation (16) we define a characteristic wavelength λ_0 connecting the c.m. of the DEMS with the observer. The wave at low energy corresponds to the Compton wavelength and at high energy is modulated by a Doppler factor due to the relative motion between the two frames S and S_0:

$$\lambda_0 = \lambda_c\gamma\left(1-\beta\cos\theta\right), \tag{25}$$

the wavelength of the c.m. (25) is a generalization of the Compton wavelength of the source for observers in relative motion respect the c.m. of the DEMS, proving as the impinging particle has a wave behaviour respect the observer [9] when the observer interact trough out the wave emitted by a DEMS produced in the lab, *i.e.* interacts indirectly, but has a particle behaviour as described in the Equation (20) when they interacts directly with the observer producing a DEMS.

4. Application to the Compton Experiment Phenomenology

A historical step in the birth of the Quantum Mechanics was done with the Compton experiment. In this paragraph is explained the Compton's experiment without to use the usual approach.

When a pair electron-positron interact with respect to the lab frame S at very low relative velocity $\beta_1 \approx \beta_2 \approx 0$ it follows $\beta \approx 0$ and $\gamma \approx 1$, Equation (21) gives a rest energy $\varepsilon \approx 2m_ec^2$ coinciding with the total energy of the particles, *i.e.* the Compton and the de Broglie wavelengths have an identical value. Under these conditions the wavelength (25) of a photon emitted from the c.m. S_0 of the DEMS toward an atomic electron is the Compton's wavelength (17) of the incoming electron or positron in which the carried rest energy is all that of the pair.

Now following the experimental procedure, we know that during a collision of an X-ray photon with an orbital electron of an atom of graphite, the photon could be bounced away only like massive particles can do. Following BT phenomenology, when the photon with energy E and momentum P impinges on an electron at rest, the intense electric field existing in the neighbourhood of the atomic electron polarises locally the photon in a electron-positron virtual pair with a near zero kinetic energy. The pair can live only a short time during which

the atomic electron interacting with the virtual positron of the pair produces a new real DEMS which is observed in the lab-frame as a bounced photon with energy and momentum $E' < E$ and $P' < P$. The residual virtual electron of the pair not directly involved in the DEMS production is scattered away with an amount of energy and momentum bigger than the energy of the atomic electron. The phenomenology above, describes a process in which two electrons exchange their role. In fact, the atomic electron and the virtual electron of the pair switch their physical identities.

The wavelength of the photon bounced away and collected in the lab-frame S along a direction forming an angle θ with the beam axis, is different from the wavelength produced in the DEMS performed by the positron-electron interaction during the X-electron scattering. In fact, the virtual positron interacting with the atomic electron of the graphite produces a low energy local DEMS in the layer, with a resulting wavelength equal to the Compton one, whereas in the lab-frame S, on the calorimeter are collected all the photons emitted by the DEMS with a de Broglie wavelength. Hence considering the X-electron scattering, when the polarised positrons interact with the atomic electrons the energy of the interaction is low enough to converge in the c.m. of the DEMS to the Compton wavelength of the positron. By using this local equivalence, we combine the Compton and de Broglie wavelengths and frequencies obtaining in agreement with the formal result proposed by de la Peña and Cetto and Kracklauer the transformation

$$\begin{cases} \lambda_{db} = \dfrac{\lambda_c}{\beta\gamma} \\ \nu_{db} = \gamma\nu_c \end{cases} \tag{26}$$

from the Compton wavelength and frequency in the frame of the c. m. to the de Broglie wavelength and frequency in the lab-frame [10] [11].

To analyse the emission of the DEMS produced in the graphite layer, *i.e.* the Doppler modulations (25) of the Compton wavelength λ_c of the scattered photons varying with respect to the collection angle θ, we use the S_0 frame of the c.m. of the DEMS produced during the positron-electron interaction. Since velocity and Compton wavelength are constant with respect to the variation of the angle, the differential of the Doppler wavelength (25) gives

$$\mathrm{d}\lambda_0 = \beta\gamma\lambda_c \sin\theta \mathrm{d}\theta \tag{27}$$

which describes in the frame S_0 of the scattered photon the differential behaviour of the generalised Compton wavelength of the DEMS. Applying the transformation (26) to the Equation (27) in order to obtain the de Broglie wavelength variation in the frame S where the photons are collected

$$\mathrm{d}\lambda = \lambda_c \sin\theta \mathrm{d}\theta \tag{28}$$

integrating on an arbitrary interval [λ, λ'] corresponding to an angular interval [0, θ] in which are collected the scattered photons. Using the Compton wave-

length definition (17) where the rest energy (21) in terms of rest mass gives $\varepsilon = 2m_e c^2$ Equation (28) becomes:

$$\lambda' - \lambda = \frac{h}{m_e c}\left(1 - \cos\theta\right) \tag{29}$$

fully in agreement with the experimental result.

5. Electron-Positron Annihilation

If we consider the lab-frame placed in the c.m. of the two impinging particles, in such a way that the observed energy along the sight line is half of the total energy (16) of the DEMS

$$E_\Gamma = \frac{\gamma\varepsilon}{2} \tag{30}$$

the angle at which the DEMS is able to emit two photons with an energy equal to half of the total energy of the source produced is:

$$\theta = \arccos\sqrt{1 - \frac{1}{\gamma^2}}\,. \tag{31}$$

Considering a low energy $\gamma \cong 1$, the electron-positron annihilation occurs with a null total momentum and a total energy $\varepsilon \cong 2m_e c^2$.

In agreement with the Equation (31), we observe in the lab-frame the emission of two opposite photons at an angle of 90˚ respect the trajectory of the two colliding particles, each with a frequency coinciding with the Compton one $\nu \cong \frac{m_e c^2}{h}$.

In general, for $\gamma > 1$ the c.m. of the pair is moving away from the lab-frame with a speed βc and the photon emission occurs with two symmetric angles of scattering lower than 90˚ degrees.

Using the principle of the time reversal we can consider a pair creation from a polarized source. In this case at low energy electrons can be created and successively annihilated producing two photons.

6. The Cherenkov Limit Angle

In order to define the emission angle in which a particle crossing a media S is seen to emit photons by an observer, according to the existence and positivity of the Doppler energy (16) we have:

$$\cos\theta < \frac{1}{\beta} \tag{32}$$

always verified in vacuum where the source can emit photons in any direction, whereas for observers embedded in a polarizable medium with a relative refraction index $n > 1$ Equation (32) gives for a crossing particle:

$$\theta \geq \arccos\frac{1}{n\beta} \tag{33}$$

describing the characteristic Cherenkov effect with a limit angle for the photon emission in a medium crossed by electrical particles moving at velocity greater then light in the medium.

7. Deduction of the Lorentz-Einstein's Transformations

The use of the generalised Compton wavelength allows to deduce the Lorentz-Einstein transformations, in fact, if a particle interacts in the lab-frame with many antiparticles each DEMS produced emits a wave. When the waves achieve the positions of two different observers, each wave allows to the observers to perform independent measures of energy and momentum of the same interacting particle, each wave is associated to a measure of time and position of the same particle. Is fundamental to know how the measures are interconnected.

We consider the c.m. S_0 of a DEMS placed in a whatever lab in space. When two different observers receive the electromagnetic signal emitted by the same DEMS S_0, the Compton wave is observed in two different places S and S' with different wavelength for the Doppler effect (25) produced between the DEMS and each observer.

Assuming arbitrarily the observer $\mathcal{S}$ to be at rest with respect S_0 in such a way that the emission of the DEMS along the sight line connecting S_0 to S forms a null angle with respect the direction of observation, and the observer $\mathcal{S}'$ to be in motion in such a way that the sight line connecting S_0 to $\mathcal{S}'$ forms a non null angle with respect to the direction of emission connecting S_0 and $\mathcal{S}$, the measures of time and position of the event "emission from the c.m. S_0 of the DEMS", realized independently by the two observers $\mathcal{S}$ and $\mathcal{S}'$ are connected by the generalized Compton wavelengths (25):

$$\frac{x}{\lambda_c}=\frac{ct}{\lambda_c}=\frac{x'}{\lambda_0}=\frac{ct'}{\lambda_0}=a \tag{34}$$

where $a>0$ is equal for each observer. Using the Equation (25) and (34), we write two space and time transformations able to interconnect the measures of position and time of the two inertial observers $\mathcal{S}$ and $\mathcal{S}'$:

$$\begin{cases} x'=\gamma\left(x-vt\cos\theta\right) \\ t'=\gamma\left(t-v\dfrac{x}{c^2}\cos\theta\right) \end{cases} \tag{35}$$

the transformations (35) agree with the generalized Lorentz-Einstein's transformations, which in standard configuration ($\theta=0$) describe the observer $\mathcal{S}'$ moving along the X-axis toward the observer $\mathcal{S}$.

In this context the derivation of the relativistic transformations (35) takes origin from a typical EM wave-connection between the DEMS and the observers. This result proves that the measures of space and time can be performed only if the two observers $\mathcal{S}$ and $\mathcal{S}'$ are reached by the same wave signal emitted by a DEMS in S_0. To do that is necessary each pair of observers are causally connected with a same DEMS. In general if a particle moving in spacetime produc-

ing a great number of DEMS, each in a different points P of space, each observer can be connected with all the points P of space by means of the own interaction with all the DEMS produced, *i.e.* the wavelengths of each DEMS realise a different metric (34) for each pair of observers and empty spacetime is not a static primitive geometric notion, but a variable active consequence of the existence of infinite wave connections among observers.

8. Information Transfer between Two or More Observers

In Relativity a phenomenon of great relevance and mystery is the impossibility to define an inertial frame $\mathcal{S}$ with respect of which a system S_0 in motion with respect to the frame S has a relative velocity greater than c. Analysing this effect in the present context, considering a signal as an elementary information, is proved as the direct transferring of information violates the cause-effect principle, because occurs with a superluminal velocity. On the otherwise, when the transferring of information is produced indirectly by successive interactions involving two or more inertial observers, the velocity cannot exceed the speed of light.

To prove that is considered the differentials of the Equation (34) for a motion between the observers S and $\mathcal{S}$ at speed component $\pm v_x = v\cos\theta$:

$$\begin{aligned} \mathrm{d}x' &= \gamma\left(\mathrm{d}x \pm v_x \mathrm{d}t\right) \\ \mathrm{d}t' &= \gamma\left(\mathrm{d}t \pm v_x \frac{\mathrm{d}x}{c^2}\right) \end{aligned} \tag{36}$$

Dividing the differential of space with the one of the time, Equations (36) give the usual relativistic sum of the velocity for an observer S_0 in motion with speed component u_x along the X-axis in the frame S in relative motion with speed component v_x respect $\mathcal{S}$

$$u'_x = \frac{\mathrm{d}x'}{\mathrm{d}t'} = \frac{u_x \pm v_x}{1 \pm \dfrac{u_x v_x}{c^2}} \tag{37}$$

If the motion of S_0 with speed u_x respect to S or the motion of S with speed v_x respect to $\mathcal{S}$ were to occur at infinite velocity, the relativistic sum of the velocities (37) cannot be infinite but would give respectively c^2/v_x or c^2/u_x, each value of which is a finite superluminal speed coinciding with the phase velocity of the de Broglie's wave observed in the frame $\mathcal{S}$ as it were emitted respectively from a DEMS associated to the moving frames S and S_0.

8.1. Superluminal Communication between Two Interacting Observers

In order to the previous consideration we take in to account a pair of charged particles placed in the frames S_1 and S_2. When two charged particles reach a reciprocal distance of interaction equal to 3/2 of the wavelength of the source zone of the DEMS that will produced, the principle of cause-effect was been violated. In that instant the source zone starts to expand it localising inside the spherical crown of the source zone centred in the c.m. of the interacting pair, an amount

of energy and momentum greater than zero. The energy localised inside the source zone increases until the charges reach the minimum interaction distance compatible with their trajectories, this minimum value sets the final wavelength λ of the DEMS equivalent to the exchanged photon. How does the source before that the phase A of the interaction ends, at know the minimum distance of interaction? During the DEMS formation, the progressive expansion of an ideal spherical surface from the initial diameter λ and the final diameter $3\lambda/2$ delimits the source zone. During the expansion, the diameter of the surface increases with the angular phase φ of the spinning of the field of the Poynting vector around the DEMS. Its expansion speed is $u_{\exp} = c/\varphi$, *i.e.* when at the beginning the phase is $\varphi = 0$ the source zone starts to expand it with an infinite velocity decreasing rapidly with the phase value. After a time $T/2$ the source zone ends to expand it and the DEMS starts to emit as an ideal electromagnetic dipole.

Considering the observer S_1 placed on the particle #1 in motion with a relative velocity v_{12}, at $\varphi = 0$ using Equation (37) the observer S_2 measures the velocity of propagation of the spherical front of the DEMS as

$$u'_{\exp} = \lim_{\varphi \to 0} \frac{\frac{c}{\varphi} + v_x}{1 + \frac{v_x}{\varphi c}} = \frac{c^2}{v_x} \tag{38}$$

coinciding with the speed of the de Broglie wave (19). In this sense the de Broglie wave carries superluminally the information of the reciprocal interaction in a way such that each particle know the energy and momentum that will be exchanged before really the true interaction occurs.

8.2. Subluminal Communication between Inertial Observers

Considering the relative velocity $\boldsymbol{u} = (u_x, 0, 0)$ of an observer placed in S_0 with respect an observer S, the transformations (38) give the velocity of S_0 with respect the observer S' when S and S' are in relative motion along the X-axis at a velocity $\boldsymbol{v} = (v\cos\theta, 0, 0)$.

Since the position of S_0 on the X-axis is settled by the coordinate $x = a\lambda_0$ on the lab-frame S at time $t = aT_0$, where wavelength and period characterise the wave signal emitted towards the observer S from the DEMS placed in S_0. The Compton's wave emitted from S_0 is received in the frame S in a Doppler wave mode coinciding with a de Broglie's wave, so to measure position and time of S_0 with respect S we apply the transformations (26) on the signal emitted from S_0 obtaining:

$$\begin{cases} x = a\dfrac{\lambda_0}{\beta_x \gamma} \\ t = a\dfrac{\lambda_0}{\gamma c} \end{cases} \tag{39}$$

Since S_0 is in relative motion with respect the frame S at velocity u_x, calcu-

lating the speed component $u_x^* = \mathrm{d}x/\mathrm{d}t$ of the DEMS in S_0 with respect the observer S, the Equation (39) gives

$$u_x^* = \frac{c}{\beta_x} \equiv \frac{c^2}{u_x} \tag{40}$$

which is equal to the phase velocity of the de Broglie's wave received in the frame S.

Considering a particle #1 in relative motion respect the observer in the lab-frame S, the direct interaction produces a DEMS SS_1 connecting the two systems with an electromagnetic signal propagating with superluminal velocity (40). Similarly occurs considering the direct interaction between the frames S and S', the direct interaction connects the observers with a signal propagating with velocity

$$v_x^* = \frac{c}{\beta_x'} \equiv \frac{c^2}{v\cos\theta} \tag{41}$$

To obtain information about the velocity of a system S_0 respect the frame S' we use the Equation (39) obtaining

$$u_x' = \frac{u_x^* + v_x^*}{1 + \dfrac{u_x^* v_x^*}{c^2}} = \frac{u_x + v\cos\theta}{1 + \dfrac{u_x v\cos\theta}{c^2}} \tag{42}$$

always lower than c. The Equation (40) and (42) prove that the observer S can measure for an incoming particle a velocity greater than c only when interacts directly with it, in this case the wave emitted toward S is a monochromatic Compton's wave, received as a shifted Doppler wave due to the relative motion of the impinging particle in the frame. The wave measured by the observer is coinciding with the de Broglie's wave of the impinging particle. For observations occurring in a frame S' on which are collected in a unique wave-packet more waves, each emitted from a DEMS produced during the direct interaction of the particle with a different inertial observer, the velocity measured by the Equation (40) is equivalent at the group velocity of the wave-packet describing the particle, always lower than the light speed.

8.3. Direct Entanglement

By considering the case in which two particles are created in pair with a kinetic energy enough to escape each from the other, this is the act of formation of a primary DEMS in which the two particles vary their interaction distance with continuity increasing the wavelength due to the direct interaction and remaining entangled for ever with their direct connection. In fact, the DEMS has a decreasing wavelength in time but the Planck's action of the corresponding exchanged photons remains with the same value. Each interaction involving one of the two particles in time, for the energy and momentum conservation laws of the DEMS, maintain the correlation in spacetime in such a way that any modification of spin, energy and momentum occurring on one of the two particles, produces a simultaneous correlate modification in the twin particle, independently

from their effective distance. The modification is occurring at superluminal velocity (40) and corresponds to an instantaneous revision of the direct interaction to maintain continuously unchanged the electromagnetic structure of the DEMS which for a free direct interaction has a constant coupling value α.

9. Conclusion

In order to reduce the number of models and theories required to describe exhaustively a phenomenon with manifold aspects, are ever necessary new powerful ideas. In this article an extension of the Bridge Theory is proposed to describe in a single self-consistent theoretical and phenomenological context the quantum-relativistic behaviours appearing experimentally in the interactions among photons and charged particles. The present theoretical formulation proves that the wave-particle duality is the experimental evidence of a common origin of two much different behaviours of a charged particle, as the ones described by Quantum Mechanics and by Special Relativity. The emerging theory shows that superluminality and entanglement both have to do with the direct electromagnetic interaction of a pair of charged particles producing a DEMS. In fact, after the production of the dipole, the electromagnetic source continues to exist independently by their effective distance achieved during their removal phase and independently by the occasional external actions that could occur on one of the two particles forming the DEMS. Each action modifying the dynamic state of one of the two particles produces an instantaneous reaction on the dynamic state of the other to keep their coupling constant. In fact, for all free interactions, independently of the dynamics of the two particles and their distances, the constant of fine structure is numerically invariant.

Acknowledgements

With great pleasure I thank Prof. Guido Dematteis for his contribution to the understanding of this new emerging theory.

Conflicts of Interest

The authors declare no conflicts of interest regarding the publication of this paper.

References

[1] Auci, M. and Dematteis, G. (1999) *International Journal of Modern Physics*, **B13**, 1525-1557. https://doi.org/10.1142/S0217979299001569

[2] Auci, M. (1989) *Physics Letters A*, **135**, 86-88. https://doi.org/10.1016/0375-9601(89)90650-6

[3] Auci, M. (2003) On the Compatibility between Quantum and Relativistic Effects in an Electromagnetic Bridge Theory. arXiv:1003.3861

[4] Auci, M. (1990) *Physics Letters A*, **148**, 399-404. https://doi.org/10.1016/0375-9601(90)90488-A

[5] Auci, M. (1990) *Physics Letters A*, **150**, 143-150. https://doi.org/10.1016/0375-9601(90)90109-2

[6] Feshback, H. and Villars, F. (1958) *Reviews of Modern Physics*, **30**, 24. https://doi.org/10.1103/RevModPhys.30.24

[7] Bhaumik, M. (2016) Deciphering the Enigma of Wave-Partcle Duality. arXiv:1611.00226

[8] Einstein, A. (1905) *Annalen der Physik*, **17**, 891. https://doi.org/10.1002/andp.19053221004

[9] Auci, M. (2003) Wave-Particle Behaviour in Bridge Theory. arXiv:1201.4577

[10] de la Peña, L. and Cetto, M. (1996) The Quantum Dice: An Introduction to Stochastic Electrodynamics. Kluwer Academic Publishers, Norwell, MA, Chap. 12. https://doi.org/10.1007/978-94-015-8723-5

[11] Kracklauer, A.F. (1992) *Physics Essays*, **5**, 226. https://doi.org/10.4006/1.3028975

Journal of Modern Physics, 2018, 9, 2223-2232
http://www.scirp.org/journal/jmp
ISSN Online: 2153-120X
ISSN Print: 2153-1196

Statistical Derivation of the Fundamental Scalar Field

B. I. Lev[1,2]

[1]Bogolyubov Institute for Theoretical Physics of the NAS of Ukraine, Kyiv, Ukraine
[2]Department of Physics, Chungnam National University, Daejeon, Korea
Email: bohdan.lev@gmail.com

How to cite this paper: Lev, B.I. (2018) Statistical Derivation of the Fundamental Scalar Field. *Journal of Modern Physics*, **9**, 2223-2232.
https://doi.org/10.4236/jmp.2018.912140

Received: September 14, 2018
Accepted: October 15, 2018
Published: October 18, 2018

Copyright © 2018 by author and Scientific Research Publishing Inc.
This work is licensed under the Creative Commons Attribution International License (CC BY 4.0).
http://creativecommons.org/licenses/by/4.0/

Open Access

Abstract

Based on a nonequilibrium statistical operator, it has been shown that the fundamental scalar field provides a natural representation of the repulsive interaction that produces scattering in the system and thus motivates law of entropy increasing.

Keywords

Statistical Physics, Fundamental Scalar

The standard methods of the equilibrium statistical mechanics cannot be applied to the study of systems with long-range interactions because relevant thermodynamic ensembles can be nonequivalent inasmuch as equilibrium states correspond only to local entropy maxima [1] [2], in particular, since energy is not-additive, and cannot use the canonical ensemble to study the system with long-range interaction. Two types of approaches (statistical and thermodynamic) have been developed to determination the equilibrium states of such interacting system and describe possible phase transition. It is generally believed that mean field theory is exact for systems. Since in mean field theory any thermodynamically function depends on the thermodynamically variables only through the dimensionless combinations and the system is thermodynamically stable but the thermodynamically limit does exist [3].

The purpose of this paper is to develop a new approach [4] [5] to the statistical description of a system of interacting particles with regard for spatial inhomogeneity of the particle or the field distribution. In order to describe such structures, it is necessary to work out a method that would enable us to select the states with thermodynamically stable particle distributions [6]. The main idea is

to give a detailed treatment of an interacting system in terms of the principles of nonequilibrium statistical mechanics [7]. The representation of the partition function in terms of the functional integral over external fields makes it possible to employ the methods of the quantum field theory [8]-[15]. The extension to the complex plane provides a possibility to apply the saddle-point method to find the dominant contributions to the partition function and to obtain all the thermodynamical functions of the system. It allows selecting the system states associated both with homogeneous and inhomogeneous particle distributions.

This method is based on the Hubbard-Stratonovich representation of the partition function [16]. We employ the saddle-point approximation taking into account the conservation laws for the number of particles and energy and thus obtain a nonlinear equation. The latter provides a statistical description in terms of mathematical physics and may be treated as a natural definition of the field variables. In this way we can answer the question of how the fundamental scalar field appears in the field theory with the necessary condition, to consider the nature of this field and the spatial features of its behavior. The answer to this question should follow from the statistical nature of the interaction and the thermodynamic law of entropy increase.

The phenomenological thermodynamics is based on the conservation laws for the average values of physical parameters, *i.e.*, the number of particles, energy, and momentum. The statistical thermodynamics of nonequilibrium systems is also based on the conservation laws, but for the dynamical variables rather than their average values. It represents local conservation laws for the dynamical variables. In order to determine the thermodynamical functions of a nonequilibrium system, a representation of the relevant statistical ensembles is needed with allowance for the nonequilibrium states of the system. The concept of Gibbs ensemble can provide a description of nonequilibrium stationary states. In this case we can determine a nonequilibrium ensemble as a totality of systems contained under similar stationary external conditions. To determine a local equilibrium ensemble exactly, we have to find the distribution function or the statistical operator of the system [7]. We can assume that nonequilibrium states of the system can be written in terms of the spatial distribution energy $H(\mathbf{r})$ and the microscopic particle density $n(\mathbf{r})=\sum_i \delta(\mathbf{r}-\mathbf{r}_i)$. Then the statistical operator [7] of the local equilibrium distribution is given by:

$$Q_l = \int D\Gamma \exp\left\{-\int\left(\beta(\mathbf{r})H(\mathbf{r})-\eta(\mathbf{r})n(\mathbf{r})\right)\mathrm{d}\mathbf{r}\right\} \tag{1}$$

The integration in this formula should be carried out over the whole phase space of the system. It should be noted that in the case of local equilibrium distributions the Lagrange multipliers $\beta(\mathbf{r})$ and $\eta(\mathbf{r})$ are functions of spatial points. The local equilibrium distributions may be introduced provided the relaxation time of the whole system is much longer than the relaxation time in any local macroscopic area contained in this system. The thermodynamic relation for interacting systems can be obtained under this condition. The variation of the statistical operator with respect to the Lagrange multipliers yields the

required thermodynamic relations as given by [7] $-\frac{\delta \ln Q_l}{\delta \beta(\mathbf{r})} = \langle H(\mathbf{r}) \rangle_l$ and $\frac{\delta \ln Q_l}{\delta \eta(\mathbf{r})} = \langle n(\mathbf{r}) \rangle_l$. These relations provide a natural general extension of the well-known relation for equilibrium systems to the case of non-equilibrium systems.

In the general case, the Hamiltonian of a system of interacting particles can be written as

$$H = \sum_i \frac{p_i^2}{2m_i} + \frac{1}{2}\sum_{i,j} U(\mathbf{r}_i \mathbf{r}_j) \tag{2}$$

where p_i and m_i is impulse and mass every particle and $U(\mathbf{r}_i \mathbf{r}_j)$ determines the energy of the repulsive interaction. The energy density can present in the form:

$$H(\mathbf{r}) = \frac{p^2(\mathbf{r})}{2m(\mathbf{r})} n(\mathbf{r}) + \frac{1}{2}\int U(\mathbf{r},\mathbf{r}') n(\mathbf{r}) n(\mathbf{r}') \mathrm{d}\mathbf{r}' \tag{3}$$

The nonequilibrium statistical operator of an interacting system is given by

$$\begin{aligned} Q_l = \int D\Gamma \exp\Bigg\{ -\int \Bigg(\beta(\mathbf{r}) \frac{p^2(\mathbf{r})}{2m(\mathbf{r})} - \eta(\mathbf{r}) \Bigg) n(\mathbf{r}) \mathrm{d}\mathbf{r} \\ -\frac{1}{2}\int \beta(\mathbf{r}) U(\mathbf{r},\mathbf{r}') n(\mathbf{r}) n(\mathbf{r}') \mathrm{d}\mathbf{r}\mathrm{d}\mathbf{r}' \Bigg\} \end{aligned} \tag{4}$$

where $D\Gamma = \frac{1}{(2\pi\hbar)^3}\prod_i \mathrm{d}r_i \mathrm{d}p_i$ for the integration over the phase space.

In order to perform formal integration in the second term of this presentation, we introduce additional field variables within the context of the theory of Gaussian integrals [8] [16] *i.e.*,

$$\begin{aligned} &\exp\Bigg\{ -\frac{\nu^2}{2}\int \beta(\mathbf{r}) \omega(\mathbf{r},\mathbf{r}') n(\mathbf{r}) n(\mathbf{r}') \mathrm{d}\mathbf{r}\mathrm{d}\mathbf{r}' \Bigg\} \\ &= \int D\psi \exp\Bigg\{ -\frac{\nu^2}{2}\int \beta(\mathbf{r}) \omega^{-1}(\mathbf{r},\mathbf{r}') \psi(\mathbf{r}) \psi(\mathbf{r}') \mathrm{d}\mathbf{r}\mathrm{d}\mathbf{r}' - \nu \int \sqrt{\beta(\mathbf{r})} \psi(\mathbf{r}) n(\mathbf{r}) \mathrm{d}\mathbf{r} \Bigg\} \end{aligned} \tag{5}$$

where $D\psi = \frac{\prod_s \mathrm{d}\psi_s}{\sqrt{\det 2\pi\beta\omega(\mathbf{r},\mathbf{r}')}}$ and $\omega^{-1}(\mathbf{r},\mathbf{r}')$ is the inverse operator that satisfies the condition $\omega^{-1}(\mathbf{r},\mathbf{r}')\omega(\mathbf{r}',\mathbf{r}'') = \delta(\mathbf{r}-\mathbf{r}'')$. Thus, the interaction energy is represented by the Green function for this operator and $\nu^2 = \pm 1$ in accordance with the sign of the interaction of the potential energy. The introduced field variable $\varphi(\mathbf{r})$ contains information similar to the original distribution function, *i.e.*, complete information concerning probable spatial states of the system. In this way introduced field which describe behavior of the distribution of the interacting particles.

The statistical operator can be rewritten in the form given by

$$Q_l = \int D\Gamma \int D\psi \exp\left\{-\int\left(\beta(\mathbf{r})\frac{p^2(\mathbf{r})}{2m(\mathbf{r})} - \eta(\mathbf{r}) - i\sqrt{\beta(\mathbf{r})}\psi(\mathbf{r})\right)n(\mathbf{r})\mathrm{d}\mathbf{r}\right\}Q_{int} \quad (6)$$

where $Q_{int} = \exp\left\{-\frac{1}{2}\int\beta(\mathbf{r})U(\mathbf{r},\mathbf{r}')^{-1}\psi(\mathbf{r})\psi(\mathbf{r}')\mathrm{d}\mathbf{r}\mathrm{d}\mathbf{r}'\right\}$ follows from the interaction in terms of the field variable. The latter general functional integral can be integrated over the phase space. We substitute the definition expression for the density, then the nonequilibrium statistical operator reduces to

$$Q_l = \int D\psi \int \frac{1}{(2\pi\hbar)^3 N!}\prod_i \mathrm{d}r_i \mathrm{d}p_i \xi(\mathbf{r}_i)\exp\left\{-\left(\beta(\mathbf{r}_i)\frac{p_i^2}{2m_i} - i\sqrt{\beta(\mathbf{r}_i)}\psi(\mathbf{r}_i)\right)\right\}Q_{int} \quad (7)$$

where $\xi(\mathbf{r}) \equiv \exp\eta(\mathbf{r})$ is the chemical activity. Integration over all the moments reduces the real part of the non-equilibrium statistical operator to a simple expression [4] [9] given by

$$Q_l = \int D\psi Q_{int}\exp\left\{\int\left[\xi(\mathbf{r})\left(\frac{2\pi m(\mathbf{r})}{\hbar^3\beta(\mathbf{r})}\right)^{\frac{3}{2}}\cos\left(\sqrt{\beta(\mathbf{r})}\psi(\mathbf{r})\right)\right]\mathrm{d}\mathbf{r}\right\} \quad (8)$$

For the general case of long-range interaction, e.g., Coulomb like or Newtonian gravitation interaction in continuum, the limiting inverse operator should be treated in the operator sense, *i.e.*, $U^{-1}(\mathbf{r},\mathbf{r}') = -L_{\mathbf{rr}'} = -L_{\mathbf{r}'}\delta(\mathbf{r}-\mathbf{r}')$. For the case of long-range interaction between particles, the non-equilibrium statistical operator can be written as

$$Q_l = \int D\psi \exp\left\{\int\left[\psi(\mathbf{r})L_{\mathbf{rr}'}\psi(\mathbf{r}') + \xi(\mathbf{r})\Lambda^{-3}(\mathbf{r})\cos\left(\sqrt{\beta(\mathbf{r})}\psi(\mathbf{r})\right)\right]\mathrm{d}\mathbf{r}\right\} \quad (9)$$

where $\Lambda(\mathbf{r}) = \left(\frac{\hbar^2\beta(\mathbf{r})}{2m(\mathbf{r})}\right)^{\frac{1}{2}}$ is the thermal de-Broglie wavelength in each spatial point. In the general case, the non-equilibrium statistical operator is given by

$$Q_l = \int D\psi \exp\left\{S(\psi(\mathbf{r}),\xi(\mathbf{r}),\beta(\mathbf{r}))\right\} \quad (10)$$

with the effective non-equilibrium "local entropy" being described by the expression

$$S = \int\left[\psi(\mathbf{r})L_{\mathbf{rr}'}\psi(\mathbf{r}') + \xi(\mathbf{r})\Lambda^{-3}(\mathbf{r})\cos\left(\sqrt{\beta(\mathbf{r})}\psi(\mathbf{r})\right)\right]\mathrm{d}\mathbf{r} \quad (11)$$

The statistical operator is suitable to apply the efficient methods developed in the quantum field theory without additional restrictions on either integration over the field variables or the perturbation theory. The functional $S(\psi(\mathbf{r}),\xi(\mathbf{r}),\beta(r))$ depends on the field distribution, the chemical activity, and the inverse temperature. After that we can apply the saddle-point method to find the asymptotic value of the statistical operator Q_l as the number of particles N tends to infinity. The dominant contribution is given by the states that satisfy the extremum condition for the functional. It can be easily shown that the saddle-point equation represents the thermodynamic relation and can be

reduced to an equation for the field variable, $\frac{\delta S}{\delta \psi(\mathbf{r})}=0$, the normalization condition $\int \frac{\delta S}{\delta \xi(\mathbf{r})}\xi(\mathbf{r})\mathrm{d}\mathbf{r}=N$, and the energy conservation law for the system $\int \frac{\delta S}{\delta \beta(\mathbf{r})}\xi(\mathbf{r})\mathrm{d}\mathbf{r}=E$. The solution of this equation completely determines all the thermodynamical functions and describes the general behavior of interacting systems with both spatially homogeneous and inhomogeneous particle distributions. The above set of equations in principle solves the many-particle problem in the thermodynamical limiting case. The spatially inhomogeneous solution of these equations corresponds to the distribution of interacting particles. It is very important to note that only this approach makes it possible to take into account the inhomogeneous distribution of the temperature that can depend on the spatial distribution of particles in the system.

From the normalization condition and definition $\int \rho(\mathbf{r})\mathrm{d}\mathbf{r}=N$ can introduce some new variable which present the macroscopic density function $\rho(\mathbf{r})\equiv \Lambda^{-3}(\mathbf{r})\xi(\mathbf{r})\cos\left(\sqrt{\beta(\mathbf{r})}\psi(\mathbf{r})\right)$. In the case without interaction $\varphi(\mathbf{r})=0$ for free particles, if write the chemical activity in terms of the chemical potential $\xi(\mathbf{r})=\exp\left(\mu(\mathbf{r})\beta(\mathbf{r})\right)$ from present definition can obtain the well-known relation $\beta(\mathbf{r})\mu(\mathbf{r})=\ln\rho(\mathbf{r})\Lambda^{3}(\mathbf{r})$ that generalizes the relation of the equilibrium statistical mechanics [17] [18]. The equation for energy conservation in this case can present in the new form:

$$\frac{1}{2}\int \frac{\rho(\mathbf{r})}{\beta(\mathbf{r})}\left(3-\sqrt{\beta(r)}\psi(\mathbf{r})tg\left(\sqrt{\beta(\mathbf{r})}\psi(\mathbf{r})\right)\right)\mathrm{d}\mathbf{r}=E \tag{12}$$

Derivation of the energy-conservation equation over the volume yields a relation for the chemical potential, *i.e.*,

$$\frac{1}{2}\frac{\rho(\mathbf{r})}{\beta(\mathbf{r})}\left(3-\sqrt{\beta(r)}\psi(\mathbf{r})tg\left(\sqrt{\beta(\mathbf{r})}\psi(\mathbf{r})\right)\right)=\frac{\delta E}{\delta V}\frac{\delta V}{\delta N}=\mu(\mathbf{r})\rho(\mathbf{r}) \tag{13}$$

hence the chemical potential is given by

$$\mu(\mathbf{r})\beta(\mathbf{r})=\frac{3}{2}-\frac{1}{2}\sqrt{\beta(r)}\psi(\mathbf{r})tg\left(\sqrt{\beta(\mathbf{r})}\psi(\mathbf{r})\right). \tag{14}$$

This approach also provides the equation of state for the system within the context of the thermodynamic relation for pressure $P=\frac{1}{\beta}\frac{\delta S}{\delta V}$ for the case of energy conservation. The local equation of state is now reduced to

$$P(\mathbf{r})\beta(\mathbf{r})=\rho(\mathbf{r})\left(\mu(\mathbf{r})\beta(\mathbf{r})-\frac{1}{2}\right) \tag{15}$$

In the case of an ideal gas $\psi(\mathbf{r})=0$ we have $\mu\beta=\frac{3}{2}$ and obtain the usual equation of state $P\beta=\rho$. Thus the equation of state reproduces the equation of state of the ideal gas. The energy of the system is equal to $E=\frac{3}{2}NkT$, this

formula is in accordance with the previous well-known results [18]. Within the context of the definition (15) we can conclude that, under the condition $\mu(\mathbf{r})\beta(\mathbf{r})<\frac{1}{2}$, there appears negative pressure $P(\mathbf{r})<0$ that satisfies the necessary vacuum condition in the cosmology. It holds under the special condition $\sqrt{\beta(r)}\psi(\mathbf{r})tg\left(\sqrt{\beta(\mathbf{r})}\psi(\mathbf{r})\right)<2$, for constant temperature and for the total energy of the system $E<\frac{1}{2}NkT$. This condition implies that the energy of each particle is lower than the thermal energy. In this special case the energy of the system is lower than the total thermal energy of particles, that is impossible.

The possibility to apply the saddle-point method and thus to select the system states whose contributions in the partition function are dominant [6]. The solutions obtained equations associated with the finite values of the functional may be regarded as thermodynamically stable particle and field distributions. On this solution we must determine the general relation between thermodynamic parameter and their spatial dependence. Thus the spatially inhomogeneous distribution of the fields can be unambiguously related to the spatially inhomogeneous particle distribution. In general approach all thermodynamic parameter *i.e.* (pressure, chemical potential, density) dependence from spatial point and dependence one from other. Actually, this approach extends the average field approximation to involve into consideration spatially inhomogeneous field distributions. In our case the introduced field describes the nature of repulsive interaction and can present the fundamental scalar field which correspond for the scattering in the system.

If introduce the new field variable $\varphi=\sqrt{\beta(r)}\psi(\mathbf{r})$ and take into account the definition of the chemical potential (14) can rewrite the macroscopic density in the form given by

$$\rho(\mathbf{r})\equiv\Lambda_e^{-3}(\mathbf{r})\exp\left\{-\frac{1}{2}\varphi(\mathbf{r})tg\varphi(\mathbf{r})\right\}\cos\varphi(\mathbf{r}) \tag{16}$$

where the de-Broglie wavelength is renormalized, *i.e.*, $\Lambda_e=\left(\frac{\hbar^2\beta(\mathbf{r})e}{2m(\mathbf{r})}\right)^{\frac{1}{2}}$. The local entropy in terms of the new variable after substitution obtained relation in (11) is given by

$$S=\int\left[\frac{\varphi(\mathbf{r})}{\sqrt{\beta(r)}}L_{\mathbf{rr}'}\frac{\varphi(\mathbf{r}')}{\sqrt{\beta(r)}}+\Lambda_e^{-3}(\mathbf{r})\exp\left\{-\frac{1}{2}\varphi(\mathbf{r})tg\varphi(\mathbf{r})\right\}\cos\varphi(\mathbf{r})\right]\mathrm{d}\mathbf{r} \tag{17}$$

For constant temperature and equal particles masses the local entropy in the mean-field approximation can be presented as

$$S=\int\left[\frac{1}{\beta}\varphi(\mathbf{r})L_{\mathbf{rr}'}\varphi(\mathbf{r}')+\Lambda_e^{-3}\exp\left\{-\frac{1}{2}\varphi(\mathbf{r})tg\varphi(\mathbf{r})\right\}\cos\varphi(\mathbf{r})\right]\mathrm{d}\mathbf{r} \tag{18}$$

Now the equation for the field variable can be rewritten as

$$2L_{\mathbf{rr}'}\varphi(\mathbf{r}')-\beta\frac{\mathrm{d}V(\varphi)}{\mathrm{d}\varphi}=0 \tag{19}$$

where the potential energy $V(\varphi)\equiv\rho(\mathbf{r})=\Lambda_e^{-3}\exp\left(-\frac{1}{2}\varphi(\mathbf{r})tg\varphi(\mathbf{r})\right)\cos\varphi(\mathbf{r})$ is a function of the field variable in the above form. This potential has a minimum for $3\sin 2\varphi=-2\varphi$. For small values of φ we have two different solutions $\varphi=0$ and $\varphi^2=1$. For small φ the effective potential is given by a very simple expression $V(\varphi)=\left(1-\varphi^2\right)$ and the equation for the field variable reduces to $2L_{\mathbf{rr}'}\varphi(\mathbf{r}')+2\beta\varphi(\mathbf{r}')=0$. In the general case the potential energy of the field possesses oscillation character with decreasing amplitude. This fully relation with necessary condition of the cosmological model natural inflation was proposed in article [19]. After that we can analyze the probable spatial solution for the field variable and the behavior of the field in the time. In order to provide this, the knowledge of particle interaction energy with relevant specifics is required. It is well-known from cosmology reasoning that galaxy scattering is associated with the fundamental scalar field. We have shown above that the repulsive statistical interaction can be described in terms of the field $\varphi=\sqrt{\beta(r)}\psi(\mathbf{r})$. We suppose that the introduced fields are fundamental scalar fields responsible for the statistical motivation of the scattering of matter. From this assumption we can find the energy of interaction between two masses located in different spatial point. As follows from cosmology, two masses scatter with the velocity $v=H(\mathbf{r}-\mathbf{r}')$ where H is the Hubble constant and $\mathbf{r}-\mathbf{r}'$ is the distance between them. The kinetic energy of the relative motion for each mass is given by $T=\frac{m(\mathbf{r})}{2}H^2(\mathbf{r}-\mathbf{r}')^2$ and thus the energy of interaction between two masses located in different spatial points is $W(\mathbf{r}-\mathbf{r}')=\frac{m(\mathbf{r})}{2}H^2(\mathbf{r}-\mathbf{r}')^2+\frac{m(\mathbf{r}')}{2}H^2(\mathbf{r}-\mathbf{r}')^2$. For homogeneous distribution of masses, the last expression can be rewritten as $W(\mathbf{r}-\mathbf{r}')=m(\mathbf{r})H^2(\mathbf{r}-\mathbf{r}')^2$. In terms of such interaction energy, the inverse operator is given by

$$L_{\mathbf{rr}'}=\frac{1}{mH^2}\frac{\mathrm{d}^2}{\mathrm{d}r^2} \tag{20}$$

Having determined the inverse operator, we can present the spatial dependence of the fundamental scalar field as the solution of the equation

$$\frac{2}{mH^2}\frac{\mathrm{d}^2\varphi}{\mathrm{d}r^2}-\beta\frac{\mathrm{d}V(\varphi)}{\mathrm{d}\varphi}=0. \tag{21}$$

For small values of φ the latter transforms to the equation

$$\frac{\mathrm{d}^2\varphi}{\mathrm{d}r^2}+\beta mH^2\varphi=0 \tag{22}$$

that has a periodical solution $\varphi=\cos\left(\sqrt{m\beta}Hr\right)$ with the spatial period $\frac{1}{\sqrt{m\beta}H}$. For distances shorter than this value we can regard the fundamental

scalar field to be invariable. However, the fundamental scalar field can change in time. To describe the evolution of such fields, we can present a dynamical equation.

In our case, however, this field motivates the repulsive interaction in the system and the entropy increase. The behavior of the solution of the equation is similar to the behavior that follows from the usual equation for the scalar field and formation of a new-phase bubble of the fundamental scalar field. The present solution can describe the formation of a bubble of a new phase in the theory of inflation of the Universe [20] [21] [22], and the field variable introduced plays the role of the fundamental scalar field and takes into account the repulsive interaction in the system under consideration. In the general presentation, formula (11) can describe the condition of new phase formation, the size of the bubble, and other parameters of the thermodynamical behavior of such systems. This non-equilibrium statistical description concerns only probable dilute structures of such systems, it does not describe metastable states and tells nothing about the time scales in the dynamical theory. In this way, however, we can solve complicated problems of the statistical description of interacting systems. For this purpose we have to derive a dynamical equation for the field. In this sense we can use the Ginsburg-Landau equation for the fundamental scalar field in the standard form given by

$$\frac{\partial\varphi(\mathbf{r},t)}{\partial t}=-\gamma\frac{\delta S}{\delta\varphi(\mathbf{r})} \tag{23}$$

where γ is the dynamical viscosity coefficient [23]. In this case all the necessary conditions satisfy the thermodynamic relation. We can suppose that the motivation of the Universe dynamics is associated with the entropy increase. The evolution in the non-equilibrium state is governed by the local entropy landscape and the morphological instabilities of the parameter. The dynamics of the system is dissipative, and it should result in the decrease of the local entropy. This solution obtained equation which gives the answer on the equation: what is motive scattering of the matter. Dynamic of formed Universe can be only dissipative and for description of existence of Universe we must take into account its nonequilibrium conditions.

Interacting particle systems are non-equilibrium a priory. Before relaxing to the thermodynamic equilibrium, isolated systems with long-range interactions are trapped in non-equilibrium quasi-stationary states whose lifetimes diverge as the number of particles increases. A theory was presented which allows us to quantitatively predict the instability threshold for spontaneous symmetry breaking for a class of d-dimensional systems [24]. Non-equilibrium stationary states of the systems were described in article [25] which concluded that three-dimensional systems do not evolve to thermodynamic equilibrium but are trapped in non-equilibrium quasi-stationary states. We propose an approach that provides a possibility to quantitatively predict the particle distribution in a system with special repulsive interaction. In this way we can solve the compli-

cated problem of the statistical description of systems with special repulsive interactions and introduce a new field variable that reduces this task to the solution of the cosmological problem. Moreover, this method may also be applied for the further development of physics of self-gravitating and similar systems that are not far from equilibrium.

Acknowledgements

This article carry out for financial support from theme department of physics and astronomy of NAS Ukraine "Dynamic formation spatial uniform structures in many-body system" PK 0118U003535. This work was supported in part by Brain Pool program by Grant N 218H1D3A2065894 through the National Research Foundation of Korea (NRF).

Conflicts of Interest

The author declares no conflicts of interest regarding the publication of this paper.

References

[1] Thirring, W. (1970) *Zeitschrift für Physik*, **235**, 339-352. https://doi.org/10.1007/BF01403177

[2] Chavanis, P.-H., Rosier, C. and Sire, C. (2002) *Physical Review E*, **66**, Article ID: 036105.

[3] Laliena, V. (2003) *Nuclear Physics B*, **668**, 403-411. https://doi.org/10.1016/j.nuclphysb.2003.07.005

[4] Lev, B.I. and Zhugaevych, A.Ya. (1998) *Physical Review E*, **57**, 6460. https://doi.org/10.1103/PhysRevE.57.6460

[5] Lev, B.I. and Zagorodny, A.G. (2011) *Physical Review E*, **84**, Article ID: 061115. https://doi.org/10.1103/PhysRevE.84.061115

[6] Lev, B.I. (2011) *International Journal of Modern Physics B*, **25**, 2237-2249. https://doi.org/10.1142/S0217979211100771

[7] Zubarev, D.N. (1974) Non-Equilibrium Statistical Thermodynamics. Consultans Bareu, New York.

[8] Kleinert, H. (1989) Gauge Fields in Condensed Matter. World Scientific, Singapore. https://doi.org/10.1142/0356

[9] deVega, H.J., Sanchez, N. and Combes, F. (1996) *Physical Review D*, **54**, 6008. https://doi.org/10.1103/PhysRevD.54.6008

[10] Lipatov, L.N. (1977) *JETP* (*Sov*), **72**, 412.

[11] Edward, S. and Lenard, A. (1962) *Journal of Mathematical Physics*, **3**, 778. https://doi.org/10.1063/1.1724281

[12] Hubbard, J. (1959) *Physical Review Letters*, **3**, 77. https://doi.org/10.1103/PhysRevLett.3.77

[13] Grigorishin, K.V. and Lev, B.I. (2005) *Physical Review E*, **71**, Article ID: 066105. https://doi.org/10.1103/PhysRevE.71.066105

[14] Bilotsky, Y.D. and Lev, B.I. (1984) *Teoreticheskaya i Matematicheskaya Fizika*, **60**, 120.

[15] Samuel, S. (1978) *Physical Review D*, **18**, 1916. https://doi.org/10.1103/PhysRevD.18.1916

[16] Stratonovich, R.L. (1958) *Soviet Physics*, *Doklady*, **2**, 416.

[17] Ruelle, D. (1969) Statistical Mechanics. Rigorous Results, New York, Amsterdam.

[18] Huang, D. (1969) Statistical Mechanics. W. A. Benjamin, New York.

[19] Adams, F.C., Richard Bond, J., Freese, K., Frieman, J.A. and Olinto, A.V. (1993) *Physical Review D*, **47**, 426. https://doi.org/10.1103/PhysRevD.47.426

[20] Linde, A.D. (1990) Elementary Particle Physics and Inflationary Cosmology. Horwood Academic, Chan. https://doi.org/10.1201/b16971

[21] Linde, A.D. (1979) *Reports on Progress in Physics*, **42**, 389-437. https://doi.org/10.1088/0034-4885/42/3/001

[22] Coleman, S. (1977) *Physical Review D*, **15**, 2929-2936. https://doi.org/10.1103/PhysRevD.15.2929

[23] Landau, L.D. (1973) Statistical Mechanics. Nauka, Moskwa.

[24] Pakter, R., Marcos, B. and Levin, Y. (2013) *Physical Review Letters*, **111**, Article ID: 230603. https://doi.org/10.1103/PhysRevLett.111.230603

[25] Benetti, F.P.C., Ribeiro-Teixeira, A.C., Pakter, R. and Levin, Y. (2014) *Physical Review Letters*, **113**, Article ID: 100602. https://doi.org/10.1103/PhysRevLett.113.100602

Journal of Modern Physics, 2018, 9, 2233-2256
http://www.scirp.org/journal/jmp
ISSN Online: 2153-120X
ISSN Print: 2153-1196

Merger of Compact Binaries in the Context of Gravitational Waves and Short-Lived Gamma-Ray Bursts

Shawqi Al Dallal[1], Walid J. Azzam[2]

[1]College of Graduate Studies and Research, Ahlia University, Manama, Bahrain
[2]Department of Physics, College of Science, University of Bahrain, Zallaq, Bahrain
Email: shaldallal@gmail.com

How to cite this paper: Al Dallal, S. and Azzam, W.J. (2018) Merger of Compact Binaries in the Context of Gravitational Waves and Short-Lived Gamma-Ray Bursts. *Journal of Modern Physics*, **9**, 2233-2256.
https://doi.org/10.4236/jmp.2018.912141

Received: September 20, 2018
Accepted: October 19, 2018
Published: October 22, 2018

Copyright © 2018 by authors and Scientific Research Publishing Inc.
This work is licensed under the Creative Commons Attribution International License (CC BY 4.0).
http://creativecommons.org/licenses/by/4.0/

Open Access

Abstract

The discovery of gravitational waves resulting from the merger of two massive black holes (GW150914) has revolutionized our view of merging compact binaries. Recently, the Swope Supernova Survey of the optical counterpart of a gravitational wave event in the NGC 4993 galaxy, GW170817, emanating from the merger of two neutron stars, has triggered a lot of research work. Emphasis has been on comparing the existing theoretical models with the observational data, allowing for the prospect of an even more stringent test of general relativity. The afterglow of this event was observed in a wide range of wavelengths extending from radio waves to gamma rays. In this work, we first explore the evolutionary pathways of compact binary systems following the in-spiral, merger, and ring down sequence. We then proceed to discuss the processes leading to the production of gravitational waves and electromagnetic emission resulting from the merger of compact objects, particularly neutron star binaries and neutron star-black hole systems. We construct a basic inventory of the energy released during the merger of compact binaries in all bands of the electromagnetic spectrum with emphasis on gamma-ray burst emission. The constraints on certain wavelength emissions, such as gamma-ray bursts, are discussed in terms of orbital dynamical instabilities, energy transfer processes, and possible jet orientations with respect to the observer. Finally, we explore the futuristic perspective of the impact of gravitational waves detection on our understanding of the working of the universe.

Keywords

Merging Binaries, Compact Objects, Gravitational Waves, Gamma-Ray Bursts

1. Introduction

Gravitational waves are ripples in the fabric of spacetime generated by accelerating masses. They are generated also by a change in the quadruple moment, which is produced only when there is an asymmetrical movement of mass. They propagate outward as a wave from their source with the speed of light, and transport energy as gravitational radiation.

The possibility of the existence of gravitational waves (GW) was discussed in 1893 by Oliver Heaviside evoking the analogy between the inverse square law in electromagnetism and gravitation [1]. In 1905, Henri Poincaré proposed their existence as being required by the Lorentz transformation, and suggested that, in analogy to accelerating electrical charge emitting electromagnetic waves, an accelerating mass should generate GWs [2]. Subsequently, gravitational waves were predicted in 1916 by the general theory of relativity [3] [4].

Gravitational waves can provide deeper insight into important natural phenomena in the universe. They can penetrate regions of space prohibited to electromagnetic radiation. Thus, they allow, for example, the observation of the merger of compact objects in remote galaxies billions of light years away. Gravitational waves can also be used to probe the very early universe before the era of recombination when the universe was opaque to electromagnetic radiation. Primordial gravitational waves were predicted by the theory of inflation during the very early universe when spacetime experienced a short period faster than light expansion. However, this background signal is very weak to be observed by current instruments.

An observer of a GW will discover that spacetime is distorted by the effect of strain. This effect will produce a rhythmic increase and decrease of distances between objects at the frequency of the wave, and its magnitude decreases in proportion to the inverse square law from the source. However, this effect when measured on Earth after propagating through astronomical distances is extremely small, having strains of the order 10^{-21}. This strain is within the accuracy limit of the LIGO and Virgo instruments [5].

The first indirect evidence of the existence of GWs was discussed by Russell Alan Hulse and Joseph Hooton Taylor. They discovered the first binary pulsar in 1974 [6]. The characteristics of the orbit can be inferred from the Doppler shifting of radio signals generated by the pulsar. Accumulated data in 1979 showed a gradual decay of the orbital period fitting precisely the expected loss of energy and angular momentum as predicted by the general theory of relativity.

In the first part of this work, we introduce the theoretical framework characterizing gravitational waves produced by the merger of compact binaries. In the second part, we proceed to discuss evolutionary pathways leading to the formation of compact binaries. In the third part, the processes and constrains involved in the merger of compact binaries are discussed. In the fourth part, the methods of detection of gravitational waves are introduced. This is followed by describing real merger events of black hole binaries and neutron star binary systems. In the

last part of this paper we explore the futuristic perspective of gravitational waves and their impact on new horizons in astrophysics.

2. Parameters Characterizing Gravitational Waves

In this section we introduce some parameters describing the behavior of gravitational waves generated by the merger of compact binaries. These parameters will be helpful in shedding light on the nature of the processes leading to the merger of compact binaries. Let us first consider the merger of NS-NS binaries at a separation of "a". External perturbation may cause the decay of their orbits, until they merge, at a rate of $\mathrm{d}a/\mathrm{d}t = -a/\tau_{GW}$, where τ_{GW} is the gravitational merger timescale. For circular binary orbit decay, and assuming both NS can be approximated as point masses, the gravitational merger timescale is given by [7]:

$$\tau_{GW} = \frac{5}{64}\frac{c^5}{G^3}\frac{a^4}{\mu M^2} = \frac{5}{64}\frac{c^5}{G^3}\frac{a^4}{q(1+q)M_1^3} \tag{1}$$

Employing geometrized units ($G = c = 1$), the above equation can be written as:

$$\tau_{GW} = 2.2\times 10^8 q^{-1}(1+q)^{-1}\left(\frac{a}{R_\odot}\right)^4\left(\frac{1.4M_\odot}{M_1}\right)^3 \tag{2}$$

In the above equations M_1 and M_2 are the individual NS masses, M is the combined total mass ($M = M_1 + M_2$), $\mu = M_1M_2/M$ is the reduced mass, and $q = M_2/M_1$ is the binary mass ratio, c is the velocity of light, G is the gravitational constant, and $M_\odot$ and $R_\odot$ are the solar mass and the solar radius, respectively. For an elliptical orbit, τ_{GW} is shorter, and the eccentricity is gradually reduced by the emission of gravitational waves, until circularization is achieved as they decay. The merger lifetime can be obtained by integration as $\tau_{merger} = \tau_{GW}/4$. The luminosity of the emitted gravitational waves by NS binary systems is given by [7]:

$$\begin{aligned} L_{GW} &= \frac{32}{5}\frac{\mu^2M^3}{a^5} = \frac{32}{5}\frac{M_1^2M_2^2(M_1+M_2)}{a^5} \\ &= 5.34\times 10^{32} q^2(1+q)\left(\frac{M_1R_\odot}{1.4M_\odot}\right)^5\frac{1}{a^5}\ \mathrm{erg/s} \end{aligned} \tag{3}$$

At the end of the binary lifetime, the distance between its components shrinks to within a few NS radii, and the luminosity increases enormously, as predicted by the above equation, approaching the luminosity of all visible matter in the universe $\left(\approx 10^{53}\ \mathrm{erg/s}\right)$.

The strain amplitude h observed face-on at a distance D from the source can be approximated by [7]:

$$h = \frac{4M_1M_2}{aD} = 5.53\times 10^{-3} q\left(\frac{M_1}{1.4M_\odot}\right)^2\left(\frac{a}{100\ \mathrm{km}}\right)^{-1}\left(\frac{D}{100M_{pc}}\right)^{-1} \tag{4}$$

LIGO and Virgo instruments are sensitive enough to observe strain ampli-

tudes of the order 10^{-21}. The corresponding gravitational wave characteristic frequency is given by:

$$f_{GW} = 2 f_{orb} = \frac{1}{\pi}\left(M/a^3\right)^{1/2} = 194\left(\frac{M}{2.8M_\odot}\right)^{1/2}\left(\frac{a}{100\text{ km}}\right)^{-3/2}\text{ Hz} \quad (5)$$

Again, the frequency increases appreciably as the distance between the NS binary shrinks to a few NS radii. Gravitational waves are expected to have a wide range of frequencies: $10^{-16}\text{ Hz} < f < 10^{4}\text{ Hz}$ [8].

An interesting measurement that can be achieved with direct GW observations, is the orbital decay rate, with the period evolving according to the relation:

$$\frac{\mathrm{d}T}{\mathrm{d}t} = -\frac{192\pi}{5}\left(M_C\omega\right)^{5/3} \quad (6)$$

where ω is the angular frequency, and M_C is the chirp mass given by [7] [9]:

$$M_C = \mu^{3/5}M^{2/5} = \frac{\left(M_1M_2\right)^{3/5}}{\left(M_1+M_2\right)^{1/5}} = \frac{c^3}{G}\left[\frac{5}{96}\pi^{-8/3}f^{-11/3}\dot{f}\right]^{3/5} \quad (7)$$

This is a parameter that can be determined readily from GW observations.

3. Evolutionary Pathways for Compact Binary Formation

Merger of neutron stars or neutron star-black whole (BH) systems, with merger timescales smaller than the Hubble time, are typically formed via similar evolutionary pathways in stellar-field galaxy populations [10]. Several scenarios were proposed for the formation of compact binaries. In one scenario, the standard channel for NS-NS or BH-NS merging binaries is that the first-born compact object passes through a common envelope (CE) phase. Other models have also been proposed. One of these models assumes that the progenitor binary stars have nearly equal mass, and that they evolve off the main sequence and enter a CE phase prior to either undergoing a supernova [11] [12]. Simulation of this latter process shows that NS-NS systems could be formed by twin giant stars with core masses $\geq 0.15M_\odot$. The standard pathway assumes a high-mass progenitor binary with both stars having a mass in the range $M \geq 8\text{-}10M_\odot$ to ensure the burst of a pair of supernovae [11] [12]. In this system, the most massive star evolves over just a few million years before leaving the main sequence. It then passes through a giant phase and undergoes a Type Ib, Ic, or II supernova producing what will become the heavier compact object: a BH in BH-NS systems, or the most massive NS in NS-NS systems. Subsequently, the secondary star leaves the main sequence and enters a CE phase as it evolves to the giant phase, overflowing its Roche lobe [7]. The binary separation then shrinks dramatically as a result of dynamical friction until sufficient energy is produced to expel the envelope. This is an important step to keep the binary compact objects close enough through the emission of the gravitational waves within the Hubble time. In this scenario, the exposed helium-rich core of the secondary star undergoes a supernova with the consequence of either unbinding the system or producing a tight binary. The outcome of this process depends on the magnitude and orien-

tation of the supernova kick.

The implications of the above scenarios:

- Accretion of matter by a NS has a limit beyond which accretion-induced collapse may take place [11]. In fact, the CE efficiency as determined by the range of binary separation and the mass of the primary compact object following the accretion phase, is very poorly constrained [9] [13] [14] [15].
- The relation between the initial star mass and the final compact object mass is fairly understood. However, uncertainties may arise from poor knowledge of the metallicity, which is a crucial factor when considering the effect of mass loss in stellar winds [16] [17].
- The fate of the system after the merger is determined by the maximum mass of the newly formed NS. It either undergoes accretion-induced collapse to a BH or survives as a NS. At present, a maximum mass of $1.97 \pm 0.04 M_{\odot}$ was obtained for a NS by the Shapiro time delay measurements [18]. GW observations may provide further constrains [19] [20] [21]. Supernova remnants may indicate whether the NS has a classic hadronic composition or instead consists of some form of strange quark matter or other particle condensates [22] [23] [24] [25]. On the other hand, the supernova kick velocity distribution is not fully understood. This is an important issue that determines whether the system becomes unbound or remains bound after the second explosion [23] [24] [25] [26]. **Figure 1** summarizes the various scenarios of the evolutionary pathways for binary compact object formation.

Many population synthesis models have been proposed to understand binary system evolution in our Milky Way Galaxy. Assumptions about the CE evolution, the supernova kick distribution, and other parameters have been advanced. In certain models, population synthesis is normalized by estimating the star formation history in the Milky Way Galaxy [27] [28]. Other works involve the choice of the best judged parameters capable of reproducing the observed Galactic binary pulsar sample [29] [30].

A quantity of interest is the number of BH-NS and NS-NS mergers. Interferometric detection has a high sensitivity to the chirp mass M_C (see Equation (7)), and to the binary mass ratio q [31] [32] [33] [34]. If the signal to noise ratio is sufficiently high, it is possible to determine whether the primary's mass exceeds the maximum mass of a NS, even for frequencies outside the range of the LIGO band [7].

4. Merger of Compact Stars Binaries

The merger of compact binaries follows roughly three phases: in-spiral, merger, and ring down. Each of these phases constitutes a set of challenges for numerical modeling and detection.

The quazi-equilibrium (QE) formalism describes accurately the binary in-spiral phase, up until the point where the gravitational radiation timescale becomes comparable to the dynamical timescale. When the binary separation

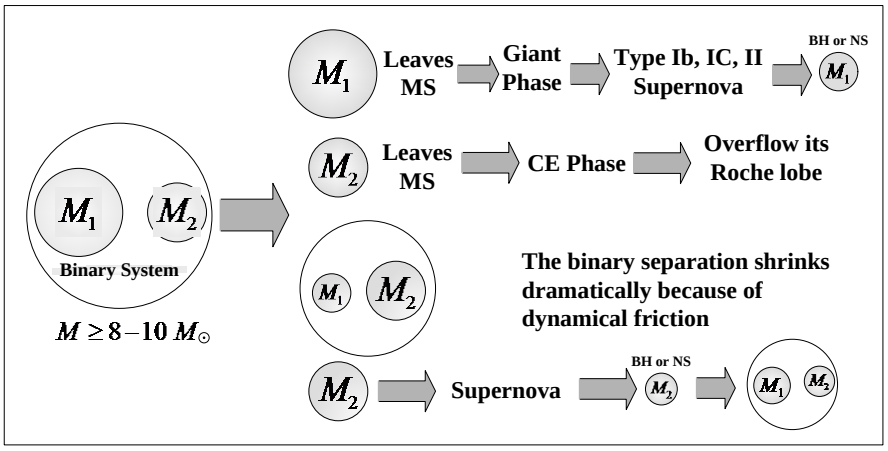

Figure 1. Evolutionary pathways of compact binaries formation.

shrinks to a few radii of the two NSs, the binary system becomes rapidly unstable. Dynamical instability causes the neutron stars to plunge and enter the merger phase. This is a complicated hydrodynamic phase that requires full GR simulations to be fully understood. Simulations show that if the NSs are of equal mass, the merger resembles a slow collision. On the other hand, if the primary is substantially more massive, then the secondary will be tidally disrupted during the plunge phase and will accrete onto the primary. Prior to merging, the NSs are most likely irrotational, leading to a substantial velocity discontinuity at the surface of contact and giving rise to a rapid production of vortices [7]. Meanwhile, a disk will form around the central remnant from the material that escapes from the outer Lagrange points of the system. Numerical simulation predicts that this phase produces the maximum GW amplitude. Gravitational waves during merger provide important information about the NS equation of state (EOS); in particular, it provides information about the gravitational wave frequency f_{orb} at which the binary orbit becomes unstable (see Equation (5)). The merger may generate the thermal energy necessary to power the short-lived gamma-ray bursts (sGRB). This occurs when neutrinos and antineutrinos produced by the shock-heated material enter an annihilation phase around the remnant, producing high-energy gamma-ray photons.

In the ring-down phase, the system is finally settled in a dynamically stable configuration. The GW signal depends in this case on the remnant's mass and rotational profile. If the remnant is massive enough, it becomes gravitationally unstable, and it collapses to form a spinning BH. Alternatively, three possible scenarios are expected, depending on the total mass of the remnant [7]:

- If the *remnant mass* is less than the maximum mass of an isolated (M_{iso}) nonrotating NS, then it will survive and become stable forever.
- A *supermassive remnant* with a mass exceeding the isolated stationary mass limit, but below that allowed for a uniformly rotating NS (typically $\leq 1.2M_{iso}$, and assuming weak dependence on the ESO), may become unstable [35] [36] [37]. Supermassive remnants are usually stable against gravita-

tional collapse, unless angular momentum losses drive the angular velocity below the allowed value for stability. Angular momentum losses may originate from pulsar-type emission or magnetic coupling to the outer disk.

- A remnant entering the *hypermassive* regime, may be supported by a rapid differential rotation. Hypermassive NS remnants (HMNR) may have significantly larger masses, depending on the EOS, and will survive for a timescale much larger than the dynamical time, exhibiting a wide range of oscillation modes [38] [39] [40] [41] [42]. Eventually, differential rotation decreases gradually due to some combination of radiation reaction and magnetic viscous dissipation resulting in a collapse of the HMNS to a spinning black hole. The energy released from the collapse to HMNS may cause a delay in the sGRB, and the peak of the GW emission, powered by the collapse of the HMNS into a BH, occurs only at a later time. The discrepancy in the time of arrival between the GW and the sGRB was observed for the first NS-NS merger detected by LIGO (see sec. 7.2.3).

Calculations have shown the possible formation of gravitationally-bound thick disks of material around the remnants. These types of disks are expected to heat-up appreciably, possibly yielding electromagnetic emission. However, these disks are not GW emitters, because of their relatively axisymmetric configuration and their inherently low densities. Under certain circumstances, a gravitational unbound outflow from mergers may occur. This outflow may be the site of exotic nuclear reactions produced by the *r*-process and leading to the formation of heavy elements.

5. Merger of Black Hole-Neutron Star Binaries

In-spiral of BH-NS system can also be described by post-Newtonian (PN) expansion, up until shortly before merger [7]. However, the parameter space is profoundly different from the NS-NS case. In the first place, a BH is heavier than a NS, and consequently the dynamics can follow a different pathway. Furthermore, BHs may be spinning rapidly, and the spin-orbit coupling can play a decisive role in the orbital dynamics of the binary giving rise to a larger number of oscillation modes in the GW signal [43] [44]. The larger mass of BH-NS binaries implies that instability occurs at a lower GW frequency (see Equation (5)). The instability of BH-NS binary systems is determined primarily by the binary mass ratio, NS compactness, and to a lesser extent by the BH spin [45]. Generally, the binding energy assumes its lowest value as the radius increases. For systems with high BH masses and/or more compact NS, the system is driven to dynamical orbital instability that occurs near the classical innermost stable circular orbit. In this case, the NS plunges toward the BH before the onset of tidal disruption, and the NS is typically swallowed as one piece by the BH with no material left behind to form a disk [7]. The GW emission from such systems is severely reduced after the merger event, leaving only a low-amplitude, rapidly decaying ringdown signal [46].

An interesting case to consider occurs when the NS and the BH have a mass ratio close to unity, the NS is less compact, and the BH has a prograde spin direction. In this case, the NS will reach the mass-shedding limit prior to dynamical instability, leading to its tidal disruption. The in-spiral is immune to angular momentum transfer via mass-shedding, and has never been seen in full or even approximate GR calculations [47]. However, unstable mass transfer may lead to the formation of a substantial disk around the BH. In this process, the NS matter is accreted promptly by the BH [45].

6. Detection of Gravitational Waves

In the late 1950s, the scientific community was focused on whether GWs could transmit energy. Richard Feynman settled this question by a thought experiment known as the "sticky bead argument", presented during the First Gravitational Relativity Conference at Chapel Hill in 1957. In this argument, he noted that the effect of passing a GW on a rod with beads would be to move the beads along the rod, and consequently heat is generated, implying that GWs produce work. The Chapel Hill Conference inspired Joseph Weber to start designing and building a GW detector, known as the Weber bar, which is a large solid bar isolated from environmental vibrations. During the period 1969-1970, he claimed detecting gravitational waves emanating from the Galactic Center. However, the rate of this detection raised doubts on the validity of his observations, as this would drain our galaxy of energy at a time scale shorter than its inferred age. These doubts were further confirmed by other research groups. By the late 1970s, there was a general consensus that Weber's observations were spurious.

Modern GW detectors employ interferometry to achieve the required detection sensitivity. The most sensitive detectors using this scheme are the LIGO instruments at Hanford and Livingstone, and the Virgo instrument in Italy. These instruments are sensitive to strains of the order $h = 10^{-21}$. One of the most promising future GW detection instruments is under development at Chongqing University. It is planned to detect high frequency gravitational waves with typical parameters: $f = 100$ GHz and $h = 10^{-31}$ to 10^{-32} [48].

The LIGO and Virgo detectors are modified Michelson interferometers. GW strain is measured as the difference in length between its orthogonal arms. Each arm has two mirrors at its ends and is 4 km in length. A passing GW alters the arm length (ΔL) in the x and y directions, such that, $\Delta L = hL$, where h is the GW strain amplitude. This change in length produces a phase difference between the two laser beams passing through the beam splitter, and thus transmits an optical signal proportional to the GW strain to the output detector. To achieve the required sensitivity, each arm contains a resonant optical cavity formed by two test mass mirrors, which multiplies the effect of the GW on the light phase by a factor of 300 [49]. Additional resonant buildup of the laser light in the interferometer is achieved by placing a partially transmitting power-recycling mirror at the input [50]. Thus, the 20 W of laser input is increased

to 700 W incident on the laser beam splitter, which is further increased to 100 kW that circulates in each arm cavity. Furthermore, the GW signal is optimized by placing a partially transmitting signal-recycling mirror at the output. This allows the extraction of the signal by broadening the bandwidth of the arm cavities [51] [52]. **Figure 2** illustrates the modified Michelson interferometer used for GW detection.

7. Observational Evidence of Gravitational Waves Emanating from the Merger of Compact Binaries

The completion of the LIGO and Virgo detectors has enabled the scientific community, for the first time, to detect gravitational waves. In the following sub-sections, the characteristics of the detected gravitational waves and their progenitors are discussed.

7.1. Gravitational Waves from Binary Black Hole Merger

On September 14, 2015, the LIGO Hanford, WA, and Livingstone, LA, Observatories detected the first signal carrying the signature of a black hole binary merger. A schematic diagram of the gravitational wave signal of this event is shown in **Figure 3**. In this figure, the strain h (10^{-21}) is shown as a function of time (s). Over 0.25 s the frequency increases from 35 Hz to 150 Hz, where the amplitude of the signal assumes its maximum value. This type of signal is typical of gravitational waves emanating from the merger of compact binary stars. For lower frequencies, the event is characterized by a chirp mass given by Equation (7). **Figure 3** provides an estimation of f and $\dot{f}$, leading to a chirp mass of $M_C \approx 30M_\odot$, and implying a total mass of the binary compact stars $M = M_1 + M_2 \geq 70M_\odot$ [53]. The corresponding sum of the Schwarzschild radii of the binary components is $2GM/c^2 \geq 210$ km. At a frequency of 75 Hz, which is half the maximum gravitational wave frequency, the binary objects must be very close and very compact [53]. A distance of 350 km is typical for equal Newtonian point masses orbiting at this frequency.

A chirp mass of $30M_\odot$ cannot be obtained for a pair of two neutron stars. Moreover, a BH-NS binary having the deduced chirp mass would merge at a much lower frequency. Therefore, the merger of a BH binary is the only known system that can reach an orbital frequency of 75 Hz [53]. The damping oscillation of the signal (see **Figure 3**), after reaching its maximum value, is consistent with a black hole relaxing to a final stationary Kerr configuration [53].

Using general relativity-based models [54] [55] [56] [57], and performing a coherent Bayesian analysis to derive the posterior distribution of the source parameter [58], the initial and final masses, final spin, distance, and redshift of the source are obtained [53].

Fitting numerical simulations of binary black hole mergers [59] [60], allows the estimation of the mass and spin of the final black hole, the total energy radiated in gravitational waves, as well as the peak gravitational wave luminosity

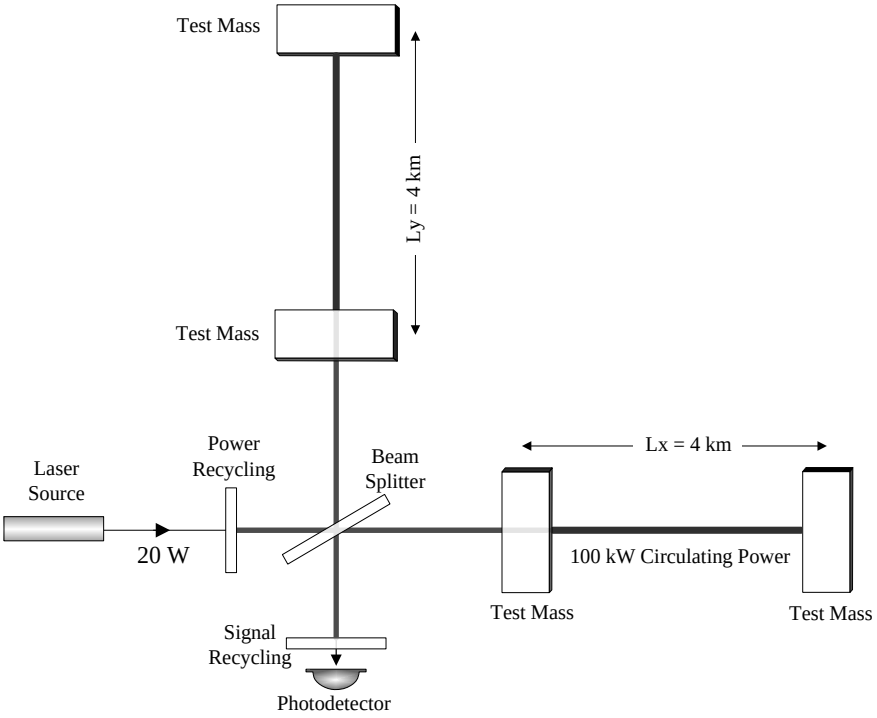

Figure 2. Advanced LIGO detector (see text) (adapted from ref. [49]).

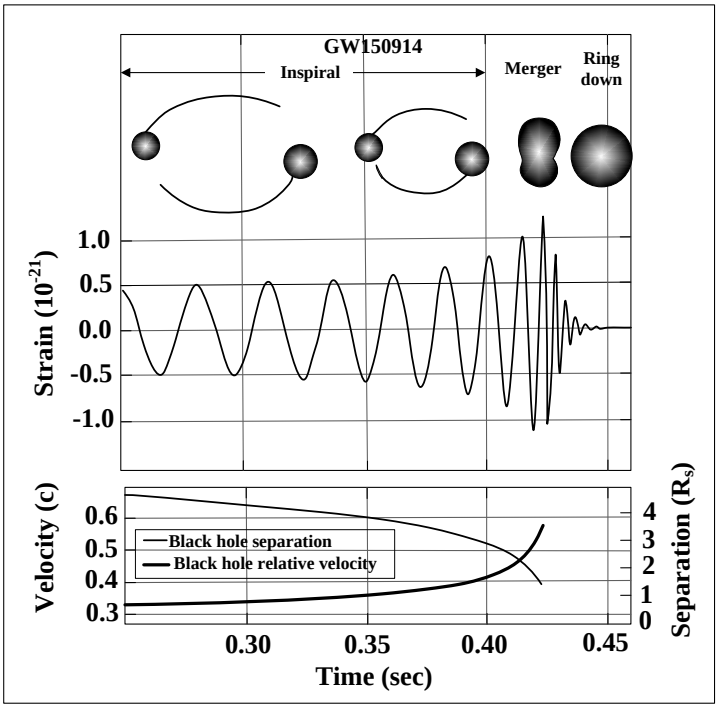

Figure 3. (Top) Estimated gravitation alwave strain amplitude for the GW150914 event. (Bottom) The Keplerian effective black hole separation in units of Schwarzschild radii and the effective relative post-Newtonian parameter $\upsilon/c = \left(GM\pi f/c^3\right)^{1/3}$, where f is the GW frequency calculated numerically, and M is the total mass (adapted from reference [49]).

[61]. The estimated total energy radiated in gravitational waves in the GW150914 event is $3.0^{+0.5}_{-0.5} M_{\odot} c^2$, and the peak gravitational wave luminosity reached a value of $3.6^{+0.5}_{-0.4} \times 10^{56}$ erg/s, which is equivalent to $200^{+30}_{-30} M_{\odot} c^2/s$. The primary and secondary black holes masse are estimated to be $36^{+5}_{-4} M_{\odot}$ and $29^{+4}_{-4} M_{\odot}$, respectively. The final black hole mass and spin are $62^{+4}_{-4} M_{\odot}$ and $0.67^{+0.05}_{-0.07}$, respectively [49].

Subsequently, gravitational waves emanating from two other binary mergers were discovered. The masses of the black holes for one of the two events is $(14+8) M_{\odot}$ (GW151226) [62] and for the other $(31+19) M_{\odot}$ [63]. As expected, no electromagnetic (EM) counterpart was discovered despite the massive efforts invested by the astronomical community.

Assuming a modified dispersion relation for the gravitational wave [64], observations constrain the Compton wavelength of the graviton to $\lambda_g > 10^{13}$ km, corresponding to a bound graviton mass $m_g < 1.2 \times 10^{-22}$ eV/c^2 [53].

The GW150914 event demonstrates the existence of stellar-mass black holes with masses exceeding $30 M_{\odot}$, and that binary black holes can form in nature and that they can merge within the Hubble time. These results can be extended to describe what happens when micro black holes collide and merge, as explained in sub-section (8.4).

7.2. Gravitational Waves from Binary Neutron Star Mergers

On 17 August 2017 at 12:41:06 UT, the advanced LIGO/Virgo instruments detected the in-spiral and merger of binary neutron stars (GW170817) [56]. The source of the GW was identified as residing in the periphery of the S0 galaxy NGC4993 at a distance of 40 ± 8 Mpc (130.4 ± 26 million ly) and has a stellar mass of $\log M/M_{\odot} = 10.49^{+0.08}_{-0.20}$ [65]. The Swope Supernova Survey 2017a (SSS17a) is the first detection of an electromagnetic counterpart to a gravitational wave source [65]. The observed optical counterpart peaks at an absolute magnitude of $M_i = -15.7$, which is 1000 times brighter than a nova [57], or a typical kilonova, as predicted originally by Metzger *et al.*, 2010 [66].

The masses m_1 and m_2 of the merging neutron stars are in the range $m_1 \in (1.36 - 2.26) M_{\odot}$ and $m_2 \in (0.86 - 1.36) M_{\odot}$ [67]. The chirp mass M_C drives the frequency evolution of the gravitational radiation in the in-spiral phase (see Equation (7)). The best measured mass parameter is $M_C = 1.188^{+0.004}_{-0.002} M_{\odot}$. The total mass is $2.82^{+0.47}_{-0.09} M_{\odot}$, and the mass ratio m_2/m_1 is bound to the range 0.4 - 1.0 [67]. These masses are consistent with a system of binary neutron stars. White dwarfs are excluded since the gravitational wave signal sweeps through the 200 Hz frequency in the instruments' sensitivity band, implying an orbit of about 100 km, which is much smaller than the typical radius of a white dwarf [68]. However, for this specific merging event, the gravitational wave data alone cannot exclude more compact objects than neutron stars, such as quark stars or black holes [67]. In the latter case, no EM component is expected to be observed, in violation of the observational evidence.

A short-lived gamma ray burst (sGRB) was observed independently in the same sky direction by Fermi-GBM [69], and INTEGRAL [59]. A more detailed description of the processes involved in generating and observing sGRB by the merging of NSs is given in sub-section (7.2.3).

Gravitational waves alone can provide only limited information about the nature of the merging progenitors. This is the case for BH-BH mergers and for BH-NS mergers when the mass of the NS is much less than the mass of the BH (see Section 3). NS-NS mergers, on the other hand, produce electromagnetic waves (EM), and when combined with GW observations, will provide a wealth of information about the nature and dynamics of the merging NS, the processes involved during the in-spiral, merger, and ringdown phases, as well as the afterglow of the shattered debris following the merger.

Gravitational wave emission probes the bulk motions, binary properties, masses, and hypothetically the composition of the NS. Electromagnetic observations, on the other hand, provide a better understanding of the astrophysics behind the event, particularly the environment of the merging compact objects, the formation of relativistic and non-relativistic outflows, and in certain cases the properties of the merging products [70] [71]. The combined measurements of GW and EM emissions permit new types of measurements, such as the Hubble constant [72] [73] and also provide rich information about the origin of short-lived gamma-ray bursts [75] (see sub-Section 7.2.3).

7.2.1. UV, Optical, and Near Infrared Transient Afterglow Emissions

Photometry is a powerful tool for probing a wide range of spectral emissions, and the resulting energy distribution inferred from this photometry can be described by a blackbody model with a well-defined temperature, a radius corresponding to an expansion velocity, and the bolometric luminosity [76]. The afterglow of the merging neutron star binary gives rise to a multi-component spectral energy distribution (SED) across the optical and NIR. It is characterized by a rapid fading of the UV and the blue optical bands, in addition to a significant reddening of the optical/NIR colors [76]. In the optical/NIR bands, the most auspicious counterpart is the kilonova. This is a roughly isotropic thermal transient powered by radioactive decay of rapid neutron capture elements synthesized in the merger ejecta [66] [77] [78] [79] [80]. The luminosity, timescale, and spectral peak of the kilonova depend precisely on the ejecta composition. For ejecta rich with the Fe group or light *r*-process nuclei with atomic mass number $A \le 140$, the kilonova emission is expected to have a peak at optical wavelengths at a luminosity $L_p \approx 10^{41}\text{-}10^{42}\ \text{erg}\cdot\text{s}^{-1}$ on a short timescale of $t_p \approx 1$ day, the so-called blue kilonova [66] [78] [81]. On the other hand, for ejecta rich with heavier lanthanide elements ($A \ge 140$) the emission is predicted to exhibit a peak at NIR wavelengths with $L_p \approx 10^{40}\text{-}10^{41}\ \text{erg}\cdot\text{s}^{-1}$ over a longer time scale of $t_p \approx 1$ week, which is known as a red kilonova [79] [80] [82]. It was shown that the data for the GRB170817 NS merger event cannot be fitted with a model with heating from ^{56}Ni radioactive decay and Fe-peak opacities, as in normal

supernovae [76]. However, heating from the *r*-process nuclei requires at least two components and is consistent with lanthanide-poor and lanthanide-rich opacities [76]. In a multi-component model, each component is considered as arising from distinct regions in the ejecta. The high velocity of the blue KN ejecta suggests that it originates from the shock-heated polar region created when the neutron stars collide (e.g., [83] [84]). On the other hand, the low velocity red KN component could originate from the vividly ejected tidal tails in the equatorial plane of the binary (e.g., [71] [85] [86]). In this case, the relatively high ejecta mass $\approx 0.01 M_{\odot}$ suggests an asymmetric mass ratio of the emerging binary ($q \leq 0.8$, [86]). The fitted opacity indicates that the hyper-massive neutron star remnant is relatively short-lived ≈ 30 ms, [87] [88].

Models of comprehensive UV, optical, and NIR data for the 170,817 merger event indicate that the total ejecta mass is $\approx 0.05 M_{\odot}$ with a high velocity, $v \approx 0.3c$, blue component and a slower, $v \approx 0.1\text{-}0.2c$, purple/red component. The presence of both components and the large ejecta mass indicates that binary neutron star mergers are a dominant factor in the cosmic *r*-process nucleosynthesis.

7.2.2. X-Ray Emission from Neutron Stars Binary Merger

The Chandra X-ray observatory was successful in detecting the afterglow of GRB170817 at 16 days post trigger. X-ray and radio emission were discovered at the transient's position about 9 and 16 days after the merger. These emissions are likely produced by processes distinct from the ones generating the UV/optical/near infrared emission [87]. The detected luminosity of the X-ray emission from SSS17a has a value of $L(0.3\text{-}10\ \text{keV}) = 2.6^{+0.5}_{-0.4} \times 10^{38}\ \text{erg}\cdot\text{s}^{-1}$, and it follows a power law spectrum with an exponent $\Gamma = 2.4 \pm 0.8$ [89]. Moreover, it was found that the X-ray light curve from the binary NS merger associated with the source is consistent with the afterglow from the off-axis short-lived gamma-ray burst, with a jet angle ≥ 23˚ from the line of sight [89]. The radio and X-ray data can be jointly explained as the afterglow emission from a sGRB with a jet energy of 10^{49} - 10^{50} erg [90].

7.2.3. Short-Lived Gamma Ray Bursts

On August 17, 2017, the Fermi Gamma-ray Burst Monitor (GBM) detected a short gamma-ray burst approximately 1.7 s after the arrival of the gravitational wave that originated from the binary neutron star merger event (170817).

The standard model of short-lived gamma ray bursts (sGRB) predicts that their prompt emission fades on a time scale < 2 s, and that the relativistic jet will be decelerated by the ambient medium. Usually, the jets launched by sGRBs are collimated and highly relativistic; implying that they are only detectable within a narrow range of viewing angles at early times [91]. However, the GRB jet emanating from the GW170817 event was observed off axis and gave rise to a faint afterglow emission at early times that grew in luminosity as the jet beaming became less severe, and its opening angle spread into the line of sight of the ob-

server [92]. GRB 170817A, which emanated from the 170817 NS merger event, has a duration of 100 ms as detected by INTEGRAL, and thus it can be assigned to the short-lived GRB class [93]. An important feature of this gamma-ray burst (GRB 170817A) is the low luminosity of its prompt γ-ray emission. The low luminosity may be due to the off-axis observation of the event. The minimum luminosity of short-lived gamma-ray bursts is not well-constrained observationally, making it difficult to definitely distinguish the luminosity of off-axis GRBs from faint on-axis GRBs.

The off-axis GRB model predicts other multi-wavelength properties, such as late-time radio emission from the afterglow that peaks on timescales of about 10 days after attaining the X-ray peak [92]. Indeed, the radio source associated with SSS17a was reported almost 15 days post-burst [92]. The γ-ray emission along our line of sight was certainly feeble, or the emission might be deficient in all directions as in the case of low-luminosity long-lived GRBs associated with Ic supernova [94]. This weak burst is thousands of millions of times fainter than the inferred energies of short-lived GRBs and could belong to a separate population of weakly jetted, low luminosity GRBs [95].

The absence of a normal GRB afterglow (e.g., in X-rays; [96]), led certain investigators to suggest the possibility of an off-axis emission mechanism, such as may be produced by a shocked cocoon around the primary jet (e.g., [97] [98]).

The energy spectrum of GRB 170817A is well described by a power law with an exponential cutoff at ≈185 KeV [99], and it has a total energy that is about 4 to 6 orders of magnitude less than a typical *Swift* sGRB [100].

7.2.4. On the Origin of Heavy Elements

Colliding neutron stars produce neutron-rich ejecta that can trigger the enhanced *r*-process and gives rise to the so-called kilonova explosion, which powered by the radioactive decay of elements synthesized in the outflow [101]. It has been argued that the high opacity of synthesized heavy elements in the ejecta, such as lanthanides and actinides, will suppress their emission in the optical and it will appear predominantly in the near-infrared on a time scale of several days [80] [101] [102]. The *r*-process is responsible for about half of the elements heavier than iron and has been traditionally attributed to core collapse supernovae [103]. Recent studies, however, disapprove supernovae as a source of at least the heaviest elements of the "platinum peak" near the mass $A = 195$ [104]. Nucleosynthesis calculations have confirmed the suitability of compact binary mergers as a source of production of the heaviest elements in the Universe [88] [105] [106] [107] [108]. Unlike colliding black holes, merging neutron stars expel metallic and radioactive debris that can be observed by ground-based telescopes or satellites. As mentioned in sub-section (7.2.1), the modeling of the multi-band light curves, leads to the presence of at least two emission components [104]. The first is characterized by a high opacity and is interpreted as being the tidal part of the dynamical ejecta, carrying a very low electron fraction ($\gamma_e < 0.25$) and resulting in a strong *r*-process that produces lanthanides/actinides [104]. The second component has a low opacity and is characterized by a weaker *r*-process

via a raised electron fraction ($\gamma_e > 0.25$). This second component may be produced by a different mechanism, such as a neutrino driven wind, and/or the unbinding of the accretion torus material [104]. Finally, these findings provide strong observational evidence that NS binary mergers can resolve the stunning and heated debate on the cosmic origin of heavy and precious elements, such as gold, silver, and platinum.

8. Gravitational Waves: A Future Perspective

The LIGO and Virgo instruments have revolutionized our understanding of one of the most challenging phenomena in astrophysics. The scientific community had to wait for about a century to finally witness the detection of gravitational waves predicted originally by the theory of general relativity in 1916. It is worthwhile at this stage to elucidate the lessons we have learned from the first generation of detected gravitational wave events and to investigate the possible impacts of future discoveries of gravitational waves on our vision about the working mechanisms in our universe.

8.1. Evaluation of Gravitational Waves Detection Events

The first generation of detected gravitational waves emanating from the merger of compact binaries involved five events, four of which were produced by the merger of binary black holes and only one was produced by the merger of neutron stars. It is to be noted that no black hole-neutron star event has been detected so far. However, it is difficult at this stage to statistically draw any conclusion regarding the frequency of occurrence of each type of binary system. This is basically because black hole binaries are more massive than neutron star binaries and, accordingly, the strain associated with gravitational waves resulting from their merger can be detected to large distances. The most powerful detected event so far involved the merger of a black hole binary with masses of 36 and $29M_{\odot}$ and a distance of about one billion light years. In comparison, in a sphere of this radius, a limited number of NS-NS binary mergers can be detected. The various types of binary systems can be statistically significant only within a sphere of radius where all these types are potentially detectable. The relative number of the various types of compact binaries can then shed light on the accuracy of the models regarding their evolutionary pathways.

An important outcome of NS-NS merger events is the peculiarity of the short-lived gamma-ray burst (sGRB) typically associated with such events. Their general features are different from most short-lived gamma-ray bursts detected by the *Swift* satellite. Future detections of GW events emanating from NS-NS mergers may constitute a statistically significant sample that could be used to elucidate the various origins of sGRBs.

8.2. Primordial Gravitational Waves from the Inflationary Era

An important prediction of the cosmological inflation theory is the generation of primordial gravitational waves [109]. The amplitude of the GW signal is charac-

terized by a ratio (r) between the tensor and scalar power spectrum amplitudes at a given pivot scale k [110]. The best bound on r obtained so far yields $r < 0.07$ at 95% confidence level, for $k = 0.05$ Mpc^{-1} [110]. An important issue is that various inflationary scenarios predict different values of r. Therefore, the observation of a gravitational signature of primordial GWs provides a powerful tool to examine the validity of the general inflationary theory and helps also to discriminate between specific inflationary models. Studying the primordial GW background may also probe a wide class of phenomena related to cosmological inflation. For example, the presence of additional field besides the inflaton can generate an extra GW background, not pertaining to vacuum oscillations [111] [112] [113]. A point of interest is the generation of the GW background during the inflationary heating phase [114], which provides a potential test for studying the mechanisms involved in this process. Detection of primordial GWs also has a direct impact on our understanding of fundamental physics. In fact, the energy scale of inflation is intimately related to the tensor-to-scalar ratio (r), whose detection may lead to the exploration of new horizons of physics beyond the standard model of particle physics. It is to be noted that at the early stages of the universe, processes other than inflation may have provided a source for GWs, including the electroweak phase transition [115], the first order phase transition [116] [117], and the topological defects [118] [119]. For all the above reasons, the detection of primordial GWs may shed light on major problems in cosmology in the forthcoming decade. The crucial observational signature of the inflationary GW background is a curl-like pattern in the polarization of the Cosmic Microwave Background (CMB), also referred to as the B-mode. Technological advances in the past decade have steered cosmology towards an exhilarating era where scientists can assess experimentally the existing theoretical models concerning our universe. A number of ground-based or balloon-borne experiments have been designed to probe the B-mode signal. These experiments include Polarbear [120], Piper [121], ACTpol [122], Spider [123], and CLASS [124]. Furthermore, satellites such as COBE, WMAP, and Planck have provided bounds on r, as reported above. In addition, several next generation CMB space missions have been planned to detect gravitational waves, and more specifically the B-mode. Among this new generation of missions are COrE [125], LiteBIRD [126], PIXIE [127], and PRISM [128]. Evidence of primordial GWs could also originate from galaxy and CMB curl-like lensing signatures induced by tensor modes [129] [130]. Other signatures of primordial GWs include parameters related to the small modification in the expansion history of the universe arising from GW contributions to the overall energy budget [131]. Finally, a direct detection by future aLIGO [132] or eLISA [133] [134] is a viable possibility, especially if some specific inflationary mechanism generates a blue-tilted primordial tensor spectrum [109].

8.3. Gravitational Waves from the Relic of Galaxy Formation

Gravitational waves may have been produced prolifically during the initial phase

of galaxy formation at the early universe. Several models have been proposed to explain the formation of massive black holes at the center of galaxies at redshifts corresponding to the era when the universe was less than one billion years old. Masses of black holes at the center of faraway galaxies can be estimated using the M-sigma relation [135]. An important question to ask is at what epoch did the seeding of black holes at the centers of galaxies take place, and what are the possible mechanisms involved in their growth. Many hypotheses have been advanced to elucidate the origin of massive or supermassive black holes at the centers of galaxies. Several possible formation channels have been proposed for the formation of massive black hole seeds, including the collapse of population III stars [136], gas dynamic instabilities where supermassive black holes are postulated to form directly out of the dense gas cloud [137] [138], the collapse of supermassive stars [139], and the merger of small and intermediate mass black holes. There is little dispute that once a black hole forms at the center of a galaxy, it can grow either by accretion of surrounding material or by merging with other black holes. In the latter case, gravitational waves will be generated, and if strong enough, they will fall in the domain of sensitivity of the current or future GWs detectors. This merging process is also more likely to happen when galaxies collide to form a cD galaxy [139] [140]. The collision of massive or supermassive black holes at the center of these galaxies will produce energetic GWs that may lie within a sphere of radius, again, corresponding to the sensitivity of the actual or future GWs detectors.

Primordial black holes (PBH) of a wide range of masses have been proposed to form in the extreme densities and inhomogeneities of the early universe [141]. More recently, Choptuik [142] and Kim [143] have demonstrated the formation of PBHs during the inflationary era, when the density of the universe experienced a dramatic decrease causing a cosmological phase transition. In this context, PBHs could be the seeding agent at the center of the first generation of galaxies in the early universe. Eventually, when the sensitivity of the gravitational wave detectors becomes capable of detecting GW events at redshifts beyond the era of star formation, it is possible that the source of GWs may be shown to be primordial in origin. Studies have shown that if the observed event rate is greater than one event per year at redshifts $z \geq 40$, then the probability distribution of primordial density fluctuations must be significantly non-Gaussian or the events may originate from primordial black holes [144]. Thus, GWs are promising tools that will refine our understanding of the workings of the universe.

8.4. Quantum Mechanical Black Holes

In this last section we investigate the possibility of the creation and merger of micro or mini black holes. These are hypothetical entities subject to the rules of quantum mechanics. The concept of micro black holes was initially introduced by Stephen Hawking in 1971 [141]. They could have been created in the high-density environment in the early universe, or possibly through subsequent

phase transitions, and therefore they are referred to as primordial micro black holes. In principle, primordial black holes may have any mass above the Planck mass, and are characterized by a Schwarzschild radius $R = 2GM/c^2$, where G is the gravitational constant, c the speed of light, and M the mass of the black hole. Some theoretical models hypothesize the existence of extra dimensions of space, where the strength of gravity increases at a faster pace than in three dimensions. Certain configurations of extra dimensions may lower the Planck scale to the TeV range, which makes the production of micro black holes in the Large Hadron Collider (LHC) a viable possibility [145] [146]. However, quantum effects will cause micro black holes to evaporate almost instantaneously by Hawking radiation, producing a burst of elementary particles [146]. A holeum is a primordial and a hypothetically stable quantized bound state [147]. It consists of a number of mini black holes bound quantum mechanically. In the case of the merger of these mini black holes due to external perturbations, quantum effects will play a major role, and in this case no gravitational waves are likely to be produced, but instead the merger will most probably give rise to a jet of elementary particles.

9. Conclusion

We have presented the theoretical framework characterizing gravitational waves emanating from the merger of compact binaries as derived from general relativity, and it was shown that this framework accurately describes the merger events of compact binaries. Detection of gravitational waves from black hole mergers provides evidence of the existence of a wide range of stellar black hole masses. Merging neutron stars give rise to gravitational waves and electromagnetic counterpart emission. The colliding and merging neutron stars give rise to a kilonova, and the observational data can only be explained by assuming multi-component ejecta that produce emissions covering all parts of the spectrum, from gamma rays to radio waves. The observed short gamma-ray bursts produced in these merging events are extremely faint as compared to the ones recorded by the *Swift* satellite, and this result has cast doubt on the origin of short gamma-ray bursts. A confirmation of the nature of short gamma-ray bursts from merging neutron stars may have to await the discovery of other merging events before a solid model can be set. Analysis of the electromagnetic counterpart of GW170817 reveals that NS-NS mergers are the main source of heavy elements in the universe. The future detection of more GWs will undoubtedly provide a wealth of information concerning the processes that shape our universe.

Conflicts of Interest

The authors declare no conflicts of interest regarding the publication of this paper.

References

[1] Heaviside, O. (1893) *Electromagnetic Theory*, **1**, 455-466.

[2] Poincaré, H. (1905) *Note*: *Sur la dynamique de l'électron. C.R. T*, **140**, 1504-1508.

[3] Einstein, A. (1916) *Prussian Academy Proceedings*, **1**, 688-696.

[4] Einstein, A. (1918). *Prussian Academy Proceedings*, **1**, 154-167.

[5] LIGO Scientific Collaboration; Virgo Collaboration (2012) *Physical Review D*, **85**, Article ID: 082002.

[6] Hulse, R.A. and Taylor, J.H. (1975) *The Astrophysical Journal Letters*, **195**, L51-L53. https://doi.org/10.1086/181708

[7] Faber, J.A. and Rasio, F.A. (2012) *Living Reviews in Relativity*, **15**, 8. https://doi.org/10.12942/lrr-2012-8

[8] Huang, Y. and Weisberg, J.M. (2016) *The Astrophysical Journal*, **829**, Article ID: 55.

[9] Blanchet, L., *et al.* (1995) *Physical Review Letters*, **74**, 3515. https://doi.org/10.1103/PhysRevLett.74.3515

[10] Belczynski, K., *et al.* (2008) *The Astrophysical Journal Supplement*, **174**, 223-260. https://doi.org/10.1086/521026

[11] Bethe, H.A., Brown, G.E. and Lee, C.-H. (2007) *Physics Reports*, **442**, 5-22. https://doi.org/10.1016/j.physrep.2007.02.004

[12] Brown, G.E., Lee, C.-H. and Rho, M. (2008) *Physical Review Letters*, **101**, Article ID: 091101.

[13] Postnov, K. and Yungelson, L. (2006) *Living Reviews in Relativity*, **9**, 6.

[14] Davis, P.J., Kolb, U. and Willems, B. (2010) *Monthly Notices of the Royal Astronomical Society*, **403**, 179-195. https://doi.org/10.1111/j.1365-2966.2009.16138.x

[15] Zorotovic, M., Schreiber, M.R., Gänsicke, B.T. and Nebot Gómez-Morán, A. (2010) *Astronomy & Astrophysics*, **520**, Article ID: A86. https://doi.org/10.1051/0004-6361/200913658

[16] Zhang, W.-Q., Woosley, S.E. and Heger, A. (2007) *The Astrophysical Journal*, **679**, 639-654. https://doi.org/10.1086/526404

[17] O'Connor, E. and Ott, C.D. (2011) *The Astrophysical Journal*, **730**, 70. https://arxiv.org/abs/1010.5550

[18] Demorest, P., Pennucci, T., Ransom, S., Roberts, M. and Hessels, J. (2010) *Nature*, **467**, 1081-1083. https://arxiv.org/abs/1010.5788 https://doi.org/10.1038/nature09466

[19] Read, J.S., Lackey, B.D., Owen, B.J. and Friedman, J.L. (2009) *Physical Review D*, **79**, Article ID: 124032. https://arxiv.org/abs/0812.2163

[20] Özel, F. and Psaltis, D. (2009) *Physical Review D*, **80**, Article ID: 103003. https://arxiv.org/abs/0905.1959

[21] Markakis, C., Read, J.S., Shibata, M., Uryū, K., Creighton, J.D.E., Friedman, J.L. and Lackey, B.D. (2009) *Journal of Physics*: *Conference Series*, **189**, Article ID: 012024. https://arxiv.org/abs/1110.3759

[22] Pandharipande, V.R. and Smith, R.A. (1975) *Nuclear Physics A*, **237**, 507-532. https://doi.org/10.1016/0375-9474(75)90415-7

[23] Wang, C., Lai, D. and Han, J.L. (2006) *The Astrophysical Journal*, **639**, 1007-1017. https://arxiv.org/abs/astro-ph/0509484 https://doi.org/10.1086/499397

[24] O'Shaughnessy, R., Kim, C., Kalogera, V. and Belczynski, K. (2008) *The Astrophysical Journal*, **672**, 479-488. https://arxiv.org/abs/astro-ph/0610076 https://doi.org/10.1086/523620

[25] Kuranov, A.G., Popov, S.B. and Postnov, K.A. (2009) *Monthly Notices of the Royal Astronomical Society*, **395**, 2087-2094. https://arxiv.org/abs/0901.1055 https://doi.org/10.1111/j.1365-2966.2009.14595.x

[26] Hobbs, G., Lorimer, D.R., Lyne, A.G. and Kramer, M. (2005) *Monthly Notices of the Royal Astronomical Society*, **360**, 974-992. https://arxiv.org/abs/astro-ph/0504584 https://doi.org/10.1111/j.1365-2966.2005.09087.x

[27] Voss, R. and Tauris, T.M. (2003) *Monthly Notices of the Royal Astronomical Society*, **342**, 1169-1184. https://arxiv.org/abs/astro-ph/0303227

[28] de Freitas Pacheco, J.A., Regimbau, T., Vincent, S. and Spallicci, A. (2006) *International Journal of Modern Physics D*, **15**, 235-250. https://arxiv.org/abs/astro-ph/0510727 https://doi.org/10.1142/S0218271806007699

[29] Kalogera, V., Belczynski, K., Kim, C., O'Shaughnessy, R. and Willems, B. (2007) *Physics Reports*, **442**, 75-108. https://arxiv.org/abs/astro-ph/0612144 https://doi.org/10.1016/j.physrep.2007.02.008

[30] O'Shaughnessy, R., Kalogera, V. and Belczynski, K. (2010) *The Astrophysical Journal*, **716**, 615-633. https://arxiv.org/abs/0908.3635 https://doi.org/10.1088/0004-637X/716/1/615

[31] Buonanno, A., Chen, Y., Pan, Y., Tagoshi, H. and Vallisneri, M. (2005) *Physical Review D*, **72**, Article ID: 084027. https://arxiv.org/abs/gr-qc/0508064

[32] Babak, S., Balasubramanian, R., Churches, D., Cokelaer, T. and Sathyaprakash, B.S. (2006) *Classical and Quantum Gravity*, **23**, 5477-5504. https://arxiv.org/abs/gr-qc/0604037

[33] van der Sluys, M., Raymond, V., Mandel, I., Röver, C., Christensen, N., Kalogera, V., Meyer, R. and Vecchio, A. (2008) *Classical and Quantum Gravity*, **25**, Article ID: 184011. https://arxiv.org/abs/0805.1689

[34] Van Den Broeck, C., Brown, D.A., Cokelaer, T., Harry, I., Jones, G., Sathyaprakash, B.S., Tagoshi, H. and Takahashi, H. (2009) *Physical Review D*, **80**, Article ID: 024009. https://arxiv.org/abs/0904.1715

[35] Komatsu, H., Eriguchi, Y. and Hachisu, I. (1989) *Monthly Notices of the Royal Astronomical Society*, **237**, 355-379. https://doi.org/10.1093/mnras/237.2.355

[36] Cook, G.B., Shapiro, S.L. and Teukolsky, S.A. (1992) *The Astrophysical Journal*, **398**, 203-223. https://doi.org/10.1086/171849

[37] Cook, G.B., Shapiro, S.L. and Teukolsky, S.A. (1994) *The Astrophysical Journal*, **424**, 823-845. https://doi.org/10.1086/173934

[38] Baumgarte, T.W., Shapiro, S.L. and Shibata, M. (2000) *The Astrophysical Journal Letters*, **528**, L29-L32. https://arxiv.org/abs/astro-ph/9910565 https://doi.org/10.1086/312425

[39] Shibata, M., Baumgarte, T.W. and Shapiro, S.L. (2000) *The Astrophysical Journal*, **542**, 453-463. https://arxiv.org/abs/astro-ph/0005378 https://doi.org/10.1086/309525

[40] Duez, M.D., Liu, Y.T., Shapiro, S.L., Shibata, M. and Stephens, B.C. (2006) *Physical Review Letters*, **96**, Article ID: 031101. https://arxiv.org/abs/astro-ph/0510653

[41] Stephens, B.C., Duez, M.D., Liu, Y.T., Shapiro, S.L. and Shibata, M. (2007) *Classical*

and Quantum Gravity, **24**, S207-S220. https://arxiv.org/abs/gr-qc/0610103

[42] Galeazzi, F., Yoshida, S. and Eriguchi, Y. (2012) *Astronomy & Astrophysics*, **541**, A156. https://arxiv.org/abs/1101.2664

[43] Baumgarte, T.W., Cook, G.B., Scheel, M.A., Shapiro, S.L. and Teukolsky, S.A. (1998) *Physical Review D*, **57**, 7299-7311. https://arxiv.org/abs/gr-qc/9709026 https://doi.org/10.1103/PhysRevD.57.7299

[44] Arvanitaki, A. and Geraci, A.A. (2013) *Physical Review Letters*, **110**, Article ID: 071105.

[45] Shibata, M. and Taniguchi, K. (2011) *Living Reviews in Relativity*, **14**, 6. http://www.livingreviews.org/lrr-2011-6 https://doi.org/10.12942/lrr-2011-6

[46] Kyutoku, K., Shibata, M. and Taniguchi, K. (2010) *Physical Review D*, **82**, Article ID: 044049. https://arxiv.org/abs/1008.1460

[47] Faber, J.A., Baumgarte, T.W., Shapiro, S.L., Taniguchi, K. and Rasio, F.A. (2006) *Physical Review D*, **73**, Article ID: 024012. https://arxiv.org/abs/astro-ph/0511366

[48] Thorne, K.S. (1995) *Particle and Nuclear Astrophysics and Cosmology in the Next Millennium*, **160**, 45. https://arxiv.org/abs/gr-qc/9506086 .

[49] Abbott, B.P., *et al.* (2016) *Physical Review Letters*, **116**, Article ID: 06102.

[50] Drever, R.W.P., *et al.* (1983) The Advanced LIGO Detectors in the Era of First Discoveries. In: Meystre, P. and Scully, M.O., Eds., *Quantum Optics*, *Experimental Gravity*, *and Measurement Theory*, Vol. 94, Plunum Press, New York, 503-514.

[51] Meers, B.J. (1988) *Physical Review D*, **38**, Article ID: 2317. https://doi.org/10.1103/PhysRevD.38.2317

[52] Kwee, P., *et al.* (2012) *Optics Express*, **20**, Article ID: 10617.

[53] Fricke, T.T., *et al.* (2012) *Classical Quantum Gravity*, **29**, Article ID: 065005.

[54] Taracchini, A., *et al.* (2014) *Physical Review D*, **89**, Article ID: 061505.

[55] Pürrer, M. (2014) *Classical Quantum Gravity*, **31**, Article ID: 195010.

[56] Hannam, M., *et al.* (2014) *Physical Review Letters*, **113**, Article ID: 151101.

[57] Khan, S., *et al.* (2016) *Physical Review D*, **93**, Article ID: 044007.

[58] Veitch, J., *et al.* (2015) *Physical Review D*, **91**, Article ID: 042003.

[59] Healy, J., *et al.* (2014) *Physical Review D*, **90**, Article ID: 104004.

[60] Husa, S., *et al.* (2016) *Physical Review D*, **93**, Article ID: 044006.

[61] Abbott, B.P., *et al.* (2016) *Physical Review D*, **93**, Article ID: 122004.

[62] Abbott, B.P., *et al.* (2016) *Physical Review Letters*, **116**, Article ID: 241103.

[63] Abbott, B.P., *et al.* (2017) *Physical Review Letters*, **118**, Article ID: 221101.

[64] Will, C.M. (1998) *Physical Review D*, **57**, Article ID: 2061.

[65] Pan, Y.C., *et al.* (2017) *The Astrophysical Journal Letters*, **848**, L30. https://doi.org/10.3847/2041-8213/aa9116

[66] Metzger, B.D., *et al.* (2010) *Monthly Notices of the Royal Astronomical Society*, **406**, Article ID: 2650.

[67] Abbott, B.P., *et al.* (2017) *The Astrophysical Journal Letters*, **848**, L12. https://doi.org/10.3847/2041-8213/aa91c9

[68] Shapiro, S.L. and Teukolsky, S.A. (1983) The Physics of Compact Objects. John Wiley, New York.

[69] Goldstein, A., *et al.* (2017) *The Astrophysical Journal Letters*, **848**, L14.

https://doi.org/10.3847/2041-8213/aa8f41

[70] Metzger, B.D. and Berger, E. (2012) *The Astrophysical Journal*, **746**, 48. https://doi.org/10.1088/0004-637X/746/1/48

[71] Rosswog, S., Piran, T. and Nakar, E. (2013) *Monthly Notices of the Royal Astronomical Society*, **430**, 2585-2604. https://doi.org/10.1093/mnras/sts708

[72] Schutz, B.F. (1986) *Nature*, **323**, 310-311. https://doi.org/10.1038/323310a0

[73] Holz, D.E. and Hughes, S.A. (2005) *The Astrophysical Journal*, **629**, 15. https://doi.org/10.1086/431341

[74] Nissanke, S., *et al.* (2010) *The Astrophysical Journal*, **725**, 496. https://doi.org/10.1088/0004-637X/725/1/496

[75] Berger, E. (2014) *Annual Review of Astronomy and Astrophysics*, **52**, 43-105. https://doi.org/10.1146/annurev-astro-081913-035926

[76] Cowperthwaite, P.S., *et al.* (2017) *The Astrophysical Journal Letters*, **848**, L17. https://doi.org/10.3847/2041-8213/aa8fc7

[77] Li, L.X. and Paczynski, B. (1998) *The Astrophysical Journal Letters*, **507**, L59. https://doi.org/10.1086/311680

[78] Roberts, L.F. (2011) *The Astrophysical Journal Letters*, **736**, L21. https://doi.org/10.1088/2041-8205/736/1/L21

[79] Barnes, J. and Kasen, D. (2013) *The Astrophysical Journal*, **775**, 18. https://doi.org/10.1088/0004-637X/775/1/18

[80] Tanaka, M. and Hotokezaka, K. (2013) *The Astrophysical Journal*, **775**, 113. https://doi.org/10.1088/0004-637X/775/2/113

[81] Metzger, B.D. and Fernandez, R. (2014) *Monthly Notices of the Royal Astronomical Society*, **441**, 3444-3453. https://doi.org/10.1093/mnras/stu802

[82] Kasen, D., Badnell, N. and Barnes, J. (2013) *The Astrophysical Journal*, **774**, 25. https://doi.org/10.1088/0004-637X/774/1/25

[83] Bauswein, A., *et al.* (2013) *The Astrophysical Journal*, **773**, 78. https://doi.org/10.1088/0004-637X/773/1/78

[84] Sekiguchi, Y., *et al.* (2016) *Physical Review D*, **93**, Article ID: 124046.

[85] Rosswog, S., *et al.* (1999) *Astronomy and Astrophysics*, **341**, 499.

[86] Hotokezaka, K., *et al.* (2013) *Physical Review D*, **87**, Article ID: 024001.

[87] Fernandez, R. and Metzger, B. D. (2013) *Monthly Notices of the Royal Astronomical Society*, **435**, 502-517. https://doi.org/10.1093/mnras/stt1312

[88] Just, O., *et al.* (2015) *Monthly Notices of the Royal Astronomical Society*, **48**, 541-567. https://doi.org/10.1093/mnras/stv009

[89] Hagard, D., *et al.* (2017) *The Astrophysical Journal Letters*, **848**, L25. https://doi.org/10.3847/2041-8213/aa8ede

[90] Alexander, K.D., *et al.* (2017) *The Astrophysical Journal Letters*, **848**, L21. https://doi.org/10.3847/2041-8213/aa905d

[91] Fong, W., *et al.* (2015) *The Astrophysical Journal*, **815**, 102. https://doi.org/10.1088/0004-637X/815/2/102

[92] Hallinan, G., *et al.* (2017) *Science*, **358**, 1579-1583.

[93] Savchenko, V., *et al.* (2017) *The Astrophysical Journal Letters*, **848**, L5. https://doi.org/10.3847/2041-8213/aa8f94

[94] Kaneko, Y., *et al.* (2007) *The Astrophysical Journal*, **654**, 385.

https://doi.org/10.1086/508324

[95] Murguia-Berthier, A., *et al.* (2017) *The Astrophysical Journal Letters*, **848**, L34. https://doi.org/10.3847/2041-8213/aa91b3

[96] Evans, P.A., *et al.* (2017) *Science*, **358**, 1565-1570. https://doi.org/10.1126/science.aap9580

[97] Gottieb, O., Nakar, E. and Piran, T. (2017) *Monthly Notices of the Royal Astronomical Society*, **473**, 576-584.

[98] Lazzati, D., *et al.* (2017) *Monthly Notices of the Royal Astronomical Society*, **471**, 1652-1661. https://doi.org/10.1093/mnras/stx1683

[99] LIGO Scientific Collaboration and Virgo Collaboration (2017) *The Astrophysical Journal Letters*, **848**, L13. https://doi.org/10.3847/2041-8213/aa920c

[100] Gehrels, N., *et al.* (2009) *Annual Review of Astronomy and Astrophysics*, **47**, 567-617. https://doi.org/10.1146/annurev.astro.46.060407.145147

[101] Pian, E., *et al.* (2017) Spectroscopic Identification of r-Process Nucleosynthesis in a Double Neutron Star Merger. arXiv:1710.05858

[102] Arcavi, I., *et al.* (2017) *Nature*, **551**, 64-66.

[103] Burbidge, E.M., *et al.* (1957) *Review of Modern Physics*, **29**, 547. https://doi.org/10.1103/RevModPhys.29.547

[104] Tanvir, N.R., *et al.* (2017) *The Astrophysical Journal Letters*, **848**, L27. https://doi.org/10.3847/2041-8213/aa90b6

[105] Rosswog, S., *et al.* (1998) *Astronomy and Astrophysics*, **341**, 499-526.

[106] Freiburghaus, C., *et al.* (1999) *The Astrophysical Journal Letters*, **525**, L121. https://doi.org/10.1086/312343

[107] Goriely, S., *et al.* (2011) *The Astrophysical Journal*, **738**, L32. https://doi.org/10.1088/2041-8205/738/2/L32

[108] Mendosa-Temis, J.D.J., *et al.* (2015) *Physical Review C*, **92**, Article ID: 055805.

[109] Guzzetti, M.C., *et al.* (2016) *La Rivista del Nuovo Cimento*, **39**, 399-495.

[110] Ade, P.A.R., *et al.* (2016) *Physical Review Letters*, **116**, Article ID: 031302.

[111] Barnaby, N., *et al.* (2012) *Physical Review D*, **86**, Article ID: 103508.

[112] Binetruy, P., *et al.* (2012) *JCAP*, **1206**, 27.

[113] Biagetti, M., *et al.* (2013) *Physical Review D*, **88**, Article ID: 103518.

[114] Khlebnikov, S.Y. and Tkachev, I.I. (1996) *Physical Review Letters*, **77**, 219. https://doi.org/10.1103/PhysRevLett.77.219

[115] Huber, S.J., *et al.* (2016) *JCAP*, **1604**, 36.

[116] Caprini, C., *et al.* (2016) *JCAP*, **1604**, 1.

[117] Dev, P.S.B. and Mazumdar, A. (2016) *Physical Review* D, **93**, Article ID: 104001.

[118] Sanidas, S.A., *et al.* (2012) *Physical Review D*, **85**, Article ID: 122003.

[119] Figueroe, D.G., *et al.* (2013) *Physical Review Letters*, **110**, Article ID: 101302.

[120] Ade, P.A.R., *et al.* (2014) *The Astrophysical Journal*, **794**, Article ID: 171.

[121] Gandilo, N.N., *et al.* (2016) *PIPER*, **1607**, Article ID: 06172.

[122] Calabrese, E., *et al.* (2014) *JCAP*, **1408**, 10.

[123] Crill, B.P., *et al.* (2008) *Proceedings of SPIE—The International Society for Optical Engineering*, **7010**, Article ID: 08071548.

[124] Eimer, J.R., *et al.* (2012) *Proceedings of SPIE—The International Society for Optical*

Engineering, **8452**, Article ID: 12110041.

[125] Bouchet, F.R., *et al.* (2011) https://arxiv.org/abs/1102.2181

[126] Matsumura, T., *et al.* (2013) *Journal of* Low *Temperature Physics*, **176**, 733. https://doi.org/10.1007/s10909-013-0996-1

[127] Kogut, A., *et al.* (2011) *JCAP*, **1107**, 25.

[128] Andrè, P., *et al.* (2014) *JCAP*, **1402**, 6.

[129] Dodelson, S., *et al.* (2003) *Physical Review Letters*, **91**, Article ID: 021301. https://arxiv.org/abs/astro-ph/0301177

[130] Jeong, D. and Schmidt, F. (2012) *Physical Review D*, **86**, Article ID: 083512.

[131] Smith, T.L., *et al.* (2006) *Physical Review Letters*, **97**, Article ID: 021301. https://arxiv.org/pdf/astro-ph/0603144v1.pdf

[132] Aasi, J., *et al.* (2015) *Classical and Quantum Gravity*, **32**, Article ID: 074001.

[133] eLISA Science Collaboration. https://www.elisascience.org/

[134] Klein, A., *et al.* (2016) *Physical Review D*, **93**, Article ID: 024003.

[135] Ferrarese, F. and Merrit, D. (2000) *The Astronomical Journal*, **539**, L9-L12. https://doi.org/10.1086/312838

[136] Bromm, V., *et al.* (1999) *The Astrophysical Journal Letters*, **527**, L5-L8. https://doi.org/10.1086/312385

[137] Haehnelt, M.G. and Rees, M.J. (1993) *Monthly Notices of the Royal Astronomical Society*, **263**, 168-178. https://doi.org/10.1093/mnras/263.1.168

[138] Lodato, G. and Natarajan, P. (2006) *Monthly Notices of the Royal Astronomical Society*, **371**, 1813-1823. https://doi.org/10.1111/j.1365-2966.2006.10801.x

[139] Volonteri, M. (2010) *The Astronomy and Astrophysics Review*, **18**, 279-315. https://doi.org/10.1007/s00159-010-0029-x

[140] Leahy, J.P. (1997) An Atlas of DRAGNs, "Glossary".

[141] Hawking, S.W. (1971) *Monthly Notices of the Royal Astronomical Society*, **152**, 75-78. https://doi.org/10.1093/mnras/152.1.75

[142] Choptuik, M.W. (1993) *Physical Review Letters*, **70**, 9-12. https://doi.org/10.1103/PhysRevLett.70.9

[143] Kim, H.I. (2000) *Physical Review D*, **62**, Article ID: 063504.

[144] Koushiappas, S.M. and Loeb, A. (2017) *Physical Review Letters*, **119**, Article ID: 221104.

[145] Giddings, S.B. and Thomas, S.D. (2002) *Physical Review D*, **65**, Article ID: 056010.

[146] Dimopoulos, S. and Landsberg, G.L. (2001) *Physical Review* Letters, **87**, Article ID: 161602.

[147] Chavda, L.K. and Chavda, A.L. (2002) *Classical and Quantum Gravity*, **19**, 11. https://doi.org/10.1088/0264-9381/19/11/311

Call for Papers

Journal of Modern Physics

ISSN: 2153-1196 (Print) ISSN: 2153-120X (Online)
http://www.scirp.org/journal/jmp

Journal of Modern Physics **(JMP)** is an international journal dedicated to the latest advancement of modern physics. The goal of this journal is to provide a platform for scientists and academicians all over the world to promote, share, and discuss various new issues and developments in different areas of modern physics.

Editor-in-Chief

Prof. Yang-Hui He City University, UK

Subject Coverage

Journal of Modern Physics publishes original papers including but not limited to the following fields:

Biophysics and Medical Physics
Complex Systems Physics
Computational Physics
Condensed Matter Physics
Cosmology and Early Universe
Earth and Planetary Sciences
General Relativity
High Energy Astrophysics
High Energy/Accelerator Physics
Instrumentation and Measurement
Interdisciplinary Physics
Materials Sciences and Technology
Mathematical Physics
Mechanical Response of Solids and Structures
New Materials: Micro and Nano-Mechanics and Homogeneization
Non-Equilibrium Thermodynamics and Statistical Mechanics
Nuclear Science and Engineering
Optics
Physics of Nanostructures
Plasma Physics
Quantum Mechanical Developments
Quantum Theory
Relativistic Astrophysics
String Theory
Superconducting Physics
Theoretical High Energy Physics
Thermology

We are also interested in: 1) Short Reports—2-5 page papers where an author can either present an idea with theoretical background but has not yet completed the research needed for a complete paper or preliminary data; 2) Book Reviews—Comments and critiques.

Notes for Intending Authors

Submitted papers should not have been previously published nor be currently under consideration for publication elsewhere. Paper submission will be handled electronically through the website. All papers are refereed through a peer review process. For more details about the submissions, please access the website.

Website and E-Mail

http://www.scirp.org/journal/jmp **E-mail: jmp@scirp.org**

What is SCIRP?

Scientific Research Publishing (SCIRP) is one of the largest Open Access journal publishers. It is currently publishing more than 200 open access, online, peer-reviewed journals covering a wide range of academic disciplines. SCIRP serves the worldwide academic communities and contributes to the progress and application of science with its publication.

What is Open Access?

All original research papers published by SCIRP are made freely and permanently accessible online immediately upon publication. To be able to provide open access journals, SCIRP defrays operation costs from authors and subscription charges only for its printed version. Open access publishing allows an immediate, worldwide, barrier-free, open access to the full text of research papers, which is in the best interests of the scientific community.

- High visibility for maximum global exposure with open access publishing model
- Rigorous peer review of research papers
- Prompt faster publication with less cost
- Guaranteed targeted, multidisciplinary audience

Scientific Research Publishing

Website: http://www.scirp.org

Subscription: sub@scirp.org

Advertisement: service@scirp.org